Molecular and biochemical characterisation of the electron transport chain of *Plasmodium falciparum*

Thomas ANTOINE

Ph.D. February 2012

Molecular and biochemical characterisation of the electron transport chain of *Plasmodium falciparum*

Thesis is submitted in accordance with the requirements of the University of Liverpool for the degree of Doctor of Philosophy

By

Thomas ANTOINE

February 2012

Declaration

This thesis is the result of my own work. The material contained in the thesis has not been presented, nor is currently being presented, either wholly or as a part, for any other degree or other qualification.

The research work was carried out in the Liverpool School of Tropical Medicine, University of Liverpool, United Kingdom.

.....

Thomas ANTOINE (2012)

Acknowledgments

First of all, I would like to express my gratitude to my supervisors Pr. Steve Ward, Dr. Giancarlo Biagini and Dr. Nick Fisher for their supervision, continued support and constant encouragement throughout my PhD.

A special thank goes to the InterMal PhD program and the Marie Curie Fellowship for providing the generous funding which allowed me to undertake this research, but also for giving me the opportunity to attend conferences and workshops as well as meet so many interesting people.

I am grateful to Prof. Alister Craig and Prof. Sylke Muller for accepting to be the two members of my oral defense committee.

The members of the Ward's research group have contributed immensely to my personal and professional time at Liverpool. I am very grateful to Ashley Warman for insightful comments in my work, for reviewing my thesis and providing valuable feedback as well as for many motivating discussions. I would like also to thank David Waterhouse for his friendship, enthusiasm and support in mass spectrometry analysis. I have greatly enjoyed the opportunity to work with Enrique Salcedo and Jill Davies, whose expertise and technical excellence in malaria research have been particularly helpful. Other past and present group members that I have had the pleasure to work with are Gavin Laing, Alison Ardrey, Ally Shone and Gemma Nixon.

Thanks to Alasdair Hill, Alison Mbekiani, Doss, Murad Ali Mubaraki, Taghreed Abdulaziz Hafiz, Francesca Tamoranezzi, Alice Halliday, Susana Barbosa, Darren Cook, Archana Kaniti, Upali Goonetilleke and others who made the lab a friendly environment for working.

I would also like to acknowledge my French comrades Rodolphe and Mathieu for being great friends throughout my last year in Liverpool.

I would like to thank Natalia for her love, encouragement and support when I have needed it the most. Thank you with all my heart!

Finally, I dedicate this thesis to my mom, dad and sister for always believing in me, for their continuous love and their supports in my decisions. Merci pour tout!

Abstract

The single mitochondrion of *Plasmodium falciparum* has some unusual functional features and unconventional biochemical properties. The electron transport chain (ETC) has critical roles in generating the mitochondrial membrane potential ($\Delta\psi_m$) and driving pyrimidine biosynthesis. Enzymes of the respiratory chain became attractive targets for antimalarial drugs such as atovaquone, an inhibitor of the bc_1 complex and lethal to malaria parasites. Although much progress has been made, there are a number of knowledge gaps in our understanding of the underlying biochemical mechanisms of the respiratory chain and some major components are still not completely characterised. In addition, recent studies have generated conflicting data and hypotheses with regards to mitochondrial function. This thesis, using a multidisciplinary approach, was undertaken to improve our understanding of the mitochondrion and its function and to clarify some of the confusing and contradictory data in this area.

Due to high sequence divergence, two ETC complexes remain to be clearly annotated in *Plasmodium* species: the succinate dehydrogenase (or complex II) and ATP synthase (or complex V). A pyramid-shaped bioinformatic strategy based on structural fingerprints and motif patterns was applied to identify candidate genes encoding the membrane anchors of complex II (SdhC and SdhD) and the ATP synthase F_0 sector (subunits *a* and *b*). In order to validate the genes predicted, 2D (non-)gradient BNE/SDS-Page approaches were established to separate respiratory chain complexes from solubilised *P. falciparum* membranes and identify their subunits via NanoLC-MS/MS analysis. Although the proteomic strategy was validated with bovine mitochondrial preparation, no positive identification of the genes of interest could be obtained with *P. falciparum* extract due to low-expression of target proteins and difficulties in the preparation of isolated mitochondria of high purity.

For the first time, the direct activities (or ubiquinone reduction activity) of the five dehydrogenases delivering ubiquinol to the bc_1 complex were compared. Due to a higher rate of turnover, the type II NADH dehydrogenase (*Pf*Ndh2) appears to be the main enzyme for feeding the electron transport chain with activity two to three times greater than the other dehydrogenases (dihydroorotate dehydrogenase, malate quinone oxidoreductase, glycerol-3-phosphate dehydrogenase). Additionally, spatiotemporal confocal imaging of parasite mitochondria revealed that loss of *Pf*NDH2 function provoked a collapse of the mitochondrial transmembrane potential ($\Delta\psi_m$). This observation reinforced the interest of targeting *Pf*Ndh2 as a chemotherapeutic strategy for drug development. The catalytic properties of the *P. falciparum* complex II were also examined using various electron donors and acceptors. Although complex II has been previously considered as a succinate dehydrogenase, results obtained indicate that complex II functions as a ubiquinol-fumarate reductase (QFR) forming succinate from fumarate in the asexual stages of *P. falciparum*. The capacity of menaquinone, an alternative electron carrier of anaerobic species and recently detected in malaria parasites was also evaluated to replace

ubiquinone within the respiratory chain in anaerobic conditions. Data obtained demonstrated that the menaquinone pool is not involved in the ETC and only the ubiquinone pool interacts with the different enzymes.

Artemisinin and its derivatives are frontline drugs employed in the treatment of uncomplicated malaria usually in the form of combination therapies. The ETC has been previously implicated in the mode of action of artemisinin and its derivatives. In this chapter, this hypothesis was tested using a single-cell imaging and enzyme-assay based approach. Data presented reveal that endoperoxide drugs provoke a rapid collapse of mitochondrial and plasma membrane potentials, both essential for parasite survival. Addition of the iron chelator desferrioxamine or the superoxide scavenger Tiron drastically reduces the depolarization highlighting the role of ferrous ions and oxidant stress in the artemisinins activation process and membrane damaging activity. Deoxyartemisinin, which lacks the endoperoxide bridge, has no effect on membrane potential indicating that this peroxide functionality is the key pharmacophore responsible for the pharmacological activity of this class of compound. Thus, the results presented, suggest that artemisinin and its derivatives act as a generator of additional reactive oxygen species that overcome the oxidative defenses of the malaria parasite and cause a widespread and rapid membrane potential depolarization leading to mitochondrial dysfunction and parasite death.

Atovaquone is a bc_1 inhibitor used in combination with proguanil (e.g. Malarone^{TM}) for the curative and prophylactic treatment of malaria. However, resistance to atovaquone associated with point mutations have been detected in the field. In this thesis, the first description of the effect of the Y268S mutation (harbored by the atovaquone-resistant field isolate TM902CB) on parasite bc_1 catalytic turnover and stability has been reported. This mutation was shown to confer a 270-fold shift of the inhibitory constant (K_i) for atovaquone with a concomitant reduction in the V_{max} of the bc_1 complex of 40% and a 3-fold increase in the observed K_m for ubiquinol. Western blotting analyses revealed a reduced iron-sulfur protein content in Y268S bc_1 suggestive of a weakened interaction between this subunit and the cytochrome *b*. It was concluded that the reduced enzyme activity affects protein stability and should incur a fitness penalty to the parasite, features that were not fully discernable using the yeast model alone.

Due to a small mitochondrial genome (mtDNA), the great majority of mitochondrial proteins, including those composing the ETC, are imported post-translationally from the cytosol into the organelle. Thus, it is essential to understand the import and processing machinery of mitochondrial proteins in malaria parasites. However, the description of the apicomplexan model including *P. falciparum* is fragmented across different studies and no general overview, including recent insights, has been proposed. An updated picture of the whole protein import and processing machinery in apicomplexa is presented. Novel putative components are revealed by comparison with five other apicomplexan species (*Toxoplasma gondii*, *Cryptosporidium muris*, *Theileria parva*, *Babesia bovis* and *Neospora caninum*). Aspects of the apicomplexan model are highly divergent from that seen in yeast, mammalians or plants.

Publications and presentations

Publications:

1. Fisher N*, Abd Majid R*, **Antoine T**, Al-Helal M, Warman AJ, Johnson DJ, Lawrenson AS, Ranson H, O'Neill PM, Ward SA, Biagini GA. 287(13):9731-41. (*Join first authors).
Cytochrome *b* mutation Y268S conferring atovaquone resistance phenotype in malaria parasite results in reduced parasite bc_1 catalytic turnover and protein expression. *J Biol Chem*. 2012. PMID: 2228249.

2. Vallières C, Fisher N, **Antoine T**, Al-Helal M, Stocks P, Berry NG, Lawrenson AS, Ward SA, O' Neill PM, Biagini GA, Meunier B. [Epub ahead of print]
HDQ, a potent inhibitor of *Plasmodium falciparum* proliferation binds to the Q_i site of the bc_1 complex. *Antimicrob Agents Chemother*. 2012. PMID: 22547613.

3. Biagini GA, Fisher N, Shone AE, Mubaraki MA, Srivastava A, Hill A, **Antoine T**, Warman AJ, Davies J, Pidathala C, Amewu RK, Leung S, Sharma R, Gibbons P, Hong DW, Pacorel B, Lawrenson AS, Charoensutthivarakul S, Taylor L, Berger O, Mbekeani A, Stocks PA, Nixon GL, Chadwick J, Hemingway J, Delves MJ, Sinden RE, Zeeman AM, Kocken CHM, Berry NG, O'Neill PM, Ward SA..
Generation of quinolone antimalarials targeting the Plasmodium falciparum mitochondrial respiratory chain for the treatment and prophylaxis of malaria. *Proc Natl Acad Sci U S A*. 2012. PMID: 22566611.

Publications in preparation:

4. **Antoine T**, Fisher N, Ward SA and Biagini GA.
Import and processing of mitochondrial proteins in *Plasmodium falciparum* and other apicomplexan parasites (review). *In preparation*.

5. **Antoine T**, Shone A, Amewu R, O'Neill PM, Ward SA and Biagini GA.
Rapid Fe^{2+}-chelatable depolarization of plasma and mitochondrial membrane potential by artemisinin and semi-synthetic endoperoxides. *In preparation*.

Presentations:

8th Annual BioMalPar / EVIMalaR Conference (EMBL), Heidelberg, Germany, May 2012.
Short oral and poster presentation
"Rapid Fe^{2+}-chelatable depolarization of plasma and mitochondrial membrane potential by artemisinin and semi-synthetic endoperoxides"

7th Annual BioMalPar / EVIMalaR Conference (EMBL), Heidelberg, Germany, May 2011.
Poster presentation
"Determining the source of electrons for the respiratory chain of Plasmodium falciparum"

Annual LSTM Postgraduate Seminar, Liverpool, UK, May 2011.
Oral presentation
"Bioinformatic and proteomic analysis of Plasmodium falciparum respiratory chain components: succinate dehydrogenase and ATP synthase"

16th European Bioenergetics Conference (EBEC), Warsaw, Poland, July 2010.
Poster presentation
"Gene identification and functional characterisation of Plasmodium falciparum succinate dehydrogenase"

6th Annual BioMalPar Conference (EMBL), Heidelberg, Germany, May 2010.
Poster presentation
"Gene identification and functional characterisation of Plasmodium falciparum succinate dehydrogenase"

Annual LSTM Postgraduate Seminar, Liverpool, UK, May 2010.
Oral presentation
"Gene identification and functional characterisation of Plasmodium falciparum succinate dehydrogenase"

British Society of Parasitology Spring Meeting, Cardiff, UK, April 2010.
Poster presentation
"Bioinformatic and proteomic analysis of Plasmodium falciparum succinate dehydrogenase"

Bioenergetics Christmas Meeting (Imperial College), London, UK, December 2009.
Oral presentation
"Bioinformatic and proteomic analysis of Plasmodium falciparum succinate dehydrogenase"

Table of contents

List of figures

Chapter 1

Chapter 3

Chapter 4

Chapter 5

Chapter 6

Chapter 7

Chapter 8

List of tables

Chapter 1

Chapter 3

Chapter 4

Chapter 5

Chapter 6

Chapter 7

Abbreviations

ADP	Adenosine diphosphate
AIP	Aryl hydrocarbon receptor-interacting protein
AOX	Alternative oxidase
ATP	Adenosine triphosphate
ATQ	Atovaquone
BSA	Bovine serum albumin
BNE	Blue native electrophoresis
CSP	Circumsporozoite protein
DCPIP	2,6-dichloroindophenol
DDM	Dodecyl-β-D-maltoside
DDT	Dichlorodiphenyltrichloroethane
DFO	Desferrioxamine
DFP	Deferipone
DHO	Dihydroorotate
DHODH	Dihydroorotate dehydrogenase
DHFR	Dihydrofolate reductase
DHPS	Dihydropteroate synthase
DMSO	Dimethyl sulphoxide
DNA	Deoxyribonucleic Acid
DTT	Dithiothreitol
DV	Digestive vacuole
EDTA	Ethylenediamine-tetraacetic acid
Erv1	Essential for respiration and viability 1
ETC	Electron transport chain
EtOH	Ethanol
FAD	Flavin Adenine Dinucleotide
FCN	Falcilysin
FCCP	Carbonyl cyanide 4-(trifluoromethoxy)phenylhydrazone
FPLC	Fast protein liquid chromatography
FPPIX	Ferriprotoporphyrin IX
G3P	Glycerol-3-phosphate
G3PDH	Glycerol-3-phosphate dehydrogenase
HDQ	Hydroxy-2-dodecyl-4-(1H)-quinolone
HEPES	4-(2-hydroxyethyl)-1-piperazineethanesulfonic acid
HMM	Hidden markov model
IC_{50}	50% inhibitory concentration
IPTG	Isopropyi-β-D-thiogalactopyranoside
iRBC	Infected red blood cell
IMP	Inner membrane protease
IMS	Intermembrane space
ISP	Rieske Iron protein

KCN	Pottasium cyanide
Kd	Dissociation constant
kDa	Kilodaltons
KH	Keilin-Hartree particles
Ki	Inhibitor constant
Mia40	Mitochondrial intermembrane space import and assembly protein 40
mM	Milimolar
mg/ml	Milligram per millilitre
MIP	Mitochondrial intermediate peptidase
MPP	Mitochondrial processing peptidase
MQ	Menaquinone
MQH_2	Menaquinol
MQO	Malate quinone oxidoreductase
mRNA	Messenger RNA
MS/MS	Tandem mass spectrometry
MSF	Mitochondrial import stimulation factor
mtDNA	Mitochondrial DNA
mtOM64	64 kDa mitochondrial outer membrane protein
MTT	Methylthiazolyldiphenyl-tetrazolium bromide
MVA	Modified vaccinia Ankara
MW	Molecular weight
NAC	Nascent-associated polypeptide complex
NADH	β-Nicotinamide-Adenine-Dinucleotide (reduced form)
NADPH	β-Nicotinamide-Adenine-Dinucleotide – Phosphate (reduced form)
NanoLC	Nano Liquid Chromatography
ND	Not determined
nM	Nanomolar
nm	Nanometers
OD	Optical density
ORF	Open reading frames
OSCP	Oligomycin Sensitivity-Conferring Protein
PAM	Presequence translocase-associated motor
PBS	Phosphate Buffer Saline
*Pb*NDH2	*P. berghei* type II NADH dehydrogenase
*Pf*NDH2	*P. falciparum* type II NADH dehydrogenase
PMS	Phenazine methosulfate
QFR	Quinol:fumarate reductase
Q_i	Ubiquinone reduction site
Q_o	Ubiquinol oxidation site
RAC	Ribosome-associated complex
RBC	Red blood cell
ROS	Reactive oxygen species
rRNA	Ribosomal RNA
SAM	Sorting and assembly machinery
SD	Standard deviation

SDH	Succinate dehydrogenase
SDS	Sodium Dodecyl Sulfate
SE	Standard error
SERCA	Sarco/endoplasmic reticulum Ca2+-ATPase
SP	Sulfadoxine-pyrimethamine
SQR	Succinate:ubiquinol oxidoreductase
TBS-T	Tris buffered saline and Tween-20
TCA	Tricarboxcylic acid cycle
TTFA	Thenoyltrifluoroacetone
TIM	Translocase of the Inner Membrane
TM	Transmembrane domain
TMRE	Tetramethyl rhodamine ethyl ester
toc64	The outer chloroplast envelope 64
TOM	Translocase of the Outer Membrane
TPR	Tetratricopeptide repeat
tRNA	Transfer RNA
UQ	Ubiquinone
UQH_2	Ubiquinol
UV	Ultra violet
V_{max}	Maximum reaction velocity
v/v	Volume by volume
w/v	Weight by volume
WHO	World Health Organisation
WT	Wild type

Chapter 1

Introduction

1.1. Malaria

1.1.1. The history of malaria - key discoveries

Traces of human malaria parasites have been found in the mummified remains of individuals who lived in ancient Egypt between 3200 BC and 1304 BC (Miller et al., 1994b). The early Greeks, including Homer (*c*. 850 BC) and Hippocrates (*c*. 400 BC), were well aware of the characteristic poor health, malarial fevers and enlarged spleens seen in people living in marshy places (Cox, 2010). In the seventh century, Italians named the disease associated to with the swamps around Rome "mal aria", meaning "bad air". Alphonse Laveran, a French army physician and Nobel Prize winner in 1907, was the first to discover the causative agent of malaria in 1880 in Algeria by noticing the presence of parasites in the blood of infected patients (Laveran, 1881). This discovery was subsequently confirmed by Ettore Marchiafava and Angelo Celli in 1884 who named the protozoan observed *Plasmodium* (Smith and Sanford, 1985).

Sir Ronald Ross, a British physician in the Indian Medical Service and Nobel Prize winner in 1902, identified in 1897 the avian malaria vector by observing *Plasmodium* parasites within the *Anopheles* mosquitoes which had been previously fed on malaria-infected blood from birds (Ross, 1898). In 1898, the Italian malariologists Giovanni Battista Grassi, Amico Bignami, Giuseppe Bastianelli, Angelo Celli, Camillo Golgi and Ettore Marchiafava demonstrated conclusively that human malaria was transmitted by only female *Anopheles* mosquitoes and described the whole blood-mosquito life cycles of *P. vivax*, *P. falciparum* and *P. malariae* (Grassi, 1900). In 1948, Henry Shortt and Cyril Garnham completed the *Plasmodium* life cycle by showing that a phase of division in the liver preceded parasite development in the blood (Shortt and Garnham, 1948). The final mystery, the long period between infection and appearance and reappearance of parasites in the blood, was established by Wojciech Krotoski in 1982 who demonstrated the presence of dormant stages in the liver (Krotoski et al., 1982).

1.1.2. Malaria epidemiology

Approximately 200 species of *Plasmodium* parasites have been identified to date and have been shown to infect reptiles, rodents, birds and mammals (Perkins and Austin, 2009). Human beings are the natural hosts for five *Plasmodium* species:

- *P. falciparum:* the most virulent species and cause of the most severe form of malaria. Pre-dominantly found in sub-Saharan Africa, it causes 90% of malaria deaths.
- *P. vivax*: the second most widespread species, notably in South America and Asia, and the most frequent cause of recurring malaria. It infects an estimated 70 - 80 million people annually but is generally non fatal (Mu et al., 2005).
- *P. malariae:* distributed across the globe but rarely causes fatality.
- *P. ovale:* restricted to West Africa and some Pacific regions (Philippines and Indonesia). Due to low prevalence rates and its relatively mild and chronic nature it is, alongside *P. malariae*, considered one of the minor parasites of the five human malaria species.
- *P. knowlesi*: the cause of primate malaria, however recent findings have established it to be responsible for human malaria cases in South East Asia (Singh et al., 2004).

Malaria is one of the most important infectious diseases and a major public health problem. According to the World Malaria Report 2010, malaria is endemic in tropical and subtropical areas of over 106 countries **(Fig. 1.1)** (WHO, 2010). Almost one half of the world's population lives under constant threat of malaria and an estimated 225 million cases led to 781,000 deaths in 2009. The impact of the disease on gross domestic product is important and can reach 1.3% in countries with high malaria rates (Sachs and Malaney, 2002).

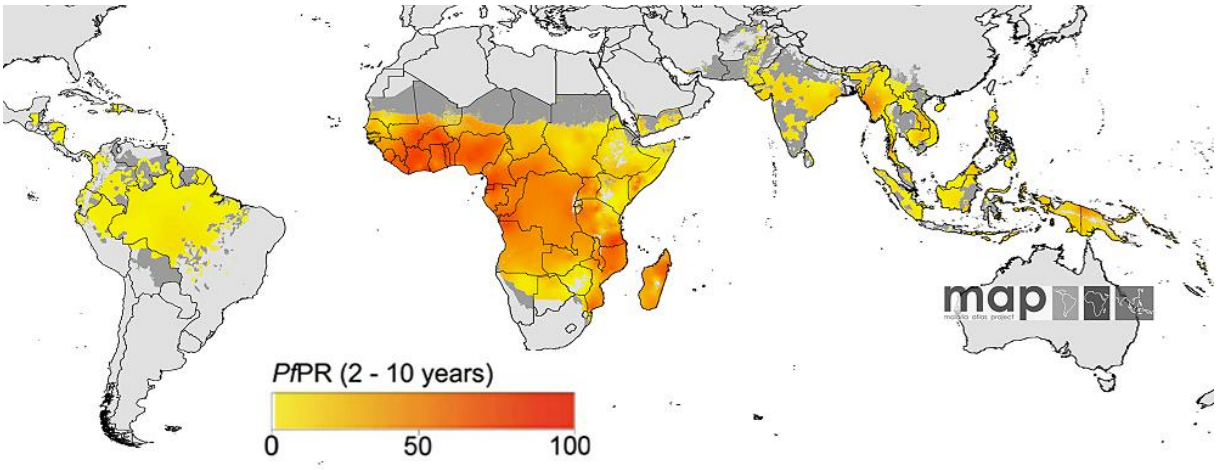

Figure 1.1. The spatial distribution of *Plasmodium falciparum* malaria endemicity for 2007 (Hay et al., 2009). The malariometric indice used is the *P. falciparum* parasite rate $Pf\text{PR}_{2\text{-}10}$ (the percentage of a 2 to 10 years age population with parasites detectable in their blood) displayed as a continuum of yellow to red from 0%–100% (see map legend). The rest of the land area was defined as unstable risk (medium grey areas) or no risk (light grey).

About 90% of malaria deaths occur in sub-Saharan Africa and the majority of them are children under 5 years whilst pregnant women are the main adult risk group. A child dies of malaria every 30 seconds in Africa (WHO, 2010).

1.1.3. The malaria parasite

1.1.3.1. A protozoan parasite

The malaria parasite is a unicellular protozoan of genus *Plasmodium,* member of the Apicomplexa phylum **(Fig. 1.2)**. By definition, the malaria parasite is a protozoan that has adapted to invade and live in cells and tissues of other organisms. Protozoan parasites are scattered in three different kingdoms according to the Simpsons and Roger classification of eukaryotes (Simpson and Roger, 2004). As for malaria, other genera of parasitic protozoans are agents of human and veterinary diseases such as leishmaniasis (caused by *Leishmania* genus), Chagas disease (caused by *Trypanosoma cruzi*), sleeping sickness (caused by *Trypanosoma brucei*), amebiasis (caused by *Entamoeba histolytica)*, trichomoniasis (caused by *Trichomonas vaginalis)*, giardiasis, toxoplasmosis (caused by *Toxoplasma gondii*), cryptosporidiosis (caused by *Cryptosporidium* genus), theileriosis (caused by *Theileria genus)*, or babesiosis (caused by *Babesia* genus)(de Souza, 2008).

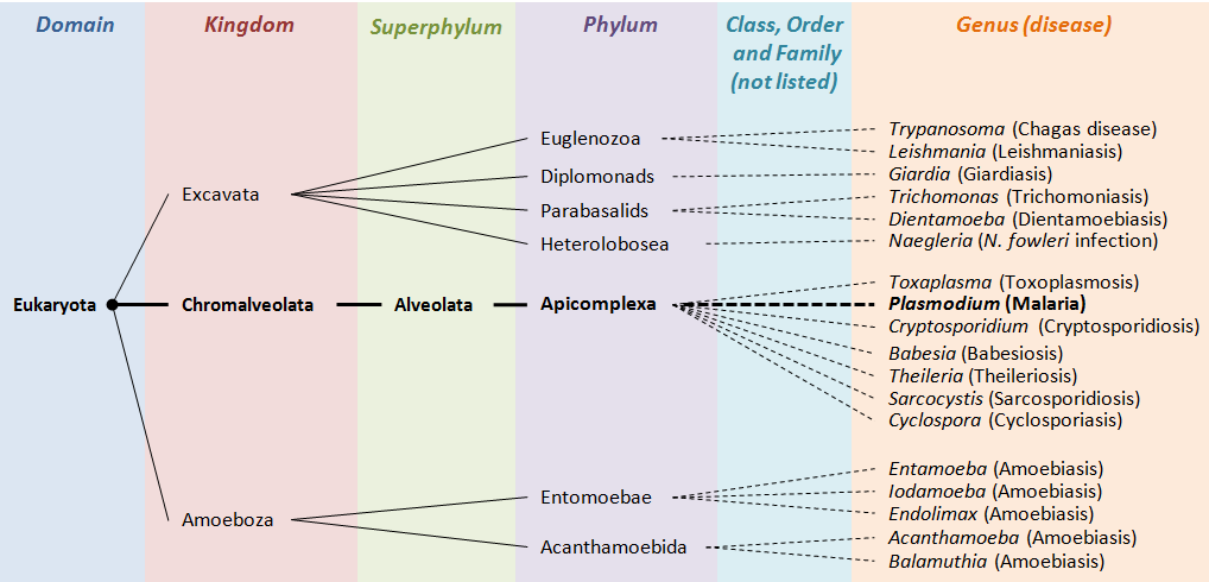

Figure 1.2. Classification of infectious parasitic protozoans based on Simpsons and Roger's eukaryote tree (Simpson and Roger, 2004).

1.1.3.2. Life cycle of human malaria parasites

Among the protozoan parasites, *Plasmodium* species have one of the most complex and multistage life cycle. As illustrated in **Figure 1.3**, human malaria parasites are heteroxenous parasites alternating between two hosts: a vertebrate (human) and invertebrate (female mosquito of genus *Anopheles*). The asexual life cycle of the malaria parasite begins during the blood meal of an infected female mosquito when sporozoites from her salivary glands are introduced into the human. These

sporozoites are carried to the parenchymal cells of the liver via the circulatory system. After invasion into the hepatocytes, parasites start an asexual replication process called exoerythrocytic schizogony where they divide to form tens of thousands of merozoites (Cowman and Crabb, 2006). The completion of this pre-erythrocytic stage varies between *Plasmodium* species **(Table 1.1)**. In the case of *P. vivax* and *P. ovale*, dormant stage parasites called hypnozoites can persist in the liver and cause relapses by invading the bloodstream months or years later (Krotoski et al., 1982). After release into the circulatory system, merozoites (1-2 µm in diameter) rapidly adhere to and invade erythrocytes (Barnwell and Galinski, 1998).

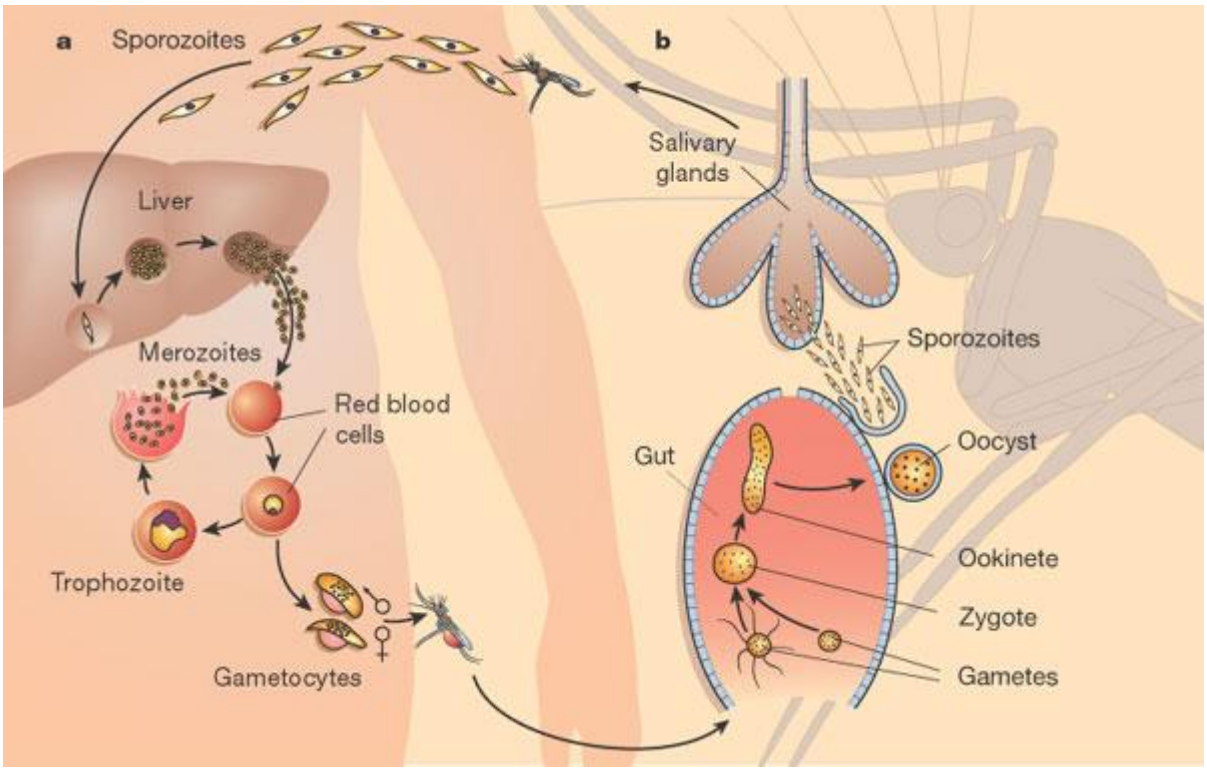

Figure 1.3. Life cycle of the parasite *Plasmodium falciparum* in the human host and female *Anopheles* mosquito (Wirth, 2002). (a) The asexual life cycle in the human host. **(b)** The sexual life cycle in the *Anopheles* mosquito. (Permission licence # 3144911355100).

Once inside the red blood cell, the parasite undergoes a 48 hours (or 72 hours for *P. malariae*) asexual multiplication cycle called erythrocytic schizogony. This blood-phase of the life cycle consists of the merozoite developing into a ring stage over the first twelve hours post-invasion. Then, it develops into a trophozoite and remains at this stage for 14 hours. Finally, the matured trophozoite is marked by multiple rounds of nuclear division resulting in the formation of merozoites into a schizont. When the red blood cell burst, each mature schizont releases about 8-32 merozoites which are ready to invade new erythrocytes (Gregson and Plowe, 2005).

Table 1.1. Characteristics of 4 species of human malaria (Looareesuwan et al., 1990). The *pre-erythrocytic stage* is the period between the time of infection and merozoite release. The *pre-patent period* is the interval between the date of infection until the first appearance of the trophozoites in erythrocytes. The *incubation period* refers to the first appearance of clinical symptoms of the disease. The *relapse* is a renewed clinical manifestation of the infection started by hypnozoites.

	P. falciparum	*P. vivax*	*P. ovale*	*P. malariae*
Pre-erythrocytic stage (days)	5.5	8	9	14-15
Presence of hypnotizes	-	+	+	-
Pre-patent period (days)	8-25	8-27	9-27	15-30
Incubation period (days)	12 (9-14)	15 (12-17)	17 (16-18)	28 (18-40)
Erythrocytic cycle (hours)	48	48	48	72
Enlargement of host erythrocyte	-	++	+	-
Primary attack	Severe in non-immune	Mild to severe	Mild	Mild
Relapse	-	++	++	-
Period of recurrence	Short	Variable	Variable	Very long
Duration of untreated infection (years)	1-2	2-5	2-5	3-50

Instead of invasion, a small proportion of merozoites will go on to develop into sexual forms, which are microgametocyte (male) and macrogametocyte (female). Gametocytes go through five morphological stages to reach full maturity within approximately 12 to 14 days (Fivelman et al., 2007; Hawking et al., 1971). If a mosquito bites an infected individual, gametocytes are taken into its midgut where they can continue their differentiation to form macrogametes and microgametes. Once matured, a single male and female gamete fusion leads to fertilization forming a diploid zygote. It will continuously divide to develop a motile ookinete which traverses the gut wall of the mosquito where it matures into an oocyst containing 4 meiotic products which replicate asexually into haploid sporozoites. They remain inside the maturing oocyst for 4-15 days before release to the mosquito's salivary glands to be passed on to another individual thus perpetuating the malaria life cycle (Sinden and Billingsley, 2001).

1.1.3.3. Ultrastructure of the asexual parasite

The work presented in this thesis is based on the asexual stage of the malaria parasite, and in particular trophozoites. The invading parasite contains several intracellular organelles, most of which are found in eukaryotic cells, for example a nucleus, a rudimentary Golgi, an endoplasmic reticulum and a single mitochondrion **(Fig. 1.4)** (Hanssen et al., 2010). Additionally, the malaria parasite possesses others organelles including a vestigial plastid (apicoplast) and a modified lysosome (digestive vacuole). In the erythrocyte, the parasite is surrounded by the parasitophorous vacuolar membrane (PVM), which serves as an interface between the parasite and host cell cytoplasm (Lingelbach and Joiner, 1998). To survive and uptake nutrients, the trophozoite ingests host cell cytoplasm across its plasma membrane via endocytic structures named cytostomes (Aikawa et al.,

1966). Malaria parasites use haemoglobin as a source of amino acids but its degradation by proteases liberates toxic heme. The free heme is polymerized into hemozoin and stored within the digestive vacuole (Dorn et al., 1995; Rosenthal and Meshnick, 1996). The apicoplast is a non-photosynthetic plastid homologous to the chloroplasts of plants with a circular genome. Its functions are still being explored but it plays an important role in the biosynthesis of fatty acid, isopentenyl diphosphate or heme in the cooperation with the mitochondrion (McFadden, 2011).

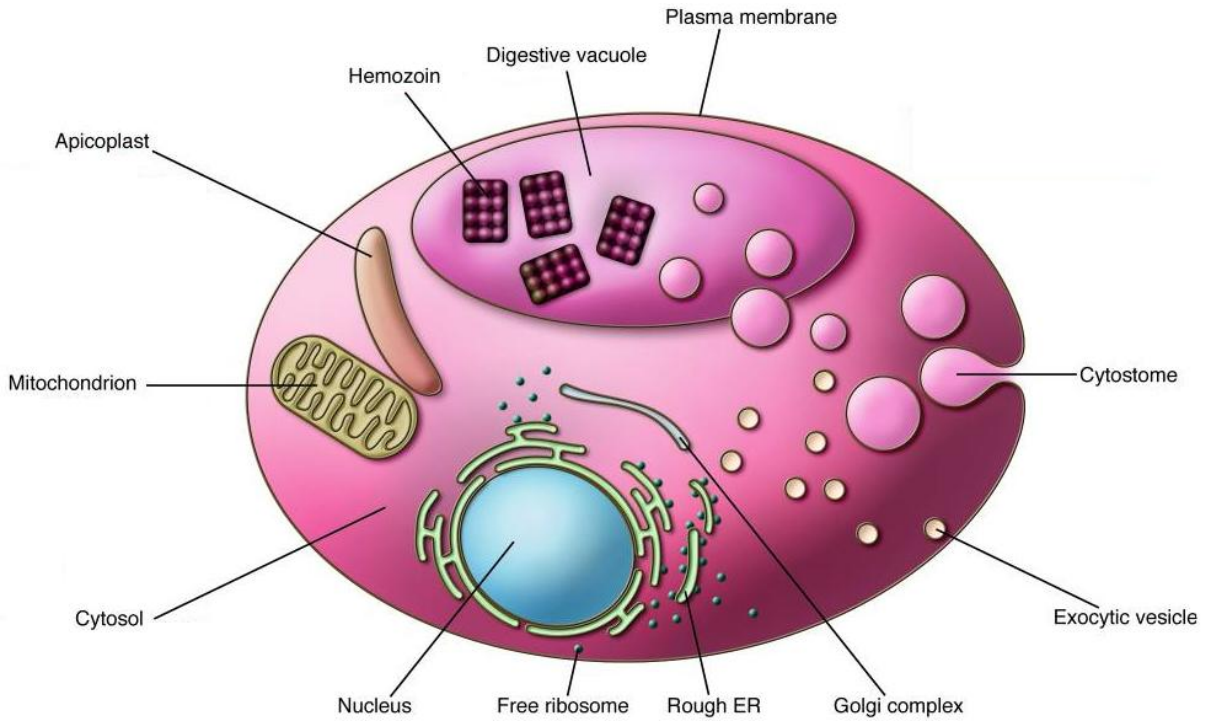

Figure 1.4. Diagram of an intraerythrocytic parasite, highlighting major organelles and cellular structures (adapted from Greenwood et al., 2008). (Permission licence # 3144921093501).

Depending on the asexual stage, the shape and size of each organelle may vary and stage-specific features may appear (Bannister et al., 2000). For example, during the invasion of host cells merozoites have specific apical organelles composed of rhoptries, dense granules, micronemes and monomenes (Bannister and Mitchell, 2009).

1.1.4. Malaria prevention

1.1.4.1. Pathogenesis and clinical features of malaria

Clinical manifestations of *Plasmodium* spp. infection are caused by the asexual stages of the parasite that develop inside red blood cells. Drastic morphological, biochemical and rheological changes of the infected erythrocyte are central to the pathology of severe malaria (Maier et al., 2009). These modifications cause cytoadherence, rosette formation and knob protrusions (Miller et al., 2002). The iRBC's (infected red blood cells) ability to adhere to the lining of small blood vessels

leads the obstruction of tissue perfusion. Additionally, the release of malaria antigens, pigment and toxins contribute to a cascade of pathological events (Mendis and Carter, 1995; Miller et al., 1994a).

Most of the morbidity and mortality attributable to malaria are caused by *P. falciparum*. Mild or uncomplicated malaria are associated with fever and nonspecific symptoms such as headache, chills and sweats, vomiting or diarrhoea (Laishram et al., 2012). The clinical pattern of severe malaria is different between non-immune adults and semi-immune African children. Death in non-immunes is often associated with high fever, multi-organ damage including renal failure, pulmonary oedema, and disseminated intravascular coagulation whereas death in children is usually due either to malarial anaemia, cerebral malaria or respiratory distress (Greenwood et al., 2008; Miller et al., 1994a).

Genetic factors, age of the patient and intensity of transmission affect susceptibility to severe anaemia or cerebral malaria (Kwiatkowski, 2005; Reyburn et al., 2005). Cerebral malaria is the most common form of severe malaria due to the cytoadherence of iRBCs to the endothelium of cerebral capillaries and venules, causing their sequestration and tight packing in these vessels (Wilairatana and Krudsood, 2009). Severe anaemia is due to direct destruction and phagocytosis of infected RBCs and unparasitized RBCs by immune responses (Ekvall, 2003). Additionally, other infectious diseases such as HIV, *Salmonella* spp or helminth infections can interact with malaria and modify the susceptibility and/or severity (Graham et al., 2000; Hartgers and Yazdanbakhsh, 2006; Korenromp et al., 2005).

1.1.4.2. Vector control

The objective of vector control is to reduce transmission of malaria by preventing human-vector contact, eliminating breeding sites, killing the mosquito larvae or reducing the longevity of adult mosquitoes. The different strategies applied are insecticides, larval and environment control.

Insecticides have been the most common form of mosquito control. From 1955 and 1969, the use of effective and inexpensive dichlorodiphenyltrichloroethane (DDT) sprayed on the inside walls of houses resulted in successful campaigns against the malaria vector and eliminated the disease in North America, Europe and parts of Asia, and tamped it down in other regions (Gravitz, 2012). The appearance of Anopheline resistance to DDT was responsible for the declining political and financial support for the Global Malaria Eradication Campaign launched by the World Health Organization (Sadasivaiah et al., 2007; van den Berg, 2009). A mix of diverse insecticides used for indoor spraying and treating bed nets (termed insecticide treated bed nets - ITNs) have been tried and showed a reduction in overall child mortality or severe pregnancy associated anaemia (Gosoniu

et al., 2008; Lengeler, 2000; ter Kuile et al., 2003). However, mosquitoes evolved resistance to effective pesticides such as pyrethroids and there is now a requirement for new insecticides (Takken and Knols, 2009). Additionally, new alternatives associated with, or replacing, insecticide-based vector control must be developed.

The larval control of *Anopheles* mosquitoes is another preventive method. Chemical and biological agents can be used to kill larvae in breeding sites. Larvivorous fishes or bacterial pathogens such as *Bacillus thuringiensis israelensis* are examples of biological solutions that attack the larval stages of the mosquito (Walker and Lynch, 2007). The elimination of breeding sites by drainage or by applying locally grown plants are environmental methods to prevent malaria.

1.1.4.3. Malaria vaccines

Vaccine development is a long process that takes years of clinical testing and trials until licensing and public availability are reached. *P. falciparum* is the main target of the vaccine trials of the different initiatives and programs. To develop malaria vaccines, different stages of the parasite development have been targeted such as pre-erythrocyte asexual or sexual stages.

Pre-erythrocyte vaccines provide humoral immunity by extracting antibodies that target sporozoites to prevent their invasion into the liver. The most developed pre-erythrocyte vaccine RTS,S/AS02A is based from the circumsporozoite protein (CSP), a cell surface protein located on sporozoites and infected hepatocytes (Girard et al., 2007). This vaccine showed promising protection levels in phase IIb trials with high immunogenicity for anti-CSP and anti-HBsAg antibodies for children younger than 24 months (Aide et al., 2011; Alonso et al., 2004; Bejon et al., 2008). Initial results of phase III trials presented reduction of malaria by half in children from 5 to 17 months of age during the 12 months after vaccination and the vaccine may have an important effect on malaria in young African children (Agnandji et al., 2011). Other vaccines based on the CSP antigen such as plasmid DNA vaccines and live recombinant vaccines that use the attenuated modified vaccinia Ankara (MVA) strain or the fowlpox virus (FPV) have undergone clinical trials but didn't show evidence of protective efficacy against invading sporozoites (Walther et al., 2006). For example, results of several phase I studies testing DNA/MVA vaccines have been disappointing even though they are safe and have strong immunogenicity (Moorthy et al., 2004a; Moorthy et al., 2004b).

Asexual blood stage vaccines are developed to primarily protect against severe malaria by eliminating or reducing the number of erythrocytic stage parasites. Development of blood-stage vaccines have been mainly focused on antigens taking part in erythrocyte invasion (Greenwood et al., 2008). The SPf66 developed in Colombia was the first asexual blood stage vaccine tested in phase III

(Patarroyo et al., 1992). However, the efficacy of this synthetic and multi-epitope vaccine candidate has been reported to be low in several clinical studies (Alonso et al., 1994; Alonso et al., 1996; Beck et al., 1997). To date, the most advanced vaccines in this class are based on antigens from merozoite surface proteins 1 (MSP-1), 2 (MSP-2) and 3 (MSP-3), the glutamate-rich protein (GLURP) and the apical membrane antigen 1 (AMA-1) (Girard et al., 2007). All were, or are, undergoing phase I trials in different countries (Genton et al., 2002; Hermsen et al., 2007; Malkin et al., 2005a; Stoute et al., 2007). Additional antigens from merozoite surface antigens such as MSP-4, -5, -8, -9, serine repeat antigen (SERA) or the erythrocyte protein 1 (PfEMP1) are under development as vaccine candidates (Girard et al., 2007).

Sexual vaccines, also termed transmission-blocking vaccines, are designed to produce antibodies against the sexual stages to prevent sporozoite development in *Anopheles* mosquitoes (Carter et al., 2000). Transmission-blocking vaccine candidates based on ookinete surface antigens S25 and S28 from *P. falciparum* or *P. vivax* are currently being developed and undergoing phase I trials (Arakawa et al., 2005; Hisaeda et al., 2000). For example, clinical trials of a vaccine based on *Pv*S25 reported safety and modest immunogenicity (Malkin et al., 2005b). Another sexual stage antigen *Pf*S230 are studying for being a possible sexual vaccine candidate (Bustamante et al., 2000).

1.1.4.4. Malaria chemotherapy

In the absence of effective malaria vaccine, chemotherapy remains the mainstay of malaria control by clearing the parasites from mammalian (human). Antimalarials can be classified according to their chemical structures and biological activities into five main groups **(Table 1.2)**. They can disrupt processes or metabolic pathways within different subcellular organelles of the malaria parasite.

To date, malaria parasites have developed partial resistance to nearly every antimalarial drug due to overuse, environmental factors, spontaneous genetic mutations in the parasites, etc. (Ekland and Fidock, 2008; Wongsrichanalai et al., 2002). To reduce the risk of resistance and increase treatment efficacy, the use of combination antimalarial drug therapy using two or three compounds with different modes of action and molecular targets has been recommended as the best option (Kremsner and Krishna, 2004).

Table 1.2. Antimalarial drug classes, their target locations, parasite stages and their possible combinations. For the target location, 'C' indicates the cytosol, 'M': the mitochondrion, 'DV': the digestive vacuole and 'A': the apicoplast. For the parasite stage, 'AS' indicates the asexual stage, 'LS': the liver stage, GS: the gametocytes or sexual stage; 'HS': hypnozoites stage, 'SS': sporozoites stage.

Drug	Target location				Parasite stage					Combination	References
	C	M	DV	A	AS	LS	GS	HS	SS		
Quinoline related compounds											
Quinine			●		●		●			+ Sulfadoxine-pyrimethamine (SP); + Tetracycline; + Clindamycin; + Doxycycline	Sullivan, 2012 O'Neill et al., 2012 Waters and Edstein, 2012 (Nosten et al., 2012)
Chloroquine			●		●		●			+ Sulfadoxine-pyrimethamine (SP)	
Amodiaquine			●		●		●			+ Sulfadoxine-pyrimethamine (SP)	
Piperaquine			●		●					+ Dihydroartemisinin	
Primaquine			●			●	●	●			
Tafenoquine			●			●	●				
Mefloquine			●		●		●			+ Sulfadoxine-pyrimethamine (Fansimef®)	
Halofantrine			●		●						
Lumefantrine			●		●					+ Artemether (Coartem®, Riamet®)	
Antifolates											
Pyrimethamine	●				●	●			●	+ Sulfadoxine (SP)	Nzila, 2012 Friesen et al., 2011
Sulfadoxine	●				●					+ Pyrimethamine (SP)	
Proguanil	●				●	●			●	+ Atovaquone (Malarone®)	
Chlorproguanil	●				●					+ Dapsone + Artesunate (Dacart®); + Dapsone (LapDap®)	
Dapsone	●				●					+ Artesunate + Chloroproguanil (Dacart®); + Chloroproguanil (LapDap®)	
Hydroxynapthaquinones											
Atovaquone		●			●				●	+ Proguanil (Malarone®)	Vaidya, 2012
Antibiotics											
Doxycycline				●	●					+ Quinine	Krishna and Staines, 2012
Clindamycin				●	●					+ Quinine	
Endoperoxide compounds											
Artemisinin	●	●?	●		●		●?				Karunajeewa, 2012
Artemether	●	●?	●		●		●?			+ Lumefantrine (Coartem®, Riamet®)	
Artesunate	●	●?	●		●		●?			+ Dapsone + Chloroproguanil (Dacart®); + amadioquine (ASAQ); + Mefloquine (ASMQ); + Sulfadoxine-pyrimethamine (SP)	
Dihydroartemisinin	●	●?	●		●		●?			+ Piperaquine	

1.1.4.4.1. Quinoline related compounds

The quinoline-containing drugs include some of the most common antimalarials:

- Cinchona alkaloids such as quinine, quinidine, cinchonidine and cinchonine.
- 4-aminoquinolines such as chloroquine, amodiaquine, piperaquine and pyronaridine.
- 8-aminoquinolines such as primaquine and tafenoquine.
- Quinoline methanol derivatives such as mefloquine, halofantrine and lumefantrine.

Quinine, an extract from *Cinchona bark*, is one of the oldest antimalarial drugs, having been used by the native population of Peru for centuries to treat fevers and chills (Ridley, 2002). In the 19th century, active components of the cinchoma alkaloids were isolated including quinine, cinchonidin and cinchonine. With remarkable antimalarial properties, quinine is often the first therapeutic choice for the treatment of severe malaria (Pasvol, 2005). The elucidation of quinine structure and then the identification of quinoline ring as key pharmacophore led to the development of synthetic 4-aminoquinolines **(Fig. 1.5. A)**. Chloroquine became for several decades the first choice of malaria treatment and prophylaxis because it was highly effective, safe and inexpensive (Hyde, 2007a). 8-aminoquinolines were synthesized to eradicate malaria hypnozoites from the liver and have been used for malaria prophylaxis (Tschan et al., 2012). In order to respond to an increase in drug resistance, a new generation of quinoline related antimalarials emerged with such as mefloquine (a quinoline methanol), lumefantrine and halofantrine (Schlitzer, 2007).

The widely accepted mechanism of action for this class of compounds is the inhibition of haemozin formation in the parasite digestive vacuole (DV) (Muller and Hyde, 2010) **(Fig. 1.5. B)**. The malaria parasite survival and development is dependent on host cell haemoglobin degradation as a source of amino acids (reviewed in Francis et al., 1997). Up to 80% of haemoglobin in the host cell is degraded by the parasite during its 48 h asexual cycle. However, haemoglobin digestion in the DV releases a large amount of toxic free heme also called ferriprotoporphyrin IX (FPPIX). Toxic heme monomers are suggested to generate oxidative radicals provoking parasite membrane permeabilization and leading to parasite death (Zhang et al., 1999). The FPPIX is biocrystallized to form inert crystals of hemozoin (the malaria pigment), which is not toxic to the malaria parasite (Pagola et al., 2000). 4-aminoquinolines act by binding to heme molecules in the DV and interfere with their process of detoxification (Fitch, 2004).

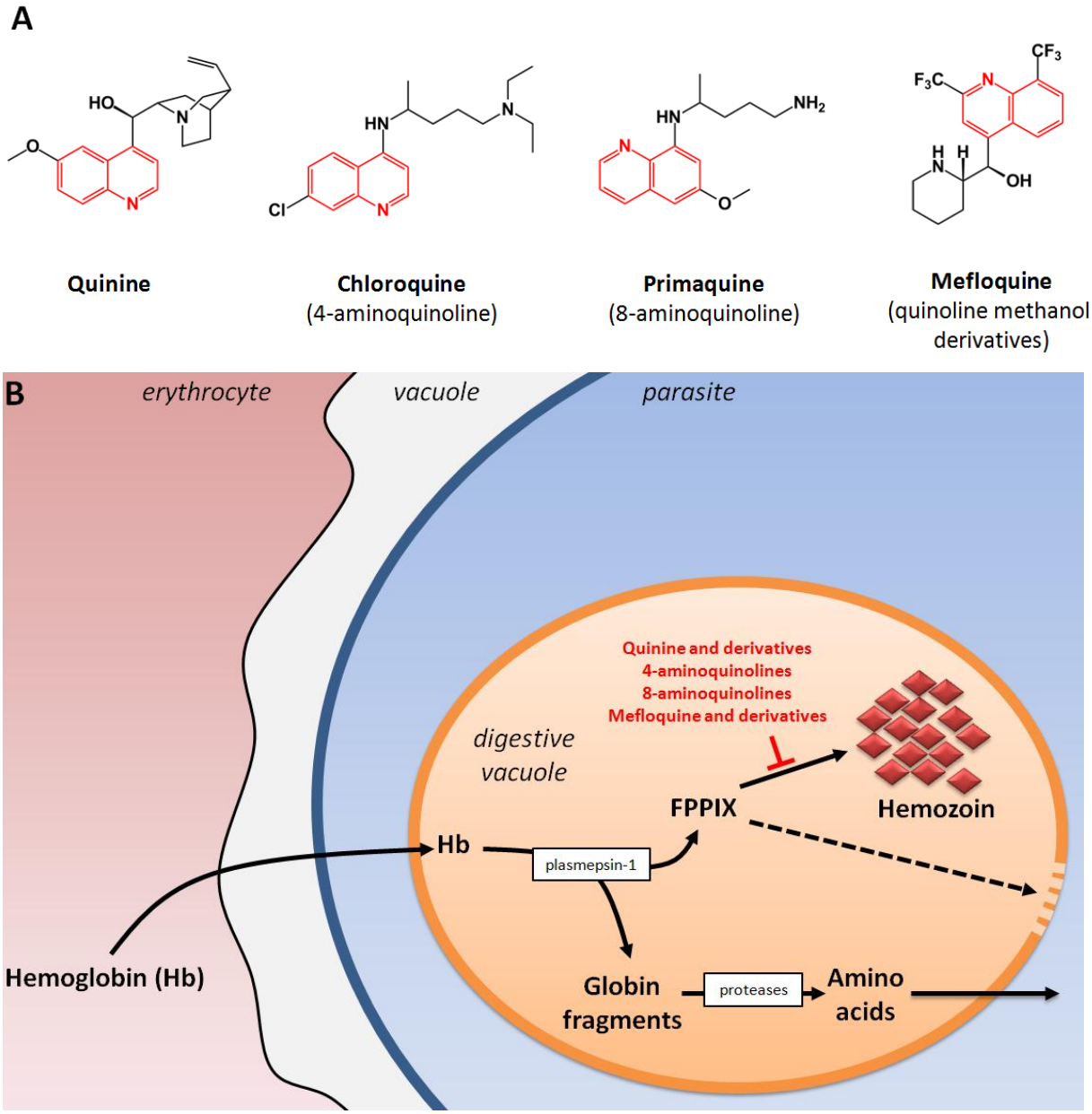

Figure 1.5. Chemical structures of quinoline containing drugs and their mode of action. (A) Chemical structures of quinine, chloroquine, primaquine and mefloquine. The quinoline ring is highlighted in red. **(B)** Schematic diagram for the mechanism of action of quinoline derivatives.

Resistance to quinolines emerged approximately 10 years after its introduction, along the Thai-Cambodian border in 1957, the Colombia-Venezuela border in 1970s and all sub-Saharan Africa in 1980s (Mita et al., 2009). Several studies have demonstrated resistance due to point mutations in *P. falciparum* chloroquine resistance transporter (*Pf*CRT) and *P. falciparum* multidrug resistance transporter 1 (PfMDR1), both located in the membrane of the food vacuole. Other mutations occurring in two plasma membrane transporters, the *P. falciparum* multidrug resistance-associated protein (*Pf*MRP) and *P. falciparum* Na^+/H^+ exchanger 1 (*Pf*NHE1) were also found to be related to quinoline antimalarial drug resistance. The involvement of *Pf*CRT polymorphisms, in particular the K76T mutation, has been established for chloroquine and 4-aminoquinoline resistances (Fidock et al.,

2000; Lakshmanan et al., 2005; Martin et al., 2009). This chloroquine resistance could allow the active efflux of diprotonated chloroquine out of the digestive vacuole (Martin and Kirk, 2004). *Pf*MDR1 has been linked to the altered susceptibility of parasites to mefloquine, halofantrine and quinine but their association remains unclear and other genetic factors may be involved such as *Pf*CRT. *Pf*MDR1 is a homolog of the multidrug resistance (MDR) transporter family, which is associated with drug resistance in mammalian tumor cells (Foote et al., 1989; Wilson et al., 1989). Mutations in MDR-like proteins in mammalian cancer cells lead to an increased drug efflux and decreased intracellular drug accumulation (Peel, 2001). Although *Pf*MDR1 is not essential in asexual stages, mutations lead to increased parasite susceptibility to chloroquine, quinine, piperaquine and primaquine (Mu et al., 2003; Raj et al., 2009). The function of *Pf*NHE1 located in the plasma membrane remains unclear but it is speculated to actively efflux protons to maintain a pH around 7.4 within the parasite (Bosia et al., 1993). The association of *Pf*NHE1 mutations with quinine resistance has been proposed but remains controversial (Andriantsoanirina et al., 2010; Briolant et al., 2011; Henry et al., 2009; Okombo et al., 2010).

1.1.4.4.2. Antifolate drugs

Antifolate antimalarial drugs are classified into two classes:

- Class I or inhibitors of the dihydropteroate synthase (DHPS) such as sulfadoxine and dapsone
- Class II or inhibitors of dihydrofolate reductase (DHFR) such as proguanil and pyrimethamine

Antifolates are widely used in fixed-ratio combinations, most commonly sulfadoxine-pyrimethamine (SP, Fansidar™), in first-line treatment for uncomplicated *P. falciparum* infection in chloroquine-resistant regions of Africa (Winstanley and Ward, 2006). Antifolate combinations are also used as intermittent preventive malaria therapies in pregnant women and infants in malaria endemic areas or in countries without supplies of Artemisinin Combination Therapy (ACT) (Gutman et al., 2012).

Growth of malaria parasites requires folate derivatives (folic acid or folinic acid) which are important cellular cofactors for the production of deoxythymidylate (dTMP) and thus DNA synthesis **(Fig. 1.6)**. The folate synthesis is essential for the malaria parasite survival which relies on *de novo* dTMP synthesis because of its incapacity to salvage pyrimidine from the exogenous medium (Hyde, 2007b). Both DHFR and DHPS catalyze two steps in the folate pathway. DHFR is present in both parasite and human host and is an essential enzyme for synthesis of the reduced form of folate (tetrahydrofolate, THF) while DHPS is only found in malaria parasites with a function of *de novo* synthesis of folate coenzymes.

Unfortunately, antifolate resistance emerged rapidly after extensive administration of sulphadoxine/pyrimethamine (SP) combinations due to point mutations in both targeted enzymes (Mita et al., 2009; Uhlemann and Krishna, 2005). The "quintuple mutant" consisting of three DHFR point mutations (S108N, N51I and C51R) and two DHPS substitutions (A437G and K540E) has been strongly associated with treatment failure (Kublin et al., 2002). *Pf*MRP1 is also proposed to affect intracellular folate homeostasis in parasites. Its point mutation K1446R has been proposed to increase exogenous folate efflux, decrease the competition with the incoming drugs for their targets and contribute to antifolate resistance (Dahlstrom et al., 2009).

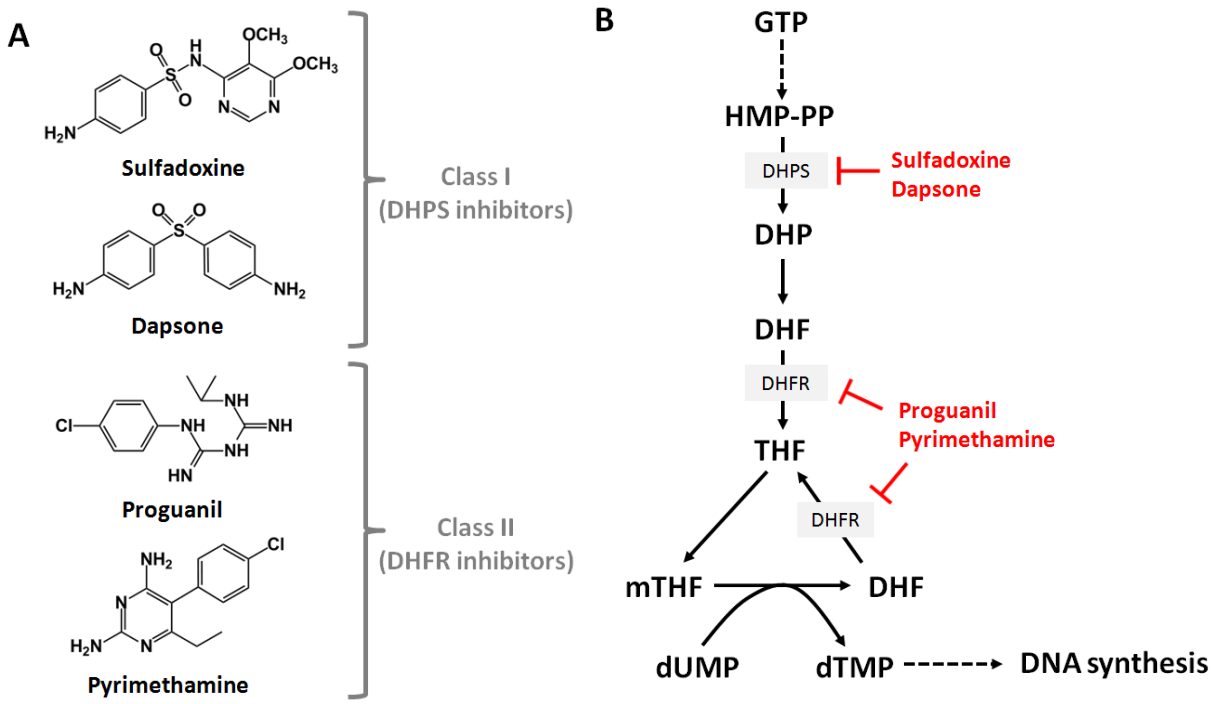

Figure 1.6. Chemical structures of antifolate drugs and their mode of action. (A) Chemical structures of sulfadoxine, dapsone, proguanil and pyrimethamine. **(B)** Folate biochemical pathway in *P. falciparum* and mechanisms of action for antifolate antimalarial drugs. Abbreviations: DHF, dihydrofolate; DHP, dihydropteroate; THF, tetrahydrofolate; DHFR, dihydrofolate reductase; DHPS, dihydropteroate synthase; GTP, guanosine triphosphate; mTHF, methylene-THF-Glu(n); dUMP, deoxy-urinidine monophosphate; HMP-PP, hydroxymethyl-pteridine-PP; dTMP, thymidine monophosphate.

1.1.4.4.3. Hydroxynapthoquinones (atovaquone)

Hydroxynapthoquinone compounds have been known as competitive inhibitors of the coenzyme ubiquinone (CoQ) and have been investigated as antimalarials since 1940s (Wendel, 1946). However, the enthusiasm for these compounds as potential antimalarial drugs has been inhibited due to their toxicity, poor bioavailability and lack of metabolic stability (Hudson et al., 1991). Atovaquone, a novel hydroxynaphthoquinone (2-[*trans*-4-(4'-chlorophenyl)cyclohexyl]-3-hydroxy-1.4-napthoquinone), was therefore developed and showed excellent antiparasite activity **(Fig. 1.7. A)**

(Hudson et al., 1991; Hudson et al., 1985). Additionally, atovaquone was found to be well tolerated and metabolically stable (Srivastava and Vaidya, 1999). However, it presented 30 % treatment failure against *P. falciparum* malaria in clinical trials and exhibited rapid emergence of resistant parasites (Chiodini et al., 1995; Looareesuwan et al., 1996). To minimise resistance and clinical failures, atovaquone is combined with the antifolate proguanil which displayed synergistic effects *in vitro* and in clinical trials (Canfield et al., 1995; Looareesuwan et al., 1996; Radloff et al., 1996). The combination of atovaquone-proguanil when given in a fixed dose tablet drug combination (Malarone™) produces a near 100% curative rate but due to its costly production this drug is used mainly as chemoprophylaxis for travellers visiting malaria endemic areas (Kessl et al., 2007; Looareesuwan et al., 1999).

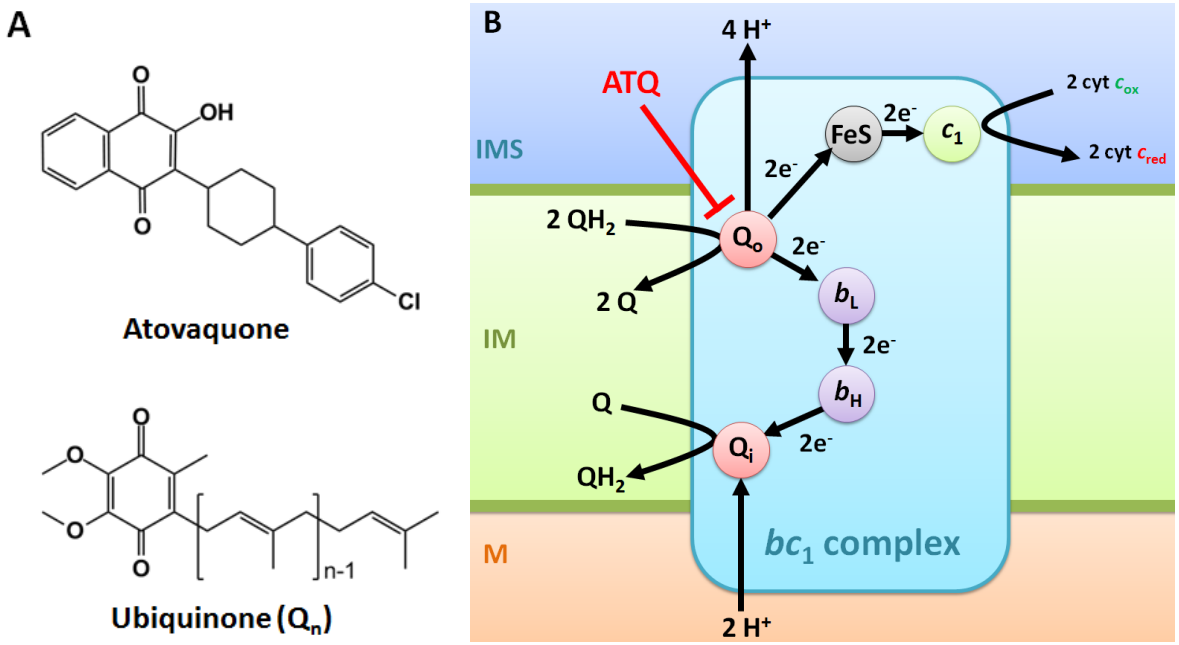

Figure 1.7. Chemical structure of atovaquone and its mode of action. (A) Chemical structure of atovaquone and its analogue, the coenzyme ubiquinone. **(B)** Schematic diagram of bc_1 complex reactions and its inhibition with atovaquone (ATQ). Abbreviations: Q, ubiquinone; QH_2, ubiquinol; b_L, heme b_L binding site; b_H, heme b_H binding site; Fe-S, iron-sulfur cluster; cyt *c*, cytochrome *c*; c_1, cytochrome *c* binding site.

Atovaquone is an inhibitor of the ubiquinol oxidation site (Q_o) of the *P. falciparum* bc_1 complex **(Fig. 1.7. B)**. The mechanism of action and emergence of resistances are comprehensively described in Chapter 6. To summarize, atovaquone inhibits the catalytic turnover of bc_1 complex, collapsing the mitochondrial membrane potential and resulting in the loss of essential mitochondrial function such as pyrimidine biosynthesis (Painter et al., 2007). In combination with atovaquone, proguanil has been suggested to inhibit the mitochondrial phosphate transporter and thereby synergises with the inhibition of bc_1 complex activity but this hypothesis remains to be supported by biological proofs (Painter et al., 2007). Different point mutations at the Q_o site associated with

Malarone™ failure have been reported (Berry et al., 2006; Korsinczky et al., 2000; Musset et al., 2006). Y268S, and less frequently Y268N, are the most common mutations observed, increasing the atovaquone IC_{50} by several hundred fold compared to sensitive parasite strains (Barton et al., 2010).

1.1.4.4.4. Artemisinin and endoperoxide derivatives

Artemisinin is a sesquiterpene lactone extracted from the chinese plant *Artemisia annua* which kills asexual stage parasites but also affects sexual stage gametocytes of *Plasmodium falciparum* (Chen et al., 1994; ter Kuile et al., 1993). A first generation of semi-synthetic derivatives (known as dihydroartemisinin, artesunate and artemether) were synthesized with higher antimalarial activity and better solubility in order to replace original artemisinin as treatment of malaria (O'Neill and Posner, 2004). Initially used as monotherapies, dihydroartemisinin (DHA), artesunate or artemether are employed in combination with a longer half-life drugs such as mefloquine (in combination with artesunate - ASMQ) or lumefantrine (in combination with artemether - Coartem®) for treatment of uncomplicated malaria (White, 2008). These artemisinin-based combination therapies (ACTs) are also widely used to treat drug-resistant malaria strains with a high efficiency, rapid clearance and minimal toxicity in humans (Nosten and White, 2007; White, 2008). The discovery of the activation mode of artemisinins opened the way for the development of novel endoperoxide bridge-based drugs displaying superior activities than artemisinins against malaria parasites and leading to the identification of a promising 1,2,4,5-tetraoxane drug candidate (RKA-182) (O'Neill et al., 2010a).

Several insights into artemisinin resistance have been reported recently. A reduced efficacy of artemisinin derivatives as monotherapy was observed recently along the Thai-Cambodian border (Dondorp et al., 2009). Several mutations in *Pf*ATPase6 (sarco/endoplasmic reticulum Ca^{2+} -ATPase) have been associated with decreased artemether susceptibility in field isolates from French Guyana and PfMDR1 amplification can significantly reduce parasite susceptibility to artemisinins (Chavchich et al., 2010; Jambou et al., 2005; Sidhu et al., 2006). Because the mode of action of artemisinin derivatives remains unclear, resistant mechanisms are also not well understood and further studies have to be performed to support genetic and biochemical evidence (Eastman and Fidock, 2009). The structure of artemisinin and its derivatives, their modes of activation and action are described in the Chapter 5.

1.2. The mitochondrion of the malaria parasite

The mitochondrion of *Plasmodium* species has unusual structural and functional features that distinguish it from mammalian mitochondria. Because it is essential for parasite survival, the mitochondrion has been successfully targeted with malaria chemotherapies and contains promising targets for the development of new antimalarial drugs. However, our knowledge regarding this organelle is limited with functions such as the tricarboxylic acid cycle or the election transport chain remaining unclear. This introduction aims to present an overview of the recent data on the structure, genome and functions of the mitochondrion.

1.2.1. Morphology of the mitochondrion in asexual and sexual stages

In the 1960s, electron microscopy studies identified a single mitochondrion with a double membrane located in the cytoplasm of *Plasmodium* parasites (Aikawa, 1966; Rudzinska, 1969). The evolution of microscopic techniques permitted a better observation of the morphology, the size and the number of mitochondria which vary between asexual and sexual stages.

As shown in **Figure 1.8**, in the ring and early trophozoite stages of the asexual parasites the mitochondrion is a single organelle. Before the transition between mature trophozoite and shizont, it evolves to a wider, branched and elongated structure (van Dooren et al., 2005). During shizogony, the mitochondrion becomes highly branched before the start of cytokinesis. When cytokinesis starts the branched mitochondrion is divided by fission into multiple organelles and the divided mitochondria move into newly formed merozoites. Mitochondrion of gametocytes undergoes morphological development throughout gametocytogenesis (Okamoto et al., 2009). In stages II and III the mitochondrion is elongated and branched, then it becomes clustered towards the center of the cell (stages IV) and finally forms a denser cluster with short, round branches when the gametocytes mature to stage V. The mitochondrion retains closely association with the apicoplast throughout the whole gametocyte developmental process (Okamoto et al., 2009). During the sexual stage, gametocyte mitochondria also develop the tubular mitochondrial cristae that are largely absent in the asexual stages but are required for full mitochondrial function (Krungkrai et al., 2000).

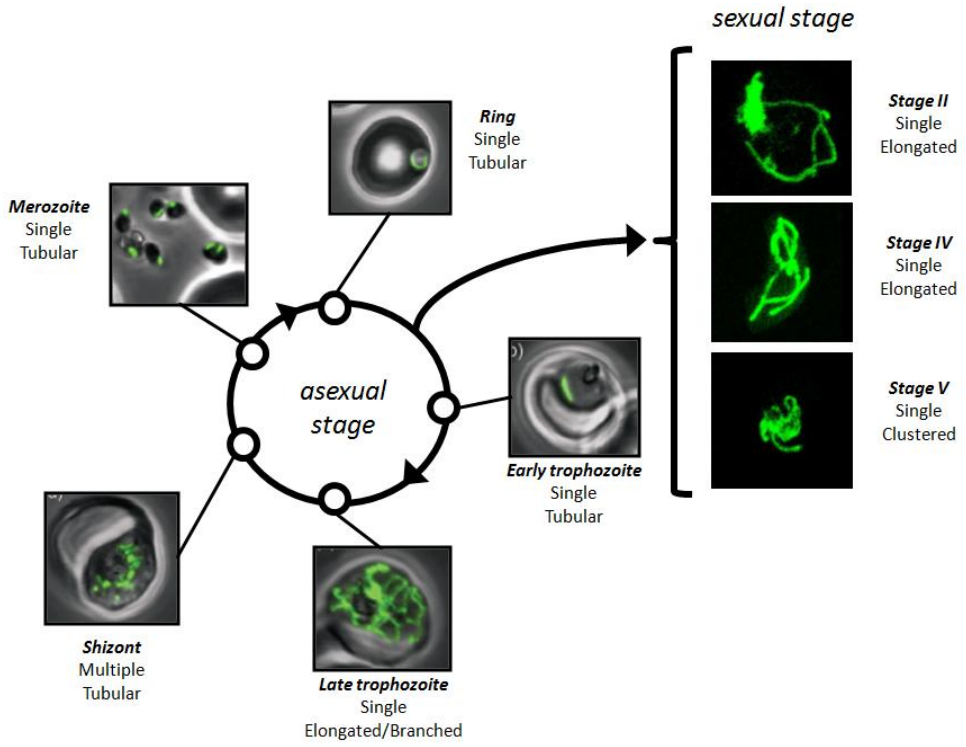

Figure 1.8. Mitochondrial morphology during asexual and sexual stages of *Plasmodium falciparum* (adapted from van Dooren et al., 2006 and Okamoto et al., 2009). (Permission licence # 3144930064779).

1.2.2. The mitochondrial genome

Malaria parasites have a 6 kb linear mitochondrial DNA (mtDNA) which is the smallest one known among eukaryotes. The mitochondrial genome is highly conserved between *Plasmodium* spp. with more than 90% of sequence similarities between human *Plasmodium* species **(Table 1.3)** (Hikosaka et al., 2011). The mtDNA is present as multiple copies with about 30 in *P. falciparum* to about 150 in *P. yoelli* and these sequences are tandemly arranged in head-to-tail configurations (Vaidya and Arasu, 1987). The mitochondrial genetic material is exclusively transmitted by the female gamete of malaria parasites during mating with male gametocyte in the mosquito gut (Vaidya et al., 1993).

Table 1.3. Sequence identity of intergenic regions in the mitochondrial DNA of the five human *Plasmodium* species (Hikosaka et al., 2011).

	P. falciparum	*P. vivax*	*P. malariae*	*P. ovale*	*P. knowlesi*
P. falciparum					
P. vivax	91.7%				
P. malariae	91.2%	96.2%			
P. ovale	92.2%	96.0%	96.8%		
P. knowlesi	90.6%	96.8%	94.5%	94.3%	

As shown in **Figure 2.2**, it contains three Open Reading Frames (ORFs) encoding for three subunits of the mitochondrial electron transport chain (ETC): the subunits I and III (Cox1 and Cox3) of the cytochrome c oxidase (or Complex IV) and the cytochrome b (Cytb) subunit of the ubiquinol:cytochrome c reductase (or Complex III) (Aldritt et al., 1989; Feagin, 1992; Vaidya et al., 1989). Other subunits of complexes comprising the mtETC, which are encoded usually by the mtDNA in other organisms like the subunit II of the cytochrome c oxidase (Cox2), are encoded in the nuclear DNA. Because the conventional NADH dehydrogenase (or Complex I) is absent in *Plasmodium* species, and is replaced by a type II NADH dehydrogenase, some of its subunits are not encoded in the parasite mtDNA like in eukaryotes (Feagin and Drew, 1995).

The mtDNA also encodes fragmented ribosomal RNAs which are able to associate to reconstitute functional ribosomal subunits (Feagin et al., 1997). They are scattered across the entire genome on both strands of the DNA **(Fig. 1.9)**. Specific identities to large and small subunits of rRNA have been previously identified on a basis of 23 small transcripts. Based on sequence and structural conservation, thirteen have similarities to regions in the large subunit rRNA (lsrRNA) and seven have been identified with specific regions in the small subunit rRNA (ssrRNA) (Feagin, 2000; Feagin et al., 1997). The transcript mtR-26 has been recently suggested to be a fragment of the LSU rRNA gene (Raabe et al., 2010). Functions of the unassigned rRNA fragments could not be identified because of their poor sequence conservation. In malaria parasites, functional ribosomes have an unusual assembly composed of the small and large subunits rRNA structures formed by mitochondrial rRNA fragments and with imported ribosomal proteins (Feagin et al., 1992).

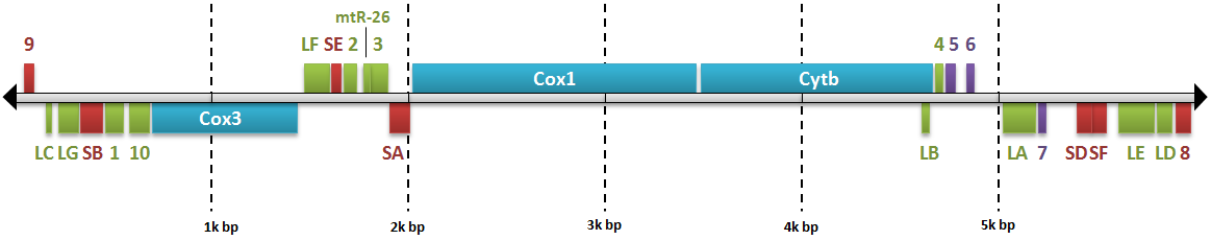

Figure 1.9. Genomic view of the linear *Plasmodium falciparum* mitochondrial DNA (adapted from Feagin, 2000; Hikosaka et al., 2011; Raabe et al., 2010). Genes above the line are transcribed from left to right and those below from right to left. The three genes encoding for Cox1, Cox3 and Cytb are indicated in blue. Fragments of ribosomal RNA genes are shown in coloured boxes: those with similarity to the large subunit rRNA (lsrRNA) in green, those with similarity to the small subunit rRNA (ssrRNA) in red and those which are currently not assigned in purple. (Permission licence # 3144930784297).

Unlike higher eukaryotes, transfer RNA (tRNA) are not encoded in the mtDNA but probably in the nuclear DNA or apicoplast (Esseiva et al., 2004). Necessary for the protein synthesis, the entire set of tRNA is imported into the mitochondrion from the cytoplasm like the majority of mitochondrial proteins (Mi-Ichi et al., 2003).

1.2.3. Mitochondrial imported proteins

All proteins required for mitochondrial functions, with the exceptions of COX I, COX II and Cytb, are encoded by the nuclear chromosomes and imported into the mitochondrion. After synthesis in the cytoplasm, mitochondrial proteins are imported into the mitochondrion via different pathways. In Chapter 7, the current state of art and new insights with regards to import and processing pathways of mitochondrial proteins, in apicomplexans including *P. falciparum,* is reviewed.

With PlasMit (gecco.org.chemie.uni-frankfurt.de/plasmit) - a neural network approach for the prediction of mitochondrial transit peptides (mTPs) from *P. falciparum* - 381 annotated genes of the *P. falciparum* genome have been predicted to have mitochondrial targeting signals **(Fig 1.10)** (Bender et al., 2003). These predicted proteins are involved in different metabolic pathways but the function of the majority remains unknown.

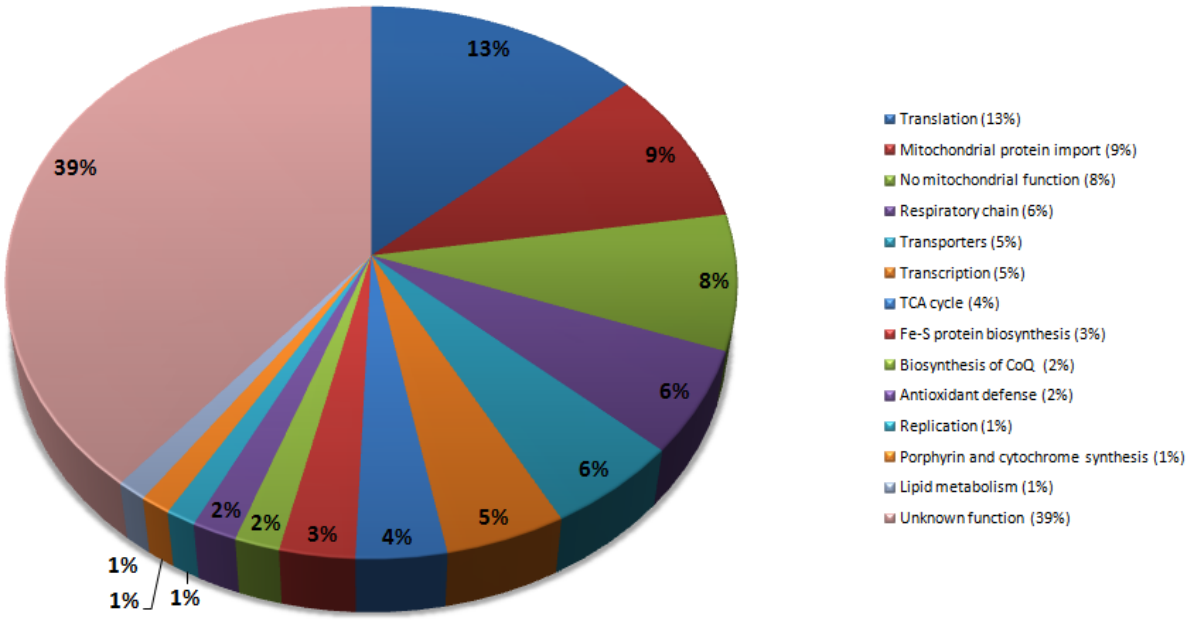

Figure 1.10. Functional distribution of 341 proteins with a mitochondrial signal peptide (Torrentino-Madamet et al., 2010). Different cellular processes implicated in the physiology of the mitochondrion have been identified through 341 putative mitochondrial proteins predicted with PlasMit (Bender et al., 2003).

1.2.4. Physiology of the mitochondrion

1.2.4.1. The TCA cycle

In higher eukaryotes, the mitochondrion is a source of cellular energy in the form of ATP. The role and contribution of the tricarboxylic acid (TCA) cycle to the bioenergetics of blood stage malaria parasites have been debated for many years (Vaidya and Mather, 2009). In higher eukaryotes, the TCA cycle occurs under aerobic conditions and is a series of chemical reactions that generate energy

by consuming acetyl-CoA. The *Plasmodium* genome encodes all the necessary enzymes for TCA cycle which are actively synthesized during the asexual stages and possess putative mitochondrial signal sequences (Bozdech et al., 2003; Gardner et al., 2002). However, the lack of a mitochondrial pyruvate dehydrogenase suggests that the TCA cycle in malaria parasite is different from pathways in other eukaryotes (Foth et al., 2005). In line with this, a bifurcated TCA pathway, one part being oxidative and the other reductive, has been suggested before to be recently retracted (Olszewski et al., 2010).

After entrance into the parasite, the molecule of glucose is metabolised into two molecules of pyruvate via the glycolysis pathway. In higher eukaryotic organisms, the molecule of pyruvate is transported into the mitochondrion where it is converted to acetyl-CoA which integrates with the TCA cycle. Deficient of pyruvate dehydrogenase into the mitochondrion, the malaria parasite cannot generate acetyl-CoA from pyruvate which is fermented into lactate yielding only two molecules of ATP for each glucose molecule consumed (Foth et al., 2005). Depending on the atmospheric culture conditions used, the glycolysis pathway is estimated to consume 60 to 70% of glucose imported in *P. falciparum* (Jensen et al., 1983). In absence of a mitochondrial pyruvate dehydrogenase, the acetyl-CoA source cannot result directly from glycolysis. The acetyl-CoA is only produced from phosphoenolpyruvate in the apicoplast in order to synthesize amino sugars in the endoplasmic reticulum (Foth et al., 2005). In future, it will be essential to clarify the source of mitochondrial acetyl-CoA in order to understand the TCA metabolism in blood-stage *P. falciparum.*

1.2.4.2. *De novo* pyrimidine synthesis

In *P. falciparum* parasites, many metabolomic pathways are absent, with essential metabolites salvaged from the host (Gardner et al., 2002; Ginger, 2006). However, the salvage pathway of pyrimidines is missing which renders its biosynthesis essential for nucleic acid synthesis (Gutteridge et al., 1979). Formation of uridine monophosphate (UMP), a pyrimidine derivative, is catalysed via a pathway including six enzymes **(Fig. 1.11)**. One of them, the dihydroorotate dehydrogenase (DHODH), is a component of the electron transport chain (ETC) localised in the inner mitochondrial membrane. DHODH, a flavin-dependent enzyme, catalyzes the oxidation of dihydroorotate to orotate and couples the *de novo* pyrimidine biosynthesis to the respiratory chain by reducing the coenzyme ubiquinone (CoQ) to ubiquinol (Krungkrai, 1995; Malmquist et al., 2008). The main role of the *P. falciparum* ETC has been proposed to regenerate CoQ required as an electron acceptor for DHODH and to maintain the mitochondrial electrochemical gradient or membrane potential ($\Delta\psi_m$) (Malmquist et al., 2008; Painter et al., 2007). Thus, inhibition of pyrimidine biosynthesis is suggested to be the consequence of atovaquone leading to parasite death via inhibition of the bc_1 complex and collapse of the $\Delta\psi_m$. Transgenic *P. falciparum* parasites expressing DHODH from yeast, which is not linked with mitochondria and utilizes fumarate rather than

ubiquinone as electron acceptor, became resistant to bc_1 inhibitors by synthesis of pyrimidine independent to the ETC (Painter et al., 2007). This result highlights the essential role of the DHODH, which became an attractive drug target for the development of novel antimalarials (Baldwin et al., 2005; Patel et al., 2008; Phillips et al., 2008). Recently, a drug discovery study developed substituted triazolopyrimidine compounds that are highly selective to DHODH, exhibiting high antimalarial activity (EC_{50}s below 20 nM against *P. falciparum* 3D7) and metabolic stability (Coteron et al., 2011; Gujjar et al., 2011).

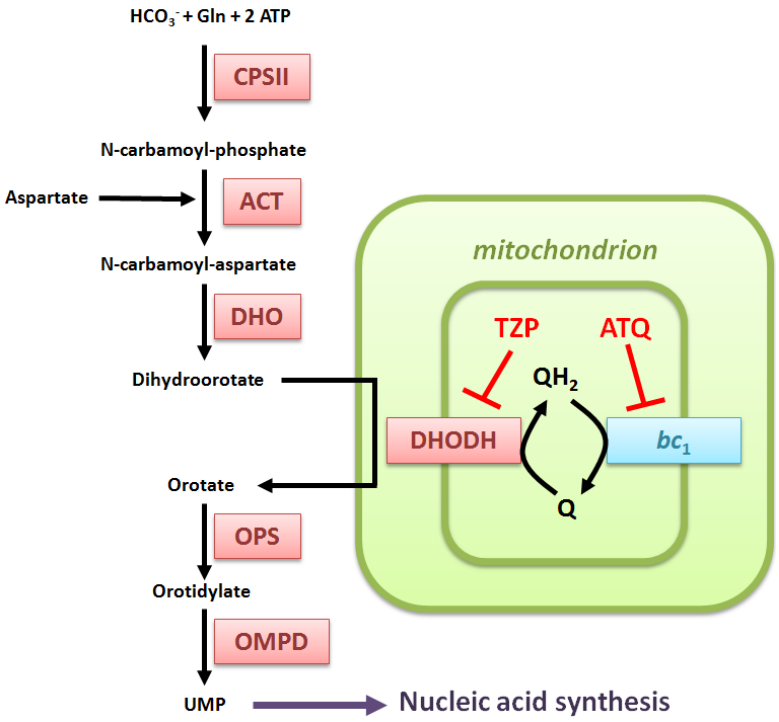

Figure 1.11. Pyrimidine biosynthesis pathway in *P. falciparum*. Enzymes involved in the *de novo* pyrimidine biosynthesis are indicated in red boxes**.** Abbreviations: CPSII, Carbomoyl phosphate synthatase II; ACT, Aspartate carbamoyl transferase; DHO, Dihydroorotase; DHODH, Dihydroorotate dehydrogenase; OPS, Orotate phosphoribosyltransferase; OMPD, Orotidine 5'-monophosphate decarboxylase; ATQ, atovaquone inhibitor; TZP, triazolopyrimidine compound.

1.2.4.3. The electron transport chain (ETC)

Plasmodium spp. have a functional respiratory chain and an oxygen-requiring system that is important for parasite growth and survival. Based on the oxygen consumption of *P. falciparum* and *P. yoelii yoelii* free parasites, the ETC was detected to be functional during the asexual and sexual stages (Krungkrai et al., 1999; Krungkrai et al., 2000; Uyemura et al., 2004). The *Plasmodium* respiratory chain is composed of five dehydrogenases namely type II NADH dehydrogenase (*Pf*NDH2 or rotenone-insensitive complex 1), succinate:quinone oxidoreductase (SDH or complex II), malate:quinone oxidoreductase (MQO), dihydroorotate dehydrogenase (DHODH) and glycerol-3-phosphate dehydrogenase (G3PDH) **(Fig. 1.12** and **Table 1.4)**. Each dehydrogenase can potentially donate electrons to the ETC via redox reactions involving the oxidation of substrates coupled to the

reduction of coenzyme ubiquinone (Q) to ubiquinol (QH_2). Downstream oxidation reactions by ubiquinol:cytochrome *c* oxidoreductase (cytochrome bc_1 or complex III), and cytochrome *c* oxidase (complex IV) are coupled to the vectorial translocation of protons (H^+), generating a transmembrane electrochemical potential ($\Delta\psi_m$). The transmembrane proton gradient is utilized by an ATP synthase (complex V) to synthesize ATP but its contribution to the whole ATP synthesis remains minimal (Balabaskaran Nina et al., 2011). In *P. falciparum*, the native ubiquinone is CoQ_8 but due to its hydrophobic nature, it cannot be used as an exogenous substrate for enzymatic assays (Biagini et al., 2006).

In most of eukaryotic species, the resulting membrane potential generated by the respiratory chain across the inner membrane is the central energy provider in the form of ATP. However, in blood stages of malaria parasites, glycolysis metabolism is favoured over the oxidative phosphorylation pathway for ATP generation (Vander Jagt et al., 1990). Although the apparent low expression levels and activities of the respiratory enzymes in the asexual stages, the respiratory chain is the primary source of mitochondrial membrane potential generation which is essential to parasite survival (Fry and Beesley, 1991; Krungkrai et al., 1993; Krungkrai et al., 1997; Painter et al., 2007). Indeed, the sensitivity of *Plasmodium* parasites to ETC inhibitors such as atovaquone, a bc_1 inhibitor, demonstrates an indispensible role (Srivastava et al., 1997).

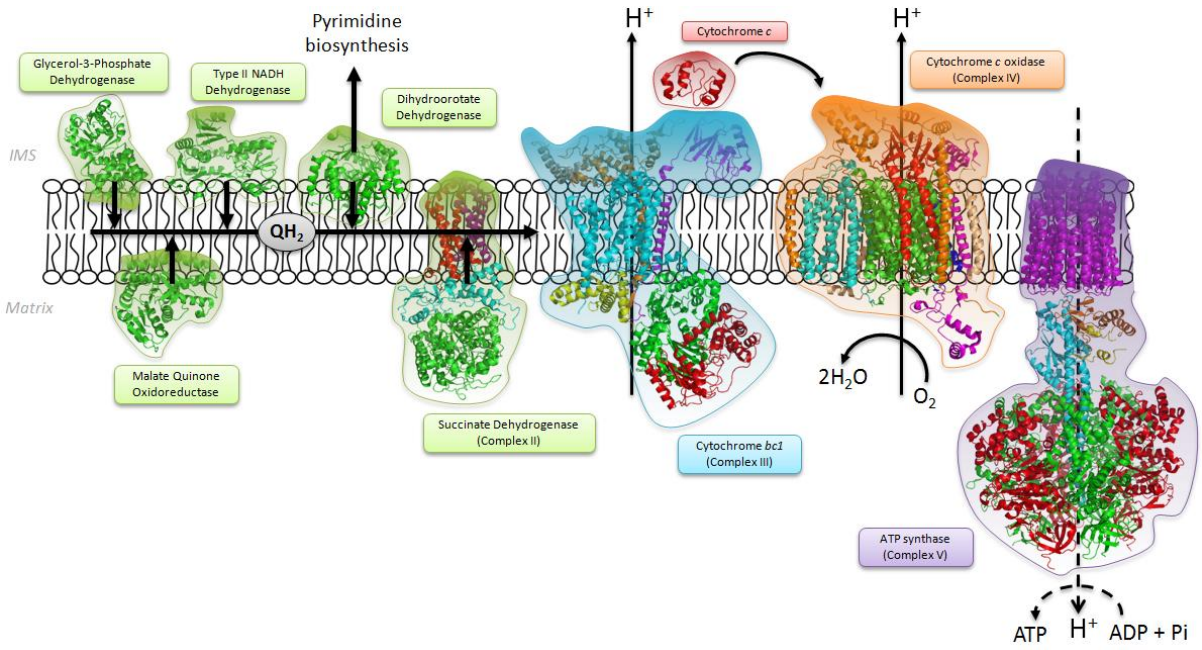

Figure 1.12. Mitochondrial electron transport chain (ETC) of malaria parasites. The enzyme complexes of the ETC are embedded in the inner membrane of the mitochondrion. Enzymes are drawn as ribbon diagrams of the crystal structures known or from orthologues available in the Protein Data Bank. Abbreviations: IMS, Intermembrane space; QH_2, ubiquinol. Proton movements are indicative only and do not represent H^+/e^- ratios for the respective complexes.

Table 1.4. Genes composing the mitochondrial electron transport chain in *P. falciparum*. Abbreviation: MW, molecular weight.

Enzyme	Subunit	PlasmoDB entry	MW (Da)	Chromosome	PlasmoDB description
Type II NADH: quinone oxidoreductase	-	PF3D7_0915000	61,671	9	Type II NADH:quinone oxidoreductase
Glycerol-3-phosphate dehydrogenase	-	PF3D7_1462800	36,636	14	Glycerol-3-phosphate dehydrogenase, putative
Malate:quinone oxidoreductase	-	PF3D7_0616800	59,508	6	Malate:quinone oxidoreductase, putative
Dihydroorotate dehydrogenase	-	PF3D7_0603300	65,559	6	Dihydroorotate dehydrogenase, mitochondrial precursor
Succinate dehydrogenase	SDHA	PF3D7_1034400	70,696	10	Flavoprotein subunit of succinate dehydrogenase
	SDHB	PF3D7_1212800	37,752	12	Iron-sulfur subunit of succinate dehydrogenase
	SDHC	Unknown	-	-	-
	SDHD	Unknown	-	-	-
bc_1 protein	Cyt b	mal_mito_3	43,377	mtDNA	Ubiquinol-cytochrome c reductase complex subunit, putative
	Rieske FeS	PF3D7_1439400	40,982	14	Ubiquinol-cytochrome c reductase iron-sulfur subunit, putative
	Cyt c1	PF3D7_1462700	46,187	14	Cytochrome c1 precursor, putative
	Hinge (QCR6)	PF3D7_1426900	10,587	14	Ubiquinol-cytochrome c reductase hinge protein, putative
	Core 1	PF3D7_0523100	61,774	5	Mitochondrial processing peptidase alpha subunit, putative
	Core 2	PF3D7_0933600	55,736	9	Organelle processing peptidase, putative
	QPK (QCR7)	PF3D7_1012300	23,020	10	Ubiquinol-cytochrome c reductase complex subunit, putative
Cytochrome *c*	-	PF3D7_1404100	12,894	14	Cytochrome c, putative
	-	PF3D7_1311700	17,965	13	Cytochrome c2 precursor, putative
Cytochrome *c* oxidase	COX I	mal_mito_2	52,973	mtDNA	Cytochrome c oxidase I, putative
	COX IIa (N-term)	PF3D7_1361700	27,262	13	Cytochrome c oxidase subunit 2, putative
	COX IIb (C-term)	PF3D7_1430900	19,786	14	Cytochrome c oxidase subunit II precursor, putative
	COX III	mal_mito_1	28,809	mtDNA	Cytochrome c oxdase III, putative
	COX Vb	PF3D7_0927800	32,364	9	Cytochrome c oxidase subunit, putative
ATP synthase	ATP1 (α)	PF3D7_0217100	61,771	2	ATP synthase F1, alpha subunit, putative
	ATP2 (β)	PF3D7_1235700	58,395	12	ATP synthase beta chain, mitochondrial precursor, putative
	ATP3 (γ)	PF3D7_1311300	35,756	13	ATP synthase gamma chain, mitochondrial precursor, putative
	ATP4 (*b*)	Unknown	-	-	-
	ATP5 (OSCP)	PF3D7_1310000	30,199	13	Mitochondrial ATP synthase delta subunit, putative
	ATP6 (*a*)	Unknown	-	-	-
	ATP9 (*c*)	PF3D7_0705900	18,559	7	ATP synthase subunit C, putative
	ATP15 (ε)	PF3D7_0715500	8,496	7	Mitochondrial ATP synthase F1, epsilon subunit, putative
	ATP16 (δ)	PF3D7_1147700	17,617	11	Mitochondrial ATP synthase delta subunit, putative

1.2.4.3.1. Type II NADH: quinone oxidoreductase (*Pf*NDH2)

Plasmodium spp. lost the conventional large multisubunit complex I found in most mammalian mitochondria. However, they acquired a single-subunit non-proton pumping NADH dehydrogenase similar to the yeast alternative complex I (or Type II NADH:quinone oxidoreductase). Also termed *Pf*NDH2, this flavoenzyme is found in a broad range of organisms including fungi, bacteria, protozoa and plants. *Pf*NDH2 catalyze the oxidation of NADH and NADPH coupled with reduction of quinone (Q) **(Equation 1)**. Type II NADH:quinone oxidoreductases from anaerobic species such as *Mycobacterium tuberculosis* use menaquione (MQ) instead of ubiquinone as electron acceptor (Weinstein et al., 2005). The type II NADH dehydrogenases can either orient to the intermembrane space or to the matrix, oxidizing cytosolic or matrix NADH respectively (Kerscher, 2000). The observation that exogenous NAD(P)H could stimulate the electron transport in *P. yoelii yoelii* suggests that *Plasmodium* NDH2 is located on the external face of the inner membrane to recycle cytosolic NAD(P)H (Uyemura et al., 2004).

$$NAD(P)H + Q \rightarrow NAD + QH_2 \quad \textbf{(Equation 1)}$$

The first crystal structure of a type-II mitochondrial NADH dehydrogenase was newly solved in yeast (Feng et al., 2012). Because such crystal structure information was unavailable until recently, structure-function relationships have been determined with modelling studies based on sequence and structure similarities of others flavoenzymes with X-ray crystallography data available such as the NADH (per)oxidases, NADH-dependent ferredoxin reductase, and lipoamide dehydrogenases (Kerscher, 2000; Mattevi et al., 1992; Schmid and Gerloff, 2004). *Pf*NDH2 structure and membrane-bound orientation have been predicted by homology modelling as well as its anchoring region and NADH-, flavin- and quinone-binding sites **(Fig. 1.13)** (Fisher et al., 2007). The quinone binding site was predicted to be formed by two short antiparallel β sheets - relatively well conserved across type II dehydrogenases - close to the surface of the membrane with sufficient distance with NAD(P)H- and flavin-binding domains for rapid electron transfer. This proximity with the membrane surface lipid bilayer facilitates quinone access to the "quinone pool" contained in the inner membrane.

Although *Pf*NDH2 is not directly involved in proton pumping, its inhibition has been demonstrated to collapse the mitochondrial membrane potential by starving the bc_1 of the reduced form of quinone (Biagini et al., 2006). Indeed, NADH-dependent respiration represents the major contributor to the *Plasmodium* respiratory chain by generating to ∼50% of the quinol flux to the bc_1 complex at maximal capacity (compared to only 1% by DHODH) (Fisher et al., 2007;

Fry and Beesley, 1991). Additionally, the *Pf*NDH2 inhibition by the flavin antagonist DPI (diphenylene iodonium chloride) or the alternative NADH dehydrogenases inhibitor HDQ (1-hydroxy-2-dodecyl-4(1H)quinolone) leads in a loss of membrane potential causing parasite death. Based on these observations and due to the emergence of atovaquone resistance, as well as the cost of Malarone™ treatment, *Pf*NDH2 has been highlighted as an attractive target for new cost-effective antimalarial drugs. Recently, Biagini *et al*. undertook a hit-to-lead study and identified a promising class of compounds inhibiting both *Pf*NDH2 and bc_1 complex (Biagini et al., 2012; Leung et al., 2012). One of the leading compounds, CK-2-68, shows antimalarial activity in the nanomolar range (IC_{50} = 31 ± 3 nM against *P. falciparum* 3D7 parasite growth) and specific *Pf*NDH2 inhibition (IC_{50} = 16 ± 2 nM). Furthermore, with nanomolar activity against the atovaquone-resistant strain TM902CB (IC_{50} = 184 ± 16 nM against *P. falciparum* TM902CB parasite growth compared to 12 ± 1.6 µM with atovaquone), CK-2-68 is a proof-of-concept inhibitor.

Recently, the type II NADH dehydrogenase has been shown to be dispensable for the sexual blood stage of *P. berghei* parasites, which rely on the glycolysis pathway as the main ATP generator (Boysen and Matuschewski, 2011). However, *Pb*NDH2-depleted rodent parasites fail to develop into mature oocysts in the mosquito midgut. Thus it is proposed that the *Pb*NDH2 gene is only essential in a glucose-deprived environment such as in the mosquito. Although non-overlapping functions of paralogous genes may appear across *Plasmodium* species, it is suspected by the authors that the NDH2 enzyme is not a promising drug target.

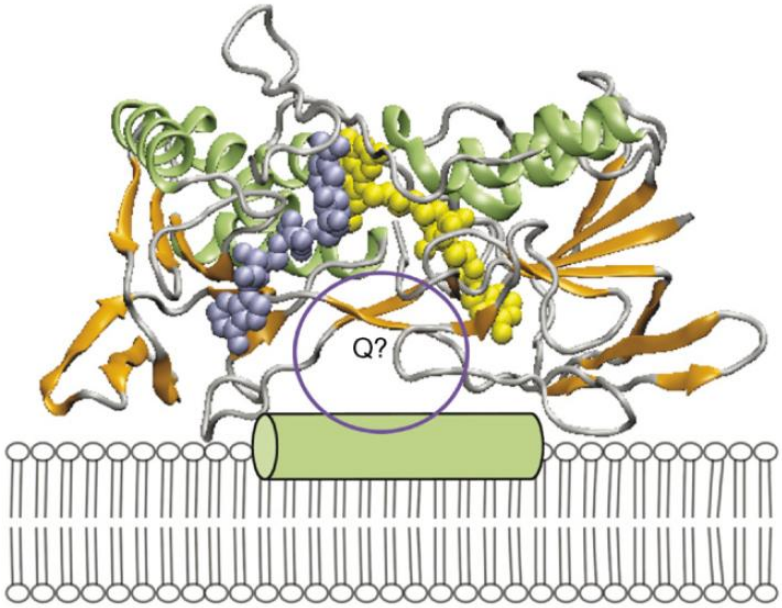

Figure 1.13. Predicted structure of *Pf*NDH2 and its membrane orientation (Fisher et al., 2007). FAD is indicated in yellow, NADH is cyan, the predicted Q-site location is circled and the predicted C-terminal amphipathic helix is represented by a green cylinder at the membrane surface.

1.2.4.3.2. Succinate: quinone oxidoreductase (complex II)

The succinate:quinone oxidoreductase (termed also succinate dehydrogenase or complex II) converts succinate to fumarate by reducing FAD in the process **(Equation 2)**.

$$\text{Succinate} + Q \rightarrow \text{Fumarate} + QH_2 \quad \textbf{(Equation 2)}$$

Succinate dehydrogenases are generally composed of four subunits: a flavoprotein (SDHA), an iron-sulfur protein (SDHB) and two membrane anchor subunits (SDHC and SDHD). In *P. falciparum,* two major catalytic subunits SDHA and SDHB composing the soluble part have been identified, cloned and characterised (Takeo et al., 2000). However, the membrane anchor *b*-type cytochrome heterodimer is highly divergent across species and remains unannotated in current databases. An attempt to solve this knowledge gap is addressed in Chapter 3.

Complex II activities have been measured in *P. falciparum* and *P. yoelii yoelii* and kinetic properties obtained are similar to mammalian succinate dehydrogenases (Fry and Beesley, 1991; Kawahara et al., 2009; Suraveratum et al., 2000).

1.2.4.3.3. Malata:quinone oxidoreductase (MQO)

The malate:quinone oxidoreductase (MQO) is a peripheral membrane-bound flavoprotein which catalyses the oxidation of malate to oxaloacetate **(Equation 3)** (Molenaar et al., 1998).

$$\text{Malate} + Q \rightarrow \text{Oxaloacetate} + QH_2 \quad \textbf{(Equation 3)}$$

MQOs can be subdivided into two major families: the MQO-1 family including mainly bacterial MQOs and the MQO-2 group containing actinobacterial MQOs (Ɛ-proteobacteria) and those from apicomplexan species (*P. falciparum*, *Toxoplasma gondii*, *Babesia bovis*) (Mogi et al., 2009). *Pf*MQO is involved in the TCA cycle by being a substitute of mitochondrial malate dehydrogenase (MDH) (Uyemura et al., 2004; van Dooren et al., 2006). The contribution of MQO in the mitochondrial ETC has been supported by measuring oxygen consumption and membrane potential $\Delta\Psi_m$ generation induced by malate in *P. yoelii yoelii* (Uyemura et al., 2000; Uyemura et al., 2004). To date, no crystal structure of *Plasmodium* MQO is available.

1.2.4.3.4. Dihydroorotate dehydrogenase (DHODH)

The *Plasmodium* DHODH is a flavin-containing enzyme that catalyzes the conversion of dihydroorotate to orotate using the flavin cofactor FMN **(Equation 4)**.

Dihydroorotate + Q → Orotate + QH_2 **(Equation 4)**

DHODH activity has been measured in parasite extracts and its gene has been identified in every parasite genome (Fry and Beesley, 1991; Gardner et al., 2002). The enzyme has been purified and characterized from the parasite mitochondria (Ittarat et al., 1994; Krungkrai, 1995; Krungkrai et al., 1992). Two types of DHODHs exist: the cytosolic DHODHs-1 use different soluble molecules as electron acceptors whereas the inner membrane DHODHs-2 (including *Plasmodium* DHODH) with the active site facing the mitochondrial intermembrane space use quinone as cofactor**.** The X-ray structure of a N-terminal truncated *Pf*DHODH has been solved bound with two inhibitors (Hurt et al., 2006).

As mentioned previously (see section: 1.2.4.2. *De novo* pyrimidine synthesis), *Plasmodium* DHODH is the fourth and only redox reaction of the essential *de novo* pyrimidine biosynthesis pathway. It also regenerates ubiquinone in the respiratory chain **(Fig. 1.14)**. Thus, *Plasmodium* DHODH became a potential target for drug discovery efforts (Baldwin et al., 2005; Coteron et al., 2011; Gujjar et al., 2011; Phillips et al., 2008; Skerlj et al., 2011). Several drug discovery programs identified promising compounds but the mechanism of inhibitions remains poorly defined. Indeed, the quinone binding site has only been predicted and not proven even on the basis of crystallographic data. However, the different inhibitors developed by different research groups share an overlapping binding site.

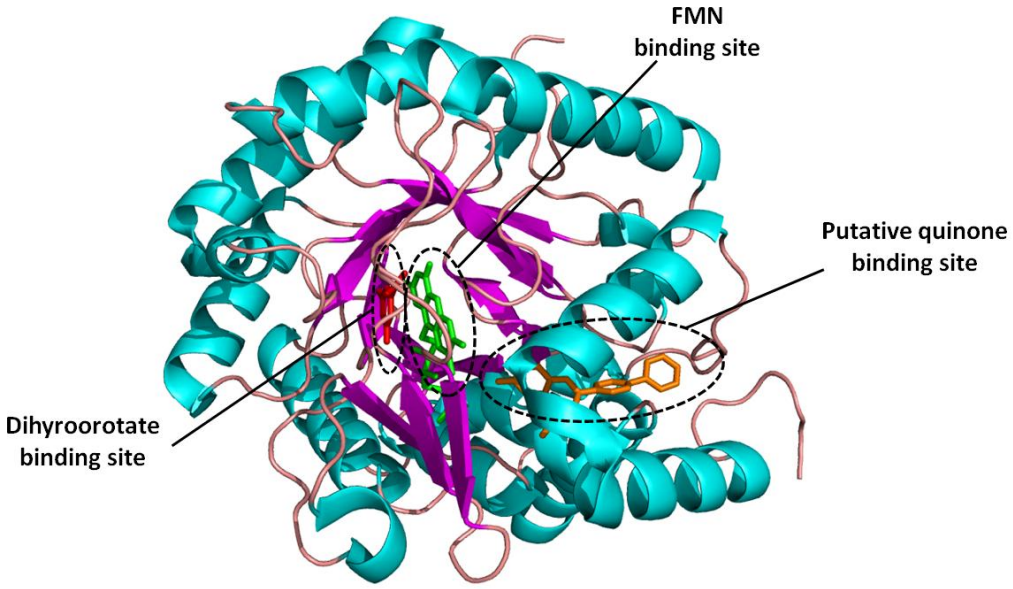

Figure 1.14. Overall structure of the N-terminal truncated *P. falciparum* dihydroorotate dehydrogenase (*Pf*DHODH). The dihydroorotate binding site is inside the barrel (purple). Dihydroorotate (red) is stacked against the internal FMN (green) (PDB entry 1TV5). The quinone binding site has been predicted via the binding site of atovaquone (orange) in aligned human DHODH structure (PDB entry 1D3G).

1.2.4.3.5. Glycerol-3-phosphate dehydrogenase (G3PDH)

The *P. falciparum* genome encodes two glycerol-3-phoshapte dehydrogenases (G3PDH), one being NAD-dependent (G3PDH-1) and the other FAD-dependent (G3PDH-2) **(Fig. 1.15)** (van Dooren et al., 2006). The NAD-dependent G3PDH (PlasmoDB entry PF3D7_1216200 in *P. falciparum*) is a cytosolic enzyme converting dihydroxyacetone phosphate (DHAP) into glycerol-3-phosphate (G3P) coupled with oxidation of NADH. G3PDH-1 is involved in the lipid biosynthesis pathway and plays an important role in the transport of reducing equivalents from the cytosol to the mitochondria (Mitamura and Palacpac, 2003). For the latter function it acts in association with the mitochondrial G3PDH-2 localized in the outer surface of the inner mitochondrial membrane. The G3P produced can integrate the lipid synthesis pathway or passes through the permeable outer mitochondrial membrane where it is re-oxidized to DHAP by the FAD-dependent G3PDH **(Equation 5)**.

Glycerol-3-phosphate + Q → Dihydroxyacetone phosphate + QH_2 **(Equation 5)**

Both enzymes perform the glycerol-3-phosphate shuttling function at the central junction of glycolysis, phospholipid biosynthesis and oxidative phosphorylation. This shuttle provides an alternative way to transport electrons from the cytosolic NADH to the mitochondrial quinone (van Dooren et al., 2006).

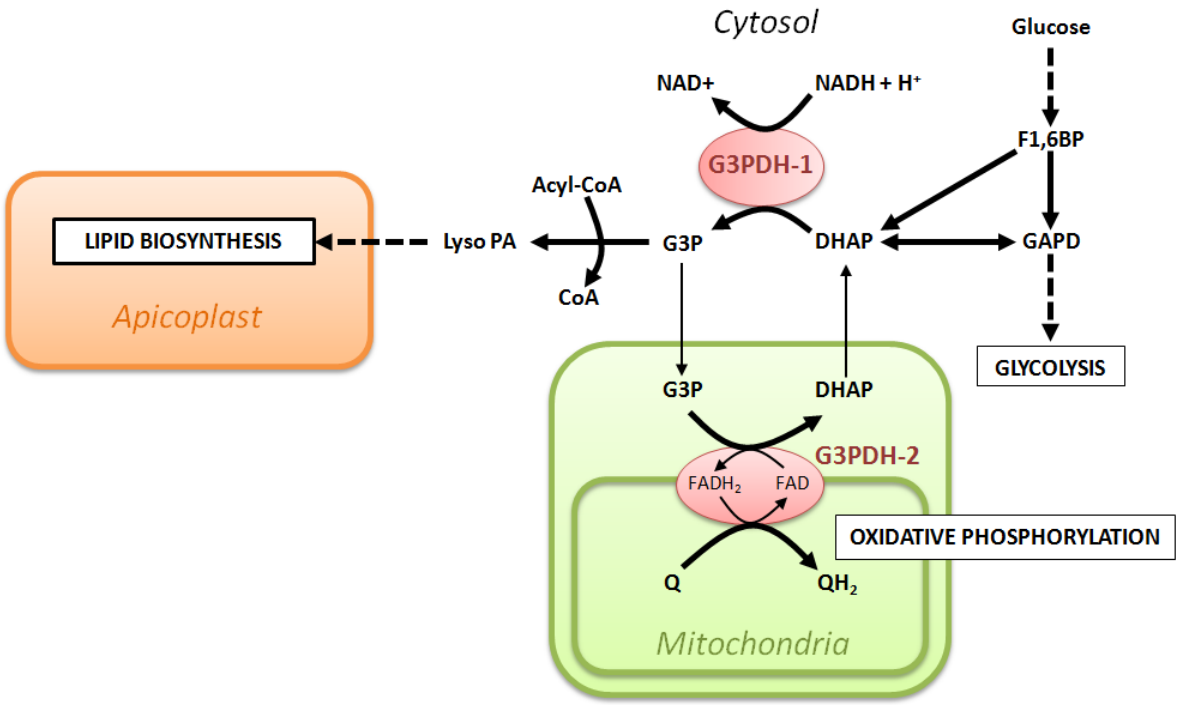

Figure 1.15. Involvement of glycerol-3-phosphate dehydrogenase-1 and -2 in three pathways. Abbreviations: G3P, Glycerol-3-phosphate; DHAP, dihydroxyacetone phosphate; LysoPA, lysophosphatidic acid; F1,6BP, fructose-1,6-bisphosphate; GADP, glyceraldehyde-3-phosphate.

1.2.4.3.6. The bc_1 complex (complex III) and Q cycle

The coenzyme ubiquinone reduced to ubiquinol by five different dehydrogenases donates electrons to the cytochrome bc_1 complex (also termed ubiquinol:cytochrome *c* oxidoreductase or complex III) **(Fig. 1.16)**. Eukaryotic bc_1 is a dimeric enzyme complex inserted into the mitochondrial inner membrane and composed of 11 non-redundant subunits (Iwata et al., 1998; Lange and Hunte, 2002; Xia et al., 1997). Crystal structures have been determined for yeast, chicken, and bovine bc_1 complexes but remain unsolved in *Plasmodium* spp (Iwata et al., 1998; Lange and Hunte, 2002; Zhang et al., 1998). So far, seven subunits have been shown to form the *Plasmodium* bc_1 complex including the cytochrome *b* encoded by the 6 kDa mitochondrial DNA **(Table 1.4)** (Petmitr and Krungkrai, 1995). The catalytic core participating directly in the electron transfer pathway is composed of three subunits: cytochrome *b*, cytochrome c_1 and the Rieske iron–sulfur protein (Zara et al., 2009). The bc_1 complex catalyses the electron transfer from ubiquinol to cytochrome *c*, coupled with the vectorial translocation of protons thus generates the transmembrane electrochemical gradient ($\Delta\Psi_m$). The catalytic mechanisms of bc_1 complex is known as the Q cycle which was first postulated by Mitchell (Mitchell, 1975).

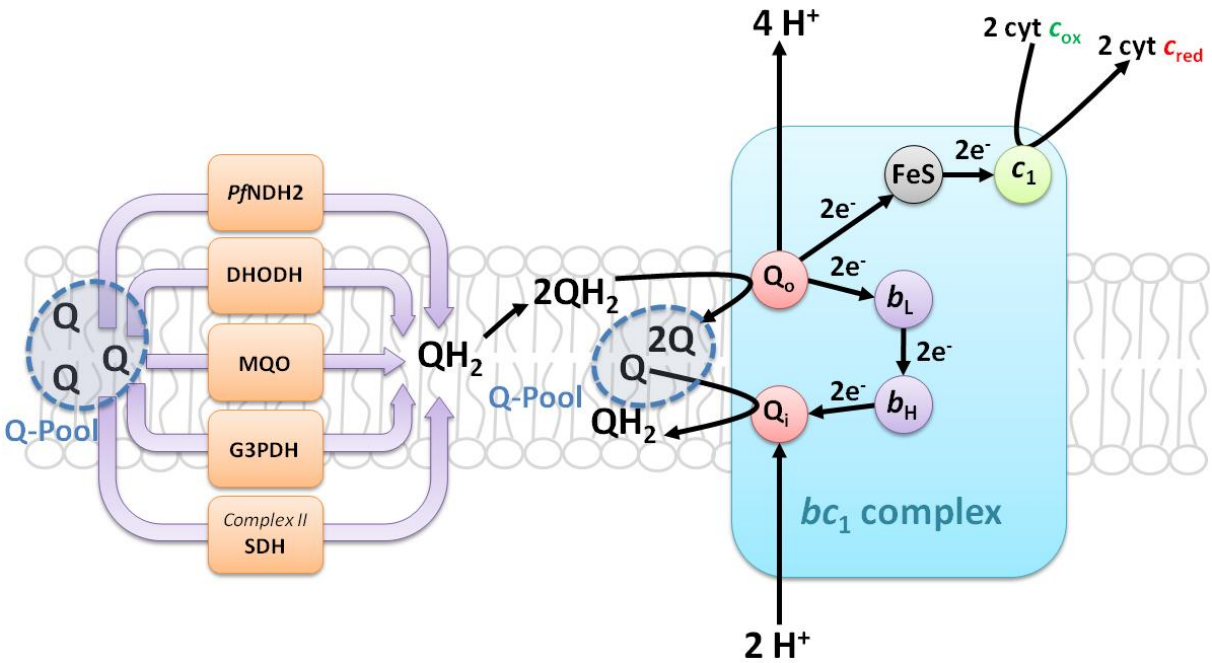

Figure 1.16. Schematic drawing of the Q cycle in the mitochondrial bc_1 complex. Abbreviations: *Pf*NDH2, type II NADH dehydrogenase; DHODH, dihydroorotate dehydrogenase; MQO, malate:quinone oxidoreductase; G3PDH, Glycerol-3-Phosphate dehydrogenase; SDH, succinate dehydrogenase; Q, ubiquinone; QH_2, ubiquinol; b_L, heme b_L binding site; b_H, heme b_H binding site; Fe-S, iron-sulfur cluster; cyt *c*, cytochrome *c*; c_1, cytochrome *c* binding site.

The mitochondrial Q cycle necessitates two different quinone-binding sites: Q_o, the quinol oxidation site and Q_i, the quinone reduction site. Q_o and Q_i binding sites are located on opposite sides of the inner membrane and are linked by a transmembrane pathway through two *b*-type

hemes, b_L and b_H (reviewed in Barton et al., 2010). The ubiquinol (QH_2) generated by dehydrogenases binds the Q_o binding sites to be oxidised to ubiquinone (Q) releasing two protons in the intermembrane space and two electrons per QH_2 molecule. One electron is transferred via the iron-sulfur cluster of the Rieske subunit to the cytochrome *c*, the electron donor to cytochrome *c* oxidase. In a bifurcated reaction, the other electron reduces the heme b_L. Afterwards, the heme b_L is oxidised by neighbouring heme b_H that recycles the electron by reducing ubiquinone to ubiquinol at the reduction site Q_i. To resume, during a complete cycle two molecules of QH_2 are oxidised to ubiquinone at Q_o site, one quinone molecule is reduced at Q_i site and four protons are translocated to the intermembrane space. During the Q cycle, electrons are transferred from ubiquinol to feed the mitochondrial respiratory chain and to regenerate ubiquinone to supply the ubiquinone pool (Q-pool) in the lipid bilayer.

The cytochrome bc_1 complex is an essential enzyme of the oxidative phosphorylation pathway in many organisms (Rich, 2003). Several quinol antagonists are complex III inhibitors known to collapse the mitochondrial membrane potential and inhibit mitochondrial respiration. For example, myxothiazole and stigmatellin binds the Q_o site while antimycin A is a potent inhibitor of the Q_i site. However, these compounds are often highly toxic to mammals and are not suitable for antimalarial use. Previously it has been demonstrated that the parasite bc_1 complex could be inhibited by atovaquone, a Q_o site inhibitor, at a 1000-fold lower concentration than the similar complex in mammalian species (Hudson et al., 1991) (see section 1.1.4.4.3. Hydroxynapthoquinones (atovaquone)). The malaria parasite sensitivity to atovaquone indicates that complex III and its contribution to membrane potential as well as Q-pool regeneration is indispensible to the parasites. Unfortunately, atovaquone resistance emerged and is correlated with a mutation in the Q_o site of the cytochrome *b*. Details of atovaquone resistance are described in Chapter 6**.**

1.2.4.3.7. Cytochrome *c* oxidase (complex IV)

The cytochrome *c* oxidase (also termed complex IV) is the terminal oxidation step in the mitochondrial respiratory chain. This enzyme receives electrons from reduced cytochrome *c* and passes them on to oxygen via two *a*-type hemes, *a* and a_3, and two copper centers, cu_a and cu_b. Four electrons are transferred per molecule of oxygen giving water as a product **(Fig. 1.17)**. For each pair of electrons passing through the complex IV, two protons are translocated across the mitochondrial inner membrane and contribute to the electrochemical gradient. Its presence in malaria parasites has been confirmed in different stages in *P. berghei* (Howells, 1970; Howells et al., 1969; Theakston et al., 1969)*, P. falciparum* (Scheibel and Pflaum, 1970) or *P. yoelii yoelii* (Fry

and Beesley, 1991). Afterwards, the enzyme has been partially purified and characterized from *P. berghei* mitochondria (Krungkrai et al., 1993). The enzyme has also been purified from *P. falciparum* mitochondrial extracts and was found to be sensitive to cyanide inhibition causing a reduction of the oxygen consumption and a depolarization of the membrane potential (Krungkrai et al., 1999; Krungkrai et al., 1997).

In mammals, complex IV is composed of 13 subunits (Richter and Ludwig, 2003; van Dooren et al., 2006). To date, five proteins have been clearly identified as components of *Plasmodium* complex IV **(Table 1.4)**. Subunits COX I, COX II and COX III form the catalytic centre of the enzyme. With the bc_1 cytochrome *b* subunit, COX I and COX III are the two other proteins encoded in the malaria parasite mtDNA. COX II is split into two nuclear-encoded subunits known as COX IIa and COX IIb while it is encoded by a single gene in most other organisms. Because COX II is a highly hydrophobic subunit, the splitting of its gene may reduce its overall hydrophobicity and facilitate its importation into the mitochondrion (van Dooren et al., 2006). *P. falciparum* also has a nuclear-encoded COX Vb subunit which may have the function to regulate the flow of electrons between the different reactions centres of the enzyme (Burke and Poyton, 1998).

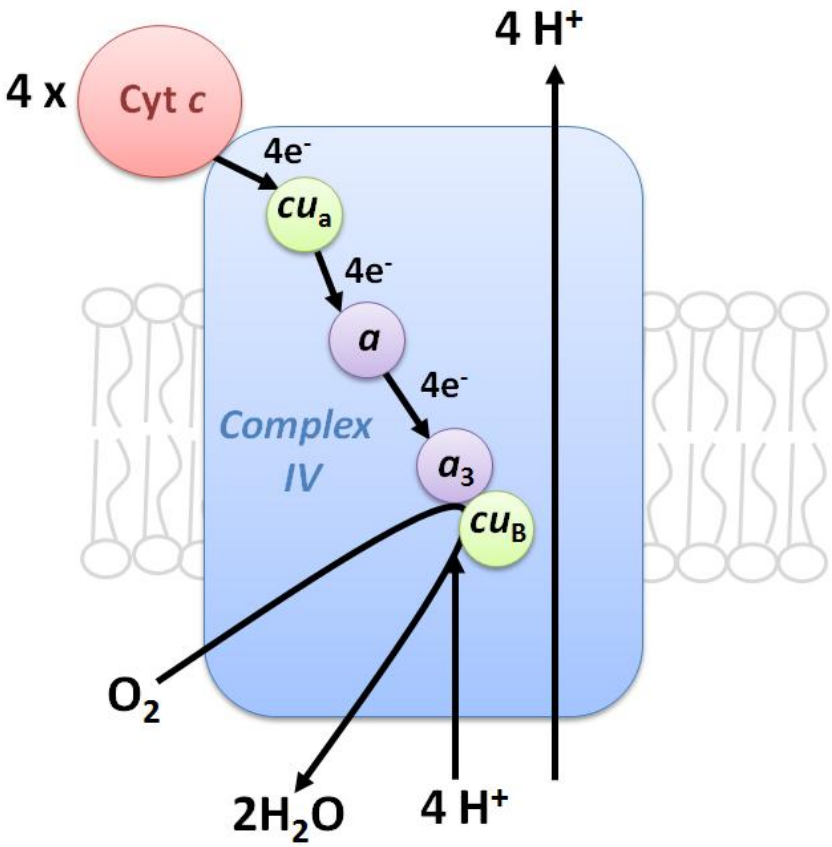

Figure 1.17. Schematic drawing of the mitochondrial cytochrome c oxidase (complex IV). Abbreviations: *a*, a-type heme *a*; a_3, a-type a_3; cu_A, copper center cu_A ; cu_B, copper center cu_B; cyt *c*, cytochrome *c*.

1.2.4.3.8. ATP synthase (complex V)

F_1F_o-ATP synthase (also termed complex V), is a rotary machine that couples ATP synthesis to the proton gradient generated across the inner mitochondrial membrane (Boyer, 1997; Capaldi and Aggeler, 2002; von Ballmoos et al., 2008). ATP synthesis requires a regular supply of inorganic phosphate (Pi) and ADP imported via the membrane potential-dependent ATP/ADP carrier (van Dooren et al., 2006). In eukaryotic species, the complex V drives the ATP synthesis in the mitochondrial matrix (a process also called oxidative phosphorylation) but the role of this enzyme in *Plasmodium* spp. is subject to debate (Vaidya and Mather, 2009). The oxidative phosphorylation integrity in the malaria parasite has been discussed for many years, supported by opposing data. Because the glycolysis pathway is the major source of ATP during the asexual stage, it was suggested that malaria parasites lost their ability to carry out oxidative phosphorylation. Biochemical studies using mitochondrial extracts from asexual and sexual blood stages proposed that oxidative phosphorylation was absent in *P. falciparum* (Fry and Beesley, 1991; Fry et al., 1990; Krungkrai et al., 1999). However by indirect measurement of respiratory control, Uyemura *et al*. showed evidence of functional oxidative phosphorylation in *P. berghei* and *P. yoelii yoelii* (Uyemura et al., 2000; Uyemura et al., 2004). Additionally, they reported an inhibition of phosphorylating respiration with oligomycin, a known ATP synthase inhibitor, supporting the presence of an operational enzyme. This observation is in contrast to previous findings that oligomycin does not appear to inhibit mitochondrial ATP hydrolase activity, the reverse action of the ATP synthase which maintains for a certain period the disrupted membrane potential by pumping protons into the intermembrane space (Fry et al., 1990; Vaidya and Mather, 2009). Evidence for the direct activity of ATP synthase is lacking and therefore the question of oxidative phosphorylation in *Plasmodium* parasites remains confused.

Moreover, the absence of ATP synthesis in the parasite mitochondrion has been corroborated with the lack of two essential subunits normally required for enzyme activity. Indeed, both subunits *a* and *b* of the F_0 sector are not yet annotated in the parasite genome due to their high divergence between species (Mogi and Kita, 2009). Thus, it has been proposed that subunits *a* and *b* are probably absent which explains why the malaria parasite lost the capacity for ATP synthesis and hydrolysis (Mather and Vaidya, 2008). Recently, attempts to disrupt both genes encoding α and β subunits of the *P. falciparum* ATP synthase were unsuccessful (Balabaskaran Nina et al., 2011). Additionally, *P. falciparum* ATP synthase was showed to be partly assembled in a dimeric complex. These results suggest that ATP synthase plays an essential role in blood stages of malaria parasite and confirm the presence of both key subunits *a* and *b* despite them

remaining unidentified. In Chapter 3 of this thesis, the identification of these two subunits was attempted by using bioinformatic and proteomic strategies.

.

1.2.4.3.9. Uncoupled protein (UCP) complex?

Under some conditions, protons can be translocated into the mitochondrial matrix without contributing to ATP synthesis by a process called "mitochondrial uncoupling" or "proton leak" (Ledesma et al., 2002). This alternative flow of protons back to the matrix is supported by enzymes or transporters located in the inner membrane and termed uncoupled proteins (UCPs). Uyemera *et al*. reported the first evidence of UCPs located in *P. falciparum* in the form of immunoblots using anti-UCP antibodies (Uyemura et al., 2004). Because a doubt remains about the ATP synthase functionality in *Plasmodium* spp, the presence of UCPs may be sufficient to complete the ETC circuit and generate a stable mitochondrial membrane potential. However, the presence and role of UCPs in the malaria parasite have to be clarified.

1.2.4.3.10. The ETC components as drug targets

Unique features of the *Plasmodium* mitochondrion suggest that enzymes composing the respiratory chain could be exploited as antimalarial drug targets (Kita et al., 2001; Mather et al., 2007; Monzote and Gille, 2010; Vaidya, 2004; Vaidya and Mather, 2009). Despite ATP being obtained via the glycolysis pathway in the asexual stage, a functional mitochondrial ETC and its related components have been shown to be a valid drug target.

As described earlier, the cytochrome bc_1 and atovaquone (a constituent of Malarone^{TM}) are the "proof-of-concept" of this strategy. Due to the expense of atovaquone and the emergence of resistant strains, attempts to develop alternative compounds have been initiated including (i) acridines and acridinediones (Biagini et al., 2008), (ii) quinolones (Biagini et al., 2012; Winter et al., 2008) (iii) and pyridones, analogues of the clopidol (Xiang et al., 2006; Yeates et al., 2008). New insights regarding the mechanism of atovaquone resistance in the parasite bc_1 are useful information for development of novel bc_1 inhibitors. This knowledge gap has been studied in Chapter 6 of this thesis which describes the molecular and biochemical characterisation of an atovaquone resistant *P. falciparum* isolate (TM902CB).

The *Plasmodium* ETC contains two untypical components, *Pf*NDH2 and MQO, which have no homologues in higher eukaryotic species including mammals. The absence of both dehydrogenases in the human host has led several research groups to suggest that they may be promising drug targets for the development of new antimalarials. In order to perform high-

throughput screens (HTS) or *in silico* rational-drug design, the generation of functional enzyme either purified or from enriched heterologous expression have been performed. In the case of *Pf*NDH2, a recombinant enzyme has been reported and its validation as a potential drug target demonstrated (Biagini et al., 2006; Fisher et al., 2007). The first results of a drug discovery project developing *Pf*NDH2 inhibitors were recently published (Biagini et al., 2012). Concerning MQO, no recombinant protein is yet available and to date attempts to generate a functional recombinant MQO have been unsuccessful (Biagini personal communication).

Due to the crucial role of the pyrimidine synthesis, the *Plasmodium* DHODH has also been validated as a possible drug target. Different studies have been performed to generate novel DHODH inhibitors by exploiting small differences in the active site of *Plasmodium* and human DHODH (Baldwin et al., 2005; Booker et al., 2010; Coteron et al., 2011; Phillips et al., 2008; Skerlj et al., 2011). To date, one of these projects has advanced to the late pre-clinical phase with the compound DSM265 (Coteron et al., 2011).

Downstream of the cytochrome bc_1 complex, the cytochrome *c* oxidase complex appears to be simpler than in higher organisms or yeast with a restricted subunit composition and an unusual split of COX II. These differences might be exploitable for a future drug development program.

1.3. Research aims

The general objective of the thesis was to take a multidisciplinary approach to study different aspects of the *Plasmodium falciparum* respiratory chain biochemistry, physiology and pharmacology.

The first results chapter of the thesis, Chapter 3, focuses upon the identification of missing ETC subunits to answer two knowledge gaps: the two anchor subunits SDH3 and SDH4 of the succinate dehydrogenase and subunit *a* and *b* of the ATP synthase. By using a bioinformatic approach, the detection of potential candidate genes is attempted and validation of the predictions is attempted using a proteomic strategy.

Chapter 4 presents for the first time the direct quinone reductase activity of all dehydrogenases composing the ETC in order to estimate their real contribution to the mitochondrial membrane potential generation. Additionally, the physiological consequence of inhibiting dehydrogenase activities on the mitochondrial electrochemical gradient ($\Delta\psi_m$) has been determined with real-time single-cell imaging assays. Moreover, menaquinone, a mitochondrial

electron carrier of anaerobic species, has been recently identified in malaria parasites and its capacity to replace ubiquinone within the ETC system in anaerobic conditions has been evaluated in this chapter.

In the Chapter 5, the previously held hypothesis that artemisinins target the parasite ETC is tested. In addition, single-cell imaging is used to measure the effect of endoperoxides against plasma ($\Delta\Psi_p$) and mitochondrial membrane potential ($\Delta\Psi_m$), and use this end-point measure to elucidate upstream mechanisms of activation.

In the Chapter 6, atovaquone sensitive and resistant parasites are compared at the biochemical level with the aim of uncovering the complex mechanisms underpinning atovaquone resistance, both at the enzyme level and at the pathway/cellular level.

Chapter 7 presents an updated picture of the mitochondrial importation and processing machinery for nuclear-encoded proteins in *Plasmodium falciparum*. Using comparative genomics and Hidden Markov Model approach, potentially new components involved in these mechanisms are presented.

Chapter 2

General Material & Methods

2.1. *In vitro* parasite culture

In vitro P. falciparum strains 3D7 and TM90 were maintained in continuous culture using standard methods (Bray et al., 2006; Trager and Jensen, 1976). Parasites were grown in 2% O+ erythrocytes (supplied by the Blood Transfusion Centre, Liverpool, UK) in RPMI 1640 medium with L-glutamine and sodium bicarbonate (R8758, Sigma-Aldrich, St. Louis, USA) supplemented with 25 mM HEPES pH 7.4, 20 µg/ml gentamicin sulphate and 10% human serum (or 0.5% Albumax (Invitrogen, Carlsbad, USA), 40 µM hypoxanthine). Cultures were grown under a gaseous headspace of 3% CO_2, 4% O_2 and 93% N_2 (BOC, Guilford, UK) (Scheibel *et al.,* 1979). Parasites were synchrony maintained by treatment with 5% sorbitol at ring stages (Lambros and Vanderberg, 1979). The parasitaemia was monitored daily by Giemsa-stained blood smears and observed under a light microscope (100 x magnification).

2.2. Drug sensitivity assays

Drug susceptibilities were determined with an inoculum size of 0.5% parasitemia (ring stage) and 1% hematocrit and were assessed by the measurement of fluorescence after the addition of SYBR Green I as described in (Smilkstein et al., 2004). Drug IC_{50} (50% inhibitory concentration) values were calculated from the log of the dose/response relationship, as fitted with Grafit software (Erithacus Software, Horley, United Kingdom). Results are given as the means of at least three separate experiments.

2.3. Cell-free parasite extract

Prior to Western blot and kinetic studies, malaria parasites were extracted from the erythrocytes. The synchronised parasites (5-10% trophoziotes) were collected by centrifugation at 3,000 g for 5 minutes. The pellet was resuspended in 5 volumes of 0,15% saponin in phosphate-buffered saline (PBS) for 30 sec, followed by three washes by centrifugation (2,500 g for 5 min) in ice-cold intracellular buffer (110 mM KCl, 30 mM NaCl, 2 mM $MgCl_2$, 20 mM glucose and 5 mM HEPES pH 7.4). The samples were checked microscopically to ensure lysis of all erythrocytes, and stored at -80 °C.

2.4. Protein quantification

The Bradford assay (Bradford, 1976) was carried out to determine the protein concentration used for SDS gel electrophoresis and to quantify the specific enzyme activity from free parasites preparation. The reaction was set up using the Bradford assay reagent (Bio-Rad, Hercules, USA). A standard curve was generated using bovine serum albumin (Sigma Aldrich, Saint-Louis, USA) at concentrations ranging from 0.2-0.9 mg/ml. Briefly, 200 µl Bradford reagent was added to 5 µl of sample and incubated for 5 min at room temperature. The assay was quantified spectrophotometrically at 595 nm (Varioscan^{TM}, Thermo Fisher Scientific, Waltham, USA). All assays were performed in triplicate and data are presented as the mean ± standard deviation.

2.5. Cell-free parasite membranes preparation

Cell-free parasites were disrupted with a sonicating probe in lysis buffer (50 mM Tris-HCl, 150 mM NaCl, 2 mM EDTA, pH 7.4) in the presence of protease inhibitor mixture (Complete Mini, Roche Applied Science, Germany). The lysate was centrifuged at 17,000 g for 30 min at 4 °C to pellet the membrane fraction. The supernatant was saved for analysis as the cytosolic fraction.

2.6. Bovine mitochondrial membranes preparation

Mitochondrial cytochrome bc_1 complex was isolated from bovine heart muscle by the method described by Kuboyama and colleagues (Kuboyama et al., 1972). All steps were performed at 0-4 ºC. First, bovine mitochondrial membranes (also called Keilin-Hartree particles) were prepared: 660 g of fresh lean beef heart muscle was diced and washed with water to remove haemoglobin prior to placing in a blender with 2 L of 50 mM sodium bicine pH 8.0. 20 ml of 2 M sodium bicine pH 9.0 was added prior to blending for 30 seconds at low speed, 30 seconds at medium speed then 45 seconds at high speed with the blender vessel briefly cooled by plunging into ice between each step. The pH was then adjusted to 8.0 with 2 M sodium bicine pH 9.0 and the sample pressed through a layer of muslin prior to centrifugation at 3,000 g for 40 minutes. The supernatant was passed through 2 layers of muslin then centrifuged at 20,000 g for 1 hour. The resulting pellet was resuspended with a Dounce homogeniser to 100 ml with 0.1 M sodium borate (orthoborate, BO_3^{3-}), 0.1 M sodium phosphate at pH 8.5. The resulting 100 ml suspension was diluted to 1 L in 0.1 M sodium borate, 0.1 M sodium phosphate pH 8.5 and centrifuged at 20,000 g for 1 hour. The supernatant was discarded to leave a pellet of Keilin-Hartree (KH) particles that were resuspended in approximately 100 ml 0.1 M sodium borate, 0.1 M sodium phosphate pH 8.5. The total concentration of protein was estimated from cytochrome *c* oxidase concentration, determined spectrophotometrically from a sodium dithionite-reduced

minus potassium ferricyanide-oxidised difference spectrum ($\varepsilon_{606\text{-}630nm}$ = 25.7 $mM^{-1}.cm^{-1}$). Mitochondrial protein concentration was estimated from this value using a figure of 0.4 nmoles cytochrome *c* oxidase/mg mitochondrial protein. Typically, a two batch preparation, processed in a single day, yielded around 100 ml of ~ 45 mg of protein/ml resuspended KH particles. These were stored at -80 °C until required.

2.7. Yeast mitochondrial membranes preparation

Wild type and mutant yeast strains were grown to stationary phase (48 h) in yeast extract peptone dextrose (YPD) at 28°C. Cells were harvested by centrifugation at 4,000 g for 5 minutes. The cells were washed with approximately 10 pellet volumes of 50 mM potassium phosphate (pH 7.5), 2 mM EDTA. The resuspended cells were centrifuged again at 4,000 g for 5 minutes and the pellet collected (it can be frozen at this stage with a few ml of glycerol for storage at -80°C if need be). The washed cells were resuspended in a total volume of 10 - 15 ml in 50 mM potassium phosphate (pH 7.5), 2 mM EDTA by using an hand homogeniser. The disrupted cells were centrifuged at 10,000 g for 20 min at 4°C to pellet debris. The supernatant was collected and centrifuged at 100,000 g for 1 h at 4°C to pellet the crude mitochondrial membranes. The pelleted membrane were resuspended in 1 ml 50 mM potassium phosphate (pH 7.5), 2mM EDTA with an hand homogeniser. 50% (v/v) glycerol (cryoprotectant) were added to the membranes preparation before to be aliquoted and stored at -80°C.

2.8. SDS-Polyacrylamide gel electrophoresis (PAGE) electrophoresis

SDS-Page were run according to the Laemmli method (Laemmli, 1970). A Laemmli sample buffer (62.5 mM Tris-HCl pH 6.8, 0.01% (w/v) bromophenol blue, 10% (v/v) glycerol, 2% (w/v) SDS, 5% (v/v) 2-mercaptoethanol) was added to each sample (1 : 2, v/v). Protein samples (containing between 10 to 50 µg of total protein) were then heated for 5 min at 95°C before to be electrophoresed on SDS/polyacrylamide gels (between 5 to 15% resolving and 4% stacking polyacrylamide gels) via the mini-gel electrophoresis system Mini-PROTEAN® II (Biorad, Hercules, USA) using Laemmli running buffer (25 mM Tris, 0.192 mM Glycine, 0.1% SDS, pH 8.8) at a constant current of 30 mA per mini-gel. The Spectra™ Multicolor Broad Range Protein Ladder (Fermentas, USA) was then used to estimate the resulting protein band.

For vizualization, proteins patterns were stained by Coomassie blue staining or by silver staining. For Coomassie Blue staining, proteins were stained in a one-step procedure by incubating the entire gel in Coomassie-based Instant Blue™ (Expedeon, Cambridge, UK) for 1h at room remperature. The gel was finally rinsed with distilled water to visualize protein bands

according to manufacturer instructions. For silver staining, proteins in gel were fixed with 10% (v/v) acetic acid, 40% (v/v) ethanol for 1 h, then oxidized in 1.72 mM sodium hydrosulfite for 2 min, washed with water and treated with ice-cold silver nitrate solution (11,8 mM silver nitrate, 0,025% (v/v) formaldehyde) for 30 min. After being washed several times with water, the gel was developed in 283 mM sodium carbonate, 63.2 µM sodium thiosulfate, 0,025% (v/v) formaldehyde. Color development was stopped with 412 mM Tris, 2% (v/v) acetic acid when the desired staining intensity has been achieved.

2.9. Western Blot analysis

After SDS-Page, proteins resolved in the gel were electrophoretically transferred to Hybond ECL nitrocellulose membrane (GE Healthcare, UK) using the wet blotting system Mini Trans-Blot® Electrophoretic Transfer Cell (Bio-Rad, Hercules, USA) in a Towbin buffer (25 mM Tris, 192 mM glycine, 20% (v/v) methanol) at the constant current of 250 mA for 1h at 4°C, The membrane was blocked with 5% skim milk in TBS-T (137 mM NaCl, 20 mM Tris, 0.1% (v/v) Tween-20) for 1h at room temperature or overnight at 4 °C. Then, the membrane was incubated with appropriate dilutions of primary polyclonal antibody in blocking buffer at room temperature for 2 hours or overnight at 4°C. After being washed in TBS-T, the membrane was incubated with 1/10000 dilution of horseradish peroxidase-conjugated goat anti-rabbit IgG secondary antibody for 1 hour at room temperature. Membrane was then washed in TBS-T, immersed in ECL™ Western blotting detection reagent kit (Amersham Pharmacia Biosciences, Amersham, UK) for 5 min in the dark and visualized on X-ray BioMax MR film (Kodak, New York, USA).

Chapter 3

Bioinformatic and proteomic identification of *Plasmodium falciparum* succinate dehydrogenase and ATP synthase

3.1. Introduction

The mitochondrial proteome from *Plasmodium falciparum* has been intensively characterized by sequence homology searching since the mapping of their genomes. Several mitochondrial proteins are part of complexes composing the electron transport chain (ETC; see Chapter 1, section 1.2.4.3) and only those having conserved amino acid sequences across species or being highly abundant have been characterized. However, a small number of ETC proteins, especially those of high hydrophobicity and/or low abundance, remain to be identified in *Plasmodium* spp. Due to high sequence divergence, the membrane anchor subunits of succinate dehydrogenase (SdhC and SdhD) and ATP synthase (subunit *a* and *b*) are still not annotated in *Plasmodium* databases. Their identification is crucial to validate the functionality and integrity of both enzymes. In this chapter, candidate genes encoding for these four missing subunits were determined based on a bioinformatic approach. The identification of the subunits was then attempted using classical proteomic approaches involving protein separation by two-dimensional (2D) blue native/SDS-polyacrylamide gel electrophoresis coupled with liquid chromatography tandem mass spectrometry (LC-MS/MS).

3.1.1. Identification of succinate dehydrogenase SdhC and SdhD subunits

3.1.1.1. The eukaryotic succinate dehydrogenase

As mentioned previously (see Chapter 1, section 1.2.4.3.2), the succinate:quinone oxidoreductase (also referred to as SDH, SQR or Complex II - EC 1.3.5.1) is a membrane protein complex that couples the two-electron oxidation of succinate to fumarate **(equation 1)** to the reduction of quinone to quinol **(equation 2)** (Hagerhall, 1997; Massey and Singer, 1957).

$$\text{succinate} \rightleftharpoons \text{fumarate} + 2\,H^+ + 2\,e^- \qquad \textbf{(equation 1)}$$

$$\text{quinone} + 2\,H^+ + 2\,e^- \rightleftharpoons \text{quinol} \qquad \textbf{(equation 2)}$$

In aerobic metabolism, eukaryotic SQRs play two roles. They are involved in the respiratory chain and constitute the only membrane-bound enzymes of the tricarboxylic acid cycle (TCA) (Saraste, 1999). Generally, eukaryotic complex II contains four subunits **(Fig. 3.1)**: two hydrophilic

subunits SdhA and SdhB attached to the inner membrane by one large or two small hydrophobic membrane-intrinsic subunits SdhC and SdhD (Horsefield et al., 2004). SdhA is a flavoprotein containing a flavin adenine dinucleotide (FAD) covalently attached to a histidine residue, and a succinate binding site (Robinson and Lemire, 1996). Succinate oxidation to fumarate releases electrons via FAD reduction. Electrons tunnel along an iron-sulfur relay constituted of three clusters [2Fe-2S], [4Fe-4S] and [3Fe-4S] located in the iron-sulfur subunit SdhB. Electrons are transferred to a ubiquinone molecule in a binding site at the interface of SdhB, SdhC and SdhD. SdhC and SdhD are two small, highly helical, membrane anchor subunits with a low spin heme b_{556} coordinated by two histidine residues (Vibat et al., 1998).

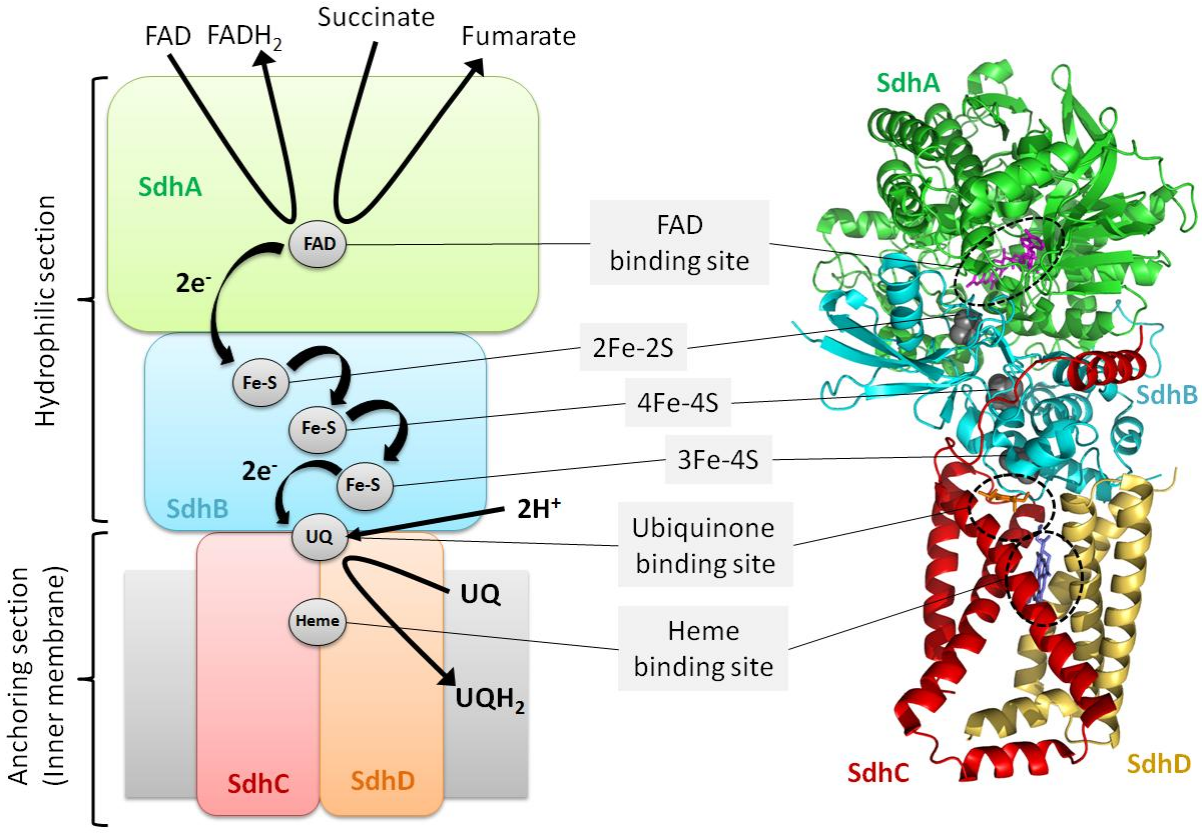

Figure 3.1. Overview and structure of the mammalian succinate dehydrogenase. The Protein Database (PDB) accession number used for the Complex II structure shown is 1ZPO (*Sus scrofa*).

SQRs crystal structures are currently available from bacteria (*Escherichia coli* - PDB entry 1NEK), pig (*Sus scrofa,* 1ZOY) and chicken (*Gallus gallus*, 2H88) (Huang et al., 2006; Sun F Fau - Huo et al.; Yankovskaya et al., 2003). Across species, the hydrophilic subunits SdhA and SdhB have high amino acid sequence identities while those of the hydrophobic subunits SdhC and SdhD are poor homologous.

Among nematode parasites, complex II has only been characterized in *Ascaris suum, Trypanosoma* and *Leishmania* species (Morales et al., 2009; Saruta et al., 1995). *A. suum* has a conventional four subunit SQR whereas its homologue in kinetoplastid species exhibits unusual features by being composed of 12 subunits.

3.1.1.2. Succinate dehydrogenase in *Plasmodium* spp.

In malaria parasites, subunits SdhA and SdhB were easily identified due to sequence similarities with other species whereas SdhC and SdhD remain unannotated in the current database. Both SdhA and SdhB subunits are encoded by single open reading frames (ORF) located on chromosomes 10 and 12, respectively.

Although the *Plasmodium* SQR integrity is not fully established by gene identification, an accumulation of evidence published in several studies suggests to the presence of a functional enzyme. Early, Fry and Beesley measured reduction of cytochrome *c* after induction with succinate in *P. falciparum* and *P. yoelii yoelii* mitochondrial fractions (Fry and Beesley, 1991). In their work, the conviction to assay the SQR enzyme has been reinforced by inhibiting the succinate:cytochrome *c* reductase activity detected with known eukaryotic complex II inhibitors such as Thenoyltrifluoroacetone (TTFA) or Malonate. Afterwards, other complex II activities have been reported in several studies using two types of assay: oxygen consumption or reduction of 2,6-dichloroindophenol (DCPIP), both induced by succinate (Krungkrai et al., 2000; Mather et al., 2010; Suraveratum et al., 2000). However, those SQR activities reported are variable and dependent on the yield and quality of the parasite preparation, as well as the type of assay performed **(Table 3.1)**.

Table 3.1. Complex II activities measured with mitochondrial extracts from *Plasmodium* spp.

Reference	Type of complex II assay (*Plasmodium* species used)	Specific activity measured (nmoles/min/mg protein)
Fry and Beesley, 1991	Cytochrome c reduction activity induced by succinate (*P. falciparum and P. yoelii yoelii*)	*Pf*: 112 ± 13; *Py*: 150 ± 24 *Pf*: 68 ± 9; *Py*: 69 ± 10 (with 20 µM TTFA) *Pf*: 77 ± 10; *Py*: 72 ± 8 (with 5 mM Malonate)
Suraveratum et al., 2000	DCPIP reduction activity induced by succinate (*P. falciparum*)	33.13[1]
Krungkrai et al., 2000	Oxygen consumption induced by succinate (*P. falciparum*)	1.45
Kawahara et al., 2009	DCPIP reduction activity induced by succinate (*P. yoelii yoelii*)	2.66 ± 0.02
Mather et al., 2010	DCPIP reduction activity induced by succinate (*P. falciparum*)	9.73 5.79 (with 10 mM Malonate)

[1] Activity monitored on the isolated complex II. *Pf* indicates *P. falciparum* and *Py*, *P. yoelii yoelii*.

The Krungkrai group was the first to isolate the *P. falciparum* complex II but containing only the SdhA and SdhB subunits with molecular weights of 55 and 35 kDa, respectively (Suraveratum et al., 2000). It has been concluded that the interaction between the hydrophobic part and the anchoring section is weak and can be easily broken during a purification process. *P. falciparum* SdhA and SdhB genes have also been cloned and characterized (Takeo et al., 2000). The genes encode subunits of 69.2 kDa (SdhA) and 37.8 kDa (SdhB), and have a presequence essential for the import into the mitochondrion. Evidence supporting the presence of SdhC and SdhD was provided by a study performed in *P. yoelii yoelii* **(Fig. 3.2)** (Kawahara et al., 2009). The molecular weight of the whole enzyme was estimated to be near 135 kDa in *P. yoelii yoelii* which is comparable to 130 kDa in mammals. A two dimensional approach identified two putative membrane anchor subunits SdhC and SdhD with molecular masses of 16 and 14 kDa respectively. However, both protein bands speculated as the two anchor subunits have not been identified by mass spectrometry.

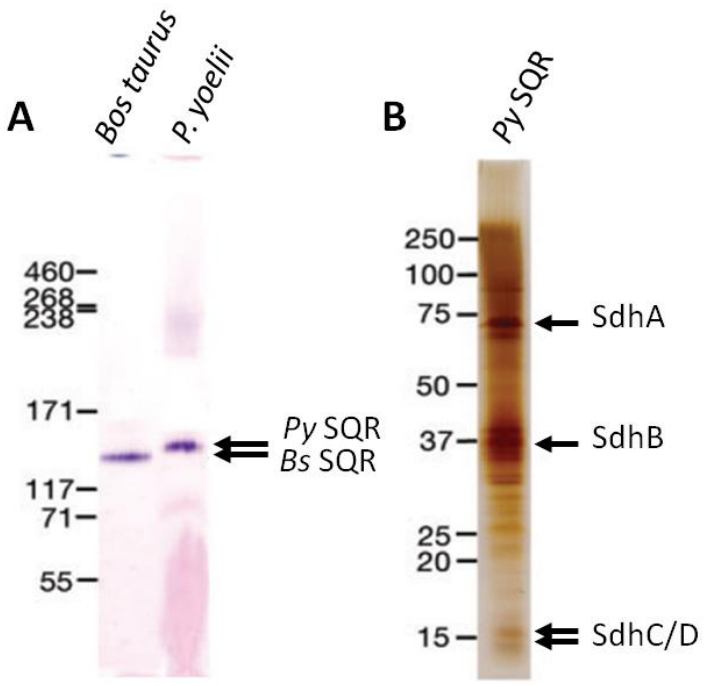

Figure 3.2. Analysis of complex II in *Plasmodium yoelii yoelii* (adapted from Kawahara et al., 2009). (A) High resolution clear native electrophoresis of mitochondrial extract in bovine (*Bos taurus*) and *Plasmodium yoelii yoelii*. Both SQRs were visualized by succinate dehydrogenase activity staining. **(B)** SDS-Page followed by silver staining of the 135 kDa band corresponding to *P. yoelii yoelii* complex II. Putative complex II subunits are indicated with arrows. (Permission licence # 3144931157373).

3.1.1.3. The membrane anchor subunits SdhC and SdhD

A first look at the primary structure among different species confirms the low sequence conservation for subunits SdhC and SdhD **(Table 3.2)**. Except subunits from animals (*S. scrofa* and *G. gallus*) which are significantly conserved (>58% similarities), sequence identities between other

species remain low (between 3% and 24%). Therefore, homology searching by conventional BLAST analysis or Hidden Markov Model (HMM) approach with eukaryotic or bacterial sequences used as templates failed to determine either subunit in apicomplexans including *Plasmodium* spp.

Table 3.2: Amino acid sequence identities between subunits SdhC and SdhD from representative species in mammals (*Sus scrofa*), aves (*Gallus gallus*), bacteria (*Escherichia coli*), yeast (*Saccharomyces cerevisiae*), plant (*Arabidopsis thaliana*) and protists (*T. cruzi*). The primary structure identities score was determined by amino acid alignment with ClustalW 2.0 (www.ebi.ac.uk/Tools/msa/clustalw2). Percentages of identity for SdhC and SdhD are highlighted in red and black respectively.

	S. scrofa	*G. gallus*	*E. coli*	*S. cerevisiae*	*A. thaliana*	*T. cruzi*
S. scrofa		70% - 58%	19% - 8%	22% - 13%	12% - 5%	4% - 7%
G. gallus			20% - 6%	24% - 15%	17% - 6%	3% - 5%
E. coli				13% - 4%	9% - 8%	3% - 12%
S. cerevisiae					12% - 6%	5% - 8%
A. thaliana						7% - 13%
T. cruzi						

UniprotKB entry (SdhC, SdhD) are for *S. scrofa* (**P35720, A5GZW8**), *E. coli* (**P69054, P0AC44**), *G. gallus* (D0VWW3, Q5ZIS0), *S. cerevisiae* (**P33421,** P37298), *A. thaliana* (A8MSF5, **Q941A0**) and *T. cruzi* (Q4D4V5, Q4D1F3).

Despite low sequence identities, high similarities were observed by aligning the anchoring section of SQR crystal structures available from bacteria, mammalian and avian species **(Fig. 3.3)**. For example, pig and bacterial SdhD show only 8% of sequence identities but share 62.7% of structural homologies. Under those observations, the hypothesis that structural features of the anchor membrane subunits are highly conserved to accomplish an analogous function can be proposed.

A

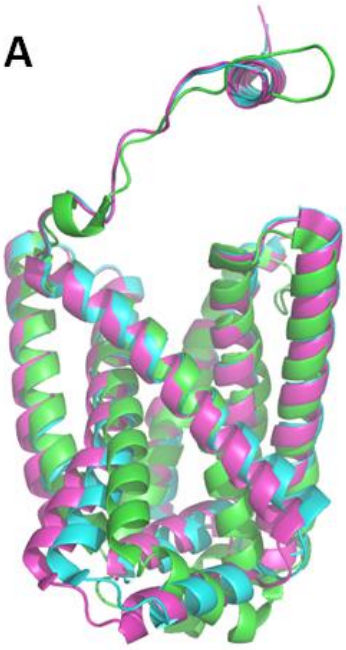

B

SQR Subunit	Species A	Species B	Sequence identities	Structure identities
SdhC	*Ss*	*Gg*	70%	**96,3%**
	Ss	*Ec*	19%	**70,8%**
	Ec	*Gg*	20%	**69,9%**
SdhD	*Ss*	*Gg*	58%	**98,5%**
	Ss	*Ec*	8%	**62,7%**
	Ec	*Gg*	6%	**62,8%**

Figure 3.3. Crystal structure alignment of SdhC and SdhD in three different species. **(A)** Structures alignment has been performed with PyMol (www.pymol.org) with membrane anchor section in *Sus scrofa* (PDB entry

1ZOY), *Escherichia coli* (1NEK) and *Gallus gallus* (2H88), highlighted in blue, green and pink, respectively. **(B)** Comparison of sequence and structure identities among three species. Sequence identities were determined with ClustalW 2.0 (www.ebi.ac.uk/Tools/msa/clustalw2). Structure identities score was calculated via crystal structure alignment with the TM-align algorithm (zhanglab.ccmb.med.umich.edu/TM-align).

3.1.2. Identification of ATP synthase subunits *a* and *b*

3.1.2.1. Eukaryotic ATP synthase

In eukaryotes, inner membrane-bound ATP synthases (F_1F_0-type ATPases, EC 3.6.3.14) catalyse two important physiological functions with the synthesis of ATP from ADP and inorganic phosphate in the mitochondrial matrix or the reverse reaction, the hydrolysis of ATP, to generate a transmembrane electrochemical gradient under conditions of low driving force (Devenish et al., 2008). The enzyme is composed of two domains: a water-soluble F_1 sector which contains the active site and consists of subunits α_3, β_3, δ, ε and γ, and the membrane-associated F_0 part made up of subunits $c_{8\text{-}12}$, *a* and *b* **(Fig. 3.4)**. The F_0 domain can be associated with additional subunits such as OSCP, *d* or F6 (Walker and Dickson, 2006). During ATP synthesis, protons from the intermembrane space are translocated to the matrix via two aqueous half-channels formed by the transmembrane domains of the subunit *a; with* one channel leading to the matrix and the other to the intermembrane space (Angevine et al., 2007).

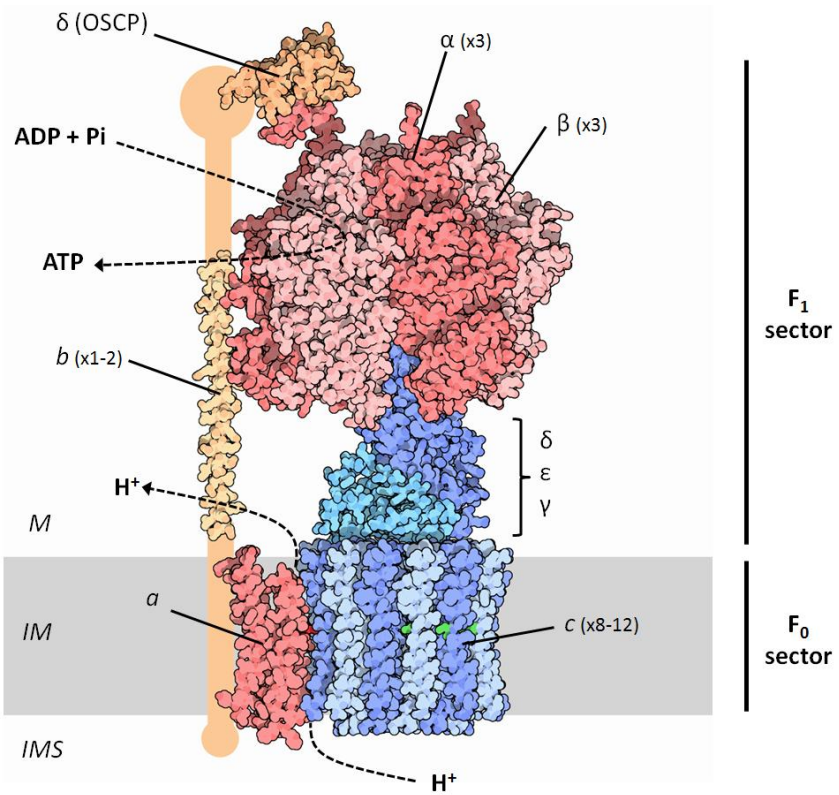

Figure 3.4. Structure and subunits composition of the F_1F_0-type ATP synthase in *E. coli*. The picture shown here is a composite of four different X-ray and NMR structures of *E. coli* F_1F_0 ATPase (PDB entry 1C17, 1E79, 2AZU and 1L2P). Abbreviations: M, matrix; IM; inner membrane; IMS, intermembrane space.

The proton flow causes rotation of the oligomeric ring formed by several subunits *c* and subsequently the central stalk composed by subunits ε, δ, γ which enforces each catalytic site in F_1 to synthesize ATP. For the reverse reaction, ATP hydrolysis in the hexameric $\alpha_3\beta_3$ drives reverse rotation of the central stalk and then *c*-ring which causes proton efflux via F_0. During translocation, the proton binding and release takes place via a carboxyl group of a strictly conserved acidic residue (Asp61 in *E. coli* or Glu59 in *S. cerevisiae*) located within the second transmembrane helix of the subunit *c* (Deckers-Hebestreit et al., 2000) **(Fig. 3.5 A and B)**. This aspartate or glutamate residue acts as the proton acceptor and donor at the subunit *a*/ring-*c* interface. The arginine conserved in subunit *a* (Arg210 in bacteria or Arg176 in yeast) is suspected to play the crucial mechanistic function to coordinate protonation and deprotonation events **(Fig. 3.5 C and D)** (Symersky et al., 2012).

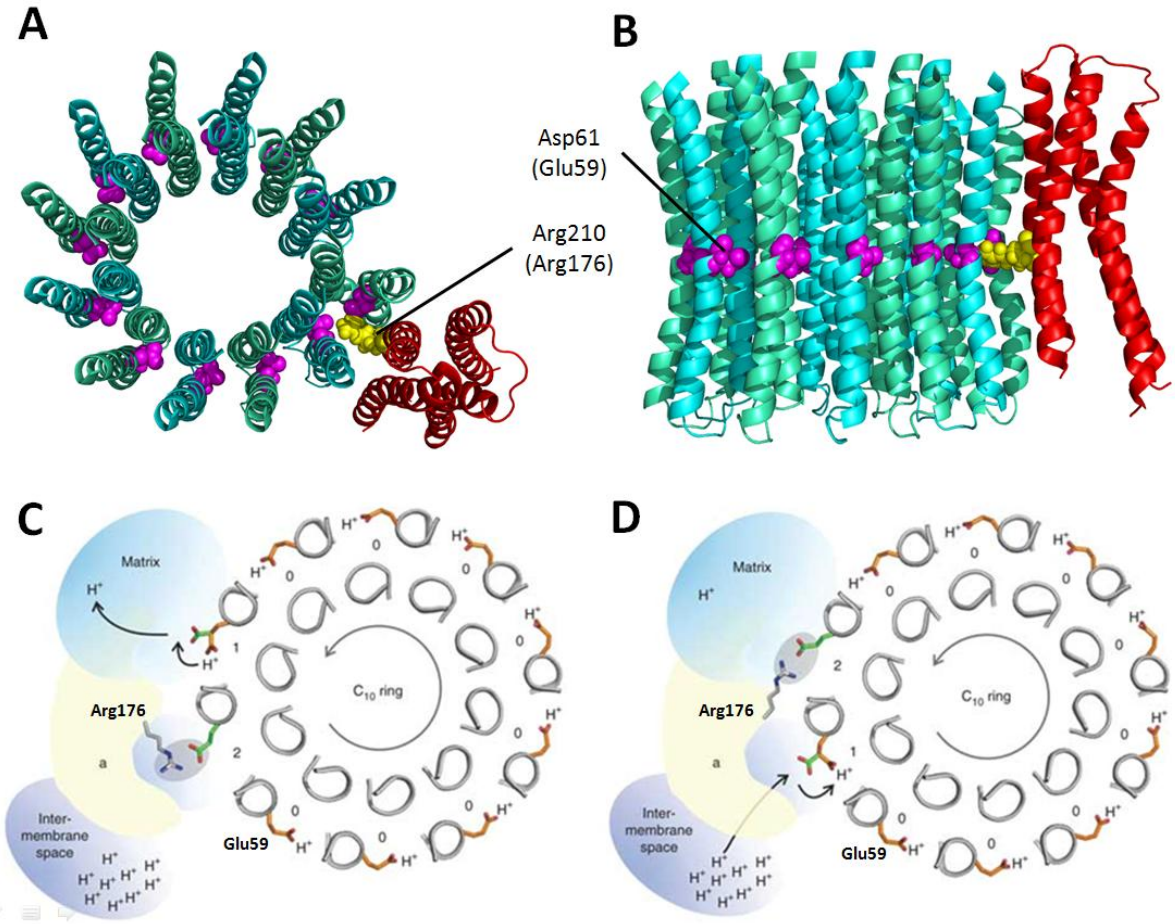

Figure 3.5. Structure of subunits *c* and *a*, and hypothetical rotary mechanism of the *c*-ring from F_1F_0 ATP synthase. (A) Cartoon representation of the *c*-ring (cyan and greencyan) and subunit *a* (red) structure viewed from the mitochondrial matrix (ATP synthase in *E. coli*; PDB entry 1C17). **(B)** Same as in A, viewed along the plane of the inner membrane. Highly conserved residues Asp61 (pink; Glu59 in yeast) and Arg210 (yellow; Arg176 in yeast) residues are represented with spheres. **(C)** Counterclockwise rotary mechanism of the ATP synthesis suggested by Symersky *et al.* and viewed from the mitochondrial matrix (Symersky et al., 2012). When facing the membrane, *c*-ring Glu59 are protonated (orange, state 0). By entering at the interface with the subunit *a,* Glu59 adopt an open conformation and release a proton into the half-channel leading to the matrix

(state 1). Glu59 in the adjacent subunit *c* interact with Arg176 (state 2) but becomes free when Arg176 switch the interaction with the newly deprotonated Glu59. **(D)** The release of the interaction enables the unengaged Glu59 residue to load another proton coming from the intermembrane space via the second water-half channel before to re-enter in the inner membrane. (Permission licence # 3144940923456)

To allow the rotational movement of the central stalk, a second structural link between F_0 and F_1 is necessary for the stabilization of the whole complex. Thus, an extended hydrophilic structure, the "second stalk" (referred also as "stator stalk") is located at the periphery and holds the $\alpha_3\beta_3$ hexamer in place during the movement of the central stalk (Wilkens and Capaldi, 1998). The stator stalk composition varies among species. In bacteria, it consists of one subunit δ (also termed OSCP, Oligomycin Sensitivity-Conferring Protein, for eukaryotes) and a dimer of subunit *b.* In cyanobacteria and other photosynthetic bacteria, two different but homologous subunits *b* and *b'* replace the dimeric structure. In the mitochondrial eukaryotic enzyme, only one subunit *b* is associated with two mitochondrial-specific subunits *d* and F6. Both subunits are wrapped around the single subunit *b* in a way to replace the function of the second subunit *b* in the bacterial enzyme (Weber, 2007). Although a complete structure of F_1F_0-ATP synthase in eukaryotes is still not available, an x-ray structure of the stator stalk from bovine heart mitochondria has been solved with large portions of subunits *b*, *d* and F6 **(Fig. 3.6)** (Dickson et al., 2006).

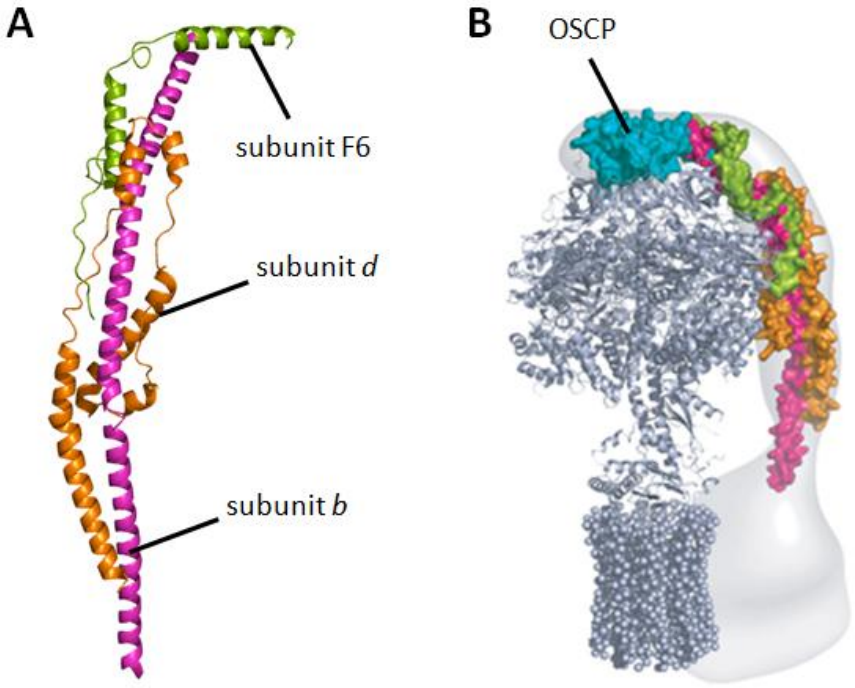

Figure. 3.6. Partial structure of the stator stalk in the ATP synthase from bovine heart mitochondria (Dickson et al., 2006). (A) X-ray structure of the stator stalk with the subunits *b* (magenta), *d* (orange) and F6 (green) (PDB entry 2CLY). **(B)** Suggested location of the stator stalk in the ATP synthase (Dickson et al., 2006). The N-terminal domain of the OSCP (cyan), the stator stalk structure and the F_1-c_{10} subcomplex (grey) were introduced by eye into an electron density map of an intact bovine ATP synthase complex determined by electron cryo-microscopy. (Permission licence # 3144940689940).

3.1.2.2. ATP synthase in *Plasmodium* spp.

It has been assumed for a long time that *Plasmodium* mitochondria cannot perform oxidative phosphorylation due to the lack of both ATP synthase subunits *a* and *b* (Fry and Beesley, 1991; Gardner et al., 2002). However, the capacity for oxidative phosphorylation in rodent parasites and *P. yoelii yoelii* was demonstrated supporting the presence of both key subunits (Uyemura et al., 2000; Uyemura et al., 2004). As mentioned previously, both subunits have major roles in H^+ translocation or maintaining stability of the whole complex. It suggests that a conventional H^+-ATP synthase lacking both subunits cannot be correctly assembled and functional. Recently, attempts to delete the genes encoding the subunit β and γ have been unsuccessful (Balabaskaran Nina et al., 2011). Therefore, the mitochondrial ATP synthase is suspected to play an important role in blood stage parasites by (i) maintaining the crucial membrane potential via ATP hydrolysis, (ii) producing ATP for local physiological processes, or (iii) contributing in mitochondrial morphogenesis. Additionally, *P. falciparum* ATP synthase has been found to be partly assembled in a dimeric complex by using a blue native gel approach **(Fig. 3.7)** (Balabaskaran Nina et al., 2011). Like in most eukaryotic organisms (Arnold et al., 1998), the dimeric ATP synthase seems to be the predominant form in *P. falciparum* parasites. The interaction between two ATP synthase monomers is mediated by the F_0 sector and probably by the subunit *a* which has the most important basis for dimerization due to its high number of transmembrane helices (Wittig and Schagger, 2008). Additionally to subunit *a*, subunit *b* and accessory subunits (*e* and A6L) can also stabilize the monomer-monomer interface (Bisetto et al., 2008; Wittig et al., 2010).

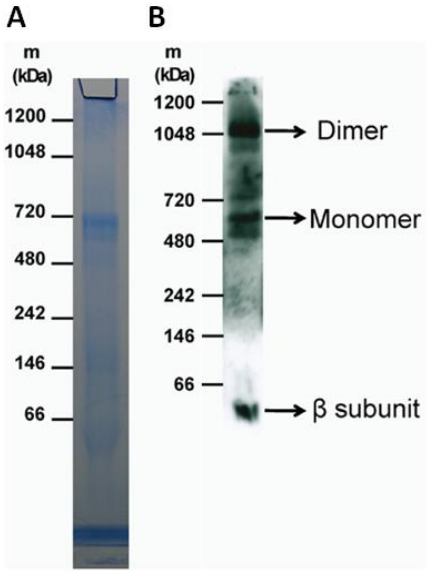

Figure 3.7. Dimeric formation of *P. falciparum* ATP synthase (Balabaskaran Nina et al., 2011). (A) Blue native gel of *P. falciparum* mitochondria extract stained with coomassie blue. **(B)** Blue native gel with mitochondria from parasites probed with anti-β antiserum.

3.1.2.3. Evidence of *Plasmodium* subunits *a* and *b* existence

Both subunits *a* and *b* are highly divergent and could not be identified by conventional bioinformatic tools like BLAST or HMM algorithms **(Table 3.3).** Recently, candidates of both subunits have been identified in the protozoan *Tetrahymena thermophilia* showing poor similarities with eukaryotic homologues (Balabaskaran Nina et al., 2010). To date, only one crystal structure of the subunit *a* (in *E. coli*) has been solved as well as a single structure of the subunit *b* (in *B. taurus*). Thus, their degree of structural similarities with homologues could not be predicted. However, the overall structure of ATP synthase remains highly conserved across species. Therefore, both subunits *a* and *b* in *Plasmodium* species can be speculated to have similar structural profiles with their homologues in bacteria or mammals.

Table 3.3. Amino acid sequence identities between subunits *a* and *b* from representative species in mammals (*H. sapiens*), bacteria (*E. coli*), yeast (*S. cerevisiae*), nematode (*A. suum*) and protist (*T. brucei)*. The primary structure identities score was determined by amino acid alignment with ClustalW 2.0 (www.ebi.ac.uk/Tools/msa/clustalw2). Percentage of identities for ATP synthase subunit *a* and *b* are highlighted in red and black respectively.

	H. sapiens	*E. coli*	*S. cerevisiae*	*A. suum*	*T. brucei*
H. sapiens		20% - 9%	34% - 15%	17% - 20%	10% - 5%
E. coli			16% - 13%	15% - 11%	20% - 8%
S. cerevisiae				17% - 15%	16% - 3%
A. suum					19% - 7%
T. brucei					

UniprotKB entry (subunits *a*, *b*) are for *H. sapiens* (**P00846, P24539**)*, E. coli* (**P0AB98, P0ABA0)***,*** *S. cerevisiae* (**P00854, P05626**)*, A. suum* (P24876, F1L7V5) and *T. cruzi* (P24499, Q57ZP0).

Only two components of the F_0 sector have been identified in malaria parasites: subunits *c* and OSCP. *Plasmodium* subunit *c* shows important identities with mammals, yeast and bacteria homologues and exhibits a glutamate residue located within its second transmembrane domain essential for protons translocation **(Fig. 3.8)**. Hence, *Plasmodium* subunit *c* displays necessary features to operate a functional rotary mechanism, supporting the presence of subunit *a* as partner.

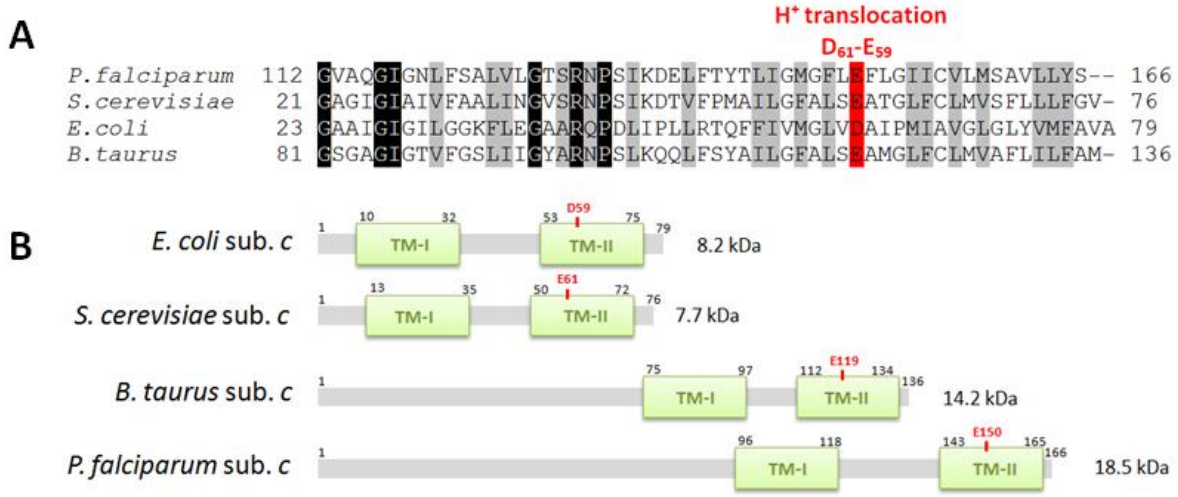

Figure 3.8. Sequence alignment of the C-terminal section from ATP synthase subunit *c* in different species and location of their transmembrane domains. (A) The sequences were aligned with ClustalW2 (www.ebi.ac.uk/Tools/msa/clustalw2). Residues are displayed with dark boxes for full conservation and grey boxes for strong similarities. In red is highlighted the Asp or Glu residue implicated in proton translocation and interaction with the Arg residue conserved in subunit *a*. The subunit *c* sequences used were from *Bos taurus* (UniprotKB entry P32876), *Saccharomyces cerevisiae* (P61829), *Escherichia coli* (P68699) and *Plasmodium falciparum* (C0H4L0). **(B)** Transmembrane helices indicated by green 'TM helix' boxes were predicted using THMMH algorithm (www.cbs.dtu.dk/services/TMHMM). The Asp or Glu essential residue is indicated in red.

3.1.3. Bioinformatic strategy

A pyramid-shaped filter was established with a series of structural fingerprints such as the molecular weight, number of transmembrane domains, secondary structure profile, conserved motifs, protein function and presence of a mitochondrial signal peptide **(Fig. 3.9)**. For each subunit searched, fingerprint cut-offs were determined by studying homologous proteins from prokaryotes, animals, yeasts or plants. Thus, candidate genes were identified by passing all the available *P. falciparum* encoding genes in the PlasmoDB database through those different filters.

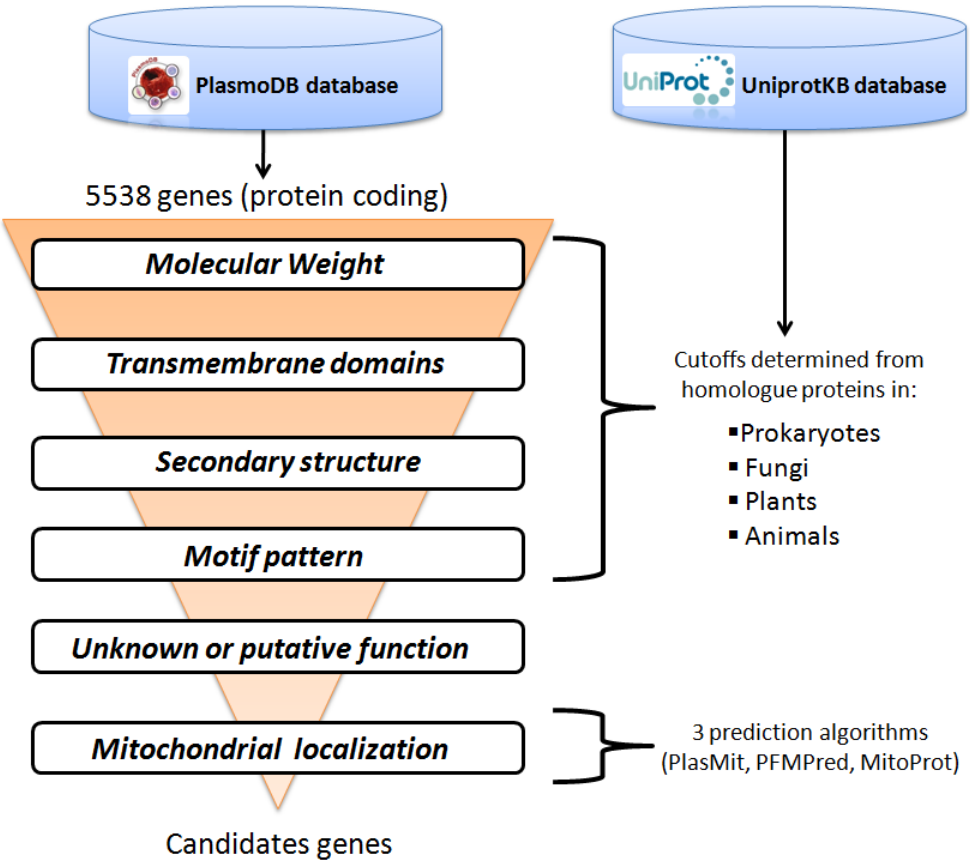

Figure 3.9. Pyramid-shaped strategy applied to identify potential candidate genes for succinate dehydrogenase and ATP synthase lacking subunits.

3.1.4. Proteomic approach

Two-dimensional (2D) blue native electrophoresis (BNE)/SDS-Page is a gel-based approach mainly used to study mitochondrial complexes (Klodmann et al., 2010; Taylor et al., 2002). In contrast to the conventional 2D isoelectric focusing/SDS-Page system, 2D BNE/SDS-Page is more adapted to characterize hydrophobic proteins even if the resolution of resulting gels is slightly reduced. The first dimension is a blue native gel electrophoresis to separate respiratory chain complexes from solubilised mitochondrial membranes. Digitonin, dodecyl-β-D-maltoside (DDM) or triton X-100 are nonionic detergents with strong delipidating properties suitable for isolation of membrane complexes. Following solubilisation, the ionic dye coomassie blue nonspecifically binds all proteins and charges them negatively. Thus, the electrophoretic mobility of complexes in the first dimension gradient gel depends on the size and shape of complexes. Separated by native gels, enzymatic complexes are still biochemically active and specific staining methods based on in-gel activity or fluorescent assays can be used to localize them on the gel (Heinemeyer et al., 2007). Subsequently, complexes are resolved from a BNE strip into their composing subunits on a second gel dimension in the presence of sodium dodecyl sulfate (SDS). Following the second dimension, gels can be stained for immediate visualization with coomassie or silver stain, as well as electroblotted for protein

detection with specific antibodies **(Fig. 3.10)**. Finally, mass spectrometry analysis can be a straightforward and sensitive approach to identify proteins from gel spots of interest.

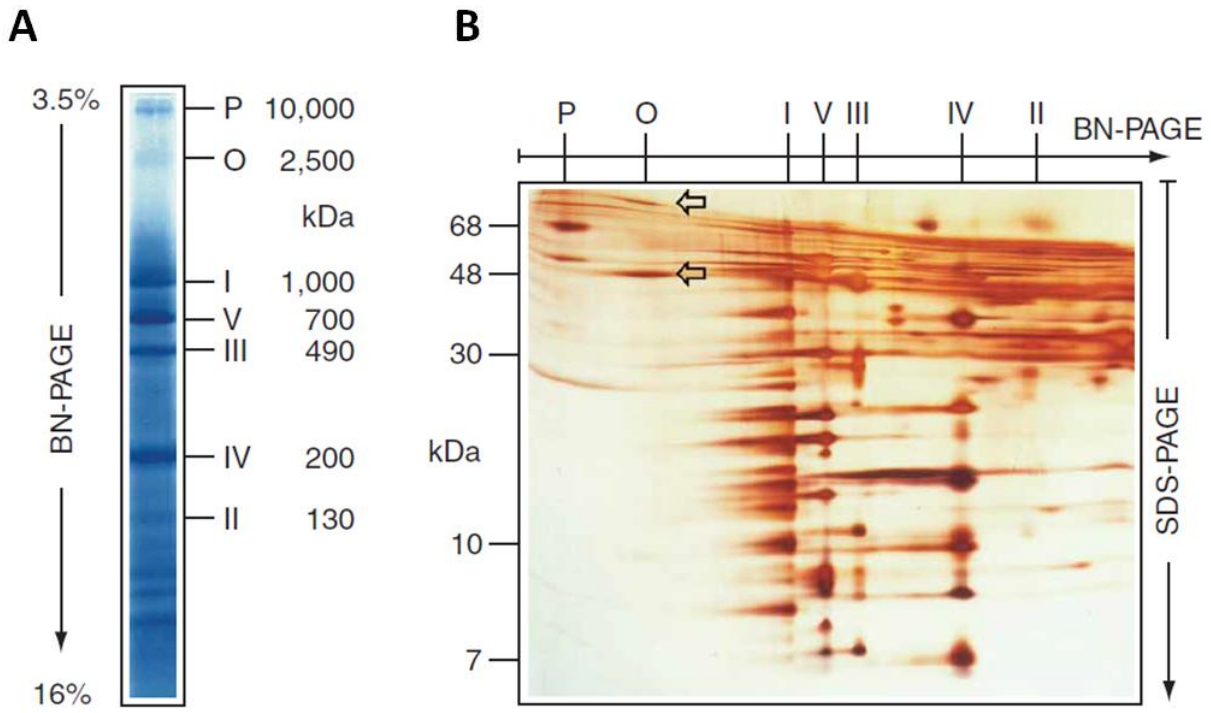

Figure 3.10. Separation of mitochondrial complexes separated by 2D BNE/SDS-Page (Wittig et al., 2006). (A) Gradient blue native gel of solubilised bovine heart mitochondrial complexes I to V, pyruvate dehydrogenase complex (P) and oxoglutarate dehydrogenase complex (O). **(B)** Silver staining of a two dimensional SDS-Page gel with subunits of each complex aligned vertically. (Permission licence # 3144940036515).

In this chapter, a conventional gradient BNE/SDS-Page approach was performed to identify lacking subunits in *P. falciparum* succinate dehydrogenase and ATP synthase **(Fig. 3.11).** The major obstacle of this strategy is the isolation of mitochondria from other components of malaria parasites as well as the low expression level of some mitochondrial proteins. Several studies on mitochondrial physiology have been handicapped by the difficulty in obtaining a clean preparation with sufficient yield of mitochondrial enzymes due to the numerous internal membrane compartments, presence of hemozoin particles, or their poor expression. To adapt the BNE/SDS-Page strategy for mitochondrial proteins, an enrichment method was added in upstream. Density gradients with sucrose, Percoll® or Ficoll are common methods to isolate subcellular fractions containing mitochondria (Tran et al., 2006). Hence, a sucrose gradient centrifugation was performed on solubilised membrane proteins. Commonly used as an alternative to BNE as first dimension, cell fractionation based on sucrose gradient density allows concentration and separation of mitochondrial complexes.

To identify our proteins of interest, two identical 2D non-gradient BN/SDS-Page gels were performed from the same protein sample. Then, one gel was stained with silver whereas the other was immunoblotted with a specific polyclonal antibody against a subunit known from *P. falciparum* complex II or V. Signals obtained from the western blot are compared with spots on the silver-stained pattern in order to localize the mitochondrial complex targeted. Spots aligned on the same vertical axis are excised, digested by trypsin and analysed by NanoLC-MS/MS to be identified.

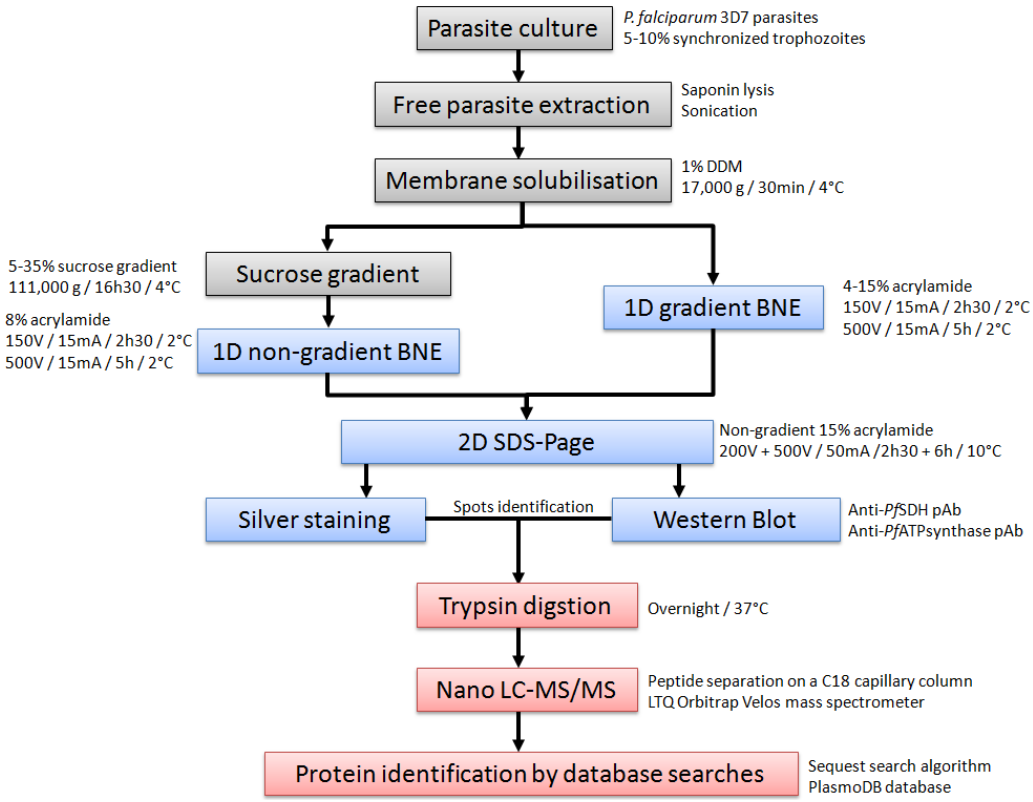

Figure 3.11 Flowchart of the proteomic approach applied for *P. falciparum* mitochondrial subunits identification. Abbreviation: pAb, polyclonal antibody.

3.2. Material & Methods

3.2.1. Bioinformatics tools

The presence of structural fingerprints in *Plasmodium* genes was determined manually from the PlasmoDB database (www.plasmodb.org). The possibility to add in a series of different structural queries with the "PlasmoDB strategy" allows filtering of the overwhelming number of encoding sequences in the *Plasmodium* genome to get only a few genes exhibiting the characteristics sought. For each structural fingerprint, the cut-off was defined by using specific bioinformatic tools and studying homologous genes from bacteria, yeast, mammal, plant and protist species **(Table 3.4)**.

Table 3.4. List of structural fingerprints chosen and bioinformatics tools used.

Filtering order	Structural fingerprint	Bioinformatic tools to determine cut-off fingerprint
1	Molecular weight	**Compute pI/Mw** (web.expasy.org/compute_pi)
2	Number of transmembrane domains	**TMHMM v2.0** (www.cbs.dtu.dk/services/TMHMM) **PSIPRED** (MENSAT3 & MENSAT-SVM options, www.bioinf.cs.ucl.ac.uk/psipred)
3	Secondary structure	**PSIPRED** (PRIPRED v3.0 option, www.bioinf.cs.ucl.ac.uk/psipred)
4	Specific motif pattern	**ClustalW2** (www.ebi.ac.uk/Tools/msa/clustalw2)
5	Protein function	**PlasmoDB description**
6	Mitochondrial signal peptide	**PlasMit** (gecco.org.chemie.uni-frankfurt.de/plasmit) **PFMPred** (www.imtech.res.in/raghava/pfmpred) **MitoProt II** (ihg.gsf.de/ihg/mitoprot.html)

3.2.2. Proteomics approach

3.2.2.1. Synthesis of anti-Sdha and anti-ATPase subunit α polyclonal antibodies

The peptide [573]AHARDDFPERDDKN[586] of the SdhA subunit (PlasmoDB entry PF3D7_1034400) was selected **(Fig. 3.12. A)**, synthesized, and used for immunization in the rabbit to generate an affinity-purified polyclonal antibody (GenScript Corp., Piscataway, NJ). In the same manner, two polyclonal antibodies were produced by targeting both peptides [520]EVEDQIKESIFQKFL[533] **(Fig. 3.12. B)** and [162]TKERRKIEIKAPGI[175] of the ATP synthase subunit α (PlasmoDB entry PF3D7_1034400) (shortly termed anti-ATPα antibodies). Rabbit anti-SdhA and anti-ATPα antibodies were lyophilized in phosphate-buffered saline (pH 7.4) with 0.02% sodium azide as preservative. Lyophilized antibodies were reconstituted with MilliQ water, and aliquots were stored at -20 °C until use.

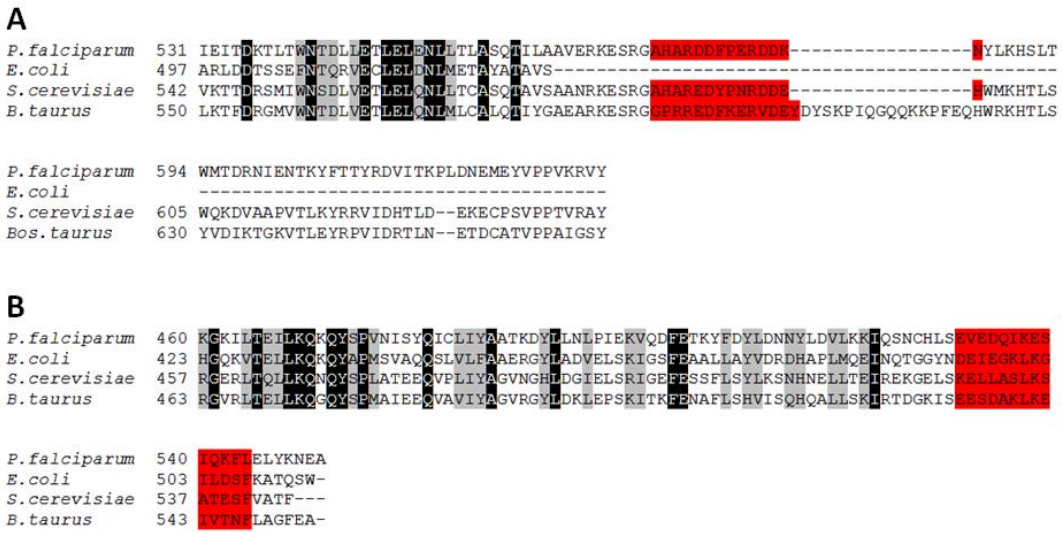

Figure 3.12. Position of the peptide chosen for polyclonal antibodies synthesis in *P. falciparum* and comparison with homologues in bacteria, yeast and bovine. (A) Sequence alignments of C-terminal section of SdhA from *P. falciparum* (PlasmoDB entry PF3D7_1034400), *E. coli* (UniprotKB entry P0AC41), *S. cerevisiae*

(Q00711) and *Bos Taurus* (**P31039**). **(B)** Sequence alignments of C-terminal section of ATP synthase subunit α from *P. falciparum* (PlasmoDB entry PF3D7_0217100), *E. coli* (UniprotKB entry P0ABB0), *S. cerevisiae* (P07251) and *Bos Taurus* (**P19483**). In red is highlighted both peptides ^{573}AHARDDFPERDDKN^{586} and ^{520}EVEDQIKESIQKFL^{533} chosen for antibody synthesis. Residues are displayed with dark boxes for full conservation and grey boxes for strong similarities.

3.2.2.2. *E. coli* crude mitochondrial membranes preparation

Wild type *Escherichia coli* cells were prepared from LB broth containing 50 µg/ml ampicillin and 25 µg/ml chloramphenicol. A 10 ml culture of bacterial cells was grown overnight at 37 °C with shaking at 200 rpm. The following day these cultures were propagated in 400 ml LB broth containing appropriate antibiotics and grown at 37°C (200 rpm shaking). The cells were harvested by centrifugation at 4,000 x *g* for 20 min. Cells were resuspended in a ice-cold buffer containing 50 mM potassium phosphate pH 7.4, 2 mM EDTA and protease inhibitors (Roche). This was followed by cell disruption using a French press at a pressure of 25,000 psi. The cell lysate was centrifuged at 4,000 x *g* for 20 min at 4°C to remove unbroken cells. Membranes were recovered from the supernatant after ultracentrifugation during 1 h at 100,000 x g and 4°C. The membranes were resuspended in 500 µl of ice-cold buffer with 50 mM KPi pH 7.4, 2 mM EDTA and protease inhibitors. Membranes were aliquoted and stored at -80°C.

3.2.2.3. Immunoprecipitation and immunobloting

For immunoprecipitation studies, *E. coli* membrane proteins were boiled (5 min at 95 °C) in denaturing lysis buffer (50 mMTris-HCl, 5 mM EDTA, 2% (w/v) SDS, 10 mM DTT) and diluted (10-fold) with non-denaturing lysis buffer (50 mM Tris-HCl, 150 mM NaCl, 1 mM EDTA, 1% (v/v) Triton X-100, pH 7.5). Following centrifugation (17,000 x *g* for 30 min), denatured proteins were collected in the supernatant and incubated overnight with 2 µg of anti-SdhA antibody, rotating at 4°C, followed by 50 µl of protein A-sepharose slurry for 3 h at 4 °C. Immunoprecipitates were washed, gently eluted with an acidic buffer (pH 2.8), and then separated by 7.5% (w/v) SDS-Page gel electrophoresis before proceeding to immunoblotting with the anti-SdhA polyclonal antibody as primary incubation as described in General Material & Methods (section 2.6 and 2.7).

3.2.2.4. Sucrose gradient density centrifugation

Parasite membrane proteins and bovine mitochondrial membranes were centrifuged 30 min at 17,000 x g and 4°C. Both pellets obtained were resuspended in ice-cold sucrose gradient buffer (50 mM Tris-HCl, 1 mM EDTA, 0.05% dodecyl-β-D-maltoside, pH 7.5) and solubilised with 1% dodecyl-β-D-maltoside for 30 min on ice with frequent mixing. Samples were centrifuged 30 min at 17,000 x g and 4°C. Supernatants were subjected to sucrose gradient centrifugation. The gradient consisted of 1.5 ml step-fractions of 35%, 32.5%, 30%, 27.5%, 25%, 22.5%, 20%, 17.5%, 15%, 12.5% 10%, (7.5%)

and 5% sucrose in ice-cold sucrose gradient buffer. 1.5 ml of solubilised membranes (supernatants) from beef heart or parasites were loaded onto the gradient and centrifuged at 100,000 x g for 16h30 at 4°C. The gradient was collected from the top in 1.5 ml fractions. In order to localize the presence of complex II in sucrose density fractions, they were assessed by 7.5% SDS-Page and Western analysis using an anti-SdhA primary antibody as described in Material & Methods (section 2.6 and 2.7).

3.2.2.5. First dimension blue native electrophoresis (BNE)

Fractions enriched in complex II were pooled and concentrated within 50 kDa cutoff Amicon centrifugal concentrators (Millipore, USA) and brought up to a final volume of 200 µl with 0.5% dodecyl-β-D-maltoside in BN sample buffer (50 mM imidazole, 50 mM NaCl, 2 mM 6-aminocaproic acid, 1 mM EDTA, pH 7.0). The protein sample concentration was determined using Bradford assays as described in General Material & Methods (section 2.2). Finally, 2.5 µl 5% Coomassie in 500 mM 6-aminocaproic acid pH 7.0 was added per 50 µg of membrane proteins. BNE were cast and performed according to published protocols (Swamy, 2006; Wittig et al., 2006). A stock solution containing 48% (w/v) acrylamide and 1.5% (w/v) bisacrylamide was prepared in deionized distilled water, filtered and used for both stacking and resolving gels. BNE resolving gels were cast in a large format (0.10 x 14 x 14 cm) with a 4-15% acrylamide gradient for only solubilised membranes supernatant or an 8% non-gradient uniform acrylamide concentration for enriched complex II preparation. Gel buffer was comprised of 500 mM 6-aminocaproic acid and 25 mM imidazole, pH 7.0. The final concentration of the stacking gel was 4% and BNE gels were stored at 4°C overnight. BNE were performed at 2-4°C by using a Hoefer® SE600 Cooled Vertical Electrophoresis Unit. Cathode buffer contained 50 mM Tricine, 7.5 mM imidazole, 0.02% coomassie blue G-250 (w/v) and 2 mM 6-aminocaproic acid, pH 7.0 while anode buffer contained only 25 mM imidazole, pH 7.0. Between 40 to 60 µg of membrane proteins were loaded. Gel was run at 150 V / 15 mA until the front line had crossed one-third of the gel, where the cathode buffer was replaced by one with only 0.002% coomassie blue G-250. Gel running was then continued at 500 V / 15 mA until complete.

3.2.2.6. Second dimension SDS-Page

For a second dimension SDS-Page, individual lanes of the first dimension gel were excised with a razor blade and incubated 1 h at 37°C with 2X loading buffer (0.125M Tris-HCl pH 6.8, 4% SDS, 20% glycerol, 0.02% Bromophenol blue, 10% 2-mercaptoethanol). The BN-Page gel strips were then rinsed briefly with SDS-Page running buffer (25 mM Tris, 0.192 mM Glycine, 0.1% SDS, pH 8.8). SDS-Page resolving gels were performed using 15% non-gradient acrylamide. The excised lanes were then placed into the top of the resolving gel (0.15 x 14 x 14 cm) and sealed with 4% stacking gel solution. A pre-stained broad range protein marker (Spectra™ Multicolor Broad Range Protein Ladder, Thermo

Scientific, USA) was loaded alongside the strip. Electrophoresis was performed at 10°C with SDS-Page running buffer at 200 V / 50 mA until the front passed into the separation gel and then continued at 500 V / 50 mA. Two identical SDS-Page were performed with two identical BNE strips from bovine mitochondrial membranes or parasite membrane proteins. One 2D gel was visualized using a standard silver staining protocol (see General Material & Methods, section 2.6.4) while the other was used for immunoblotting. For 2D immunoblots, 2D gels were transferred electrophoretically to Hybond ECL nitrocellulose (Amersham GE Healthcare, UK) using a Biorad® Trans-Blot Cell (Biorad Laboratories, USA) for 3 h at 400 mA and 4°C. Blocking and antibody incubation was carried out as described in General and Methods (section 2.7.2). For SdhA immunobloting, the customized anti-SdhA antibody described in this chapter was used. For bc_1 rieske subunit, another customized polyclonal antibody was used described in Chapter 6 (section 6.2.1). For SdhB and ATP synthase subunit α, the commercial monoclonal antibodies ab14714 and ab110273 (Abcam, UK), only specific to bovine proteins, were used respectively.

3.2.2.7. In-gel trypsin digestion, mass spectrometry and database searches

For immunoprecipitation procedure, protein spots corresponding to the signal from the anti-SdhA immunoblot were excised on the silver-stained SDS-Page. For 2D gels, proteins spots located on the same vertical that signals obtained with specific primary antibodies were excised on the similar silver-stained 2D SDS-Page.

Each sample was reduced with 10 mM DTT at 56 °C for 30 min and alkylated with 55 mM iodoacetamide at 37 °C for 30 min. Proteins contained within these gel spots were proteolyzed by addition of 190 ng of sequencing grade trypsin (Sigma) and incubated overnight at 37 °C. The resulting tryptic peptides were then dried and rehydrated in 5% (v/v) formic acid in 50% (v/v) acetonitrile. NanoLC-MS/MS analyses were performed on a Dual Gradient Ultimate 3000 chromatographic system (Dionex). A 20 µl aliquot of sample was placed into a well on a 96-well plate, of which 10 µl of sample was injected onto a C18 pre-column (Acclaim PepMap C18; 2-cm length x 100-µm inner diameter x 5-µm particle size; 100 Å porosity; Dionex). After desalting for 6 min with buffer A (water/acetonitrile/formic acid, 97.5/2.5/0.1 v/v/v) peptide separation was carried out on a C18 capillary column (Acclaim PepMap C18; 15-cm length x 75-µm inner diameter x 2-µm particle size; 100 Å porosity; Dionex) with a gradient method starting at 100% buffer A, ramping up to 50% buffer B (water/acetonitrile/formic acid, 10/90/0.1 v/v/v) over 90 min. This was then increased to 100% buffer B over 0.1 min, which was then held at 100% buffer B for 10 min. Finally, this was decreased to 0% over 0.1 min, and buffer A was increased to 100%. The column was finally re-equilibrated with 100% buffer A for 15 min. The LC eluent was nano-sprayed into the MS instrument with a glass emitter tip (Pico-tip, FS360–50-15-CE-20-C10.5; New Objective Woburn). The LTQ

Orbitrap Velos mass spectrometer (Thermo Fisher Scientific, Germany) was operated in positive ionization mode. Raw data files were processed using the software Proteome Discoverer 1.0.0 (Thermo Fisher Scientific, Germany) incorporating Sequest search algorithm. The proteins were identified by screening LC-MS sequence data against a PlasmoDB database (version 8.0). A parent mass tolerance of 1.5 Da and fragment mass tolerance of 1 Da were used, allowing for one missed cleavage. Carbamidomethylation of cysteine and oxidation of methionine were the fixed and variable modifications, respectively.

3.3. Results

3.3.1. Candidate gene identification for subunits SdhC and SdhD

First, the molecular weight (MW) of each complex II anchor subunits was estimated. Previous proteomic studies have predicted a size for each subunit between 13 to 20 kDa in *P. falciparum* and *P. yoelii yoelii* **(Table 3.5).** The theoretical MW from homologue subunits in nineteen diverse species were calculated and determined to be between 9 and 22 kDa **(Tables 3.6 and 3.7)**. Thus, a cut-off of 9 to 25 kDa for the molecular weight of each subunit has been arbitrarily determined.

Table 3.5. Molecular weight of four complex II subunits experimentally estimated and bioinformatically predicted (PlasmoDB) for *P. falciparum* and *P. yoelii yoelii*.

Complex II	Suraveratum et al., 1999 (*P. falciparum*)	Kawahara et al., 2008 (*P. yoelii yoelii*)	PlasmoDB prediction (*P. falciparum*)	PlasmoDB prediction (*P. yoelli yoelli*)
Whole Complex	90 ± 8kDa	135 kDa	-	-
Subunit *a* (SdhA)	55 ± 6 kDa	70 kDa	70696 Da	70327 Da
Subunit *b* (SdhB)	35 ± 4 kDa	35 kDa	37752 Da	37655 Da
Subunit *c* (SdhC)	15-20 kDa	16 kDa	-	-
Subunit *d* (SdhD)	13-16 kDa	14kDa	-	-

Subsequently, the number of transmembrane domains (TMs) was predicted from homologue genes and shown to be between 1 to 3 TMs depending on the prediction algorithm used **(Tables 3.6 and 3.7)**. In consequence, a cut-off of 1 to 3 TMs was chosen. The secondary structure profile was also estimated from the same set of ShdC and SdhD homologues **(Tables 3.6 and 3.7)**. Both subunits are mainly helical with 40 to 85% α-helix for SdhC and 28 to 85% for SdhD, as well as less than 15 and 22% β-strands, respectively. This observation is confirmed by the complex II X-ray structure obtained from *E. coli, G. gallus* and *S. scrofa* showing three transmembrane α-helices per subunit (Huang et al., 2006; Sun F Fau - Huo et al.; Yankovskaya et al., 2003). The part of coil secondary structure is variable with a percentage from 15 to 48% in SdhC and from 10 to 66% for SdhD.

Table 3.6. Structural fingerprints (molecular weight, number of transmembrane domains and secondary structure profile) of SdhC in 19 species representing five different kingdoms.

			Molecular weight		Transmembrane domains				Secondary structure		
	Organisms	**UniPort Acc #**	**Length**	**MW (kDa)**	**PDB**	**THMMH**	**M-SVM**	**M-V3**	**% α-helix**	**% β-strand**	**% Coil**
Animals	*Homo sapiens*	Q99643	169	18.6	-	3	3	3	76.3	0.0	23.7
	Mus musculus	Q9CZB0	169	18.4	-	3	3	3	76.3	0.0	23.7
	Gallus gallus	D0VWW3	140	15.4	3	3	3	3	74.3	0.0	25.7
	Sus scrofa	D0VWV4	169	18.5	3	3	3	3	39.3	0.0	12.2
	Drosophila menalogaster	Q9VGS3	171	18.5	-	3	3	3	67.3	0.0	32.7
	Xenopus tropicalis	A9UM72	167	18.5	-	3	3	3	76.9	0.0	23.1
	Ascaris suum	P92506	188	21.1	-	3	3	3	67.6	0.0	32.4
Protozoans	*Reclinomonas americana*	P80481	144	16.7	-	3	3	3	77.1	0.0	22.9
	Dictyostelium discoideum	Q8T2T5	192	21.4	-	2	3	3	63.5	0.0	36.5
	Cyanidioschyzon merolae	Q9ZZR3	137	16.7	-	3	3	3	81.0	0.0	19.0
	Trypanosoma cruzi	Q4D4V5	106	12.2	-	1	1	1	45.3	11.3	43.4
	Leishmania major	Q4Q708	104	11.8	-	1	1	1	48.1	11.5	40.4
Yeast	*Alternaria alternata*	B8XSR3	177	19.6	-	3	3	3	74.0	0.0	26.0
	Saccharomyces cerevisiae	P33421	198	22	-	3	3	3	72.7	0.0	27.3
Plants	*Nicotiana tabacum*	Q5M9U9	108	12.6	-	2	3	2	73.1	0.0	26.9
	Chlamydomonas reinhardtii	A8HPU2	203	21.7	-	2	3	3	57.6	1.0	41.4
Bacteria	*Escherichia coli*	P69054	129	14.3	3	3	3	3	76.7	0.0	23.3
	Enterobacter cloacae	D5CHF2	159	17.8	-	3	3	3	67.9	0.0	32.1
	Paracoccus denitrificans	Q59659	130	14.3	-	3	3	3	77.7	0.0	22.3
Minimum			**106**	**12.2**		**1**	**1**	**1**	**45.3**	**0.0**	**19.0**
Maximum			**213**	**22**		**3**	**3**	**3**	**81.0**	**11.5**	**43.4**

Table 3.7. Structural fingerprints (molecular weight, number of transmembrane domains and secondary structure profile) of SdhD in 19 species representing five different kingdoms.

			Molecular weight		Transmembrane domains				Secondary structure		
	Organisms	UniPort Acc #	Length	MW (kDa)	PDB	THMMH	M-SVM	M-V3	% α-helix	% β-strand	% Coil
Animals	*Homo sapiens*	O14521	159	17.0	-	3	3	3	48.4	6.3	45.3
	Mus musculus	Q9CXV1	159	17.0	-	2	3	3	49.1	5.7	45.3
	Gallus gallus	Q5ZIS0	157	16.4	3	2	3	3	52.9	5.1	42.0
	Sus scrofa	A5GZW8	159	17.0	3	3	3	3	47.2	6.9	45.9
	Drosophila menalogaster	Q9VCI5	182	19.3	-	2	3	2	51.6	5.5	42.9
	Xenopus tropicalis	Q6P355	152	16.4	-	2	3	3	53.9	5.3	40.8
	Ascaris suum	Q8WSR2	141	15.7	-	3	3	3	52.5	5.7%	41.8
Protozoans	*Reclinomonas americana*	P80482	120	14.2	-	3	3	3	68.3	3.3	28.3
	Dictyostelium discoideum	Q54YN1	179	19.1	-	3	3	3	33.0	5.6	61.5
	Cyanidioschyzon merolae	Q9ZZN2	79	9.6	-	2	2	1	78.5	6.3	15.2
	Trypanosoma cruzi	Q4D1F3	127	13.9	-	2	2	2	55.9	17.3	26.8
	Leishmania major	Q4Q474	147	15.7	-	2	2	2	51.4	13.3	35.3
Yeast	*Alternaria alternata*	B8XSR4	193	21.1	-	1	3	2	60.6	6.7	32.6
	Saccharomyces cerevisiae	P37298	181	20.2	-	2	3	2	51.9	5.0	43.1
Plants	*Nicotiana tabacum*	Q5M9V6	125	14.6	-	3	3	2	72.0	2.4	25.6
	Chlamydomonas reinhardtii	A8HPU1	87	9.3	-	2	1	2	35.6	3.4	60.9
Bacteria	*Escherichia coli*	P0AC44	115	12.8	3	3	3	3	80.0	0.0	20.0
	Enterobacter cloacae	D5CHF1	115	12.8	-	3	3	3	80.0	0.0	20.0
	Paracoccus denitrificans	Q59660	129	13.9	-	3	3	3	68.2	3.9	27.9
Minimum			**79**	**9.3**		**1**	**1**	**1**	**33.0**	**0.0**	**15.2**
Maximum			**226**	**21.1**		**3**	**3**	**3**	**80.0**	**17.3**	**61.5**

Highly conserved residues were identified by amino acid sequence alignment of 19 homologues and subunit-specific motifs were determined. At first sight, alignments confirmed the high divergence of those subunits across species with only a few residues conserved. The role of each residue conserved could be determined by studying the crystal structures of complex II. For SdhC, the arginine residue R_{31} (in *E. coli* sequence annotation) is fully conserved and forms a salt bridge with a heme *b* propionate moiety. This residue is also involved in the ubiquinone binding site by interacting with the conserved tyrosine Y_{83} of SdhD **(Fig. 3.13 and 3.15)**. The serine residue S_{27}, (replaced by another nucleophilic residue threonine in protozoan *Leishmania* and *Trypanosoma*) is also conserved by contributing to the formation of a hydrophobic environment surrounding the quinone-binding pocket. Finally, the histidine residue H_{84} (replaced by an aspartate in *Leishmania* and *Trypanosoma* species) plays an important role by participating in heme *b* axial ligation. Thus, "[ST]x_3R$x_{45\text{-}70}$[HD]" was identified as a specific motif for the subunit *c.*

For SdhD, the histidine H_{71} (replaced by a tyrosine in yeast) is an essential residue for stabilizing heme *b* into the enzyme **(Fig. 3.14 and 3.15)**. Moreover, two residues, aspartate D_{82} and tyrosine Y_{83}, are fully conserved due to their key role in the quinone binding site. Thus, the conserved motif "[YH]x_{10}DY" was determined for SdhD.

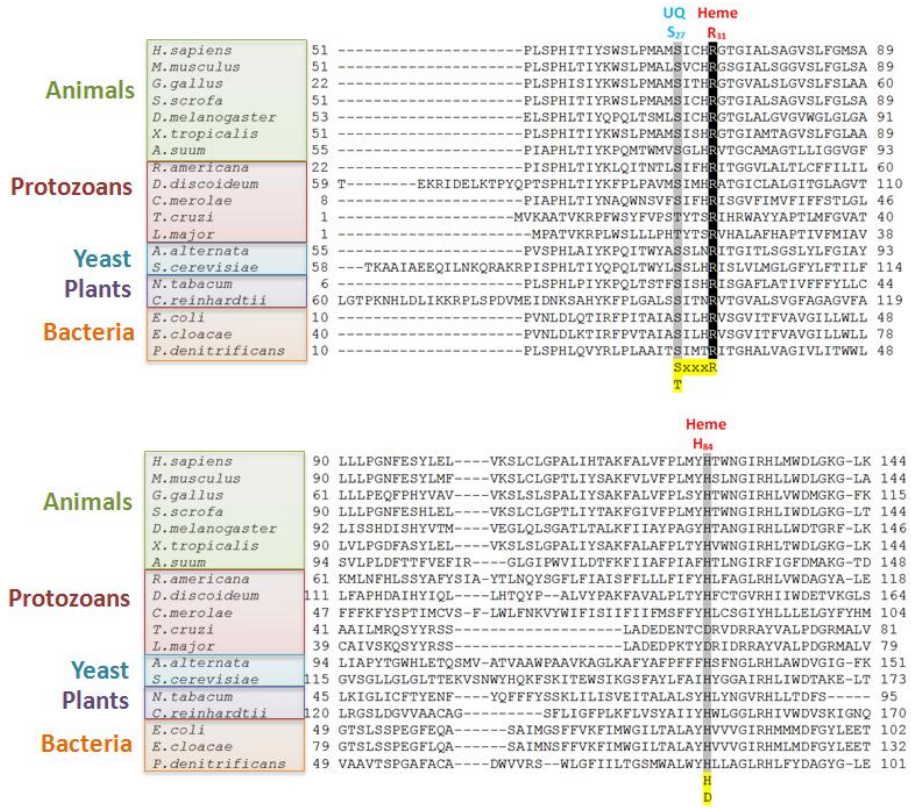

Figure 3.13. Alignment of partial SdhC sequences from 19 species. The sequences were aligned with ClustalW2 (www.ebi.ac.uk/Tools/msa/clustalw2). Residues are displayed with dark boxes for full conservation and grey boxes for strong similarities. In yellow are highlighted residues used for the SdhC motif pattern.

Figure 3.14. Alignment of partial SdhD sequences from 19 species. The sequences were aligned with ClustalW2 (www.ebi.ac.uk/Tools/msa/clustalw2). Residues are displayed with dark boxes for full conservation and grey boxes for strong similarities. In yellow are highlighted residues used for the SdhD motif pattern.

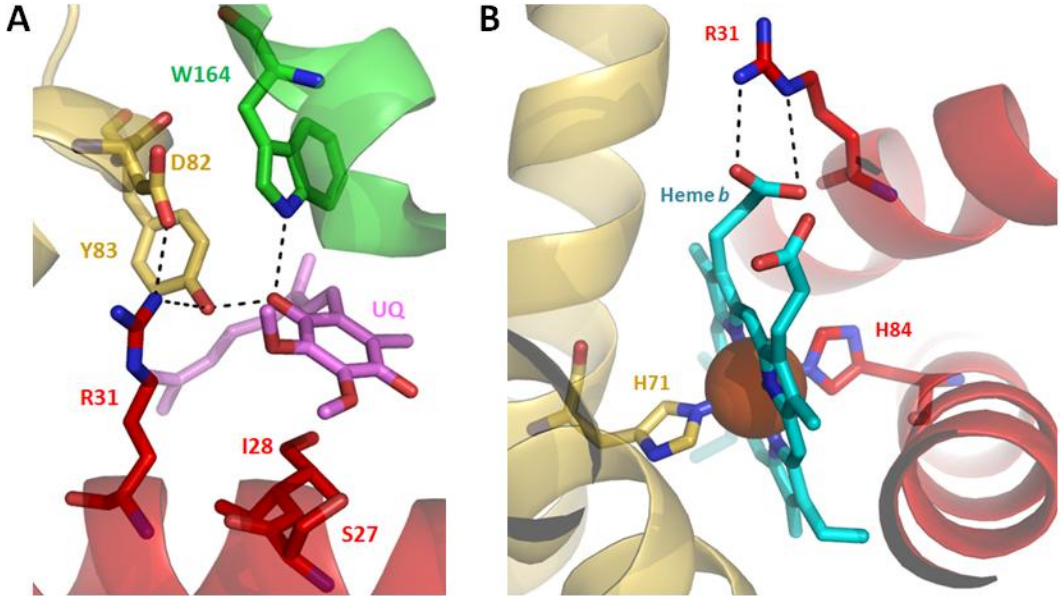

Figure 3.15. Interactions for ubiquinone-binding and heme *b* ligation in *E. coli* complex II. (A) Residues involved in ubiquinone (UQ, pink) binding are shown in stick and polar interactions are indicated with black dots. Transmembrane helices of SdhB, SdhC and SdhD are coloured in green, red, yellow, respectively. **(B)** Both histidine residues for heme *b* ligation are displayed in sticks. Polar interactions between the arginine residue and heme *b* molecule are displayed by black dots. PDB entry 1NEK.

Among 5538 *P. falciparum* genes annotated in the PlasmoDB database, 16.7% of them were shown to have the molecular weight searched and 4.0% of them displayed a number of transmembrane domains between one and three **(Table 3.8)**. Afterwards, the secondary structure profile and presence of conserved sequence motifs allowed identifyication of 18 and 5 genes with unknown functions for SdhC and SdhD, respectively. By using three different algorithms, the presence of a mitochondrial signal peptide at their N-terminal section was predicted. Five putative

genes for SdhC and two for SdhD displayed a mitochondrial peptide predicted by at least one algorithm **(Table 3.9)**.

Table 3.8. Filtering of PlasmoDB annotated genes via successive SdhC- and SdhD-specific structural fingerprints. Abbreviations: PlasMit (PM), PFMPred (PP) and MitoProt II (MP).

	Subunit *c* (SdhC, CybL)		Subunit *d* (SdhD, CybS)	
Type of filtering	Value of filtering	**Genes**	Value of filtering	**Genes**
Molecular weight	9 - 25 kDa	**925**	9 - 25 kDa	**925**
Number of transmembrane domains	1 - 3	**221**	1 - 3	**221**
Secondary structure	%Helix: 40% - 85% %Strand: 0% - 15% %Coil : 15% - 48%	**99**	%Helix: 28% - 85% %Strand: 0% - 22% %Coil : 10% - 66%	**167**
Motif pattern	$[ST]x_3Rx_{45\text{-}70}[HD]$	**27**	$[YH]X_{10}DY$	**7**
Protein function	Unknown	**18**	Unknown	**5**
Mitochondrial signal peptide	PM (strict score) PP > 0.5 MP > 0.5	**5**	PM (strict score) PP > 0.5 MP > 0.5	**2**
Candidate gene	Manually	**1**	Manually	**1**

Table 3.9. Prediction of mitochondrial signal peptide for SdhC and SdhD gene candidates. Three different webservers are used for prediction: PlasMit (PM, strict cut-off), PFMPred (PP, cut-off > 0.5) and MitoProt II (cut-off > 0.5). Abbreviation: CG, our final candidate gene.

	PlasmoDB entry	Function	MW (kDa)	PM	PP	MP	CG
SdhC	PF3D7_1371900	Plasmodium exported protein, unknown function	23.6	No	No	Yes	
	PF3D7_1476100	transcribed membrane protein 14.2	20.7	No	No	No	
	PF3D7_1310200	conserved Plasmodium protein, unknown function	16.7	No	No	No	
	PF3D7_0702400	conserved Plasmodium protein, unknown function	14.1	No	No	No	
	PF3D7_1303000	conserved Plasmodium protein, unknown function	13.7	Yes	Yes	Yes	
	PF3D7_1362300	conserved protein, unknown function	22.0	No	No	No	
	PF3D7_1243200	conserved Plasmodium protein, unknown function	9.8	No	No	No	
	PF3D7_0107400	hypothetical protein conserved in P. falciparum	18.7	No	No	No	
	PF3D7_0310800	conserved Plasmodium protein, unknown function	12.7	No	No	No	
	PF3D7_0506400	conserved Plasmodium protein, unknown function	14.0	No	No	No	
	PF3D7_1301900	Plasmodium exported protein, unknown function	15.1	No	Yes	Yes	
	PF3D7_1319800	probable protein, unknown function	16.7	No	No	No	
	PF3D7_0112100	conserved Plasmodium protein, unknown function	19.2	No	No	No	
	PF3D7_1223000	conserved Plasmodium protein, unknown function	16.0	No	No	Yes	
	PF3D7_0220200	Plasmodium exported protein, unknown function	21.4	No	No	No	
	PF3D7_1212600.2	conserved Plasmodium protein, unknown function	11.1	No	Yes	No	X
	PF3D7_1239300	conserved Plasmodium protein, unknown function	24.2	No	No	No	
	PF3D7_1356500	conserved Plasmodium protein, unknown function	22.8	Yes	Yes	Yes	
SdhD	PF3D7_0515200	conserved Plasmodium protein, unknown function	17.0	No	No	No	
	PF3D7_0611100	succinate dehydrogenase subunit 3, putative (SDH3)	9.5	Yes	Yes	Yes	X
	PF3D7_1317500	conserved Plasmodium protein, unknown function	10.4	No	No	No	
	PF3D7_1325600	conserved Plasmodium protein, unknown function	16.1	No	No	No	
	PF3D7_1458200	conserved Plasmodium protein, unknown function	13.4	No	Yes	No	

Subsequently, each gene predicted from mitochondria was analysed manually. A potential candidate for subunits *c* (PF3D7_1212600.2) and *d* (PF3D7_0611100) were identified with three and two putative transmembrane helices, respectively. Their sequence identities against counterparts in *H. sapiens* and *E. coli* are 9.0% and 4.0% for PF3D7_1212600.2 respectively, and 4.0% and 8.0% for PF3D7_0611100 respectively. It confirms the high divergence of these subunits with other mitochondrial homologues. Orthologs of both candidate genes are present in others *Plasmodium* species such as *P. vivax*, *P. chabaudi*, *P. knowlesi* or *P. berghei*.

For PF3D7_1212600.2, the motif Sx_3R, essential for ubiquinone and heme *b* binding, is located near the N-terminal region **(Fig. 3.16)**. However, this motif is not predicted to be in the first transmembrane helix of SdhC subunits in other species, but in the hydrophilic N-terminal tail as per SdhC in *Trypanosoma* and *Leishmania* spp.. Additionally, the conserved histidine residue (H_{84}) is substituted with a tyrosine located in the second transmembrane helix.

The SdhD candidate gene PF3D7_0611100 contains the conserved motif $Yx_{10}DY$ which is partially included in the second transmembrane domain (TM) **(Fig. 3.17)**. In *E. coli*, the motif is located at the second TM extremity to interact with ubiquinone. Maybe due to limitations in prediction accuracy, residues D and Y in *P. falciparum* are not localized into the second TM. Like in *S. cerevisiae*, the heme ligand histidine (H_{71}) is substituted by a tyrosine residue in the malaria parasite. The encoded gene PF3D7_0611100 has been suggested by Mogi and Kita to be the best candidate for SdhC subunit (Mogi and Kita, 2009) whereas this work identifies it as a gene candidate for SdhD. Using similar filtering based on structural fingerprints, Kita and Mogi identified the motif Sx_2HF in *P. falciparum* and Sx_2HY in other *Plasmodium* spp. as a substituted of the $H/Yx_{10}DY$ pattern.

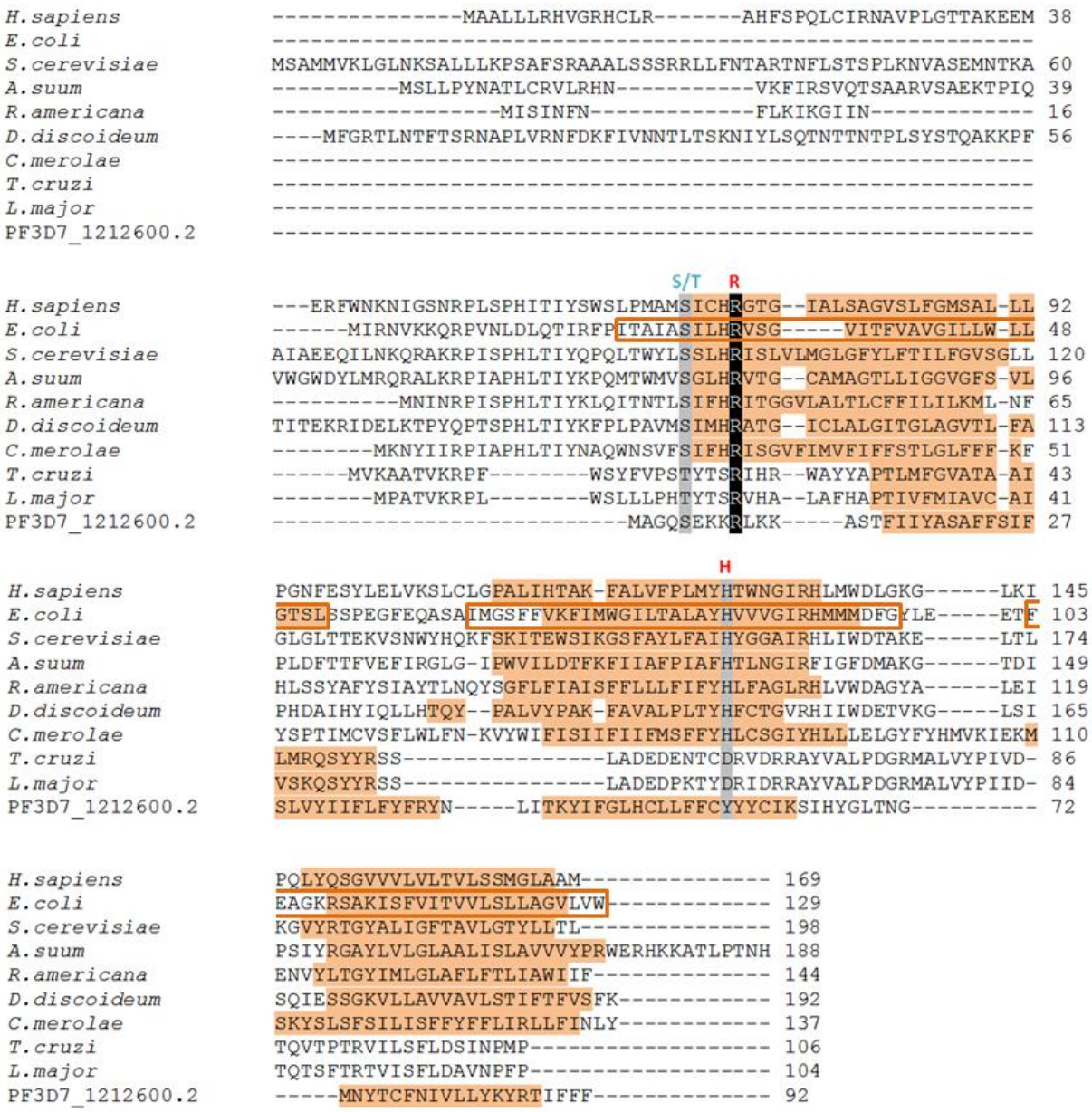

Figure 3.16. Sequence alignment of the candidate gene PF3D7_1212600.2 with SdhC homologues in other species. Transmembrane regions predicted are highlighted in orange. Transmembrane helices found in *E. coli* SdhC from the crystal structure are boxed in orange (PDB entry 1NEK). Residues are displayed with dark boxes for full conservation and grey boxes for strong similarities.

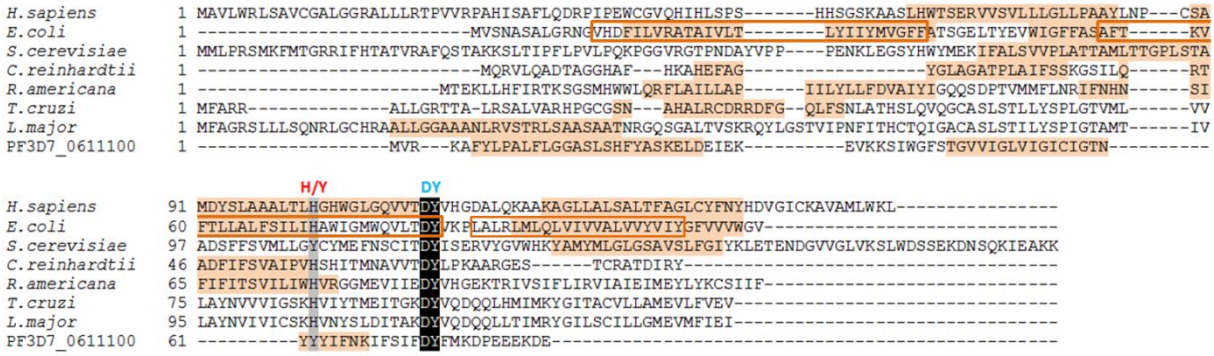

Figure 3.17. Sequence alignment of the candidate gene PF3D7_0611100 with SdhD homologues in other species. Transmembrane regions predicted are highlighted in orange. Transmembrane helices found in *E. coli* SdhD from the crystal structure are boxed in orange (PDB entry 1NEK). Residues are displayed with dark boxes for full conservation and grey boxes for strong similarities.

3.3.2. Candidate gene identification for ATP synthase subunits *a* and *b*

To identify ATP synthase subunits *a* and *b*, a similar *in silico* approach was applied. Structural fingerprints were established with 19 ATPase subunits *a* from diverse species and 15 eukaryotic subunits *b* **(Tables 3.10 and 3.11).**

The high number of transmembrane segments is a specific feature of the subunit *a* across species. In the *P. falciparum* genome, only 96 encoded genes are predicted to exhibit between 4 and 8 TMs with a molecular weight comprised between 20 to 45 kDa. Among them, genes with high helical secondary structure (> 52% helices) were filtered. On the other hand, the subunit *b* contains a single or two TM α-helices localized into the N-terminal section in order to anchor to the lipid bilayer. The 15 secondary structure predictions of subunit *b* selected have shown α-helical predominance which is consistent with the bovine subunit *b* crystal structure almost entirely composed of an extended α-helix. Therefore, genes with a molecular mass between 15 to 41 kDa as well as a helical percentage comprised between 38 and 95% were selected. Through three structural fingerprints (molecular weight, number of TMs and secondary structure profile), 0.4% and 5.9% of encoded proteins were selected for subunit *a* and *b* respectively.

For ATP synthase subunit *a,* a specific motif was identified by sequence alignment of the 19 references **(Fig. 3.18)**. It shows that arginine R_{210} is fully conserved across species. As described previously, the residue R_{210} has an essential role to coordinate protonation and deprotonation events by interacting with the aspartic acid D_{61} of each subunit *c* composing the ring **(Fig. 3.19)**. Thus, [AVFPMILW]R[AVFPMILW] was established as a subunit *a* motif with a residue arginine surrounded by two small amino acids. Mutants lacking the conserved arginine R_{210} were shown to not synthesize

ATP at significant rates (Ishmukhametov et al., 2008). Moreover, the fully conserved glutamine residue Q_{252}, located further downstream of R_{210}, may have a role into the proton translocation pathway. To confirm Q_{252} as a key component, Hatch *et al*. showed the maintenance of a functional rotary mechanism for F_0 by switching the conserved residues R_{210} and Q_{252} in a double mutant (Hatch et al., 1995). Unfortunately, no residue was fully conserved and thus no clear motif could be identified for the subunit *b* due to high sequence divergence across species.

Table 3.10. Structural fingerprints (molecular weight, number of transmembrane domains and secondary structure profile) of ATP synthase subunit *a* in 19 species representing five different kingdoms.

			Molecular weight		Transmembrane domains			Secondary structure		
	Organisms	**UniPort Acc #**	**Length**	**MW (kDa)**	**THMMH**	**M-SVM**	**M-V3**	**%Helix**	**%Strand**	**%Coil**
Animals	*Homo sapiens*	P00846	226	24.8	6	5	6	73.0%	0.0%	27.0%
	Mus musculus	Q3V2U3	226	25.1	6	5	6	72.6%	0.0%	27.4%
	Gallus gallus	E5DF83	227	24.8	6	5	6	68.3%	0.0%	31.7%
	Sus scrofa	B6EDK0	226	25.0	5	5	6	73.5%	0.0%	26.5%
	Drosophila menalogaster	P00850	224	25.2	6	4	6	74.1%	0.0%	25.9%
	Xenopus laevis	P00849	226	24.9	6	4	6	74.8%	0.0%	25.2%
	Ascaris suum	P24876	199	23.0	5	7	6	78.4%	2.5%	19.1%
Protozoans	*Reclinomonas americana*	O21289	249	27.4	7	7	8	73.1%	0.0%	26.9%
	Dictyostelium discoideum	Q27559	244	27.8	7	6	8	73.0%	0.0%	27.0%
	Cyanidioschyzon merolae	Q9ZZP8	255	28.9	6	7	8	71.4%	0.8%	27.8%
	Trypanosoma brucei	P24499	229	28.3	7	7	7	96.9%	0.0%	3.1%
	Leishmania tarentolae	Q33561	232	28.4	7	7	8	94.4%	0.9%	4.7%
Yeast	*Candida albicans*	Q9B8D4	246	26.5	7	8	8	72.8%	0.0%	27.2%
	Saccharomyces cerevisiae	P00854	256	29.1	6	6	8	72.2%	0.0%	27.8%
Plants	*Nicotiana tabacum*	Q5MA53	382	42.2	7	7	6	59.9%	1.0%	39.0%
	Chlamydomonas reinhardtii	Q8H2C1	340	35.4	5	6	8	57.1%	0.0%	42.9%
Bacteria	*Escherichia coli*	P0AB98	271	30.3	5	6	5	68.6%	1.5%	29.9%
	Enterobacter cloacae	D6DPP5	271	30.5	5	6	5	69.4%	1.1%	29.5%
	Paracoccus denitrificans	A1B619	248	26.7	6	6	7	69.8%	0.0%	30.2%
Minimum			**199**	**23.0**	**5**	**5**	**5**	**57.1%**	**0.0%**	**3.1%**
Maximum			**382**	**42.2**	**7**	**8**	**8**	**96.9%**	**2.5%**	**42.9%**

Table 3.11. Structural fingerprints (molecular weight, number of transmembrane domains and secondary structure profile) of ATP synthase subunit *b* in 15 eukaryotic species.

			Molecular weight		Transmembrane domains			Secondary structure		
	Organisms	**UniPort Acc #**	**Length**	**MW (kDa)**	**THMMH**	**M-SVM**	**M-V3**	**%Helix**	**%Strand**	**%Coil**
Animals	*Homo sapiens*	P24539	256	28.9	2	2	1	70.3%	2.0%	27.7%
	Mus musculus	Q5I0W0	256	28.9	2	2	1	72.2%	1.5%	26.3%
	Gallus gallus	F1NSC1	228	25.9	2	2	2	75.9%	2.2%	21.9%
	Sus scrofa	F1SBN7	256	28.6	2	2	1	73.0%	2.0%	25.0%
	Bos taurus	P13619	258	28.8	2	2	1	72.7%	1.6%	25.8%
	Xenopus laevis	Q9IAJ7	250	28.2	2	2	1	73.6%	2.0%	24.4%
	Ascaris suum	F1L7V5	315	36.8	2	2	2	55.2%	3.5%	41.3%
Protozoans	*Reclinomonas americana*	O21290	197	22.4	2	1	2	89.3%	2.0%	8.6%
	Dictyostelium discoideum	A9CLV8	137	14.9	1	1	1	43.8%	13.9%	42.3%
	Cyanidioschyzon merolae	Q9ZZQ7	171	20.1	1	1	1	72.5%	6.4%	21.1%
	Trypanosoma brucei	Q57ZP0	188	21.2	1	1	1	51.6%	4.8%	43.6%
	Leishmania major	Q4QFF2	187	21.3	1	1	1	54.0%	3.2%	42.8%
Yeast Plants	*Candida albicans*	Q59ZE0	233	25.8	2	2	2	77.3%	2.1%	20.6%
	Saccharomyces cerevisiae	P05626	244	26.9	2	2	1	74.6%	2.0%	23.4%
	Schizosaccharomyces pombe	O94373	244	26.7	1	2	1	76.2%	2.0%	21.7%
Minimum			**137**	**20.1**	**1**	**1**	**1**	**43.8%**	**1.5%**	**8.6%**
Maximum			**315**	**36.8**	**2**	**2**	**2**	**89.3%**	**13.9%**	**43.6%**

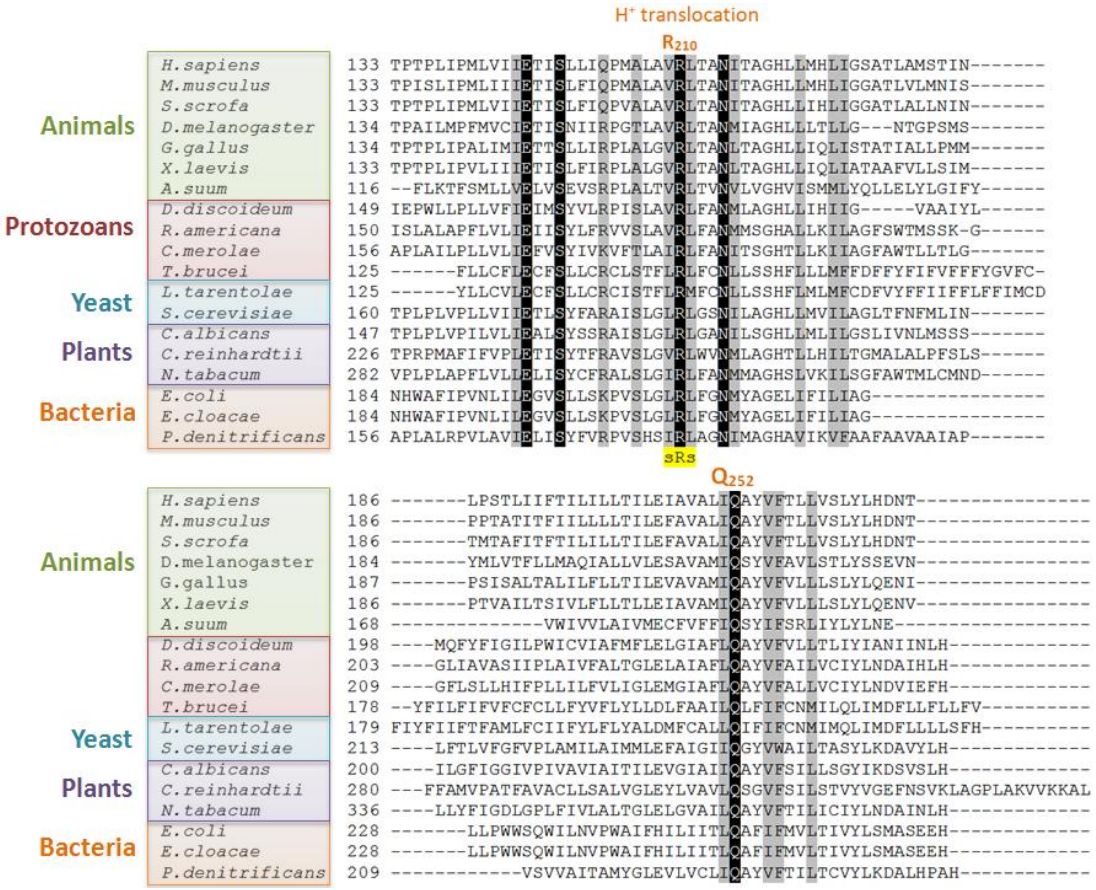

Figure 3.18. Alignment of C-terminal sections from ATP synthase subunits *a* from 19 species. The sequences were aligned with ClustalW2 (www.ebi.ac.uk/Tools/msa/clustalw2). Residues are displayed with dark boxes for full conservation and grey boxes for strong similarities. In yellow are highlighted residues used for the subunit *a* motif pattern.

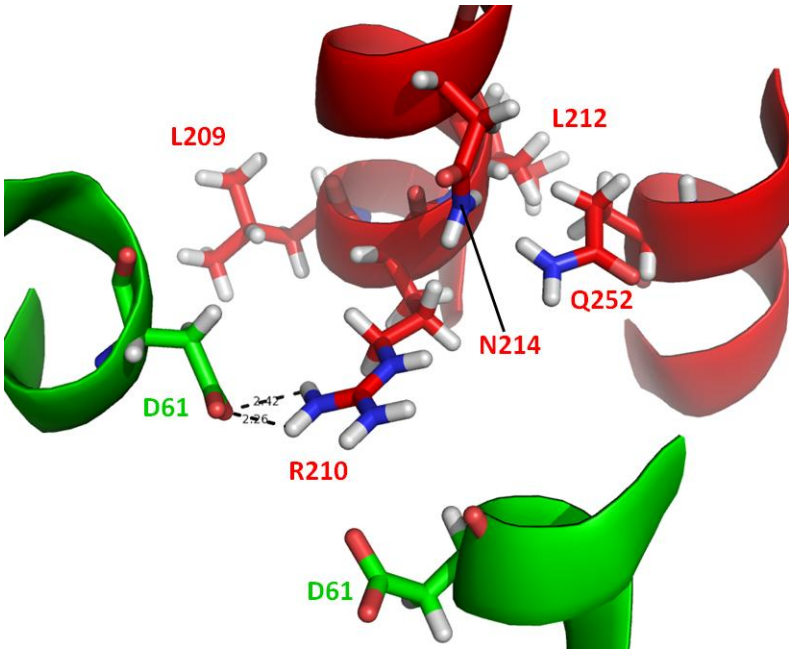

Figure 3.19. Interactions between arginine R_{210} (subunit *a*) and aspartate D_{61} (subunit *c*) in *E. coli.* Transmembrane helices of subunit *a* and subunit *c* are coloured in red and green respectively (PDB entry 1C17). Residues in the R_{210} environment are displayed as sticks. Polar interactions are indicated with black dots.

Among 5538 *P. falciparum* genes in the current PlasmoDB database, 8 and 56 candidate genes with unknown function were identified for subunit *a* and *b* respectively **(Table 3.12)**. Only three subunit *a* candidates were estimated to be mitochondrial by at least one targeting program whereas 24 genes for the subunit *b* were predicted to exhibit a mitochondrial signal peptide **(Table 3.13)**.

Table 3.12. Filtering of PlasmoDB annotated genes via successive ATP synthase subunit *a*- and subunit *b*-specific structural fingerprints. Abbreviations: PlasMit (PM), PFMPred (PP) and MitoProt II (MP).

	Subunit *a* (ATP4)		Subunit *b* (ATP6)	
Type of filtering	Value of filtering	**Genes**	Value of filtering	**Genes**
Molecular weight	20 - 45 kDa	**1724**	15 - 41 kDa	**1768**
Number of transmembrane domains	4 - 8	**96**	1- 2	**477**
Secondary structure	%Helix: 52% - 100% %Strand: 0% - 8% %Coil : 0% - 48%	**20**	%Helix: 38% - 95% %Strand: 0% - 19% %Coil : 3% - 48%	**328**
Motif pattern	[AVFPMILW]R[AVFPMILW]	**13**	No motif	**328**
Protein function	Unknown	**8**	Unknown	**56**
Mitochondrial signal peptide	PM (strict score) PP > 0.5 MP > 0.5	**3**	PM (strict score) PP > 0.5 MP > 0.5	**24**
Candidate gene	Manually	**1**	Manually	**5**

After manual observation of each mitochondrial candidate for subunit *a*, PF3D7_0611000 is the gene displaying all features required. First, the encoded protein possesses six transmembrane domains essential for insertion into the inner membrane. Moreover, it exhibits an arginine residue predicted to be embedded in the fourth TM **(Fig 3.20)**. For functional proton translocation through the F_O subcomplex, both *Plasmodium* residues arginine (subunit *a*) and glutamate (subunit *c*) have to be integrated into transmembrane domains. In PF3D7_0611000, the second site suppressor glutamine (Q_{252} in *E. coli*) is also conserved and located in the last TM. Like in other species such as *E. coli* or *A. suum*, both conserved arginine and aspartic acid in *P. falciparum* are found in adjacent transmembrane helices at a similar depth and with a slight lateral displacement relative to each other.

Without conserved motifs detected, identification of clear subunit *b* candidates was more complicated. Among mitochondrial candidates filtered, only five exhibited the presence of a single or two transmembrane domains on their N-terminal section. With the absence of other structural fingerprints to refine the identification, those five selected genes can be regarded as potential subunit *b.*

Table 3.13. Prediction of mitochondrial signal peptide for subunit *a* and *b* gene candidates. Three different webserver are used for prediction: PlasMit (PM, strict cutoff), PFMPred (PP, cutoff>0.5) and MitoProt II (Cutoff>0.5). Abbreviation: CG, final candidate gene(s).

	PlasmoDB entry	Function	MW (kDa)	PM	PP	MP	CG
Subunit *a*	PF3D7_0405600	conserved Plasmodium membrane protein, unknown function	37.8	No	No	No	
	PF3D7_0514500	conserved Plasmodium membrane protein, unknown function	25.2	No	No	No	
	PF3D7_0611000	conserved Plasmodium membrane protein, unknown function	33.3	Yes	Yes	No	X
	PF3D7_0917200	conserved Plasmodium membrane protein, unknown function	38.7	Yes	No	No	
	PF3D7_1146900	conserved Plasmodium membrane protein, unknown function	21.8	No	No	No	
	PF3D7_1237700	conserved Plasmodium membrane protein, unknown function	23.6	No	No	Yes	
	PF3D7_1318000	conserved Plasmodium membrane protein, unknown function	22.0	No	No	No	
	PF3D7_1347300	conserved Plasmodium membrane protein, unknown function	26.0	No	No	No	
Subunit *b*	PF3D7_0105400.1	conserved Plasmodium protein, unknown function	16.8	No	No	No	
	PF3D7_0107400	conserved Plasmodium protein, unknown function	18.7	Yes	Yes	Yes	X
	PF3D7_0108600	conserved Plasmodium protein, unknown function	37.6	Yes	Yes	No	
	PF3D7_0110000	conserved Plasmodium protein, unknown function	27.8	No	No	No	
	PF3D7_0112100	conserved Plasmodium protein, unknown function	19.2	No	No	No	
	PF3D7_0204200	conserved Plasmodium protein, unknown function	33.4	No	No	No	
	PF3D7_0213200	conserved Plasmodium protein, unknown function	15.3	Yes	Yes	No	
	PF3D7_0219300	conserved Plasmodium protein, unknown function	16.9	Yes	No	No	
	PF3D7_0305900	conserved Plasmodium protein, unknown function	21.3	Yes	Yes	Yes	
	PF3D7_0306000	conserved Plasmodium protein, unknown function	17.0	Yes	Yes	Yes	
	PF3D7_0306500	conserved Plasmodium protein, unknown function	36.3	No	Yes	Yes	
	PF3D7_0316000	conserved Plasmodium protein, unknown function	37.1	Yes	No	No	
	PF3D7_0403300	conserved Plasmodium protein, unknown function	18.3	No	No	No	
	PF3D7_0504500	conserved Plasmodium protein, unknown function	31.8	No	No	No	
	PF3D7_0506000	conserved Plasmodium protein, unknown function	29.6	No	No	No	
	PF3D7_0513900	conserved Plasmodium protein, unknown function	29.7	No	No	No	
	PF3D7_0515200	conserved Plasmodium protein, unknown function	17.0	No	No	No	
	PF3D7_0604400	conserved Plasmodium protein, unknown function	21.6	No	No	No	
	PF3D7_0620200	conserved Plasmodium protein, unknown function	39.0	No	No	No	
	PF3D7_0703100	conserved Plasmodium protein, unknown function	21.2	No	Yes	No	
	PF3D7_0710500	conserved Plasmodium protein, unknown function	30.2	No	No	Yes	
	PF3D7_0718900	conserved Plasmodium protein, unknown function	27.7	No	No	No	
	PF3D7_0719100	conserved Plasmodium protein, unknown function	21.1	No	Yes	Yes	
	PF3D7_0827400	conserved Plasmodium protein, unknown function	26.1	No	No	No	
	PF3D7_0830400	conserved Plasmodium protein, unknown function	15.9	No	No	No	
	PF3D7_0904200	conserved Plasmodium protein, unknown function	33.9	No	No	No	
	PF3D7_0908400	conserved Plasmodium protein, unknown function	24.0	No	Yes	No	
	PF3D7_0929900	conserved Plasmodium protein, unknown function	23.0	No	No	Yes	
	PF3D7_0931500	conserved Plasmodium protein, unknown function	27.0	No	No	Yes	X
	PF3D7_0933400	conserved Plasmodium protein, unknown function	32.0	Yes	Yes	Yes	X
	PF3D7_0934300	conserved Plasmodium protein, unknown function	16.8	Yes	No	Yes	
	PF3D7_1037900	conserved Plasmodium protein, unknown function	21.4	Yes	No	No	
	PF3D7_1105800	conserved Plasmodium protein, unknown function	30.6	No	No	No	
	PF3D7_1122700	conserved Plasmodium protein, unknown function	30.5	Yes	No	Yes	
	PF3D7_1129800	conserved Plasmodium protein, unknown function	33.6	No	No	No	
	PF3D7_1146200	conserved Plasmodium protein, unknown function	19.9	No	No	No	
	PF3D7_1147900	conserved Plasmodium protein, unknown function	24.9	No	No	No	
	PF3D7_1214000	conserved Plasmodium protein, unknown function	17.6	Yes	Yes	Yes	X
	PF3D7_1223000	conserved Plasmodium protein, unknown function	16.0	No	No	Yes	X
	PF3D7_1232800	conserved Plasmodium protein, unknown function	17.6	Yes	Yes	Yes	
	PF3D7_1239300	conserved Plasmodium protein, unknown function	24.2	No	No	No	
	PF3D7_1303600	conserved Plasmodium protein, unknown function	15.2	No	No	No	
	PF3D7_1310200	conserved Plasmodium protein, unknown function	16.7	No	No	No	
	PF3D7_1315500	conserved Plasmodium protein, unknown function	21.4	No	No	No	
	PF3D7_1325600	conserved Plasmodium protein, unknown function	16.1	No	No	No	
	PF3D7_1330100	conserved Plasmodium protein, unknown function	22.7	No	No	No	
	PF3D7_1339400	conserved Plasmodium protein, unknown function	17.7	No	Yes	Yes	

	PF3D7_1347400	conserved Plasmodium protein, unknown function	16.8	No	Yes	No	
	PF3D7_1358400	conserved Plasmodium protein, unknown function	16.6	No	Yes	No	
	PF3D7_1362300	conserved protein, unknown function	22.0	No	No	No	
	PF3D7_1366200	conserved Plasmodium protein, unknown function	17.8	No	No	Yes	
	PF3D7_1407200	conserved Plasmodium protein, unknown function	34.4	No	No	No	
	PF3D7_1416000	conserved Plasmodium protein, unknown function	26.0	No	No	No	
	PF3D7_1429600	conserved Plasmodium protein, unknown function (GEXP03)	26.1	No	No	No	
	PF3D7_1435400	conserved protein, unknown function	21.8	No	Yes	No	
	PF3D7_1469100	conserved Plasmodium protein, unknown function	31.3	No	No	No	

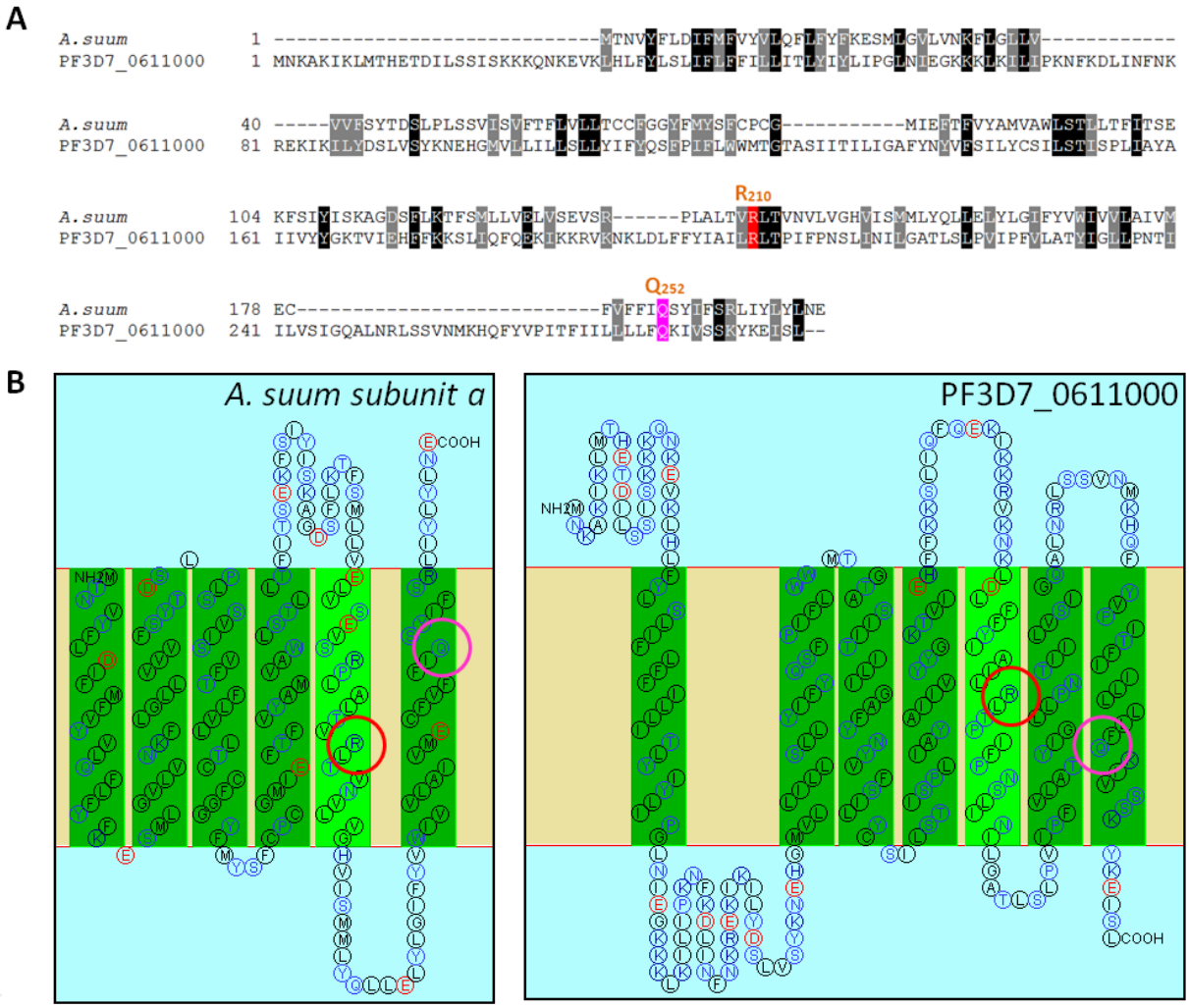

Figure 3.20. Sequence alignment and prediction of transmembrane domains in *Ascaris suum* synthase subunit *a* and the candidate gene PF3D7_0611000. (A) *A. suum* ATPase subunit *a* (P24876) and PF3D7_0611000 sequences were aligned with ClustalW2 (www.ebi.ac.uk/Tools/msa/clustalw2). Residues are displayed with dark boxes for full conservation and grey boxes for strong similarities. In red is highlighted the essential arginine (R_{210} in *E. coli*) and in pink, the conserved glutamine (Q_{252} in *E. coli*). **(B)** The helical wheel diagram of predicted segments has been carried out with SOSUI (bp.nuap.nagoya-u.ac.jp/sosui/). In red is circled the essential arginine and in pink the conserved glutamine. According the SOSUI nomenclature, in dark green are indicated primary helices while secondary helices are shown in light green.

3.3.3. Characterization of the anti-SdhA polyclonal antibody

To localize the parasite complex II into two dimensional gels, a custom polyclonal antibody against the SdhA subunit of the *P. falciparum* succinate dehydrogenase was raised using a commercial supplier (GenScript Corp., USA). The peptide ^{573}AHARDDFPERDDKN^{586} located near the C-terminal of the *P. falciparum* SdhA has been chosen for antibody generation. The anti-SdhA polyclonal antibody was raised by immunizing rabbits with the specific peptide (as peptide–KLH conjugate) and purified by affinity. This customized anti-SdhA polyclonal antibody showed a significant immunoreactivity against a 70 kDa protein, consistent with the size of the SdhA subunit in the malaria parasite, across species including *Escherichia coli*, *Bos taurus* and *P. falciparum* (soluble and membrane fractions) **(Fig. 3.21)**.

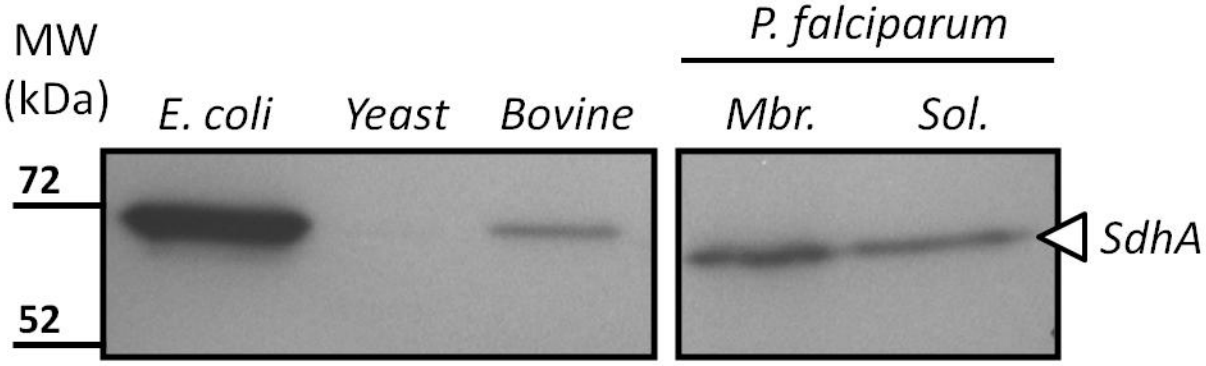

Figure 3.21. Immunobloting of the SdhA customized polyclonal antibody with bacteria, yeast, bovine and malaria parasite membrane extracts. Membrane extracts from *Escherichia coli*, *S. cerevisiae*, *B. taurus*, and *P. falciparum* 3D7 were resolved by SDS-Page and blotted to nitrocellulose. Blots were probed with anti-SdhA antibody (1:500), 2h at room temperature. Arrows on right side point to SdhA (70 kDa) immunoreactive band.

Antibody antigens were analysed by NanoLC-MS/MS to validate its specificity to SdhA. First, immunoprecipitation experiments were attempted on the membrane proteins from 3D7 free-parasite extracts, bovine and *E. coli* mitochondrial membranes. The immunocapture obtained in denaturing conditions with *E. coli* crude membranes revealed a protein captured around 70 kDa on both immunoblot and silver stained gel **(Fig. 3.22).** The band corresponding to the protein was excised from the silver-stained gel, digested with trypsin, and analyzed by NanoLC-MS/MS to obtain the peptide sequence data. The SdhA subunit was identified by 19 peptide mass fingerprints with a sequence coverage of 19.22% **(Table 3.14)**. Despite several attempts, the antibody characterization did not succeed with malaria parasite extracts or bovine mitochondria due to the low expression of complex II in *P. falciparum* and the low affinity of the antibody for the bovine SdhA.

Immunofluorescence localization of the complex II inside the parasite-infected erythrocytes has been attempted with the anti-SdhA antibody. However, no clear localization into the mitochondria has been observed which suggests the ability of the polyclonal antibody to bind the subunit in an unfolded state under denaturing conditions only.

Attempts to generate polyclonal antibodies specific to the *P. falciparum* ATP synthase were unsuccessful. Two different anti-ATPα antibodies have been raised based on two different highly immunogenic peptides but none showed immunoreactivity for a protein expected around 62 kDa. Hence, the proteomic strategy established has been performed only for the identification of complex II subunits.

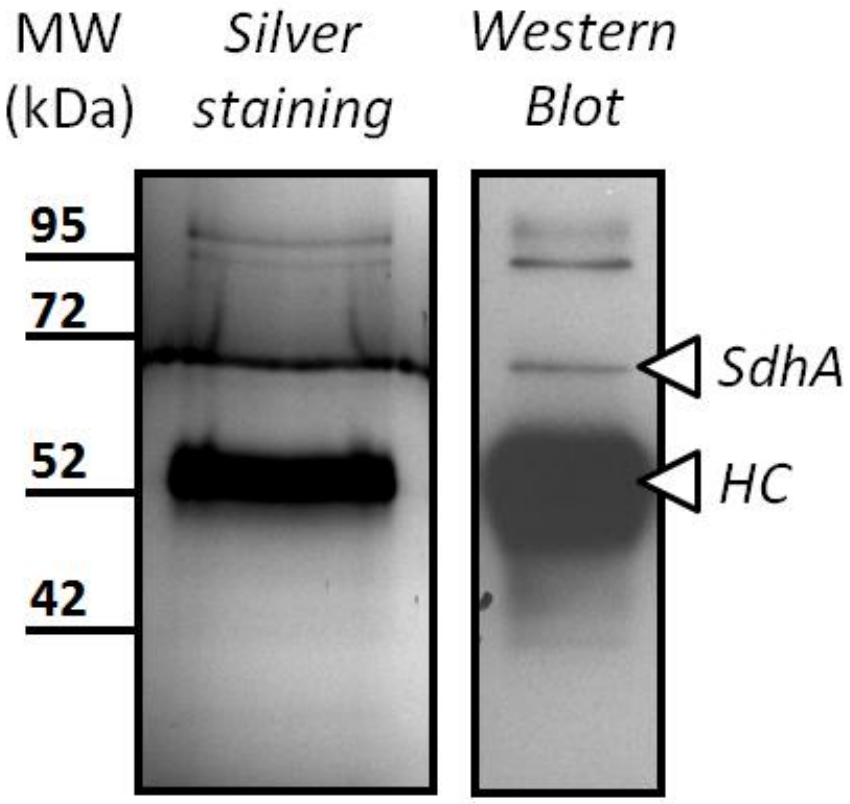

Figure 3.22. Western Blot and silver staining of the SdhA subunit (70 kDa) immunocapture from *E. coli* membrane. Arrows on right side point to SdhA (70 kDa) immunoreactive band and HC indicate the heavy chain (50 kDa) of the polyclonal antibody used for the immunoprecipitation.

Table 3.14. List of 10 first hits obtained by NanoLC-MS/MS analysis and Sequest algorithm search of the immunoprecipitated 70 kDa band. In yellow is highlighted the most significant hit.

Hits	UnitProtKB entry	Coverage	# Peptides	# AAs	MW (kDa)	calc. pI	Score	Description
1	**P0AC43**	**19.22%**	**19[a]**	**588**	**64.4**	**6.27**	**37.32**	**Succinate dehydrogenase flavoprotein subunit OS=Escherichia coli O157:H7 GN=sdhA PE=3 SV=1 - [DHSA_ECO57]**
2	P49064	15.30%	17	608	68.6	5.66	30.41	Serum albumin OS=Felis catus GN=ALB PE=1 SV=1 - [ALBU_FELCA]
3	P49822	13.82%	19	608	68.6	5.69	25.14	Serum albumin OS=Canis familiaris GN=ALB PE=1 SV=3 - [ALBU_CANFA]
4	A1AJ51	22.45%	10	548	57.3	4.94	7.58	60 kDa chaperonin 1 OS=Escherichia coli O1:K1 / APEC GN=groL1 PE=3 SV=1 - [CH601_ECOK1]
5	P0C193	14.68%	14	545	57.3	5.06	7.58	60 kDa chaperonin OS=Sodalis glossinidius GN=groL PE=3 SV=1 - [CH60_SODGL]
6	Q9ANR9	19.60%	25	546	57.6	5.29	7.58	60 kDa chaperonin OS=Wigglesworthia glossinidia brevipalpis GN=groL PE=3 SV=1 - [CH60_WIGBR]
7	A7ZUE0	3.39%	2	502	56.2	5.50	5.43	Glycerol kinase OS=Escherichia coli O139:H28 (strain E24377A / ETEC) GN=glpK PE=3 SV=1 - [GLPK_ECO24]
8	B7LAN4	10.40%	4	548	60.2	6.99	2.48	Probable malate:quinone oxidoreductase OS=Escherichia coli (strain 55989 / EAEC) GN=mqo PE=3 SV=1 - [MQO_ECO55]
9	P0AG69	7.90%	4	557	61.1	4.98	2.35	30S ribosomal protein S1 OS=Escherichia coli O157:H7 GN=rpsA PE=3 SV=1 - [RS1_ECO57]
10	P25553	5.43%	2	479	52.2	5.15	2.31	Lactaldehyde dehydrogenase OS=Escherichia coli (strain K12) GN=aldA PE=1 SV=2 - [ALDA_ECOLI]

[a] The list of 19 peptides identified are indicated in **Appendix 1**.

3.3.4. The gradient BNE/SDS-Page approach

An initial proteomic approach using gradient BNE/SDS-Page was carried out to solve complex II subunits from solubilised membranes. First, the method was validated with solubilised membranes from a beef heart mitochondrial preparation. Bovine mitochondrial proteins were analysed with a 4 to 15% gradient BNE followed by a 15% SDS-Page as the second dimension. As shown in **Figure 3.23 A**, complex I to V were isolated and clearly visible on the first dimension. Complex II appears with an unexpected size of ~200 kDa instead of ~130 kDa but protein separations on blue native gels do not exactly reflect calculated molecular masses and have to be considered with caution. Complexes were distinctly identified upon resolution of their subunits with both second dimension gels stained with silver nitrate and immunoblotted with different antibodies specific to SdhA (complex II), Rieske subunit (bc_1 complex), SdhB (complex II) and ATP synthase (subunit α) **(Fig. 3.23 B and C)**. Additionally, seven spots representing different subunits of complexes I to V were digested by trypsin and analysed by NanoLC-MS/MS. MS-based protein identifications confirmed the localization of each complex. Among complex II subunits, bands corresponding to SdhA, SdhB and SdhC were clearly visible and were identified with sequence coverage of 55.19%, 53.21% and 12.43%, respectively.

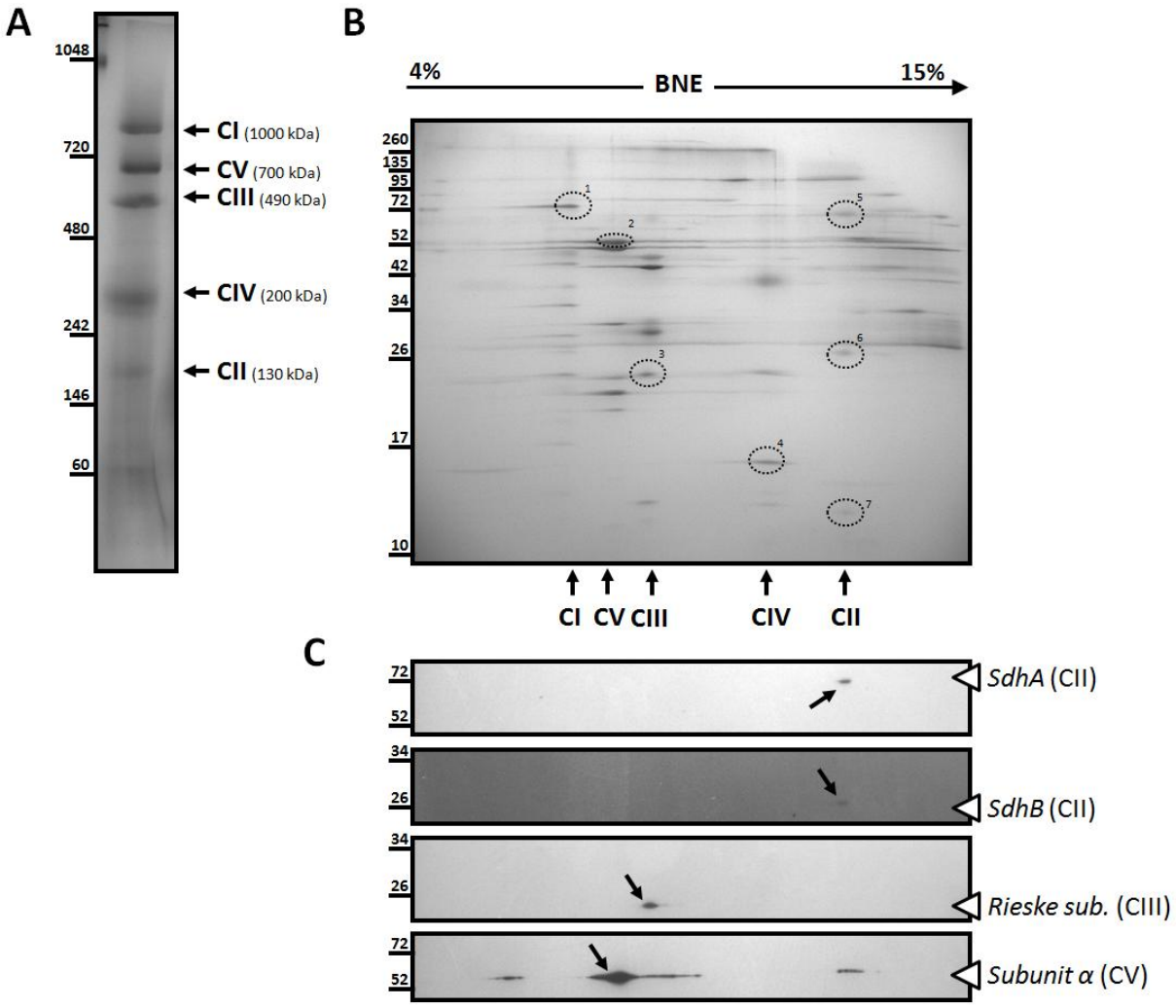

Figure 3.23. Separation of solubilised bovine mitochondrial membranes by 2D gradient BNE/SDS-Page. **(A)** Dodecyl-β-D-maltoside solubilised bovine mitochondrial membranes were separated according to their molecular weight on a gradient 4-15% blue native gel (BNE). Gels were stained with Coomassie blue. Complexes I to V are identified with arrows and their masses indicated. An unstained native protein marker (NativeMark™, Invitrogen, USA) was used as the protein ladder. **(B)** Subunits of the native complexes were separated by 15% SDS-Page and silver stained. Arrows mark the vertical alignment of subunits for each complex. A pre-stained broad range protein marker (Spectra™ Multicolor Broad Range Protein Ladder, Thermo Scientific, USA) were loaded side to the strip. Several spots indicated by dotted circles have been excised, digested by trypsin and analyzed by NanoLC-MS/MS. The protein identification was performed by database searching (UniprotKB entry, % sequence coverage): spot 1, complex I 75 kDa subunit (P15690, 74.28%); spot 2, ATP synthase subunit α (P19483, 71.79%); spot 3, complex III Rieske subunit (P13272, 28.47%); spot 4, complex IV subunit 4 (P00423, 44.38%); spot 5, complex II subunit A (P31039, 55.19%), spot 6, complex II subunit B (Q3T189, 53.21%); spot 7, complex II subunit C (P35720, 12.43%). **(C)** Immunoblot with an identical 2D gel were performed with different antibodies: our customized anti-SdhA (1/2000 dilution, antibody synthesis described in section 3.3.3) and anti-Rieske (bc_1 complex, 1/500 dilution, antibody synthesis described in section 6.2.1) polyclonal antibodies, SdhB (#ab14714, Abcam, UK) and ATP synthase subunit α (#ab110273, Abcam, UK) monoclonal antibodies. Arrows indicate localization of signals.

A similar strategy was attempted with *P. falciparum* membrane protein solubilised by 1% dodecyl-β-D-maltoside. In the first dimension, ETC complexes were not visible as with bovine extract due to the low expression of those enzymes in malaria parasites and limitations of mitochondria isolation. The second dimension gel revealed high background staining (by silver nitrate) due to the large amount of proteins solved **(Fig. 3.24 A)**. Although no clear ETC pattern could be detected on the silver stained gel, the immunoblot with anti-SdhA and anti-Rieske antibodies confirmed the presence of *P. falciparum* complex II and bc_1. Superimposition of this immunoblot onto the silver stained gel allowed determining the vertical row where complex II and III appear to be localized. However, only the SdhA subunit could be identified by NanoLC-MS/MS (13.65% sequence coverage) while no bc_1 subunits were detected. On the same vertical row of the SdhA, all spots between 10 to 20 kDa, range of molecular sizes for SdhC and SdhD, were analysed. Several attempts concluded to similar results: among all protein hits identified, no gene candidates predicted by the bioinformatic strategy for SdhC and SdhD were detected. The more noticeable identification is the unknown protein PF3D7_1117300 (27.34% sequence coverage) excised between 10 and 17 kDa. This enzyme is predicted to have 3 transmembrane domains with a molecular weight of 15.3 kDa. Nevertheless, the PF3D7_1117300 sequence doesn't exhibit any SdhC or SdhD conserved motifs nor mitochondrial signal peptides.

Although the resolution of *P. falciparum* complex II by this approach seems conceivable, its low expression in the blood stages and the limited protein loading capacity of BNE gels (maximum of 50 µg total proteins / well) is translated by non- or poorly visible spots after staining with silver nitrate which is known to be highly sensitive for protein detection in the low nanogram range. In line with this, the immunoblot with anti-SdhA and anti-Rieske antibodies revealed spots with weak intensity signals **(Fig. 3.24 B)**. Moreover, the low amount of peptides digested from SdhC and SdhD and/or obscured by others from the protein background noise can also limit the detection by mass spectrometry of clear peptide ion signals from both complex II subunits.

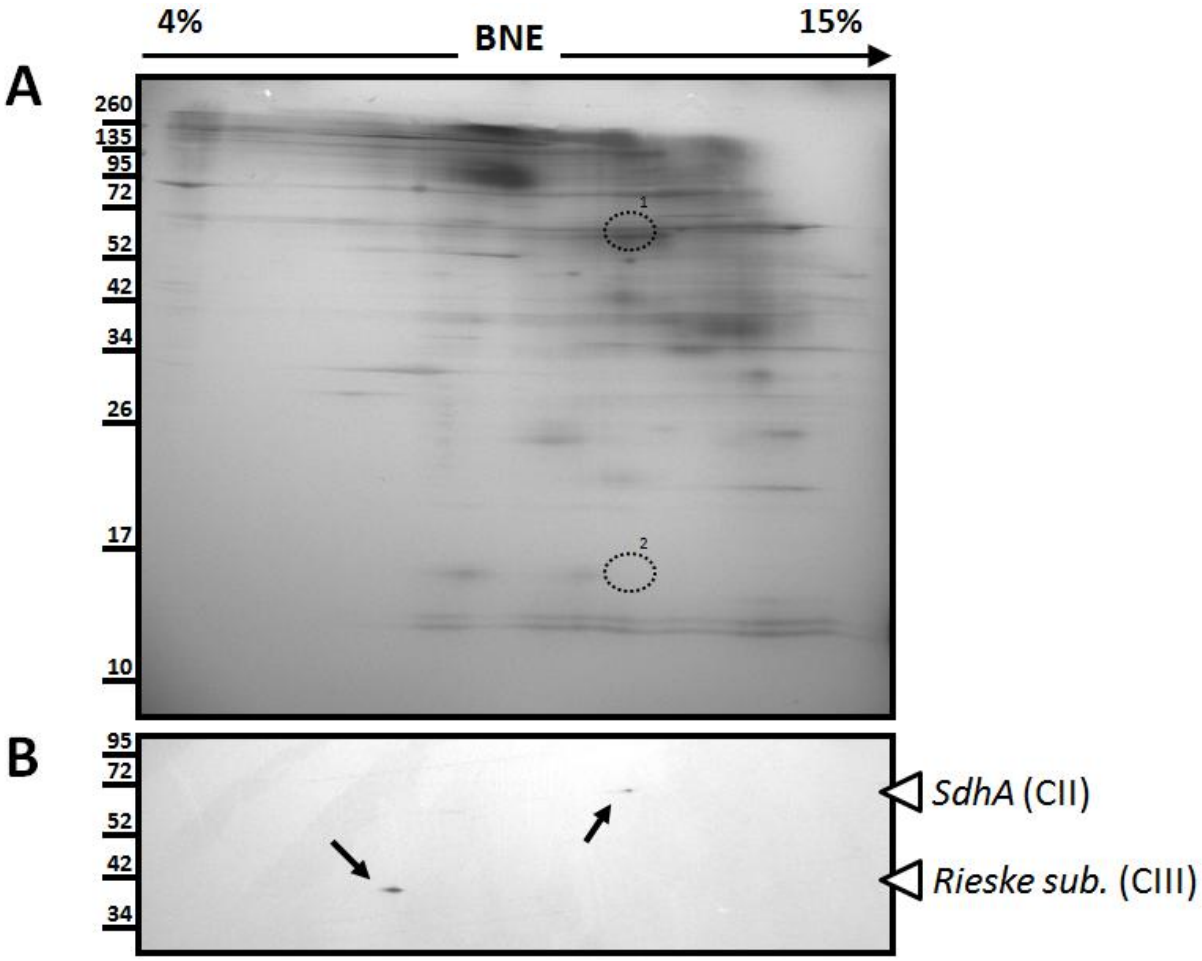

Figure 3.24. Separation of solubilised *P. falciparum* membrane proteins by 2D gradient BNE/SDS-Page. (A) Dodecyl-β-D-maltoside solubilised native membrane proteins were separated on a gradient 4-15% blue native gel (BNE) followed by a second dimension 15% SDS-Page and silver stained. Spots excised and digested by trypsin were identified by NanoLC-MS/MS and database searching (PlasmoDB entry, % sequence coverage): dotted circle 1, complex II subunit A (PF3D7_1034400, 13.65%); dotted circle 2, protein with unknown function (PF3D7_1117300, 27.34%). **(B)** Immunoblot with an identical 2D gel was performed with our customized anti-SdhA and anti-Rieske antibodies. Arrows indicate signal localization.

By superimposing both bovine and malaria parasite immunoblots, Rieske and SdhA subunits were observed to be at a very similar vertical position **(Fig. 3.25)**. This would suggest that both complexes migrated onto the blue native gel at a same distance from each other in both species. The bovine bc_1, composed of 11 subunits, has a total molecular weight (MW) of 248 kDa (Xia et al., 1997) and was visible as a dimer higher to 480 kDa on the BNE. To date, the *P. falciparum* bc_1 is composed of 7 subunits with a MW estimated of 281 kDa and appeared with a mass higher to 480 kDa on the BNE, suggesting a possible dimerization. By supposing that bc_1 complexes from *P. falciparum* and beef mitochondria are almost similar in size, their complex II should be equivalent too. Thus, the malaria parasite complex II is suspected to have a molecular weight near 130 kDa as predicted previously (Kawahara et al., 2009), which confirms the presence of both membrane anchor subunits. It also suggests that complex II from malaria parasites is not

unconventional like in *Trypanosoma cruzi* which possesses 12 subunits for a MW of 287 kDa (Morales et al., 2009).

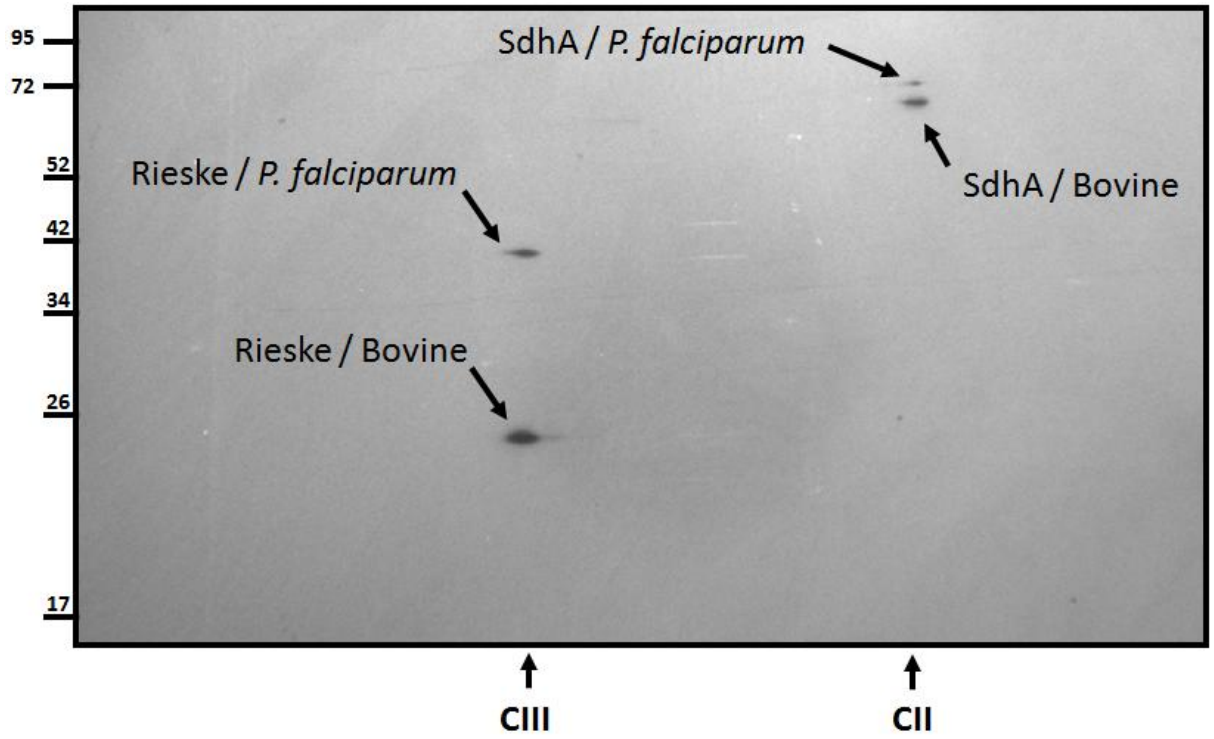

Figure 3.25. Superposition of *P. falciparum* and bovine two dimensional immunoblots. Both immunoblots were performed with both anti-SdhA and anti-Rieske polyclonal antibodies and superimposed thanks to the protein ladder. Positions of both subunits for each species are indicated with arrows. Both SdhA subunits have a molecular weight around 70 kDa in both species while the Rieske subunit (bc_1 complex) is heavier in *P. falciparum* than beef.

3.3.5. Enrichment of complex II by sucrose gradient.

The separation of ETC complexes and their assembly in supercomplexes using sucrose density gradients were shown with mitochondria from human heart, yeast or *Arabidopsis thaliana* (Heinemeyer et al., 2007; Klodmann et al., 2010; Taylor et al., 2002). Due to difficulties in isolating *P. falciparum* mitochondria as well as low expression of the complex II in trophozoite stage parasites, a sucrose gradient approach was used to substantially enrich the complex II from *P. falciparum* membranes.

P. falciparum membrane proteins were first solubilised with 1% dodecyl-β-D-maltoside followed by fractionation with a 5 to 35% sucrose step gradient. Fractions of the density gradient were collected and concentrated. Aliquots of each concentrated fraction were resolved on a 10% SDS-Page and immunoblotted with both anti-SdhA and anti-Rieske polyclonal antibodies. Immunoblot analysis showed that sucrose gradient fractions 20%, 22.5% and 25% were highly enriched in *Plasmodium* complex II **(Fig. 3.26 B)**. Because the sedimentation rate in sucrose

gradient is dependent on the molecular weight, the bc_1 complex, twice as big as complex II, is concentrated in the last fraction (35%) at the bottom of the ultracentrifugation tube. The same experiment with bovine mitochondrial membranes showed complex II sedimentation in similar fractions (from 20% to 27.5%) **(Fig. 3.26 A)**. Subsequently, fractions enriched in complex II were pooled, dialyzed and concentrated before being resolved on a first dimension non-gradient blue native gel.

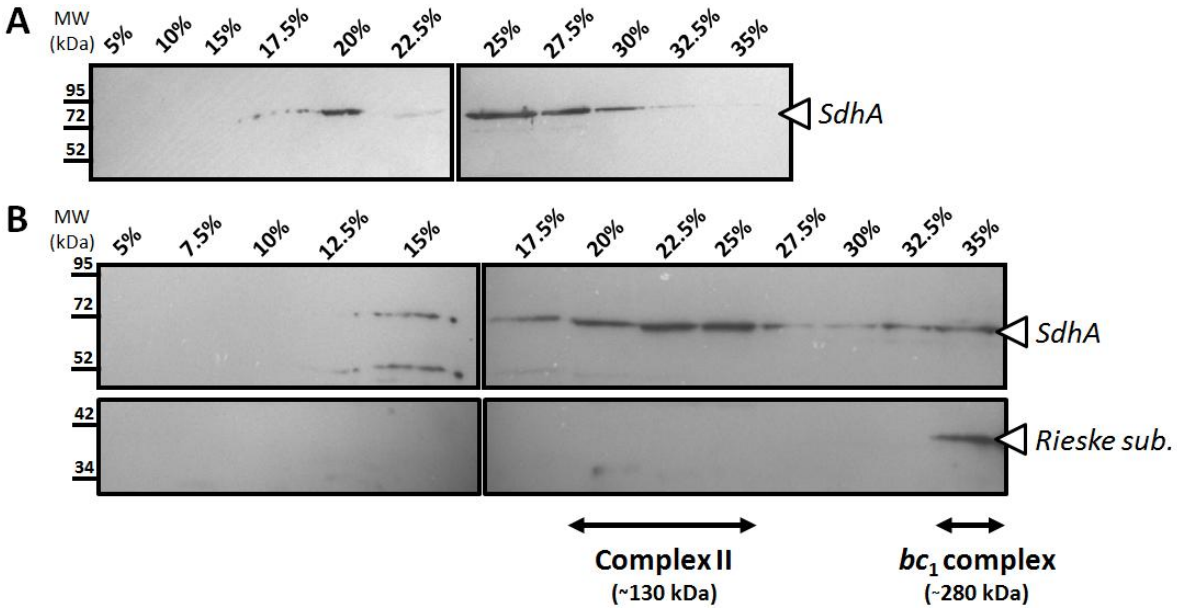

Figure 3.26. Enrichment of complex II by sucrose gradient centrifugation analysis. (A) Bovine mitochondria membranes were fractionated on a 5-35% sucrose step gradient. After concentration (with 50 kDa Amicon), an aliquot of each fraction was run on 10% SDS-Page gels followed by Western blot analysis with the anti-SdhA (70 kDa) polyclonal antibody. **(B)** In a similar manner, *P. falciparum* membranes were fractionated and aliquots separated by 10% SDS-Page. Immunoblots were performed with customized anti-SdhA (1/2000 dilution) and anti-bc_1 polyclonal antibodies (1/500 dilution). Arrows along the bottom indicate localization of complex II and bc_1 complex in the sucrose gradient fractions.

3.3.6. Non-gradient BNE/SDS-Page with enriched complex II preparation

To maximize the gel resolution between 100 kDa to 400 kDa, the previous BNE/SDS-Page approach was modified by performing a non-gradient blue native gel as first dimension instead of a conventional gradient. The suitability of using sucrose gradient fractions for non-gradient BNE/SDS-Page was firstly tested with enriched bovine complex II fractions. The enriched sample was migrated into an 8% non-gradient BNE followed by a 15% SDS-Page as a second dimension. The non-gradient BNE from bovine mitochondria showed a large band corresponding to complex II at a similar migration position to the gradient BNE **(Fig. 3.27 A)**. On the second dimension, complex II subunits became distinctly visible on the silver stained gel, except for ShdA which was confused with a strong protein background **(Fig. 3.27 B)**. Immunoblot performed with anti-SdhA

antibody confirmed the vertical row where complex II subunits are localized **(Fig. 3.27 C)**. Unlike gradient BNE, the SdhA signal around 70 kDa is widely spread due to sucrose gradient enrichment and a better gel resolution. The four subunits SdhA, SdhB, SdhC and SdhD were successfully identified by NanoLC-MS/MS analysis with sequence coverages of 53.68%, 28.21%, 21.10% and 13.25% respectively. Both bovine SdhC and SdhD with estimated molecular weight of 18.4 and 17.1 kDa respectively appeared with apparent lower sizes on the second dimension gel.

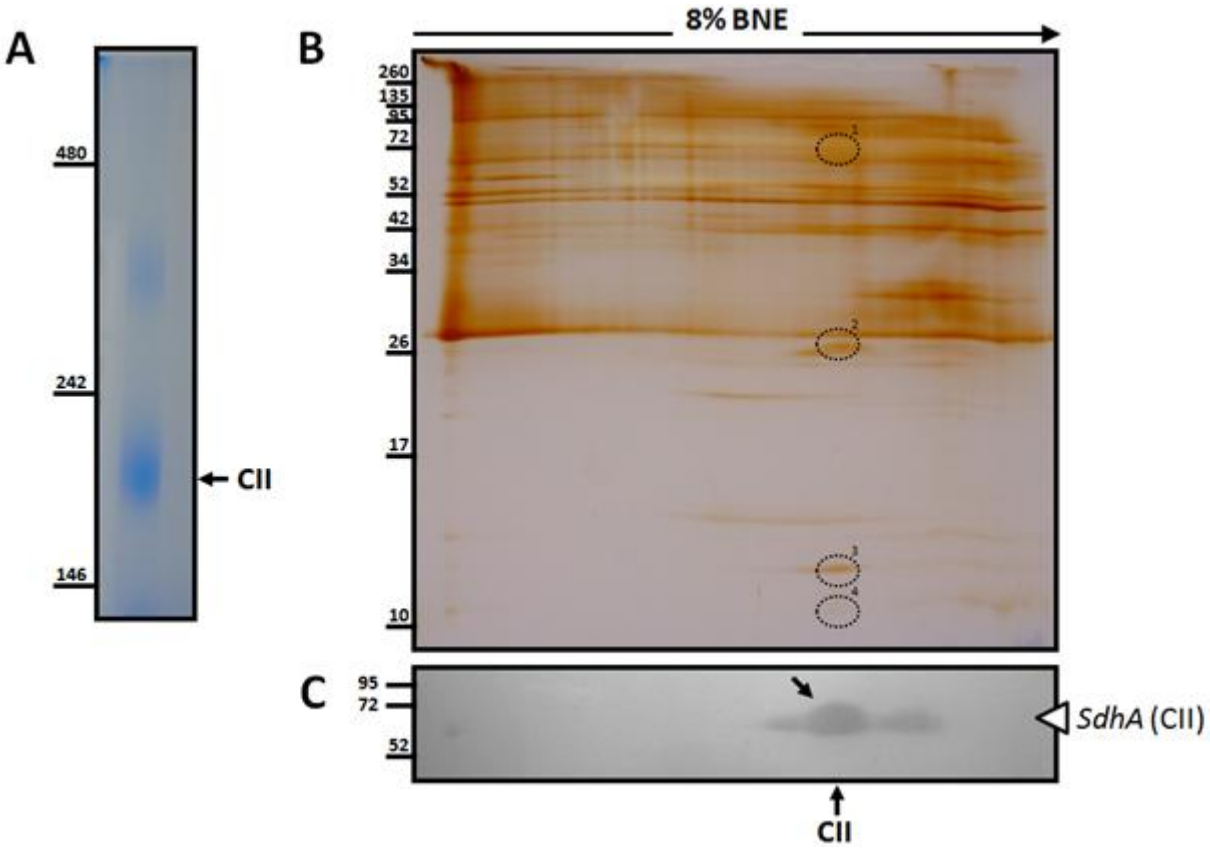

Figure 3.27. Separation of enriched bovine complex II fractions by non-gradient BNE/SDS-Page. (A) Sucrose gradient fraction (25% and 27.5% sucrose) enriched in bovine complex II were pooled, dialyzed, concentrated and separated by a non-gradient 8% blue native gel (BNE). Gel were stained with Coomassie blue. Complex II is indicated by an arrow. An unstained native protein marker (NativeMark™, Invitrogen, USA) was used as a protein ladder. **(B)** Native proteins were separated by 15% SDS-Page and silver stained. Arrows mark the vertical alignment of complex II subunits. A pre-stained broad range protein marker (Spectra™ Multicolor Broad Range Protein Ladder, Thermo Scientific, USA) was loaded alongside the strip. Several spots indicated by dotted circles have been excised, digested by trypsin and analyzed by NanoLC-MS/MS. The protein identification was performed by database searching (UniprotKB entry, % sequence coverage): spot 1, complex II subunit A (P31039, 53.68%), spot 2, complex II subunit B (Q3T189, 28.21%); spot 3, complex II subunit C (P35720, 21.10%); spot 4; complex II subunit D (Q95123, 13.25%). **(C)** Immunoblot with an identical 2D gel was performed with our customized anti-SdhA polyclonal antibody. An arrow indicates signal localization.

An identical non-gradient BNE/SDS-Page approach was carried out with *P. falciparum* enriched complex II fractions. In the same manner of gradient BNE, a strong protein background prevented the observation of a distinct complex II on the non-gradient blue native gel despite the

enzyme enrichment via sucrose gradient. The second dimension gel, stained with silver nitrate, confirmed the presence of significant background noise with no complex II subunits distinguishable by eye **(Fig. 3.28)**. However, the similar gel immunobloted using anti-SdhA antibodies confirmed the presence of the subunit with a clear signal. Thanks to the sucrose gradient enrichment and a better gel resolution, the SdhA signal appears more intense and wider than with gradient BNE/SDS-Page. Despite several attempts, *P. falciparum* SdhA and SdhB could not be identified by mass spectrometry after excision and digestion of several spots around 70 kDa (box 1) and 26 kDa (box 2) respectively. Although the sucrose gradient ultracentrifugation followed by non-gradient BNE/SDS-Page seems more appropriate to separate and visualize complex II subunits like demonstrated with bovine mitochondria, the enzyme enrichment is coupled with a concentration of other membrane proteins and complexes with similar molecular weight and probably with higher expression level. In consequence, the protein background is increased on the stained gel which makes difficult the visualization and the identification of low-expressed proteins such as Complex II subunits

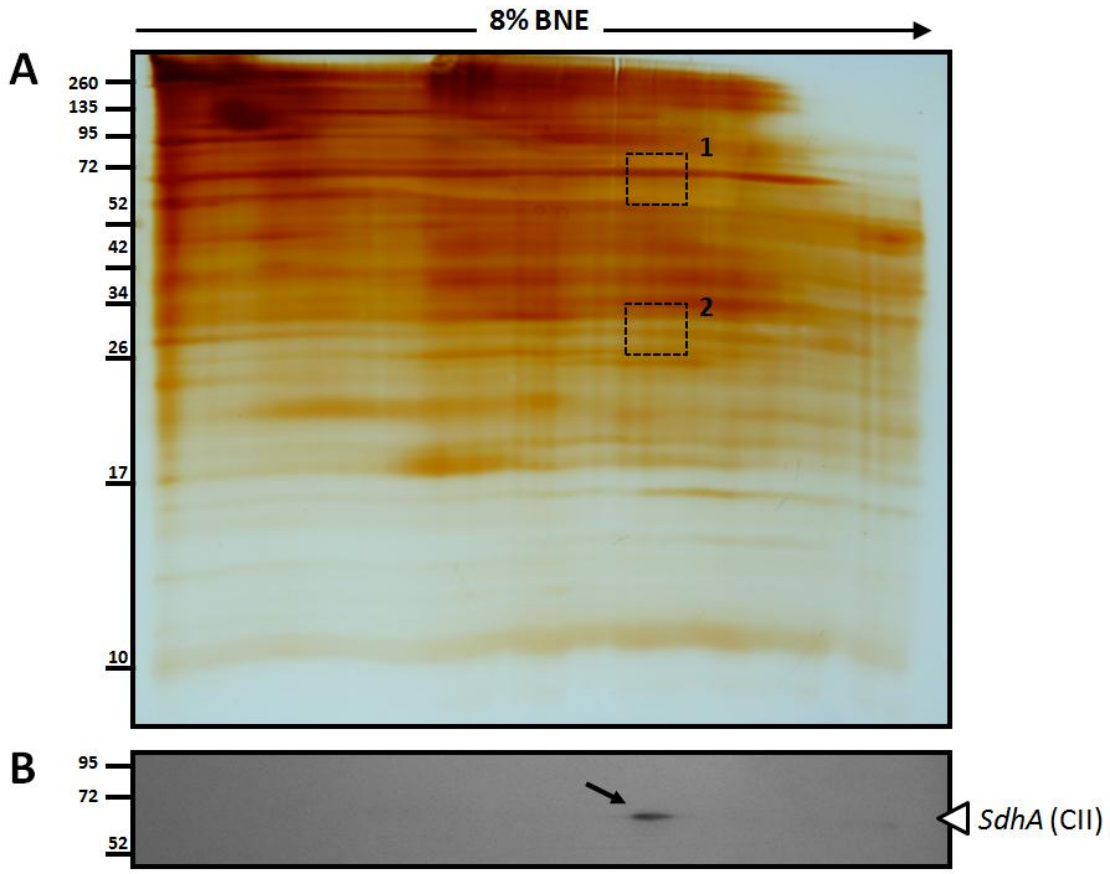

Figure 3.28. Separation of *P. falciparum* enriched complex II by 2D non-gradient BNE/SDS-Page. (A) Sucrose gradient fraction (20%, 22.5% and 25% sucrose) enriched in *P. falciparum* complex II were pooled, dialyzed, concentrated and separated by a non-gradient 8% blue native gel (BNE) followed by a second dimension 15% SDS-Page and silver stained. **(B)** Immunoblot with an identical 2D gel was performed with our customized anti-SdhA polyclonal antibody. The arrow indicates signal localization.

3.4. Discussion

The main objective of this chapter was to identify the genes encoding the membrane anchor subunits SdhC and SdhD of the complex II, as well as the *a* and *b* subunits of the ATP synthase in *Plasmodium* species. Because both enzymes are believed to be functional in malaria parasites, it suggests that those key subunits are probably not absent.

3.4.1. Proposed candidate genes by a bioinformatic approach

Because these membrane anchor subunits are highly divergent across species and difficult to identify with conventional BLAST programs, a bioinformatic strategy using structural fingerprints has been set up. PF3D7_1212600.2 and PF3D7_0611100 were identified as candidates for *P. falciparum* SdhC and SdhD respectively. The SdhC and SdhD candidate genes have the quinone/heme-binding motifs "$Sx_3Rx_{48}H$" in front of the predicted transmembrane helix I and "$Yx_{10}DY$" following the helix II. In the same manner as for *E. coli* complex II, both residues W228 in SdhB and Y72 in the SdhD "$Yx_{10}DY$" motif could hydrogen bond to the O-1 atom of ubiquinone and contribute to the binding affinity (Yankovskaya et al., 2003). The arginine in the SdhC "$Sx_3Rx_{48}H$" motif and D71 in the SdhD "$Yx_{10}DY$" motif may be in close proximity to ubiquinone and could interact with Y72 (Tran et al., 2006). The serine in the SdhC "$Sx_3Rx_{48}H$" motif, demonstrated essential in *E. coli* (Horsefield et al., 2006), may also participate in quinone binding via hydrogen bonding to the O-4 atom of ubiquinone in malaria parasites. As in *E. coli*, a heme molecule could be ligated by the histidine in the SdhC "$Sx_3Rx_{48}H$" motif and the first tyrosine residue in the SdhD "$Yx_{10}DY$" motif. It is noted that the SdhD candidate identified here, lacks a third transmembrane domain unlike its mammalian and bacterial counterparts. Mogi and Kita, recently proposed candidates for these two missing subunits but without proteomic data and motif conservation with homologues in other species to support these choices, and for this reason, they are unlikely candidates (Mogi and Kita, 2009) **(Table 3.15)**. The main difference between the study presented here and this previous work is the conserved motifs employed as subunit fingerprint. The SdhC and SdhD motifs used in this thesis are simpler and less specific due to a higher number of homologous genes used to refine both patterns. Clearly however, the bioinformatics strategy adopted here needs to be confirmed genetically or using a proteomics approach.

Table 3.15. Putative candidates of SdhC, SdhD and ATP synthase subunits *a* and *b* in *Plasmodium falciparum* proposed by Mogi and Kita, and our study.

Reference	SdhC	SdhD	ATP synthase subunit *a*	ATP synthase subunit *b*
Mogi and Kita, 2009	PF3D7_0611100	PF3D7_1010300	PF3D7_1005800	PF3D7_0703600
The present study	PF3D7_1212600.2	PF3D7_0611100	PF3D7_0611000	PF3D7_0107400 PF3D7_0931500 PF3D7_0933400 PF3D7_1214000 PF3D7_1223000

The gene PF3D7_0611000 was identified as a candidate for encoding the ATP synthase subunit *a*, on the basis that it contains a large hydrophobic section with six transmembrane domains and conserves the essential arginine residue to interact with the *c* ring. The candidate proposed by Mogi and Kita displays four transmembrane domains but lacks the crucial Arg210 which asks a question on the possible functionality of this proposed subunit (Mogi and Kita, 2009). For ATP synthase subunit *b*, no distinct gene could be determined among 5 candidates in absence of motif patterns and based only on the secondary structure profile. A recent release of the Pfam database found a "mitochondrial ATP synthase B chain precursor family" domain for the gene PF3D7_1125100. Indeed, the gene has predicted attributes expected for the subunit *b*, such as two transmembrane domains near the N-terminus, an α-helical secondary structure in the C-terminal domain, and a mitochondrial targeting peptide. However, this subunit-*b* like protein has not been selected by the bioinformatic filtering presented here due to an excessive molecular weight (59.2 kDa) which makes this subunit unconventional if its function is confirmed in future studies.

3.4.2. Proteomic attempts to validate complex II candidate genes.

2D gradient BNE/SDS-Page and non-gradient BNE/SDS-Page were performed to establish a proteomic cataloguing of all subunits that constitute the *P. falciparum* complex II. A polyclonal antibody detecting the *P. falciparum* SdhA under denaturing conditions was successfully generated but attempts to generate an anti-ATP synthase subunit α failed. Attempts to identify and characterise SdhC and SdhD subunits in *P. falciparum* by using the conventional gradient BNE/SDS-Page were unsuccessful. The protein PF3D7_1117300, detected via our proteomics analysis, was not selected by the proceeding bioinformatic analyses due to its lack of SdhC or SdhD conserved motifs. A highly divergent or unconventional subunit C or D is conceivable, and it

will be interesting in future studies to investigate whether this protein can be associated with the complex II.

3.4.3. Critical assessment of the adopted methodologies

The low number of structural fingerprints available to refine the bioinformatics filtering is a major limitation to correctly assign a unique candidate for the protein searched. Because the proteomic strategy exposed in this chapter failed to confirm predicted candidates, experimental data are still needed to evaluate the robustness of this bioinformatic approach. Thus, candidate genes proposed in this work have to be considered carefully. Additionally, this method requires manual bioinformatic processing and can be considered as a low throughput way to identify proteins. However, new bioinformatic approaches are needed to help the identification of highly divergent proteins. Indeed, BLAST or Hidden Markov Models search programs are too limited to identify those poorly-conserved proteins as well as no Pfam domains being detected in nearly 50% of *P. falciparum* proteins (Terrapon et al., 2009).

With better resolution and visualization, the non-gradient BNE/SDS-Page makes possible the identification of complex II subunits from enriched extracts. Unfortunately, no complex II subunits could be identified via this approach. This method worked well with preparation of isolated mitochondria of high purity but remains limited with poorly-expressed mitochondrial proteins included in a large membrane proteins mixture such as the *P. falciparum* membranes extract used here. Hence, a major failure of the methodological approach used was the failure to dissociate the mitochondria from other organelles (e.g. apicoplast and ER) and parasite membranes.

The subunit identification of the unusual succinate dehydrogenase in *Trypanosoma cruzi* was carried out by purifying the enzyme from isolated mitochondrial preparations before it was resolved by a classical two dimensional technique (Morales et al., 2009). To determine the seven subunits composing the unconventional complex II in plant *Arabidopsis thaliana*, the mitochondria were isolated and solubilised before being applied a 2D BNE/SDS-Page (Eubel et al., 2003). It should be noted that the different *Plasmodium* mitochondrial preparations or the purification of the enzyme by FPLC published previously could not be reproduced with our parasite strains and our laboratory conditions (Kawahara et al., 2009; Mather et al., 2010; Suraveratum et al., 2000).

3.4.4. Future potential strategies.

The identification of the lacking subunits in succinate dehydrogenase or ATP synthase remain important objectives to achieve. Alternative future experimental strategies may include:

- Determine standardized techniques to isolate the mitochondrion from malaria parasites as a routine procedure with a sufficient yield and purity, and with intact enzyme activities. For example, mitochondria isolation techniques used in other protists can be a source of inspiration. Hypotonic lysis coupled with Percoll gradient, as well as N_2 cavitation followed by Nycodenz gradient centrifugation, are common approaches to purify mitochondria from *T. brucei* parasites (Schneider et al., 2007). In the protozoan parasite *Blastocystis hominis,* the mitochondria-like organelle is isolated and purified using a sucrose gradient (Nasirudeen and Tan, 2004).

- Generate and characterise antibodies against full length SdhA or SdhB, ATPase subunit α (ATPα) or β antigens. Peptide-based antibodies, used in this study, worked predominantly in applications where the target protein was denatured whereas antibodies raised against full length protein antigens perform well against both denatured and native target (Brown et al., 2011). It may be possible to capture the whole complex II or ATP synthase from *P. falciparum* by immunoprecipitation in non-denaturing conditions with an antibody able to recognize folded antigens. Then, the subunit composition of the complex could be resolved by SDS-Page. The subunit composition of mammalian NADH dehydrogenase, F_1F_0 ATP synthase, complex II or III has been shown using one-step immunopurification with monoclonal antibodies (Aggeler et al., 2002; Murray et al., 2003; Schilling et al., 2006). To acquire the antigens needed, a recombinant subunit should be cloned, over-expressed and purified before generating polyclonal or monoclonal antibodies by immunization. However, recombinant synthesis and purification of full length proteins can be complicated tasks with uncertain success.

- Attempt a similar two-dimensional proteomic approach using gametocytes or sporozoites as source of mitochondrial enzymes instead of blood stage parasites. The expression of ETC-related genes such as type II NADH dehydrogenase, glycerol-3-phosphate dehydrogenase or cytochrome *c* were showed to be up-regulated for parasite stages having cristate mitochondria (Boysen and Matuschewski, 2011; Vontas et al., 2005). Those cristae are internal compartments of the inner membrane increasing the surface

for ETC complexes allowing for a higher rate of oxidative phosphorylation. Cristae morphology of the mitochondrion was reported for sexual and mosquito stages whereas acristate mitochondria were found for asexual erythrocytic stages (Langreth et al., 1978).

Chapter 4

Electron contribution and membrane potential generation in *Plasmodium falciparum* mitochondria

4.1. Introduction

4.1.1. Dehydrogenase contribution to the electron flow and membrane potential generation

As described in Chapter 1 section 1.2.4.3**,** the *Plasmodium* respiratory chain is composed of five dehydrogenases: type II NADH dehydrogenase (*Pf*NDH2), succinate dehydrogenase (SDH), dihydroorotate dehydrogenase (DHODH), glycerol-3-phosphate dehydrogenase (G3PDH) and malate:quinone oxidoreductase (MQO). These five membrane-bound dehydrogenases convert ubiquinone (UQ) to ubiquinol (UQH_2) which in turn is re-oxidised by the bc_1 complex (complex III), feeding the electron transport chain (ETC). Thus, these enzymes contribute to the maintenance of the membrane potential generated by the vectorial translocation of protons (H^+) from complex III and IV, and are essential for parasite survival. However, little is known about their relative contribution to the overall electron-flow at a given reduction state of the UQ-pool, and to the membrane potential generation. Furthermore, data regarding the presence and turnover of the ETC dehydrogenases have been reported in different studies but are fragmented and contradictory (Fry and Beesley, 1991; Kawahara et al., 2009; Krungkrai, 1995; Mather et al., 2010; Takashima et al., 2001).

The most accurate method to determine the activity of those five dehydrogenases is to measure the oxidation of their substrate (NADH, succinate, dihydroorotate, malate and glycerol-3-phosphate) or the reduction of their native electron acceptor (ubiquinone 8 (UQ_8)). Because UQ_8 is too hydrophobic and cannot be used as an exogenous substrate, dehydrogenase assays are commonly assayed with more hydrophilic analogues such as the artificial short-chain ubiquinone UQ_1. *Dehydrogenase s*ubstrate-product pairs cannot be detected spectrophotometrically in a reaction mixture, except for NADH which strongly absorbs ultraviolet light at 340 nm (ε_{340nm} = 6.22 $mM.cm^{-1}$). With a maximal absorption at 283 nm (ε_{280nm} = 8.10 $mM.cm^{-1}$), UQ is thus the most reliable indicator for monitoring dehydrogenase activities but can be impaired by the presence of opaque hemozoin pigments. Contained within *Plasmodium* membrane compartments, hemozoins are dark brown particles with a high propensity for light scattering. They significantly affect the absorbance spectra between the UV region and 625 nm with a peak around 400 nm. The hemozoin

particles represent a challenge to spectrophotometric measurements of enzyme activities in malaria parasites (Biagini et al., 2006; Mather et al., 2010). To overcome this problem, employment of colorimetric linked assays is an alternative way to measure dehydrogenase activities in *Plasmodium* species. Each ubiquinone reductase can be determined by two types of UQ-pool linked assays measuring either (i) the reduction of exogenous cytochrome *c* through the bc_1 complex activity which uses the generated UQH_2 as substrate (ii) or the artificial electron acceptor dichlorophenolindophenol (DCPIP) reduced by released UQH_2 in the lipid bilayer **(Fig. 4.1)**. The PMS/MTT system is another approach to evaluate the substrate oxidation from flavoproteins by reduction of the artificial electron acceptor MTT (methylthiazolyldiphenyl-tetrazolium bromide) via the artificial electron mediator PMS (phenazine methosulfate).

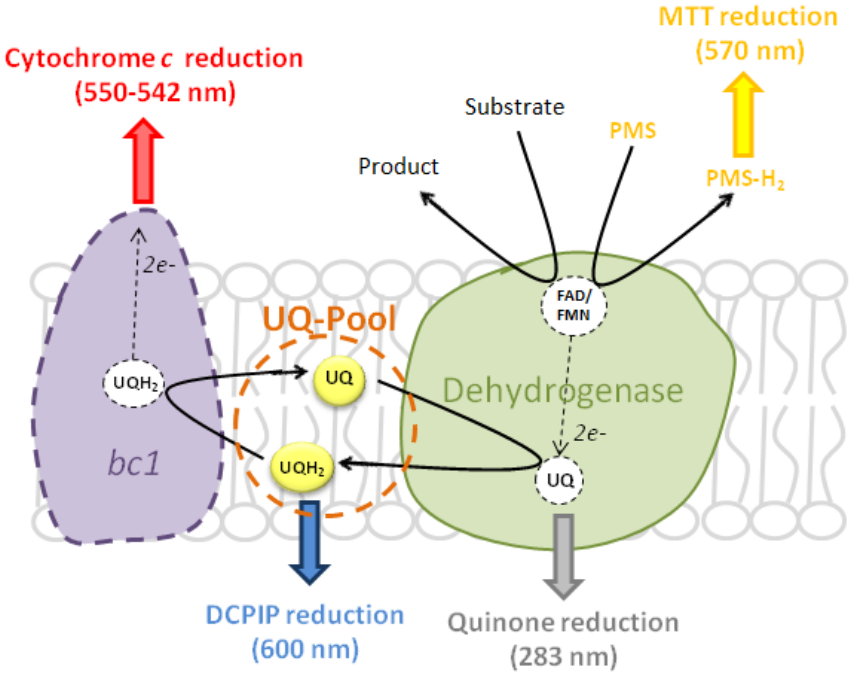

Figure 4.1. Schematic representation of different types of electron acceptors used to determine the dehydrogenase activity in *Plasmodium* species. Their peak absorptions are indicated in brackets. Abbreviations: PMS, phenazine methosulfate; MTT, methylthiazolyldiphenyl-tetrazolium bromide**;** DCPIP, dichlorophenolindophenol; UQ, ubiquinone; UQH_2, ubiquinol, bc_1; bc_1 complex.

Fry and Beesley were the first to indirectly measure different dehydrogenases by following the cytochrome *c* reduction induced by NADH, succinate, glycerol-3-phopshate and dihydroorotate from *P. falciparum* and *P. yoelii* crude mitochondria (Fry and Beesley, 1991). Several studies have since reported specific activities of the five dehydrogenases from different *Plasmodium* species. Shown in **Table 4.1**, values obtained vary depending on the type of assay used, the procedure employed to prepare the parasite extract and the *Plasmodium* species cultivated. In this study, activities from all dehydrogenases are compared for the first time with an identical type of enzymatic assay and from the same malaria parasite preparation. This homogeneity of assays allows determination of the contribution of each dehydrogenase to the oxidative phosphorylation.

Table 4.1. Summary of *Plasmodium* dehydrogenase activities determined by different studies. Abbreviations: SDH, succinate dehydrogenase; DHODH, dihydroorotate dehydrogenase; MQO, malate:quinone oxidoreductase; G3PDH, glycerol-3-phosphate dehydrogenase; N.D., Not determined; CM, Crude mitochondria.

Reference	Assay	*Plasmodium* species	Type II NADH (NADH)	SDH (Succinate)	DHODH (Dihydroorotate)	MQO (Malate)	G3PDH (Glycerol-3-phosphate)
			Specific activity (nmol.min^{-1}.mg protein^{-1})				
Fry and Beesley, 1991	Substrate:cytochrome *c* reductase (550 nm)	*P. falciparum* (CM) *P. yoelii* (CM)	385 ± 37 470 ± 45	112 ± 13 150 ± 24	11 ± 3 18 ± 3	N.D. N.D.	176 ± 24 230 ± 31
Kawahara et al., 2009	Substrate:DCPIP reductase assay (600 nm)	*P. yoelii* (CM)	N.D.	2.66 ± 0.02	10.5 ± 1.3	N.D.	N.D.
	Substrate:cytochrome *c* reductase (550 nm)		18.6 ± 1.6	N.D.	N.D.	N.D.	N.D.
	NADH:UQ_1 reductase assay (340 nm)		42.2 ± 0.3	N.D.	N.D.	N.D.	N.D.
Takashima et al., 2001	Succinate:PMS/MTT reductase (570 nm)	*P. falciparum* (CM)	N.D.	3.05 ± 0.8	N.D.	N.D.	N.D.
	Succinate:DCPIP reductase assay (600 nm)		N.D.	4.18 ± 0.0	N.D.	N.D.	N.D.
Mather et al., 2010	Substrate:DCPIP reductase assay (600 nm)	*P. falciparum* (CM)	N.D.	13.8	9.73	11.1	N.D.
Krungkrai, 1995	Dihydroorotate:DCPIP reductase assay (600 nm)	*P. berghei* (CM)	N.D.	N.D.	0.72	N.D.	N.D.

Because dehydrogenase activities are relatively low in blood-stage parasites (Mather et al., 2010; Vaidya and Mather, 2009), if the samples are not rich in mitochondria, it is important to use a relatively large amount of cell-free parasite extract per assay (e.g. 50 µg of parasite protein). This however can lead to relatively high levels of hemozoin in the reaction mixture. By monitoring the enzyme activity at 283 nm in the presence of malaria pigment, the light is scattered and a high signal background can be measured when using conventional 1 cm pathlength cuvette. To minimize the hemozoin absorbance and interference, assays were performed in a 1 mm pathlength quartz cuvettes, reducing the high signal-to-noise ratio **(Fig. 4.2)**.

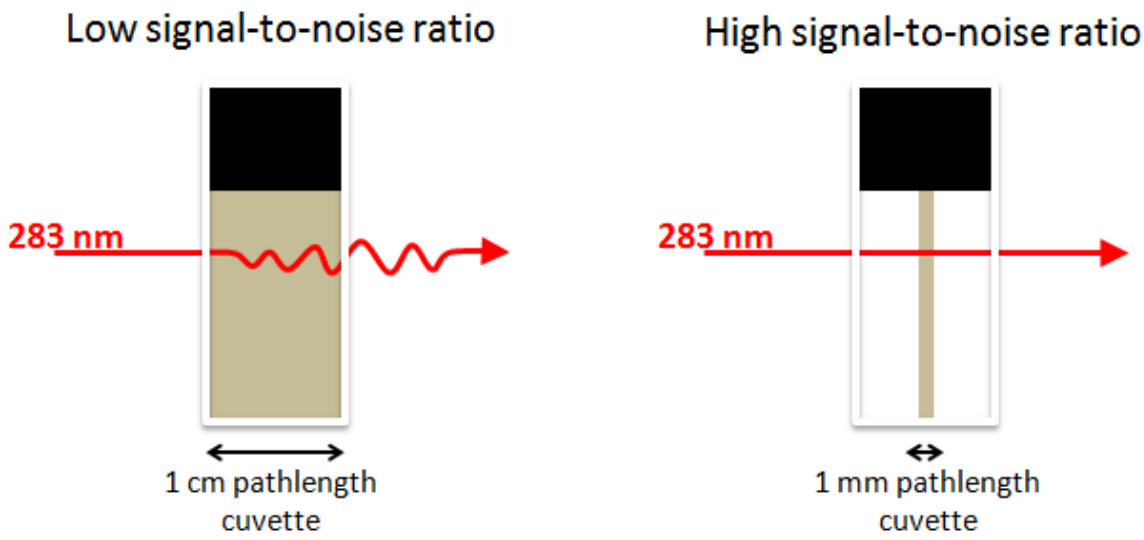

Figure 4.2. Schematic representation of 1 cm and 1 mm pathlength quartz cuvettes. With less distance of hemozoin-containing solution (indicated by a beige colour) to be crossed by the spectrophotometer beam, the 1 mm pathlength cell exhibits a lower background signal and therefore a lower signal-to-noise ratio compared to 1 cm pathlength cuvette.

With 1 mm pathlength cuvettes, quinone reduction activities (283 nm) from each dehydrogenase were assayed in *P. falciparum* cell free extract to establish their specific turnover and determine their relative contribution to the electron flow. Steady state kinetics from complex III and IV were also established in this study to determine the relative electron flux driven by both enzymes. The main providers of electrons for downstream generation of the electrochemical membrane potential were finally evaluated by monitoring the mitochondrial membrane potential in response to dehydrogenase inhibitors.

Recently, it was reported that *P. berghei* lacking the type II NADH dehydrogenase (*Pb*NDH2(-)) maintains a mitochondrial membrane potential, highlighting the hypothesis of mutual complementation among ETC enzymes (Boysen and Matuschewski, 2011). Kindly provided by Dr. Kai Matuschewski, *Pb*NDH2(-) parasites were cultivated and NADH dehydrogenase activities

were measured by direct quinone reduction and Q-pool cytochrome *c* linked assays. Compared with NADH dehydrogenase activities from *P. berghei* ANKA wild-type (WT), this work attempts to determine if the dehydrogenase complementation exists in the rodent parasite and might extrapolate to *P. falciparum.*

4.1.2. Menaquinone: an alternative electron carrier?

Menaquinone (MQ) is an alternative electron carrier of the respiratory chain mainly used by bacterial species. It is the predominant lipoquinone consumed by respiratory enzymes in Gram-positive bacteria such as *Mycobacterium* species (Collins and Jones, 1981; Pandya and King, 1966). Facultative anaerobic organisms such as *E. coli* may employ both MQ and ubiquinone (UQ) whereas mammals use only UQ **(Fig. 4.3).** In *E. coli*, the ratio MQ/UQ is regulated depending on the oxygen supply in the environment (Bekker et al., 2007; Shestopalov et al., 1997). UQ, which has a high midpoint potential (E_0' = + 110 mV), is primarily involved in aerobic respiration whereas MQ, having a low midpoint potential (E_0' = - 80 mV), is mainly consumed in anaerobic conditions.

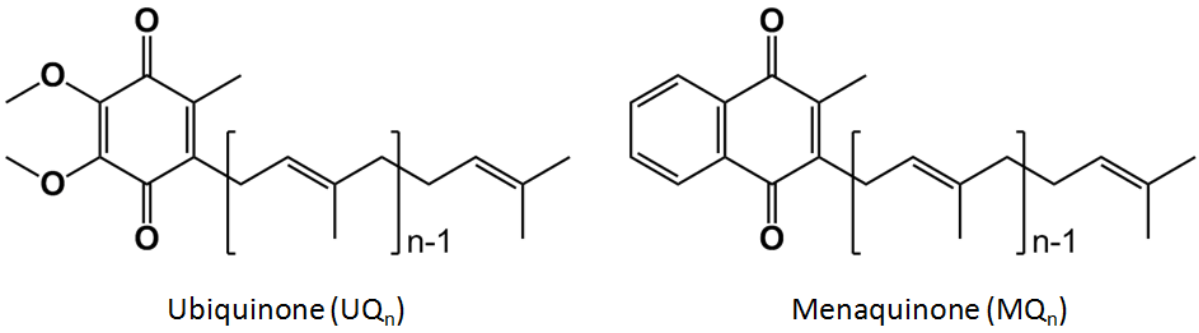

Figure 4.3. Chemical structure of ubiquinone and menaquinone.

Recently, Tonhosolo and colleagues demonstrated an active pathway for biosynthesis of menaquinone-4 (MQ_4) during the blood stage of *P. falciparum* parasites (Tonhosolo et al., 2010). This new insight suggests that MQ_4 could replace the endogenous ubiquinone as electron acceptor under anaerobic conditions. During intraerythrocytic stages, the malaria parasite might be considered as microaerophilic (Trager, 1994). Due to variations of the O_2 concentration in deep capillaries, parasites might be sequestered in an oxygen-depleted environment. Tonhosolo *et al.* confirmed that the *P. falciparum* parasite changes the content of its quinone pool depending on aeration conditions (Tonhosolo et al., 2010). Thus, parasites increase their MQ concentration by 50% and decrease their UQ counterpart by 15% after 48h of cultivation in anaerobic conditions. Additionally, they revealed that *Pf*NDH2 harvested from free parasite extracts can use MQ as an

electron carrier to oxidize NADH with an apparent K_m of 72 ± 15 µM and V_{max} of 3 ± 0.8 µmol.min^{-1}.mg^{-1}.

In mycobacteria, the menaquinol (MQH_2) produced by both type II NADH dehydrogenase and succinate dehydrogenase is directly re-oxidized by the supercomplex cytochrome bc_1 / cytochrome aa_3 or the cytochrome *bd*-type terminal oxidase (Matsoso et al., 2005). However, no data are available on the capacity of *P. falciparum* bc_1 complex to utilize MQH_2 as a coenzyme.

To determine if menaquinone might be used as an alternative electron carrier by the *P. falciparum* ETC, *Pf*NDH2 and bc_1 complex activities were measured in presence of MQ and MQH_2, respectively. These experiments were performed in anaerobic conditions to minimise possible non-enzymatic redox reactions.

4.2. Material & Methods

4.2.1. Preparation of decylubiquinol

The artificial quinol electron donor was prepared based on a previously described method (Fisher et al., 2004b). Briefly, 2,3-dimethoxy-5-methyl-n-decyl-1,4-benzoquinone (decylubiquinone), an analogue of ubiquinone (Sigma, St-Louis, USA), was dissolved (10 mg) in 400 µl of nitrogen-saturated hexane. An equal volume of aqueous 1.15 M sodium dithionite was added, and the mixture shaken vigorously until colourless. The upper, organic phase was collected, and the decylubiquinol recovered by evaporating off the hexane under N_2. The decylubiquinol was dissolved in 100 µl of 96 % ethanol (acidified with 10 mM HCl) and stored in aliquots at -80 °C. Decylubiquinol concentration was determined spectrophotometrically from absolute spectra, using $\varepsilon_{288\text{-}320}$ = 4.14 mM^{-1}.cm^{-1} **(Figure 4.4)**.

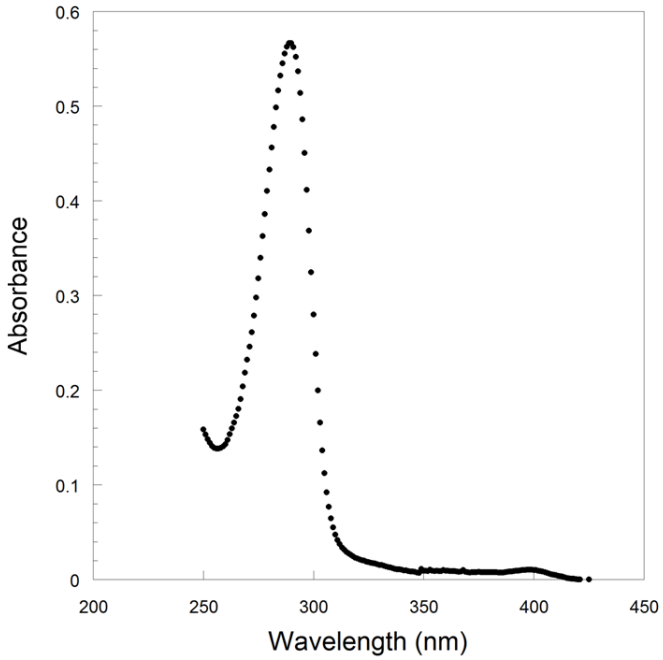

Figure 4.4. Absorption spectra of decylubiquinol. The concentration of decylubiquinol was determined by measuring the absorbance difference between 288 and 320 nm using an extinction coefficient of 4.14 $mM^{-1}.cm^{-1}$.

4.2.2. Preparation of recombinant *P. falciparum* type II NADH dehydrogenase (*Pf*NDH2).

Crude membranes containing the recombinant *Pf*NDH2 were prepared from the *E. coli* heterologous expression strain F571 according to the method described by Fisher *et al.* (Fisher et al., 2009). *E. coli* F571 cells were prepared from LB broth containing 100 $\mu g.ml^{-1}$ ampicillin, 50 $\mu g.ml^{-1}$ kanamycin and 10 $\mu g.ml^{-1}$ tetracycline. 10 ml of bacterial cells were grown overnight at 37°C in a shaking incubator (200 rpm). The following day these cultures were propagated in 400 ml LB broth containing appropriate antibiotics and grown at 37°C with shaking at 200 rpm. When the culture reached the point of inoculation (OD_{600} = 0.6), 1 mM IPTG was added to the bacterial cultures to induce expression and maximize the yield of the recombinant *Pf*NDH2. The cells were grown at 37°C for 16 h, with shaking at 200 rpm. After growth, the cells were harvested by centrifugation at 4,000 x g for 20 min. Cells were resuspended in ice-cold buffer containing 50 mM KPi pH 7.4, 2 mM EDTA and a cocktail of protease inhibitors (Roche). The resuspended cells were disrupted by two passes through a French press at a pressure of 25,000 psi. The cell lysate was centrifuged at 10,000 rpm for 20 min at 4°C to remove unbroken cells. Membranes were recovered from the supernatant after ultracentrifugation (1 h at 100,000 x g and 4°C). The membranes were resuspended via a homogenizer in 500 µl of ice-cold buffer with 50 mM KPi pH 7.4, 2 mM EDTA and protease inhibitors. Membranes were aliquoted and stored at -80°C.

4.2.3. Measurement of ubiquinone reduction induced by NADH, succinate, glycerol-3-phosphate, malate and dihydroorotate.

NADH, SDH, G3PDH, MQO and DHODH activities were measured spectrophotometrically by following the reduction of ubiquinone-1 (UQ_1) at 283 nm (ε_{283} = 8.1 $mM^{-1}.cm^{-1}$) with a Cary 4000 spectrophotometer (Varian Inc, USA). Enzyme activities were measured in a buffered solution (final volume 120 µl) containing 50 mM potassium phosphate (pH 7.5), 2 mM EDTA, 10 mM KCN (1 M stock solution, pH adjusted to 7.5) and 50 µM coenzyme Q_1 at room temperature. *P. falciparum* enzymes were present as a cell-free *P. falciparum* extract (preparation described in section 2.2) at a total protein concentration of 30-60 $\mu g.ml^{-1}$. Inhibitors were added prior the addition of substrate. The reaction volume was 120 µl and assays were performed in a 1 mm pathlength quartz cuvette (Varian, USA). Inhibitors were added prior to initiation of the reaction by addition of 200 µM NADH, 10 mM succinate, 10 mM malate, 10 mM glycerol-3-phosphate or 1 mM dihydroorotate.

4.2.4. Measurement of ubiquinol:fumarate oxidoreductase activity

The ubiquinol:fumarate reductase (QFR) reaction was assayed by following the oxidation of decylubiquinol (dQH_2) at 283 nm (ε_{283} = 8.1 $mM^{-1}.cm^{-1}$). QFR activity was initiated by addition of 10 mM fumarate in a buffered solution (final volume of 120 µl in a 1 mm pathlength quartz cuvette) containing 50 mM potassium phosphate (pH 7.5), 2 mM EDTA, 10 mM KCN, 50 µM dQH_2 and *P. falciparum* cell-free extract (concentration between 30 to 60 $\mu g.ml^{-1}$). Malonate inhibitor was added prior the addition of fumarate.

4.2.5. Measurement of Q-pool cytochrome *c* linked assay induced by dehydrogenase substrates

Cytochrome *c* reductase activity of complex III was monitored by following the reduction of cytochrome *c* at 550-542 nm ($\varepsilon_{550-542}$ = 18.1 $mM^{-1}.cm^{-1}$). The reaction buffer consisted of 50 mM potassium phosphate (pH 7.5), 2 mM EDTA, 10 mM KCN and 30 µM horse heart cytochrome *c* (Sigma, USA). The reaction volume was 700 µl and assays were performed at room temperature with a 1 cm pathlength quartz cuvette (Varian, USA). *P. falciparum* dehydrogenases were present as a cell-free *P. falciparum* extract (preparation described in section)at a total protein concentration of 30 to 60 $\mu g.ml^{-1}$. Cytochrome *c* reductase activities were initiated by the addition of 50 µM dQH_2 (to measure bc_1 complex activity), 200 µM NADH, 10 mM succinate, 10 mM malate, 10 mM glycerol-3-phosphate or 1 mM dihydroorotate.

4.2.6. Measurement of succinate:PMS/MTT oxidoreductase activity.

The ability of complex II to pass electrons from succinate to methylthiazolyldiphenyl-tetrazolium bromide (MTT) was assayed by monitoring the absorbance increase at 570 nm (ϵ_{570} = 17 $mM^{-1}.cm^{-1}$) in the presence of phenazine methosulfate (PMS) (Tran et al., 2006). The reaction volume was 700 µl and assays were performed at room temperature with a 1 cm pathlength quartz cuvette. The reaction mixture contained a reaction buffer *(*50 mM potassium phosphate, 2 mM EDTA, pH 7.5), 750 µM PMS, 75 µM MTT and 30 to 60 $\mu g.ml^{-1}$ of cell-free *P. falciparum* extract. Malonate was added prior the initiation of the reaction by addition of 10 mM succinate. IC_{50} value was calculated by fitting data to a four-parameter logistic fit function using Kaleidagraph software (Synergy Software, USA).

4.2.7. Measurement of bc_1 protein and complex IV activities

Decylubiquinol:cytochrome *c* oxidoreductase (bc_1 protein) and cytochrome *c* oxidase (complex IV) activities were measured by monitoring the increase and decrease of cytochrome *c* reduced concentration at 550-542 nm ($\varepsilon_{550-542}$ = 18.1 $mM^{-1}.cm^{-1}$), respectively. The bc_1 reaction buffer consisted of 50 mM potassium phosphate (pH 7.5), 2 mM EDTA, 10 mM KCN and 30 µM equine cytochrome *c* oxidised (Sigma, USA) (Fisher et al., 2004b). The complex IV mixture was composed of 50 mM potassium phosphate (pH 7.5), 2 mM EDTA and 5 µM antimycin A. Antimycin A is added to inhibit the bc_1 complex downstream activity and stop the production of endogenous reduced cytochrome *c*. The reaction volume was 700 µl and assays were performed at room temperature with a 1 cm pathlength quartz *cuvette. P. falciparum* bc_1 and complex IV were present as a cell-free *P. falciparum* extract at a total protein concentration of 30-60 $\mu g.ml^{-1}$. Cytochrome *c* reductase (bc_1) and oxidase (complex IV) activities were initiated respectively by the addition of 50 µM decylubiquinol (dQH_2) and 30 µM reduced equine cytochrome *c*. The horse heart cytochrome *c* was reduced by adding a pinch of sodium dithionite and then passed through a PD-10 desalting column (Pharmacia, USA). Kinetic constants, K_m and V_{max}, were determined by fitting data to a Michaelis-Menton function using Kaleidagraph software.

4.2.8. Measurement of dehydrogenases and bc_1 complex activities with menaquinone in anaerobic conditions.

All measurements were collected on a Cary 50 scanning spectrophotometer (Varian Inc., USA) in a glove box (Belle Technology, UK) under a nitrogen atmosphere and with oxygen concentration maintained at less than 2 ppm. All buffers and solutions were degassed by bubbling with argon prior to entry into the glove box to ensure removal of O_2.

P. falciparum NDH2 (cell-free *P. falciparum* extract) and recombinant *Pf*NDH2 (at a total protein concentration of 10 to 20 µg/ml) were assayed in a reaction medium consisting of 50 mM potassium phosphate (pH 7.5), 2 mM EDTA, 200 µM NADH and 10 mM KCN. NADH:menaquinone and NADH:ubiquinone oxidoreductase activities were initiated respectively by the addition of 100 µM MQ_4 and 50 µM UQ_1. Their reduction was monitored at 286 nm and 283 nm, respectively.

Malate, glycerol-3-phosphate, succinate and DHO dehydrogenase activities were monitored at 286 nm and 283 nm in presence of MQ_4 and UQ_1, respectively. The reaction was prepared in a 120 µl final volume as described previously (section 4.2.5) and was induced by addition of 10 mM malate, 10 mM G-3-P, 10 mM succinate or 1 mM DHO in presence of cell-free *P. falciparum* extract (30-60 $\mu g.ml^{-1}$).

Menaquinol:cytochrome *c* oxidoreductase and ubiquinol:cytochrome *c* oxidoreductase activities were measured as described previously (section 4.2.9). The reaction mixture was composed of 50 mM potassium phosphate (pH 7.5), 2 mM EDTA, 10 mM KCN and 30 µM oxidised equine cytochrome *c*. The reaction was initiated by the addition of 100 µM menaquinol (MQH_2) or 50 µM decylubiquinone (dQH_2) in presence of cell-free *P. falciparum* extract (30-60 $\mu g.ml^{-1}$). Menaquinol (MQH_2) was generated from an aqueous solution of menaquinone-4 by reduction with an aqueous solution of sodium dithionite in the anaerobic environment. Artificial decylubiquinol (dQH_2) was prepared as previously described (section 4.2.3) and degassed.

4.2.9. Real-time single-cell monitoring of membrane potential

The rhodamine derivative TMRE (tetramethyl rhodamine ethyl ester) was used to monitor the membrane potential of the cytoplasm and mitochondria from malaria-infected red blood cells. TMRE is cationic and reversibly accumulates inside energized membranes according to the Nernst equation. For the experiment, suspensions (5-8% parasiteamia, 1% haematocrit) of infected erythrocytes in HEPES-buffered RPMI medium (no serum) were loaded with 250 nM TMRE (Molecular Probes, USA) for 10 min at 37°C. For imaging, malaria parasite-infected erythrocytes were immobilized using polylysine-coated coverslips in a Bioptechs FCS2 perfusion chamber (Bioptechs, USA) and maintained at 37°C in growth medium (no serum). Before each assay, cells were treated with 200 nM concanamycin A for 5 minutes in order to remove the fluorescent contribution of the plasma membrane potential ($\Delta\psi_p$) and measure only the mitochondrial membrane potential ($\Delta\psi_m$). Inhibitors were added to the perfusate, and the membrane potential-dependent fluorescence responses were monitored in real time. During all manipulations, the concentration of TMRE in the perfusate was kept at 250 nM. The fluorescence signals from malaria-infected erythrocytes were collected on a Zeiss Pascal confocal laser

scanning microscope (Zeiss, Germany) through a Plan-Apochromat 63x 1.2 numerical aperture water objective. Excitation of TMRE was performed using the HeNe laser line at 543 nm. Emitted light was collected through a 560-nm long pass filter from a 543-nm dichroic mirror. For all assays, the fluorescence dynamic range was set up so that untreated TMRE-loaded cells were regarded as having complete fluorescence (100%), whereas the baseline (0%) was set by addition of 10 µM H^+ ionophore FCCP (carbonyl cyanide *p*-(trifluoromethyl) phenylhydrazone). Photobleaching (the irreversible damage of TMRE producing a less fluorescent species) was assessed by continuous exposure (5 min) of loaded cells to laser illumination. For each experiment, the laser illumination and microscope settings (laser power, scan speed, pinhole diameter, number of scan sweeps and degree of magnification) that gave no reduction in signal were used. Data capture and extraction were carried out with Zeiss Pascal software and plot design were performed with Kaleidagraph (Synergy Software, Reading, USA).

4.2.10. *In vivo* cultivation and cell-free extracts of wild-type and *Pb*NDH2-depleted rodent malaria parasites

In vivo parasite cultivation was performed under UK Home Office Animals (Scientific Procedures) Act 1986, approved by the appropriate institutional animal care and use committee, and conducted in accordance with the International Conference on Harmonization safety guidelines. *P. berghei* ANKA-GFP (WT) and *PbNDH2*(−) parasite strains were kindly provided by Dr. Kai Matuschewski (Max Planck Institute for Infection Biology, Berlin, Germany). Blood stage *P. berghei* ANKA-GFP (WT) and *PbNDH2*(−) parasites were injected via the peritoneal cavity into male CD-1 mice and the developmental stage and parasitaemia were monitored by microscopic examination of Giemsa-stained blood smears. When a parasitaemia of asynchronous blood stage parasites reached a value greater than 10% (between 120 to 170 h after infection), about 5 to 8 ml of blood was collected from 10 mice by cardiac puncture for both parasite strains. To remove serum and buffy coat, blood was washed three times in 25 mM HEPES-buffered RPMI 1640 by centrifugation at 4°C at 2,500 x *g* for 5 min. Preparation of cell-free parasites from mouse erythrocytes was performed by treatment with 0.15% (w/v) saponin in phosphate-buffered saline. The free parasite pellets were washed four times in 25 mM HEPES-buffered RPMI 1640 by centrifugation for 5 min at 6,000 x *g* and 4 °C. Before carrying out the enzymatic assays, both cell-free parasites corresponding to WT and *PbNDH2*(−) strains, were disrupted with a probe sonicator in assay buffer (50 mM potassium phosphate, 2 mM EDTA, pH 7.5) including protease inhibitor cocktail (Complete Mini, Roche Applied Science, Germany).

4.3. Results

4.3.1. Direct and Q-pool linked dehydrogenase activities

For the first time, the five dehydrogenases were assayed from *P. falciparum* cell-free extract by directly observing the reduction of UQ_1 **(Table 4.2)**. Enzyme assays measured dehydrogenase activity values in the same range (between 2 to 9 nmol UQ_1 reduced. min^{-1} .mg $protein^{-1}$) and similar to those reported by Mather *et al*. using DCPIP UQ-pool linked assays (Mather et al., 2010). *Pf*NDH2 is the most active dehydrogenase with a specific activity value of 8.80 ± 0.64 nmol UQ_1 reduced.min^{-1}.mg $protein^{-1}$. DHODH, MQO and G3PDH seem two- to three-fold less active than *Pf*NDH2. Interestingly, no succinate:UQ_1 oxidoreductase activity could be measured despite several attempts with different parasite preparations.

Table 4.2. Specific activities of *P. falciparum* dehydrogenases by measuring directly the ubiquinone reduction. The quinone reduction rate was spectrophotometrically monitored at 283 nm with a 1 mm pathlength cuvette and *P. falciparum* cell-free extract.

Dehydrogenase	Assay	Specific Activity[1] (nmol UQ_1 red/mg protein/min ± SE)
*Pf*NDH2	NADH:UQ_1 reductase	8.80 ± 0.64
SDH	Succinate:UQ_1 reductase	0.00 ± 0.00
DHODH	Dihydroorotate:UQ_1 reductase	4.41 ± 0.68
MQO	Malate:UQ_1 reductase	3.91 ± 0.64
G3PDH	Glycerol-3-phosphate:UQ_1 reductase	2.73 ± 0.29

Values are expressed as mean ± standard error from at least 3 independent experiments.
[1] Specific activity superior to the detection limit of the substrate:UQ_1 reductase assay (= 0.05 nmol UQ_1 red/mg protein/min).

Subsequently, the capacity of each dehydrogenase substrate to provide UQH_2 to the bc_1 complex was reported by performing UQ-Pool cytochrome *c* linked assays **(Table 4.3)**. As previously observed by Fry and Beesley (Fry and Beesley, 1991), the induction by NADH provided the more important cytochrome *c* reduction with a V_{max} superior to the bc_1 turnover (assayed by induction with dQH_2). Other dehydrogenases, including the succinate dehydrogenase, showed between six to seventeen-fold less cytochrome *c* reduction than *Pf*NDH2. While induction with dHQ_2 and NADH exhibited Michaelis-Menten kinetics, linear steady-state kinetics were obtained after addition of the other substrates, indicative of slower cytochrome c reductase activities. Interestingly, a low succinate:cytochrome *c* reductase activity was measured whereas no succinate:ubiquinone oxidoreductase activity has been clearly detected. First, this variation can be explained by a basal activity from the Q-pool behaviour and independent to any succinate dehydrogenase activity. On the other hand, the succinate:ubiquinone reduction activity could be underestimated due to the properties of the UQ analogue used (UQ_1) as acceptor which may

diffuse less in the lipid bilayer than the natural ubiquinone (UQ_8). Used instead of native substrates, UQ_1 is more water-soluble than the native substrate and may not diffuse correctly in the membranes which might cause different interactions with the quinone-binding site of the enzyme.

Table 4.3. Cytochrome *c* reductase activities induced by different substrates. The cytochrome *c* reductase activity was measured spectrophotometrically at 550 - 542 nm with a 1 cm pathlength cuvette and with *P. falciparum* cell-free extract Abbreviations: dQH_2, decylubiquinol; Cyt *c*, cytochrome *c*.

ETC enzyme	Assay	Specific Activity (nmol cyt c red/mg protein/min ± SE)
bc_1 complex	dQH_2: Cyt *c* reductase	97.40 ± 5.10
*Pf*NDH2	NADH:Cyt *c* reductase	112.15 ± 6.96
SDH	Succinate:Cyt *c* reductase	6.57 ± 3.87
DHODH	Dihydroorotate:Cyt *c* reductase	13.53 ± 10.44
MQO	Malate: Cyt *c* reductase	16.02 ± 9.53
G3PDH	Glycerol-3-phosphate:Cyt *c* reductase	19.33 ± 11.60

Values are expressed as mean ± standard error from at least 3 independent experiments.

Surprisingly, the cytochrome *c* reductase activity initiated by NADH is extremely high and not comparable with the rate of quinone reduction measured from *Pf*NDH2 (8.85 ± 0.64 nmol UQ_1 red/mg protein/min). Thus, another pathway is suspected to reduce exogenous cytochrome *c* by induction with NADH. The rotenone insensitive NADH:cytochrome *b*5 reductase (PlasmoDB entry PF3D7_1367500) located on the mitochondrial outer membrane is able to reduce exogenous cytochrome *c* in presence of NADH (Sottocasa et al., 1967). Both quinone reductase and UQ-pool cytochrome *c* linked assays were performed with *P. berghei* ANKA Wild Type (WT) and a mutant strain lacking the type II NADH dehydrogenase (*Pb*Ndh2 (-)) **(Fig. 4.5)** (Boysen and Matuschewski, 2011). As expected, the mutant strain did not show any quinone reduction induced by NADH whereas WT parasites exhibited a full *Pb*NDH2 activity inhibitable by ~95% with 100 nM hydroxy-2-dodecyl-4-(1H)-quinolone (HDQ). However, the NADH:cytochrome *c* reduction activity in the WT strain was inhibited by only ~10% when using the same amount of HDQ inhibitor. Thus, this inhibited fraction can be speculated to be the cytochrome *c* reduced via the contribution of *Pb*NDH2 only. The HDQ-uninhibited activity could be reduced by ~85% and ~90% in the WT and *Pb*Ndh2 (-) strains respectively using p-hydroxymercuribenzoate (pHMB), an inhibitor of the NADH:cytochrome *b*5 reductase (Barham et al., 1996). The residual activity remaining, accounting for up to 15% of the total reduction of cytochrome *c* in the WT strain, may be due to the partial inhibition of NADH:cytochrome *b*5 reductase or from another enzyme such as the NADPH-cytochrome P450 reductase. Exogenous cytochrome *c* could be also spontaneously reduced by Reactive Oxygen Species (ROS) generated through the electron transport chain. The sonication

step during the *P. falciparum* and *P. berghei* cell-free extract preparations may mix enzymes from different membrane compartments. In consequence, the cytochrome *c* reduction activity attributed to *Pb*NDH2 was overestimated due to activities from NADH:cytochrome *b*5 reductase, maybe NADPH-cytochrome P450 reductase or ROS formation.

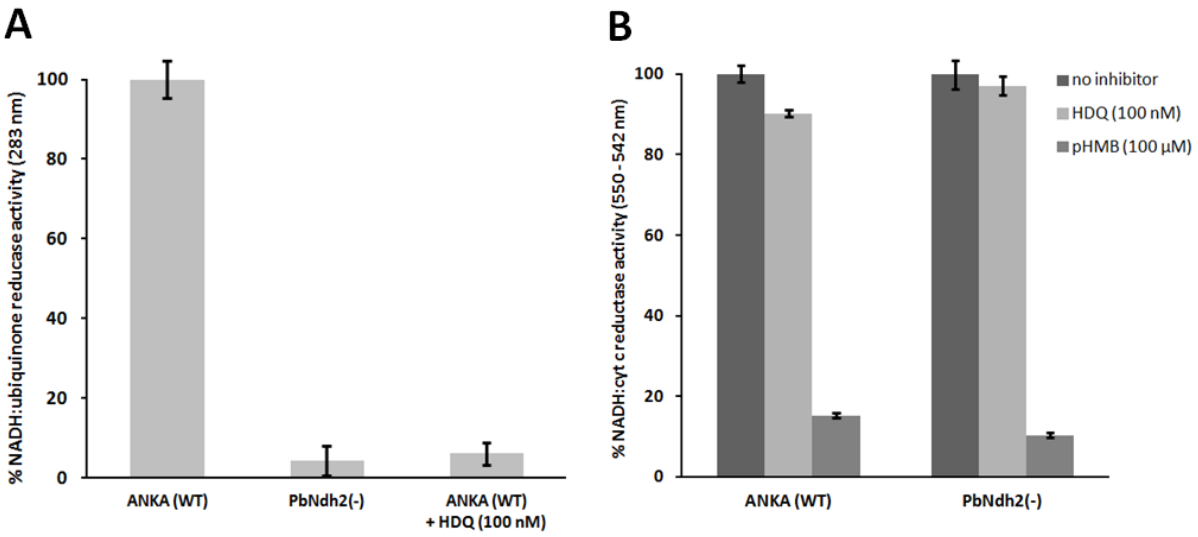

Figure 4.5. Direct quinone reduction and Q-pool cytochrome *c* linked assays with *P. berghei* ANKA wild-type (WT) and *Pb*NDH2(-). (A) Cell-free extract NADH:ubiquinone-1 reductase assay was spectrophotometrically monitored at 283 nm. **(B)** Cell-free extract NADH:cytochrome *c* reductase assay was spectrophotometrically monitored at 542-550 nm. Bars are expressed as mean ± standard error from at least 3 measurements. Abbreviations: HDQ, hydroxy-2-dodecyl-4-(1H)-quinolone; pHMB, p-hydroxymercuribenzoate.

4.3.2. Depolarization of the membrane potential by bc_1 and dehydrogenase inhibitors

To determine the consequences of inhibiting dehydrogenase activities on the mitochondrial membrane potential ($\Delta\psi_m$) real-time single-cell imaging assays were performed as described by Biagini *et al*. (Biagini et al., 2006). The measurement of mitochondrial $\Delta\psi_m$ is based on the accumulation of the cationic fluorescent probe TMRE according to the Nernst equation. The novel CK-2-68 compound, 5-fluoroorotic acid and thenoyltrifluoroacetone (TTFA) were used as selective inhibitors of *Pf*NDH2, dihydroorotate dehydrogenase and complex II, respectively **(Fig. 4.6)**. To date, no specific inhibitors for the malate:quinone oxidoreductase and the glycerol-3-phosphate dehydrogenase have been identified.

A

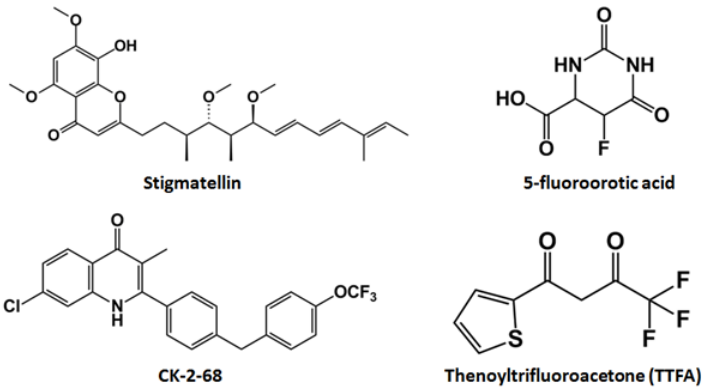

B

Enzyme	Inhibitor : IC_{50} (nM)
bc_1 complex	Stigmatellin: 12 ± 1
*Pf*NDH2	CK-2-68: 31 ± 3
Complex II	TTFA: 1,500 ± 200
DHODH	5-fluoroorotic acid: 6.1 ± 0.9
MQO	N.D.
G3PDH	N.D.

Figure 4.6. Structure and *P. falciparum* growth inhibition of bc_1 complex and dehydrogenase inhibitors. **(A)** Chemical structure of mitochondrial inhibitors used in this study. **(B)** *Plasmodium falciparum* growth inhibition IC_{50} values. Values indicated are means ± SE of results from three independent experiments. N.D.: Not determined.

In line with previous studies (Biagini et al., 2006; Srivastava and Vaidya, 1999), the inhibition of the bc_1 complex with a selective inhibitor like stigmatellin was shown to collapse the $\Delta\psi_m$ of *P. falciparum* parasites **(Fig. 4.7. A)**. Trophozoite-stage parasites were perfused with 100 nM CK-2-68 and showed a rapid and partial depolarization **(Fig. 4.7. B)**. CK-2-68 is amongst a new generation of *Pf*NDH2 inhibitors developed by a recent drug discovery project (Biagini et al., 2012). This result is consistent with the previous observation made by Biagini *et al.* where DPI, another type II NADH:dehydrogenase inhibitor, was shown to significantly reduce the TMRE fluorescence signal (Biagini et al., 2006). The $\Delta\psi_m$-dependent fluorescence of concanamycin-treated infected erythrocytes was shown to be insensitive to 5-fluoroorotic (10 µM) acid and TTFA (10 µM) **(Fig. 4.7. C and D)**. These results demonstrate clearly that *Pf*NDH2 contributes to the formation of the electrochemical gradient in our *in vitro* conditions. Although DHODH dehydrogenase is essential for pyrimidine biosynthesis, its contribution to the mitochondrial $\Delta\psi_m$ formation seems negligible due to a slower turnover. Interestingly, the conventional succinate dehydrogenase inhibitor also has no effect on the membrane potential highlighting a slow turnover or absence of the enzyme.

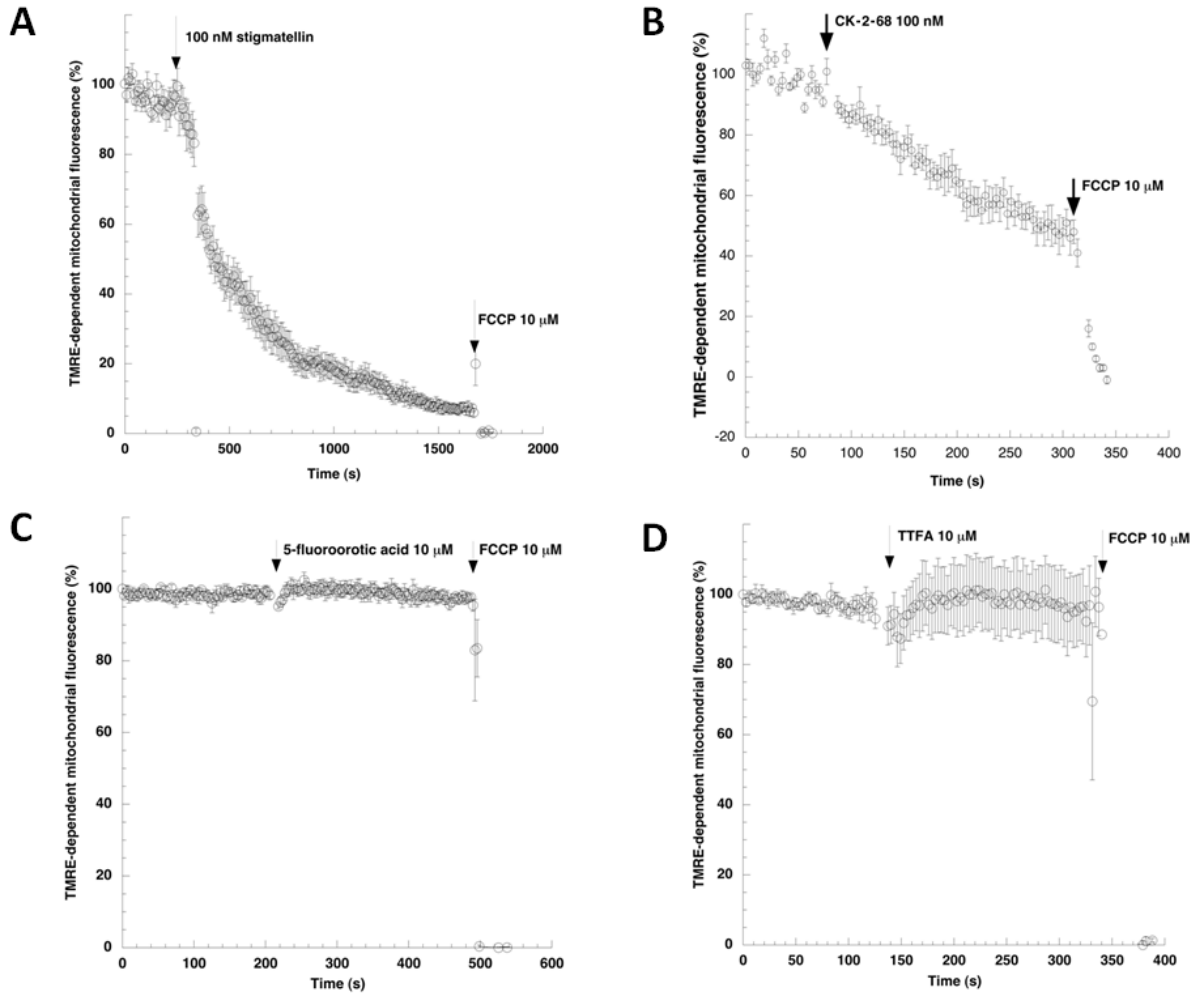

Figure 4.7. Effect of bc_1 complex and dehydrogenase inhibitors on mitochondrial membrane potential ($\Delta\psi_m$). Time course of TMRE-dependent fluorescence of *P. falciparum*-infected erythrocytes after the addition of **(A)** stigmatellin (100 nM), **(B)** CK-2-68 (100 nM), **(C)** 5-fluorootic acid (10 µM) and **(D)** TTFA (10 µM). Inhibitors were tested against concanamycin-treated cells. The baseline (0%) was set by addition of 10 µM carbonyl cyanide *p*-(trifluoromethyl) phenylhydrazone (FCCP). Data were normalized to 100% concanamycin-treated cells and to 0% in FCCP (10 µM)-treated cells. Graphs show means from experiments performed independently ± standard errors ($n \geq 7$).

4.3.3. Kinetic constants of *P. falciparum* complex III and IV.

Kinetic data from both the bc_1 complex and the cytochrome *c* oxidase are reported for the first time **(Fig. 4.8)**. Using the exogenous horse heart cytochrome *c* as electron acceptor, the bc_1 complex from *P. falciparum* cell-free parasites was shown to have a K_m value of ~5.5 µM for dQH_2. By monitoring the oxidation of reduced cytochrome *c*, the K_m and V_{max} of the cytochrome *c* oxidase were determined as ~20 µM and 2.85 nmol cytochrome *c* oxidised.min^{-1}.mg $protein^{-1}$, respectively. The relative high K_m for complex IV means a lower affinity between the enzyme and reduced cytochrome *c* than between the bc_1 complex and oxidised cytochrome *c*. The low V_{max} measured may depend on the relatively low content of cytochrome *c* oxidase in the parasite or a poor reactivity between the enzyme and the exogenous cytochrome *c* used for the assay.

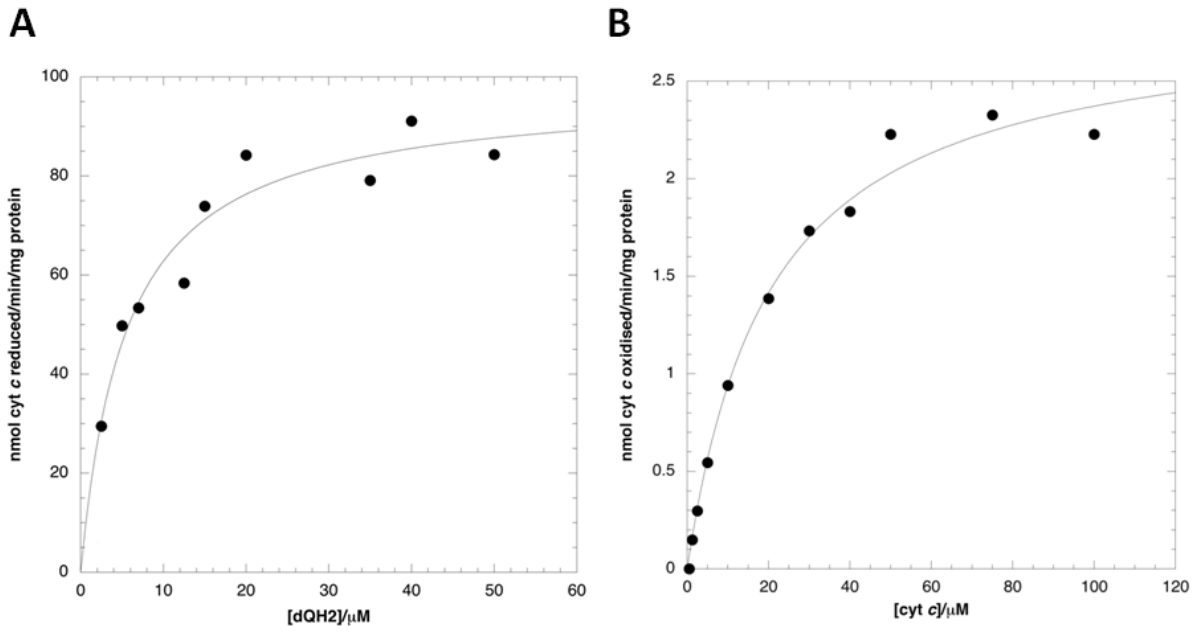

C

Enzyme	Apparent K_m (μM ± SE)	V_{max} (nmol/mg/min ± SE)
dQH_2:cythochrome *c* oxidoreductase (complex III)	5.5 ± 1.1	97.4 ± 5.1
Cytochrome *c* oxidase (complex IV)	20.3 ± 2.5	2.8 ± 0.1

Figure 4.8. Kinetics of bc_1 complex (complex III) and cytochrome c oxidase (complex IV) from cell-free *P. falciparum* extract. (A) Steady-state decylubiquinol:cytochrome *c* oxidoreductase activity of *P. falciparum* 3D7. **(B)** Steady-state cytochrome c oxidase activity of *P. falciparum* 3D7. **(C)** Kinetic constants of bc_1 complex and cytochrome *c* oxidase in *P. falciparum* 3D7.

4.3.4. Catalytic properties of *P. falciparum* complex II

As mentioned previously, no direct succinate:quinone oxidoreductase activity (SQR activity) could be detected in *P. falciparum* despite having used both ubiquinone-1 and decylubiquinone (UQ_{10} or dQ) as electron acceptors **(Table 4.4)**. Both assays showed low activities (~0.05 nmol.mg protein^{-1}.min^{-1}) corresponding to the signal background from the succinate:UQ_1 reduction. However, oxidation of succinate to fumarate (SDH activity) was detected with an activity of 4.87 ± 0.18 nmol.mg protein^{-1}.min^{-1} by monitoring the reduction of the artificial electron acceptor MTT. The succinate:PMS/MTT activity was shown to be sensitive to malonate, a complex II inhibitor, with an IC_{50} value of 4.3 ± 0.45 mM **(Fig. 4.9)**. A clear activity could be also identified (5.37 ± 0.50 nmol dQH_2 oxidized.min^{-1}.mg protein^{-1}) by monitoring the dQH_2:fumarate oxidoreduction, highlighting the presence of a ubiquinol:fumarate oxidoreductase (QFR) in malaria parasites. The QFR activity was also shown to be sensitive to a complex II inhibitor by showing 83% inhibition in presence of 10 mM malonate.

Table 4.4. The specific activities of succinate dehydrogenase (SDH) and fumarate reductase (QFR) assays from *P. falciparum* cell-free extract.

Type of assay	Specific Activity (nmol/mg protein/min ± SE)
SQR activity (succinate:UQ_1 reductase)	0.05 ± 0.03
SQR activity (succinate:dQ reductase)	0.04 ± 0.02
SDH activity (succinate:PMS/MTT reductase)	4.87 ± 0.18
QFR activity (dQH_2:fumarate reductase)	5.37 ± 0.50
QFR activity + 10 mM malonate	0.95 ± 0.40

Values indicated are means ± SE of results from three independent experiments.

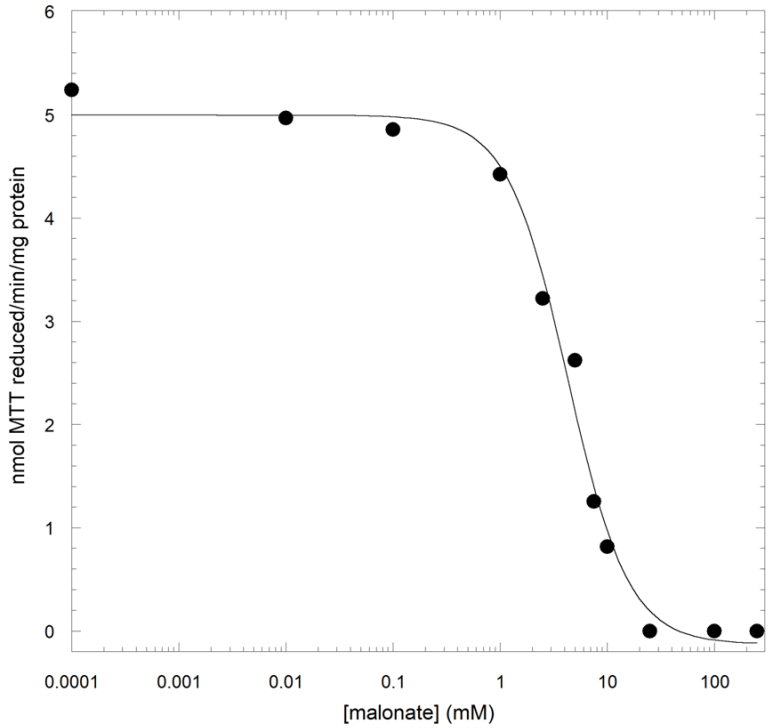

Figure 4.9. Concentration-dependent malonate inhibition of succinate:PMS/MTT activity in crude cell-free extracts. IC_{50} value was calculated by fitting of four-parameter logistic curves (Kaleidagraph software).

4.3.5. Anaerobic measurement of ETC enzymes with menaquinone as electron carrier

To determine whether menaquinone is an alternative electron carrier of the electron transport chain, NADH:quinone oxidoreductase activities induced by 100 µM menaquinone-4 (MQ) or 50 µM ubiquinone-1 (UQ) were compared in anaerobic conditions to minimise possible non-enzymatic redox reactions. With the bacterial recombinant *Pf*NDH2, depleted of hemozoin and overexpressed, no MQ reduction could be measured whereas a biphasic UQ reductase activity was obtained with an initial linear fast phase before reaching a stationary phase **(Fig. 4.10. A).** A similar result was observed with *Pf*NDH2 from cell-free parasite extract **(Fig. 4.10. B)**. No reduction of menaquinone could be measured while a slow steady-state kinetic of ubiquinone

consumption was monitored after its addition. Nonenzymatic assays demonstrated the chemical stability of MQ in the presence of NADH. The glycerol-3-phosphate:menaquinone and malate:menaquinone oxidoreductase activities were also assayed by addition of 10 mM G-3-P or 10 mM malate. **(Fig. 4.10 C and D)**. No MQ reductase activity was detected after initiation of the reaction with both substrates and in the presence of cell-free parasites, whereas slow steady-state kinetics were monitored using UQ as electron acceptor. In a similar manner, no DHO:menaquinone or succinate:menaquinone oxidoreductase activities were measured. Although carried out in an anaerobic environment, these results report that menaquinone is not an alternative coenzyme able to interact with *P. falciparum* dehydrogenases of the respiratory chain.

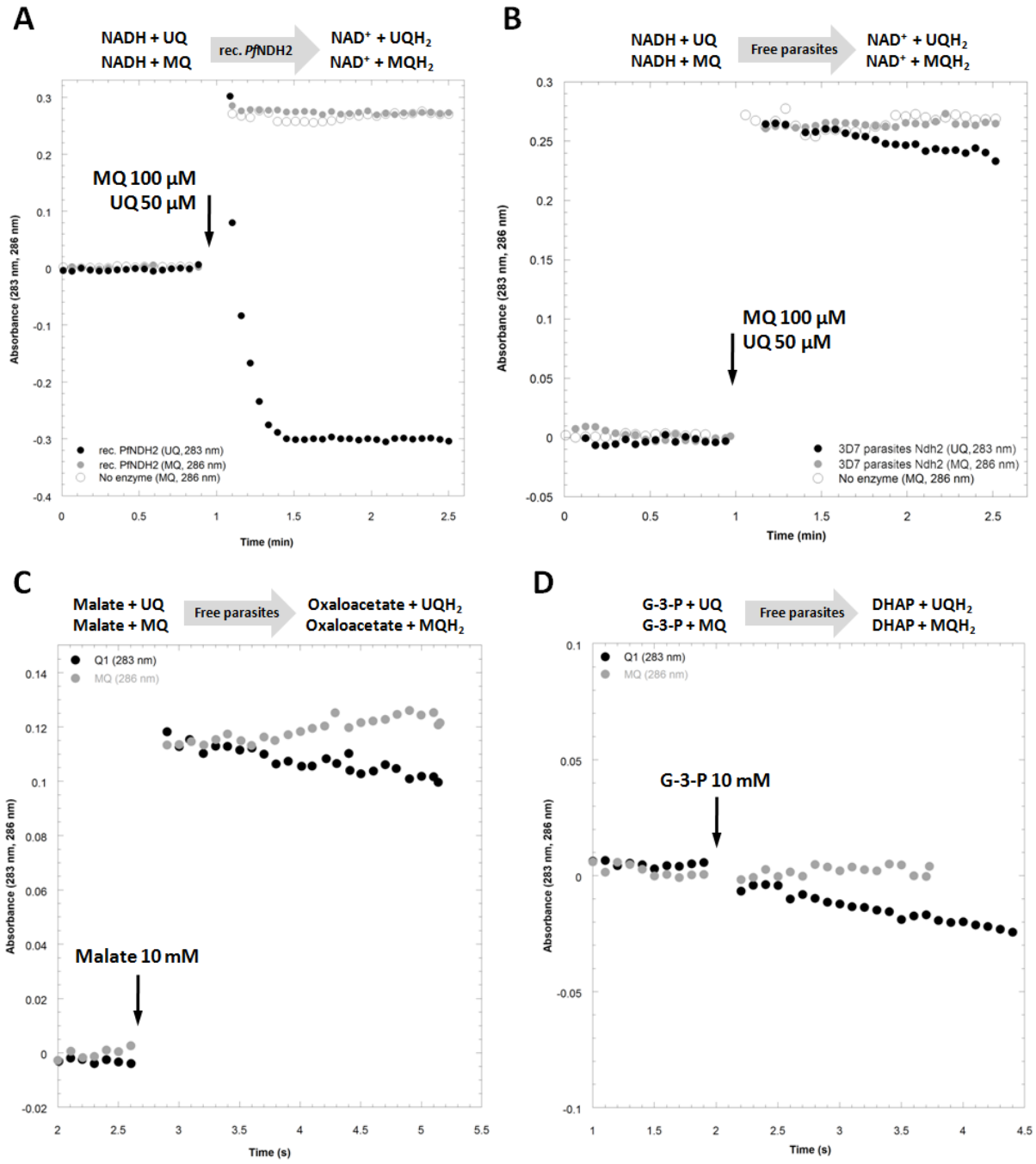

Figure 4.10. Kinetics of *P. falciparum* dehydrogenases in presence of menaquinone (MQ) or ubiquinone (UQ). (A) Recombinant *Pf*NDH2 NADH:ubiquinone (●) or NADH:menaquinone (●) oxidoreductase kinetic data monitored at 283 nm or 286 nm, respectively. The reaction was initiated by the addition of 50 µM UQ or 100 µM MQ respectively. In comparison, the nonenzymatic rate of menaquinone reduction (○, 286 nm). **(B)** Free parasites NADH:ubiquinone (●) or NADH:menaquinone (●) oxidoreductase kinetic data monitored at 283 nm or 286 nm, respectively. The reaction was initiated by the addition of 50 µM UQ or 100 µM MQ respectively. In comparison, the nonenzymatic rate of menaquinone reduction (○, 286 nm). **(C)** Free parasites malate:ubiquinone (●) or malate:menaquinone (●) oxidoreductase kinetic data monitored at 283 nm or 286 nm, respectively. The reaction was initiated by the addition of 10 mM malate. **(D)** Free parasites G-3-P:ubiquinone (●) or G-3-P:menaquinone (●) oxidoreductase steady data monitored at 283 nm or 286 nm, respectively. The reaction was initiated by the addition of 10 mM G-3-P. Abbreviations: UQ, ubiquinone-1; MQ, menaquinone-4; QH_2, ubiquinol-1; MQH_2, menaquinol-4; G-3-P, glycerol-3-phoshapte; DHAP, dihydroxyacetone phosphate; rec. PfNDH2, recombinant *Pf*NDH2.

Furthermore, the reduction of cytochrome *c* induced by menaquinol via the *P. falciparum* bc_1 complex has been tested. For this assay, menaquinol-4 (MQH_2) was used as substrate and the reduction of exogenous cytochrome *c* was monitored in strictly anaerobic conditions and with sonicated cell-free parasites. A fast cytochrome *c* reduction initiated by 100 µM MQH_2 was detected **(Fig. 4.11. A)**. However, similar kinetics were observed without parasite enzymes present in the reaction mixture. This suggests that MQH_2 directly and spontaneously reduces cytochrome *c* without enzymatic catalysis in our assay conditions. To confirm the properties of MQH_2 to be oxidised spontaneously, the reduction of NAD^+ induced by 100 µM menaquinol (*Pf*NDH2 in reverse) was assayed with and without cell-free parasite enzymes **(Fig. 4.11. B)**. High NAD^+ reduction activity initiated by MQH_2 was measured in the enzymatic and nonenzymatic assays. It suggests that menaquinol-4 (MQH_2) leads to an unspecific NAD^+ reductase activity. To conclude, electrons from MQH_2 are not used by the *P. falciparum* bc_1 complex to reduce cytochrome *c*. In anaerobic conditions, MQH_2 is stable but can be spontaneously re-oxidised to MQ in the presence of an oxidant such as cytochrome *c* oxidised or NAD^+. To note, no *Pf*NDH2 working in reverse, which reduces UQH_2 or MQH_2 in the presence of NAD^+, has been reported in the literature. In line with this, ubiquinol and NAD^+ were added together and no formation of UQ or NADH has been noted, indicative of stability between both components.

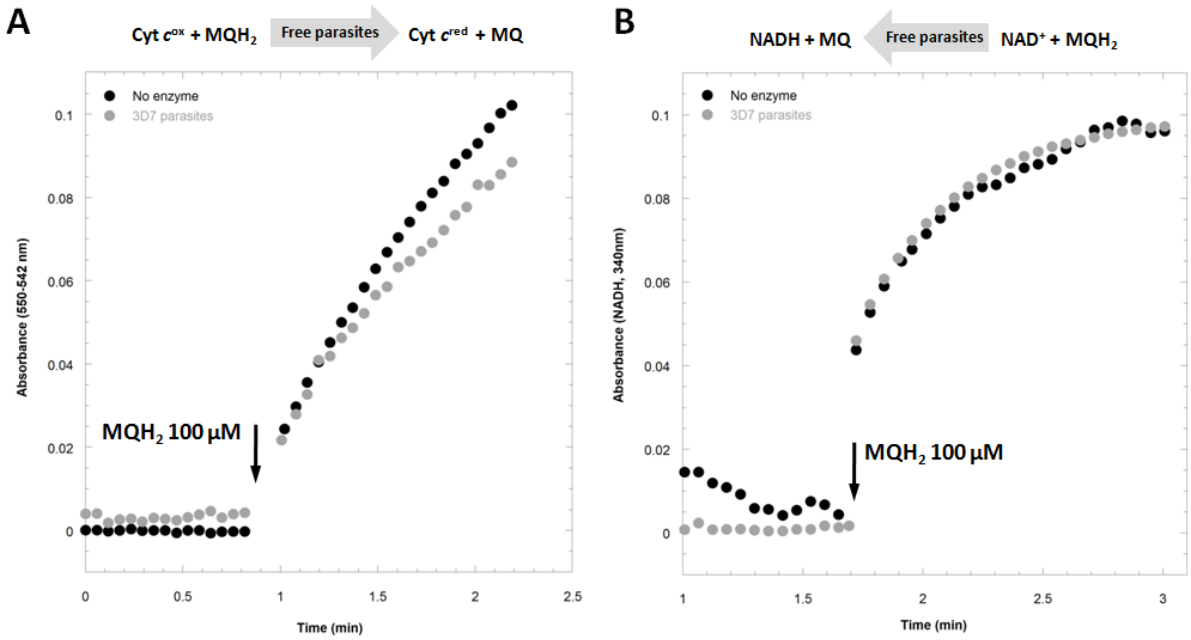

Figure 4.11. Kinetics of *P. falciparum* bc_1 complex and the reversible reaction in the presence of menaquinone. (A) Menaquinol:cytochrome *c* oxidoreductase (●) kinetic data monitored at 550-542 nm and initiated by the addition of 100 µM MQH_2. For comparison, the nonenzymatic rate of MQH_2 oxidation (●). **(B)** Electron transfer ability between MQH_2 and NAD^+ in the presence of cell-free parasites (●) or without enzymes (●).

4.4. Discussion

4.4.1. *Pf*NDH2 appears to be the main electron donor

For the first time, direct quinone reductase activities were measured for all dehydrogenases. The apparent activities of those enzymes remain low due to their low expression in the blood stages of malaria parasites (Vaidya and Mather, 2009). Those minimal dehydrogenase activities are consistent with an energy metabolism based on the glycolytic pathway during asexual stages (Fry et al., 1990).

Despite their relative low activity, dehydrogenases are the primary electron source of the mitochondrial membrane potential ($\Delta\psi_m$), which is indispensible to mitochondrial function (Srivastava et al., 1997). In this study, a robust assay developed for real-time, single-cell measurement of mitochondrial electrochemical gradient in *P. falciparum*-parasitized erythrocytes was used (Biagini et al., 2006). The inhibition of certain ETC enzymes such as bc_1 complex and *Pf*NDH2 were confirmed to collapse the $\Delta\psi_m$ of *P. falciparum* mitochondria. Thus, a partial collapse of mitochondrial $\Delta\psi_m$ was observed upon addition of CK-2-68, a novel *Pf*NDH2 inhibitor (IC_{50} = 16 ± 2 nM against the parasite enzyme). Because CK-2-68 is a moderate inhibitor of the bc_1 complex (IC_{50} = 500 ± 120 nM against the parasite *enzyme* bc_1), part of the depolarization observed (with 100 nM CK-2-68) may be caused by this inhibition. However, the contribution of *Pf*NDH2 inhibition to the collapse has been recently confirmed by demonstrating depolarization at concentration as low as 1 nM CK-2-68, 500-fold below the IC_{50} against bc_1 (Biagini et al., 2012). On the other hand, attempts to depolarize the membrane potential with inhibitors of complex II or DHODH failed. It suggests that *Pf*NDH2 is a key electron donor for downstream generation of the electrochemical membrane potential, although at this stage a contribution by G3PDH and MQO cannot be ruled out.

By monitoring the absence of NADH:ubiquinone oxidoreductase activity in the mutant *Pb*Ndh2(-), this study confirms that *P. berghei* lacking the type II NADH dehydrogenase can develop normally in asexual stages. However, Boysen *et al*. revealed that *Pb*Ndh2 (-) parasites were transformed into aberrant immature oocyst in the mosquito midgut highlighting the necessity of that enzyme for the sexual stage development (Boysen and Matuschewski, 2011). Recently, the succinate dehydrogenase has also been reported to be dispensable for the sexual blood stage of *P. berghei* parasites, via a deletion of the gene encoding the flavoprotein subunit (mutant strain termed *Pb*SdhA (-)) (Hino et al., 2012). As for *Pb*NDH2 (-), *Pb*SdhA (-) ookinetes failed in oocyst formation, leading to complete malaria transmission blockade. NDH2, complex II and maybe other dehydrogenases are not essential for *P. falciparum* blood stages which rely

mainly on cytoplasmic glycolysis raher than oxidative phosphorylation for their energy metabolism (Fry et al., 1990). Nevertheless, these enzymes seem indispensable for the parasite survival during mosquito stages. At the beginning of sexual maturation, parasites may switch their energy metabolism to oxidative phosphorylation which can explain the high number of cristate mitochondria present in gametocytes and mosquito stage parasites (Krungkrai et al., 2000). During those stages, parasites may need a large amount of ATP which could be generated by oxidative phosphorylation via a complete respiratory chain.

Furthermore, both *Pb*Ndh2 (-) and *Pb*SdhA (-) maintain a mitochondrial membrane potential, supporting the hypothesis of mutual complementation among dehydrogenases (Boysen and Matuschewski, 2011; Hino et al., 2012). This parasite adaptation highlights the crucial function of ETC enzymes to maintain the electrochemical gradient during the blood stages. It is also important to note that essentiality of genes expressing the same function are not always conserved between the human and murine malaria species, and it remains to be determined whether this is the case for mitochondrial ETC genes.

4.4.2. The bc_1 complex is the main proton pump

In *P. falciparum*, the bc_1 complex and the cytochrome *c* oxidase are the only two enzymes pumping protons from the mitochondrial matrix to the intermembrane space, in order to generate the mitochondrial electrochemical gradient (Vaidya and Mather, 2009). Both bc_1 complex and cytochrome *c* oxidase catalytic constants were determined in *P. falciparum* cell-free extract. By using substrates in excess, bc_1 complex displays a 35-fold higher V_{max} rate than complex IV. In human mitochondria, the complex IV has an activity only 1.4 ± 0.2 higher than complex III (Valnot et al., 1999). Such differences in V_{max} could be explained by a variable content in respiratory chain complexes and/or a difference in the enzyme turnover. Under the reaction conditions in the cuvette with uncoupled (i.e damaged) mitochondria, the complex III is pumping more protons than complex IV. In vivo, that situation remains quite unknown. However, it could be interesting to observe the behaviour of both enzymes from *P. berghei* mitochondria.

4.4.3. *P. falciparum* complex II: an ubiquinol:fumarate reductase?

The complex II belongs to the succinate:quinone oxidoreductases superfamily that includes succinate:quinone reductases (SQRs) and quinol:fumarate reductases (QFR). SQR oxidizes succinate to produce fumarate as a TCA cycle and respiratory chain member (Saraste, 1999). In facultative anaerobic bacteria or lower eukaryotes, QFR catalyzes the reverse reaction of SQR by reducing fumarate with ubiquinol as an electron donor (Sakai et al., 2012). SQR and QFR are

homologous proteins evolved from a common ancestor and have been shown to catalyze both reactions (Guest, 1981; Maklashina et al., 1998).

The catalytic properties of the *P. falciparum* complex II were examined using various electron donors and acceptors. By directly following quinone reduction at 283 nm, no SQR activity could be detected. This result can be explained by the lack of a suitable binding site for the ubiquinone coenzyme. This result opposes previous studies which demonstrated the presence of a SQR activity by using the DCPIP Q-pool linked assay (Kawahara et al., 2009; Mather et al., 2010; Takashima et al., 2001). The succinate oxidation (SDH activity) were only detected by using the malonate sensitive succinate:PMS/MTT assay. This enzymatic approach does not require the reduction of the ubiquinone at its binding site located into the anchoring subunits (Hagerhall, 1997). This SDH activity confirms the enzymatic functionality of the SdhA/SdhB dimer in *P. falciparum* parasites but the lack of ubiquinone reduction highlights the absence of a conventional SQR enzyme. This may be explained by the lack of SdhC and SdhD subunits or a dissociation between the SdhA/SdhB dimer and their anchor domain (SdhC/SdhD dimer). Genes encoding for SdhA and SdhB may have been annotated too soon as subunits for an SQR enzyme whereas they might be components of a QFR dehydrogenase.

The detection of a malonate sensitive QFR activity in presence of decylubiquinol as electron donor indicates that *Plasmodium* complex II functions as a quinol-fumarate reductase in intraerythrocytic parasites. Earlier, Fry and Beesley found that fumarate inhibits the reduction of cytochrome *c*, implicating the presence of a fumarate reductase activity in *P. falciparum* (Fry and Beesley, 1991). Furthermore, no succinate dependent oxygen consumption has been observed in *P. falciparum* blood or sexual stages (Krungkrai et al., 1999; Takashima et al., 2001). Recently, Tanaka *et al*, showed that *P. falciparum* parasites possessing the disrupted SdhA subunit present growth retardation and can be rescued by addition of succinate, and not fumarate, suggesting the presence of a QFR as complex II (Tanaka et al., 2012).

To conclude, *P. falciparum* complex II appears to function as a QFR, incapable of SQR activity. As in malaria parasites, the QFR from *Wolinella succinogenes* was shown to not catalyze the reversible SQR reaction (Juhnke et al., 2009). However, these results contrast with the branched TCA cycle metabolism proposed in the parasites (hypothesis recently retracted), which display a functional succinate:quinone oxidoreductase (Olszewski et al., 2010). Therefore, further enzymatic and biochemical analysis are essential to confirm the nature of this enzyme and its physiological role.

4.4.4. Menaquinone in not an alternative ETC redox exchanger

In their study, Tonhosolo et al. demonstrate that type II NADH dehydrogenase from *P. falciparum* extracts can use menaquinone-4 to oxidize NADH (Tonhosolo et al., 2010). This work presented contradictory results concerning the involvement of menaquinone in the *P. falciparum* respiratory chain. On one hand, dehydrogenases such as *Pf*NDH2, malate:quinone oxidoreductase or glycerol-3-phosphate dehydrogenase from cell-free parasite extracts has been shown to not use menaquinone-4 as an electron acceptor. On another hand, those activities performed in identical conditions in presence of ubiquinone were clearly detected which argues that it is the only electron carrier used by ETC dehydrogenases. Additionally, no menaquinol:cytochrome *c* oxidoreductase activity catalyzed by the bc_1 complex could be detected due to a certain instability of the MQH_2 which reduced cytochrome *c* or NAD^+ spontaneously. The midpoint redox potential (termed E_0' at pH 7.0) of the MQ/MQH_2 couple is around − 80 mV, thus making MQH_2 a strong reductant (Unden and Bongaerts, 1997). By contrast, the E_0' of the UQ/UQH_2 couple is around + 110 mV. The more negative midpoint potential of menaquinone, compared to ubiquinone, may contribute to its sensitivity to auto-oxidation in presence of electron acceptors such as NAD^+ or cytochrome *c* oxidised. In the line with this, an unspecific menaquinol-4:cytochrome *c* oxidoreductase activity has already been observed due to the high temperature at which the assays were performed (Refojo et al., 2012). In this study, experiments were carried out in an anaerobic glove box maintained at room temperature (between 20 to 25°C). NADH which is highly reductant with an E_0' around -320 mV, has also been demonstrated to reduce cytochrome *c* at a rate of 20 nmol.cyt *c* reduced. mg $protein^{-1}.min^{-1}$, in the absence of *Plasmodium* enzymes (Fisher et al., 2009). Moreover, no fumarate reduction induced by menaquinol could be measured (data not show). This implies that the putative QFR detected is not able to employ lower potential quinones.

To conclude, the menaquinone pool was demonstrated to not be involved in the respiratory chain and only the ubiquinone pool interacts with ETC enzymes. By inhibiting menaquinone biosynthesis with a 1,4-dihydroxy-2-naphthoate prenyltransferase inhibitor (Ro 48-8071 compound), Tonhosolo *et al.* showed a decrease of the parasitic growth (Tonhosolo et al., 2010). However, a reversal of growth inhibition by adding menaquinone failed indicating either an insufficient uptake of exogenous menaquinone by the parasites or that menaquinone is not essential for parasite growth. Further metabolomic and biochemical studies are need to clarify the physiological role of menaquinone in malaria parasites and to validate if its biosynthesis may be regarded as a potential new drug target.

The **Figure 4.12**. represents an updated picture of the electron transport chain in *P. falciparum* including new insights proposed in this chapter.

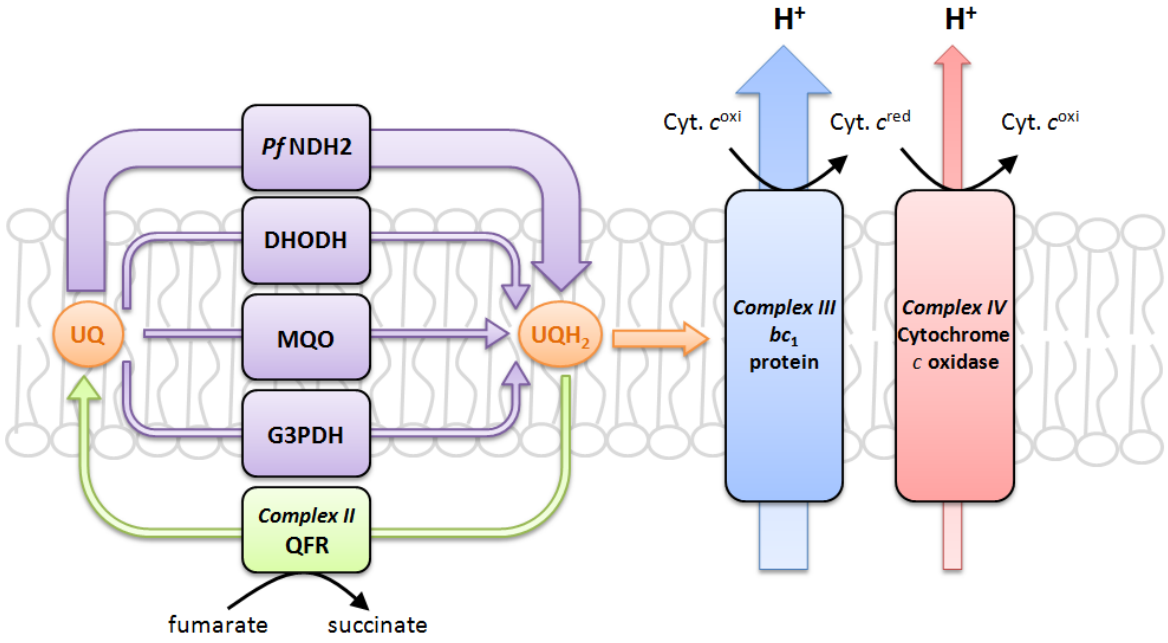

Figure 4.12. Schematic representation of the electron transport chain in *P. falciparum* parasites. The thickness of arrows represents the relative importance of the electron or proton flux catalyzed by the enzyme.

Chapter 5

Rapid Fe^{2+}-chelatable depolarization of plasma and mitochondrial membrane potential by artemisinin and semi-synthetic endoperoxides

5.1. Introduction

5.1.1. Chemical structures and characteristics of endoperoxide compounds

Artemisinin is a unique tetracyclic 1,2,4-trioxane containing an endoperoxide bridge (C-O-O-C) but lacking the nitrogen-containing ring system which is found in most antimalarial drugs (Meshnick et al., 1996; Van Geldre et al., 1997). In 1985, the endoperoxide bridge was identified as the key pharmacophore of the drug (Klayman, 1985). To improve the solubility and the pharmacological activity of artemisinin, a first series of semi-synthetic compounds was synthesized with a similar backbone but with modifications at the C_{10} position generating ester or ether derivatives like dihydroartemisinin (DHA), artemether and artesunate **(Fig. 5.1)**. Artemisinins are efficient against malaria parasites at low nanomolar concentrations while micromolar ranges are needed for toxicity in mammalian cells (O'Neill and Posner, 2004). This selectivity can be explained by a higher uptake of the trioxane drug by the parasite. Indeed by using isotopic labelled [^{3}H]-dihydroartemisinin and [^{14}C]-artemisinin, different studies showed a >100-fold higher concentration in *P. falciparum* infected erythrocytes than in uninfected red blood cells (Gu et al., 1984; Kamchonwongpaisan et al., 1994).

Based on the structure of the endoperoxide bridge, extensive studies have been devoted to the synthesis of different classes of synthetic novel compounds leading to the emergence of drug development candidates such as the trioxolane OZ439 and the tetraoxane RKA-182 with high antimalarial activities *in vitro* and in rodent models of malaria **(Fig. 5.1)** (Charman et al., 2011; O'Neill et al., 2010a).

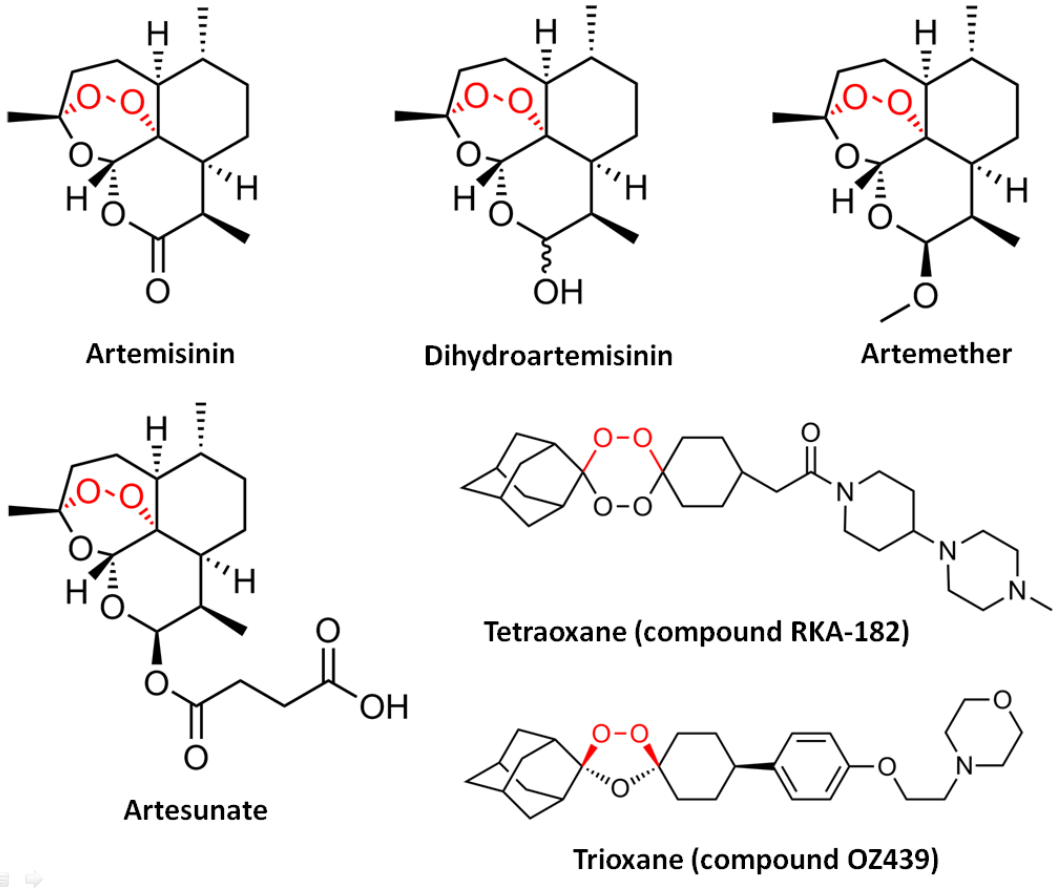

Figure 5.1. Chemical structures of artemisinin, its semi-synthetic derivatives (dihydroartemisinin, artemether and artesunate) and synthetic trioxane (compound OZ439) and tetraoxane (compound RKA-182). The endoperoxide bridge is highlighted in red.

5.1.2. Mode of activation of endoperoxide compounds

Initial studies deduced that the antimalarial activity of artemisinin, is mediated by the endoperoxide bridge. Located in the core of the structure, its cleavage generates cytotoxic oxygen-centred or alkoxyl radicals in presence of heme iron or free iron Fe^{2+} (Meshnick et al., 1991; Meshnick et al., 1993). From this premise of "endoperoxide bioactivation", two different mechanisms have been proposed.

By using [^{18}O]-labeled trioxane analogues the Posner group revealed that the oxygen-centred radicals produced were rearranged to more stable carbon-centred radicals (Posner et al., 1994; Posner et al., 1995). In this "reductive scission" model, a ferrous ion binds to either O1 or O2 cleaving the endoperoxide bond and providing respectively, an oxy radical intermediate or an oxygen-centred radical **(Fig. 5.2. B)**. Both are rearranged to primary or secondary carbon-centred radicals via a β-scission or a [1,5]-H shift which cause irreversible damage to parasite proteins. In line with this, strong evidence of the formation of these carbon-centred radical intermediates has

been raised by using electron paramagnetic resonance (EPR) spin-trapping techniques (Butler et al., 1998; O'Neill et al., 2000; Wu et al., 1998).

In the second model proposed, iron acts as a Lewis acid to facilitate ionic activation of antimalarial trioxanes generating downstream reactive oxygen species (ROS) (Haynes et al., 2007; Haynes et al., 1999). The ring opening is driven by a heterolytic cleavage of the endoperoxide bridge followed by interaction with water generating an open unsaturated hydroperoxide, capable of direct oxidation of protein residues. Fenton degradation of the oxygen-centred radical intermediate can provide hydroxyl radicals (•OH) highly reactive against amino acids, lipids or nucleic acids.

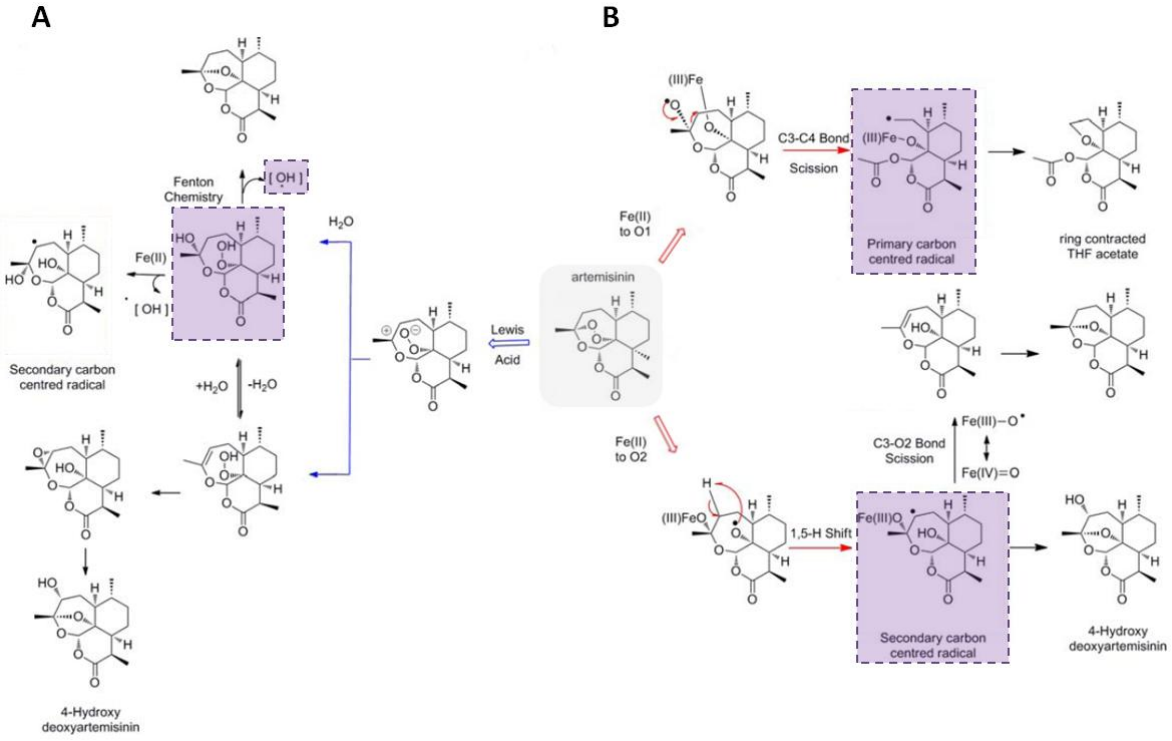

Figure 5.2. Open peroxide (A) and reductive scission (B) models of bioactivation of the endoperoxide bridge of artemisinin and its derivatives (O'Neill et al., 2010b). Radicals generated that are able to oxidise protein residues are highlighted in purple.

An alternative pathway of artemisinin activation has been suggested via the electron transport chain (ETC) components causing downstream ROS production and membrane depolarization in isolated malarial mitochondria (Li et al., 2005; Wang et al., 2010). However, the proposal of a reductive activation of the endoperoxide bridge chemically mediated by ETC activity remains unclear. Recently, the conservation of cytotoxic effects induced by artesunate in cells lacking a functional ETC has been demonstrated, contradicting the previous hypothesis proposed (Mercer et al., 2011).

Another study proposed a non iron-mediated mechanism of activation where artemisinins have a dual role. In the absence of ferrous ions, endoperoxides are proposed to oxidize $FADH_2$ contained in flavoenzymes and initiate the autoxidation of dihydroflavin coupled with ROS generation (Haynes et al., 2010). Although additional biological support is needed to validate this new hypothesis, it confirms that the activation mechanism of endoperoxide compounds remains controversial.

5.1.3. Role of heme and non heme iron in the mechanism of activation

Although the mechanism of activation involving cellular ferrous ions to produce radical intermediates is largely accepted, the origin of the iron available for bioactivation is a point of debate. Supported by experimental evidence, heme and non-heme iron were suggested to be the trigger (Golenser et al., 2006; Olliaro, 2001).

The involvement of heme in the activation of endoperoxide compounds was first proposed following isolation of heme-artemisinin in *P. falciparum* cultures (Meshnick et al., 1991). By using [^{14}C]artemisinin, Maeno and colleagues showed its accumulation in the digestive vacuole (DV) where hemoglobin degradation leads to the release of soluble heme (Maeno et al., 1993). Moreover heme has been observed to enhance the oxidising effects of endoperoxide drugs (Berman and Adams, 1997). The reaction between heme and artemisinin has been confirmed *in vitro* and *in vivo* (Kannan et al., 2002; Pandey et al., 1999; Robert et al., 2005). A recent study proposed that heme is the primary activator of artemisinin by reacting with it more efficiently than other iron-containing molecules (ferrous ions, hemin or hemoglobin) (Zhang and Gerhard, 2008). It has also been suggested that antimalarial trioxanes accumulated in the digestive vacuole are activated by neutral-lipid associated heme and induce oxidative membrane damage (Hartwig et al., 2009; Pisciotta et al., 2007).

Although the impact of heme on the activation of endoperoxide antimalarials has been demonstrated, alternative evidence shows that free ferrous ions can play a similar role. First, by using radio- or fluorescent-labeled artemisinins and high resolution microscopy, two studies contest the accumulation of trioxane drugs in the digestive vacuole and their possible interaction with heme (Eckstein-Ludwig et al., 2003; Ellis et al., 1985). Additionally, Haynes and colleagues proposed that artemisinins do not inhibit hemozoin formation and cannot react with heme according to conventional chemistry models (Haynes et al., 2004; Haynes et al., 2003). Even though 90% of iron is contained in the digestive vacuole in the form of heme, free iron is involved in free radical formation and might interact with artemisinin (Kamchonwongpaisan and Meshnick, 1996; Meshnick et al., 1993; Scholl et al., 2005; Sibmooh et al., 2001). Several studies have shown

that iron chelation antagonizes the effect of endoperoxide antimalarials *in vitro* and can prevent their toxic effects in mice (Eckstein-Ludwig et al., 2003; Meshnick et al., 1993; Pradines et al., 2002). Because iron chelators are selective to non-heme source of iron, it has been suggested that intracellular ferrous ions may have a role in artemisinins activation (Golenser et al., 2003; Golenser et al., 2006). Recent work demonstrated that three classes of endoperoxide drugs (trioxane, trioxolane and tetraoxane) have a common free-iron dependent mechanism of activation in malaria parasites (Stocks et al., 2007).

5.1.4. Proposed modes of action

Once activated, endoperoxide antimalarials were hypothesised to have several mode of action by impairing the heme detoxification pathway (Pandey et al., 1999), alkylating different proteins including the translationally controlled tumor protein (*Pf*TCTP) (Bhisutthibhan et al., 1998), inhibiting the sarco/endoplasmic reticulum membrane calcium *Pf*ATPase6 (Eckstein-Ludwig et al., 2003) and disrupting mitochondrial functions (Li et al., 2005; Wang et al., 2010).

In the first hypothesis proposed, free radicals are produced after activation, alkylate intracellular heme in the digestive vacuole and interfere with its detoxification by inhibiting its polymerization to non toxic hemozoin (Cazelles et al., 2001; Robert et al., 2005; Robert et al., 2006). The iron centre of heme plays the dual role of trigger and target of the endoperoxide bridge of artemisinins as well as causing also membrane damage to the DV (del Pilar Crespo et al., 2008; Hartwig et al., 2009). Supplementary studies suggested the same mode of action for synthetic trioxolanes and tetraoxanes (Bousejra-El Garah et al., 2011; Creek et al., 2008).

The alkylation of different malarial proteins by artemisinin has been established for many years (Asawamahasakda et al., 1994; Yang et al., 1994). Radiolabeled artemisinins were observed to form covalent bonds with several proteins and may alter their function. *Pf*TCTP, a translationally controlled tumour protein probably involved in cell growth, has been shown to react with artemisinin in the presence of hemin and bind to heme itself (Bhisutthibhan and Meshnick, 2001; Bhisutthibhan et al., 1998). Nevertheless, the importance of this potential artemisinin target remains doubtful due to the lack of data about its role and essentiality in the malaria parasite.

It has been proposed that artemisinins inhibit the sarco/endoplasmic reticulum Ca^{2+}-ATPase (SERCA) orthologue of *P. falciparum* (*Pf*ATPase6) which reduce cytosolic free calcium concentrations, an essential activity for parasite survival (Eckstein-Ludwig et al., 2003). Due to their structural similarities with thapsigargin, a specific inhibitor of *Pf*ATPase6, artemisinins

display an iron-dependent inhibition of *Pf*ATPase6 expressed in *Xenopus laevis* oocytes. However, this hypothesis has been contradicted by demonstrating no antagonistic effect between thapsigargin and artemisinin like mentioned in the original work (del Pilar Crespo et al., 2008). Additionally, the first-generation trioxolane OZ277 showed week inhibition of *Pf*ATPase6 (Uhlemann et al., 2007). Recently, no correlation between the affinity of various antimalarial drugs toward *Pf*ATPase6 was predicted *in silico*, yet their antimalarial activity has been established (Garah et al., 2009).

Finally, it has been suggested that artemisinin and its derivatives may interfere with the mitochondrial functions of *P. falciparum* after being activated by the ETC components. The administration of artemisinin to *S. cerevisiae* cultures using non-fermentable carbon sources inhibits yeast growth (Li et al., 2005). This indicates the impact of the drug on the mitochondrial membrane potential leading to a loss of mitochondrial functions, essential for the growth conditions used. This proposal has been correlated by a further study showing a mitochondrial membrane depolarization in *P. berghei* in presence of trioxane drugs (Wang et al., 2010). The observation of an artesunate distribution inside the mitochondria of infected erythrocytes support the theory of reactive oxygen species (ROS) generated by artemisinins in the organelle. The accumulation of ROS is suspected to collapse the mitochondrial membrane potential affecting the pyrimidine biosynthesis, a crucial metabolic process for parasite life. However, additional supporting data are needed to clarify the molecular mechanisms involved in this mode of action.

5.1.5. Production of radical oxygen species and lipid peroxidation

Reactive oxygen species (ROS) like superoxide anions ($^{\bullet}O_2^-$), hydroxyl radicals ($^{\bullet}OH$) or hydrogen peroxide (H_2O_2) are produced when electrons are liberated by oxidation and combine with molecular oxygen (Atamna and Ginsburg, 1993). In *Plasmodium* species, the oxidative stress is mainly generated during the haemoglobin degradation (Vennerstrom and Eaton, 1988). Parasite mitochondrion is also a source of ROS, produced by different components of the ETC via electrons transfer to O_2 but its production was considered not quantitatively significant (Atamna and Ginsburg, 1993). To control the ROS accumulation, detoxification systems are essential. Thus, the malaria parasite relies on antioxidant defences to survive such as an isoform of superoxide dismutase (SOD) and thioredoxin-dependent peroxidases (reviewed in Muller, 2004). However, an excess of ROS induced by artemisinin can overcome the oxidative defences of the parasite and initiate cell damage leading to irreversible injury (Haynes and Krishna, 2004).

Addition of artemisinins generating ROS has been demonstrated in both yeast and mammalian tumor cells (Disbrow et al., 2005; Li et al., 2005). The association between oxidant

stress and endoperoxide compounds was suggested by using ROS scavengers (tiron, N,N'-diphenyl-1,4-phenylenediamine, catalase, α-tocopherol, etc) which increase cell survival in the presence of artemisinins (Krungkrai and Yuthavong, 1987; Mercer et al., 2011; Meshnick et al., 1993; Wang et al., 2010).

The oxidative phospholipid bilayer deterioration and mitochondrial dysfunction have been demonstrated to be caused by carbon and oxygen radical species (Gardner, 1989; Richter, 1987; Zhang et al., 1990). Shown in **Figure 5.3**, O'Neill and Posner proposed a possible mechanism of parasite membrane damage induced by artemisinins via lipid peroxidation coupled by generation of reactive oxygen species (ROS) (O'Neill and Posner, 2004). After iron-induced cleavage of their endoperoxide bridge, carbon-centred radicals ($R^{\bullet}$) interact with polyunsaturated fatty acids and initiate lipid peroxidation (Porter, 1986; Yin and Porter, 2005). The free-radical mediated lipid peroxidation mechanism has been intensely studied. The initiation step starts with the loss of hydrogen from polyunsaturated fatty acids to generate carbon-centred radicals. By addition of oxygen, lipid radicals are rearranged in lipid peroxyl radicals (ROO^{-}). The chain propagation step begins with the transfer of hydrogen from unsaturated lipids to lipid peroxyl radicals producing lipid hydroperoxide (ROOH) and new lipid radicals which will initiate other chain reaction. Lipid hydroperoxides are degraded according to the superoxide-driven Fenton reaction **(reaction 2)** to hydroxyl radicals ($^{\bullet}OH$) which cause oxidative damage to receptors, enzymes or polyunsaturated lipids decreasing membrane fluidity and resulting in parasite membrane potentials depolarization (Chen and Yu, 1994; Marshansky et al., 1983; O'Neill and Posner, 2004). In the first step **(reaction 1)**, Fe^{3+} is reduced by superoxide anions ($^{\bullet}O_2^{-}$) to Fe^{2+}, which is necessary for the latter (Fenton) reaction (Gutteridge and Bannister, 1986).

$$Fe^{3+} + {}^{\bullet}O_2^{-} \rightarrow Fe^{2+} + O_2 \qquad \textbf{(reaction1)}$$

$$Fe^{2+} + H_2O_2 \rightarrow Fe^{3+} + HO^{\bullet} + HO^{-} \qquad \textbf{(reaction 2)}$$

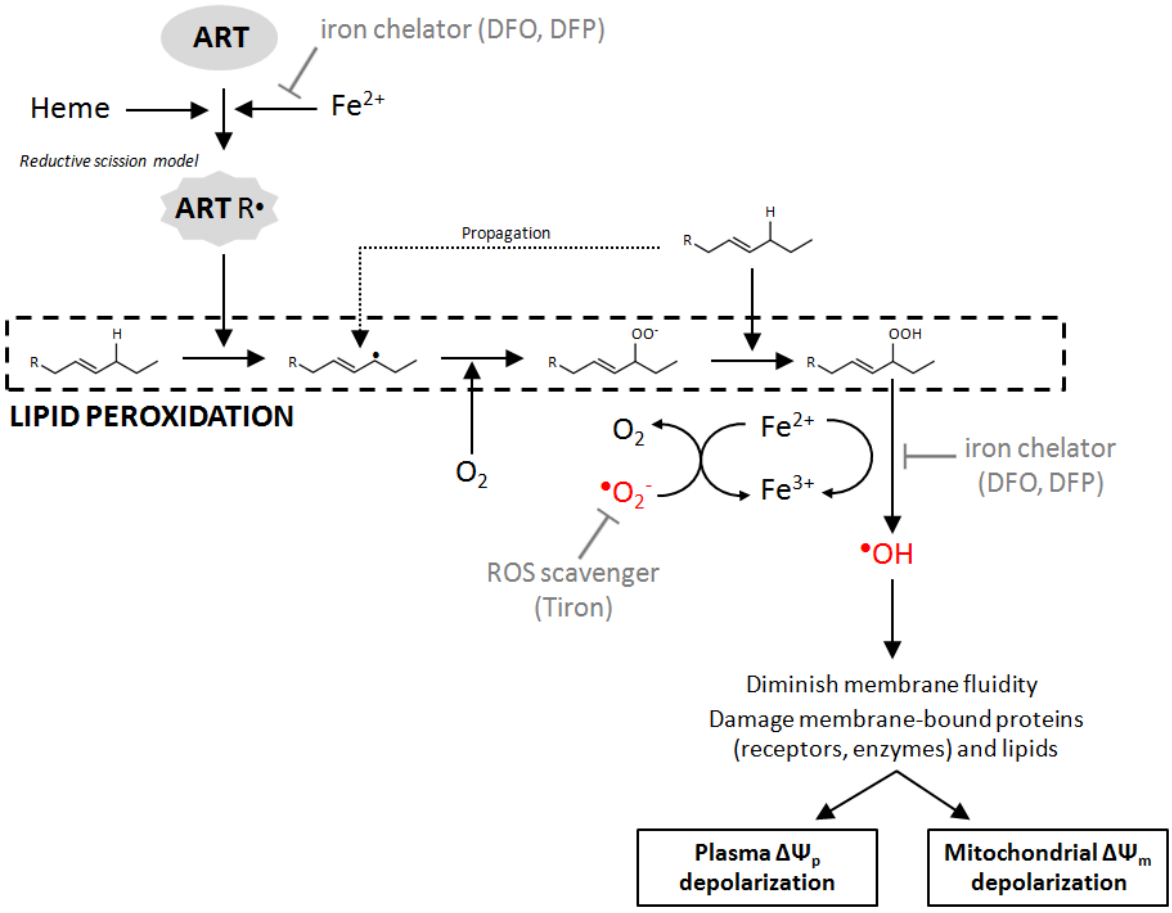

Figure 5.3. Proposition of the membrane potential depolarization pathway induced by endoperoxides. This mechanism model has been adapted from O'Neill and Posner, 2004 . Inhibitors of chemical reactions used in this study are indicated in grey.

5.1.6. The plasma and mitochondrial membrane potential

Plasmodium species have a negative electric potential ($\Delta\Psi_p$) across the plasma membrane of approximately -95 mV (Allen and Kirk, 2004; Izumo et al., 1988). It is generated by V-type H^+-ATPases which transfer protons out of the parasite cytosol (Hayashi et al., 2000; Saliba and Kirk, 1999). Localised in the plasma membrane, the V-type H^+-ATPase also plays a role in regulating a neutral cytosolic pH (near 7.3), crucial for enzyme function, incorporation of the vitamin B5 and generation of pH gradient across membranes of internal organelles (Saliba and Kirk, 1999; van Schalkwyk et al., 2010). The maintenance of the plasma membrane potential ($\Delta\Psi_p$) is also important in mediating the influx of K^+ in the parasite cytosol and the uptake of nutrients such as inorganic phosphates and choline (Allen and Kirk, 2004; Biagini et al., 2004; Lehane et al., 2004; Saliba et al., 2006). The direct inhibition of the V-type H^+-ATPase by specific inhibitors such as bafilomycin A1 or concanamycin A has been demonstrated to depolarize the plasma membrane potential and disturb the physiology of the parasite leading to its death (Allen and Kirk, 2004; Biagini et al., 2006; van Schalkwyk et al., 2010).

It was generally accepted that the maintenance of mitochondrial membrane potential ($\Delta\Psi_m$), generated by the electron transport chain (ETC), is essential for mitochondrial functions and malaria parasite survival (Biagini et al., 2008; Vaidya and Mather, 2009). In asexual parasites, the pyrimidine biosynthesis is an essential function of the mitochondrion via the activity of the dihydroorotate dehydrogenase (DHODH) (Painter et al., 2007). This function is dependent on the integrity of the ETC enzymes generating the protonmotive 'Q-cycle' and the mitochondrial membrane potential. The inhibition of cytochrome bc_1 (Complex III) of the ETC by atovaquone, an antimalarial drug, depolarizes malaria mitochondria resulting in parasite death (Srivastava et al., 1997). The Ca^{2+} homeostasis is another vital mitochondrial function driven by the mitochondrial membrane potential and modulated by a Ca^{2+} uniporter (Gazarini and Garcia, 2004).

Mitochondrial membrane potential depolarization has been noticed to be an early effect of artemisinin in isolated mitochondria of *P. berghei* (Wang et al., 2010). Moreover the induction of apoptotic cell death via the loss of membrane potential has been observed in endoperoxide treated HeLa cells (Mercer et al., 2011; Mercer et al., 2007). However, a contradictory report suggested that the lost of membrane potential is a downstream effect of cell death caused by artemisinin (del Pilar Crespo et al., 2008).

5.1.7. *In vivo* dynamic monitoring of membrane potential in malaria parasites

As described, there have been several studies that have measured the effect of artemisinin on membrane potential depolarization (Mercer et al., 2011; Mercer et al., 2007; Wang et al., 2010). In these cases, depolarization has been noted at more than 30 min after endoperoxide induction. Using rhodamine 123 and confocal microscopy, del Pilar Crespo and colleagues showed no obvious effect on mitochondrial integrity after 4 hours of treatment with artemisinin, suggesting that mitochondrial dysfunction is not an early event of endoperoxide action (del Pilar Crespo et al., 2008). However, using light and electron microscopy to demonstrate morphological changes of the mitochondrion after incubation with artemisinins, other studies have observed significant mitochondrial damage/dysfunction (Jiang et al., 1985; Kawai et al., 1993; Maeno et al., 1993). The precise involvement of the mitochondrial membrane potential in the lost of the organelle functions and induction of cell apoptosis remains a point of debate and the results obtained in these different studies may differ depending on the cell types, the monitoring techniques and the fluorochromes used.

In this chapter a highly sensitive method monitoring *in vivo* mitochondrial ($\Delta\Psi_m$) and plasma membrane potential ($\Delta\Psi_p$) is described. Their measurement is based on the accumulation of the fluorescent probe TMRE, a rhodamine 123 derivative. This dye is a lipophilic cation which can be accumulated in plasma and mitochondrial membranes of living cells according to the Nernst equation (Farkas et al., 1989; Loew, 1998; Loew et al., 1993). Combined with confocal imaging, this approach allows a rapid observation of fast changes (< 5 min) of both membrane potential in single parasite-infected erythrocytes (Biagini et al., 2008; Biagini et al., 2006)

The presented study was set out to investigate the potential of endoperoxide compounds to affect both plasma and mitochondrial electrochemical gradient. This established technique was applied to monitor the global membrane potential of *P. falciparum* infected erythrocytes treated with different endoperoxide compounds. The investigation was carried out by measuring independently the collapse of mitochondrial ($\Delta\Psi_m$) and plasma membrane potential induced by two inhibitors : a trioxolane, artemisinin and a tetraoxane, the drug-development candidate RKA-182. The role of ferrous-iron, ROS generation and the ETC in the artemisinin action pathway is also reported.

5.2. Results

5.2.1. Endoperoxide compounds collapse both plasma and mitochondrial membrane potential in *P. falciparum* infected erythrocytes

To determine the effect of endoperoxides on membrane potential, a real-time single-cell imaging approach was used (see section 4.2.9). The endoperoxide compounds used were shown to inhibit the parasite growth in a low nanomolar range **(Fig. 5.4)**. Their addition at a concentration of 100 nM was observed to reduce the total parasite fluorescence by 55 to 60% in <3 min **(Fig. 5.5 C to F)**. Atovaquone, the *bc1* complex inhibitor was used as a control, decreased the fluorescence by 30% **(Fig. 5.5 A)**, confirming previous observations performed by Biagini and colleagues (Biagini et al., 2006). Deoxyartemisinin is an artemisinin derivative lacking the endoperoxide bridge, the key pharmacophore of the anti-plasmodial activity of this class of compound **(Fig. 5.4 B)**. In contrast to other derivatives, deoxyartemisinin is an ineffective inhibitor of *P. falciparum* growth with an IC_{50} higher than 10 µM. The addition of deoxyartemisinin decreased the TMRE fluorescence to 10% **(Fig. 5.5 B)**. However, this relatively low reduction in signal could be accounted for by photobleaching and was not considered to be due to the direct effect of the drug.

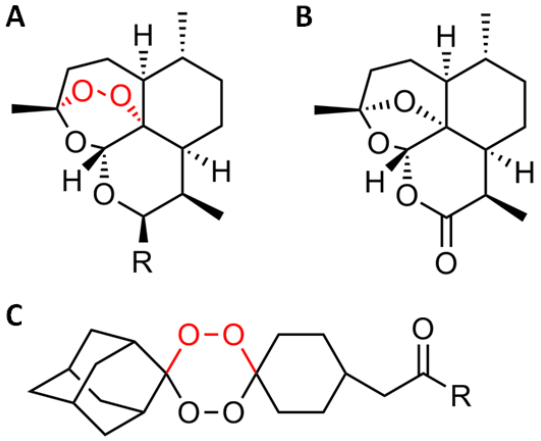

D

Drug	R	*In vitro* IC_{50} (nM)
Artemisinin	=O	7.5 ± 0.2
Dihydroartemisinin	β + α OH	3.48 ± 0.60
Artesunate	$\alpha OC(O)(CH_2)_2CO_2Na$	1.60 ± 0.40
Arthemether	$\beta O\text{-}CH_3$	4.46 ± 0.75
Deoxyartemisinin	_	> 10,000
Tetraoxane (RKA-182)	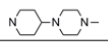	1.30 ± 0.61

Figure 5.4. Structures of endoperoxide compounds and their *P. falciparum* growth inhibition. Chemical structures of **(A)** artemisinins and its semisynthetic derivatives, **(B)** the deoxyartemisinin and **(C)** the synthetic 1,2,4,5-tetraoxane drug-development candidate RKA-182 used in this study. The endoperoxide bridge is highlighted in red. **(D)** *Plasmodium falciparum* growth inhibition IC_{50} values of endoperoxide antimalarials. Values indicated are means ± SE of results from three independent experiments.

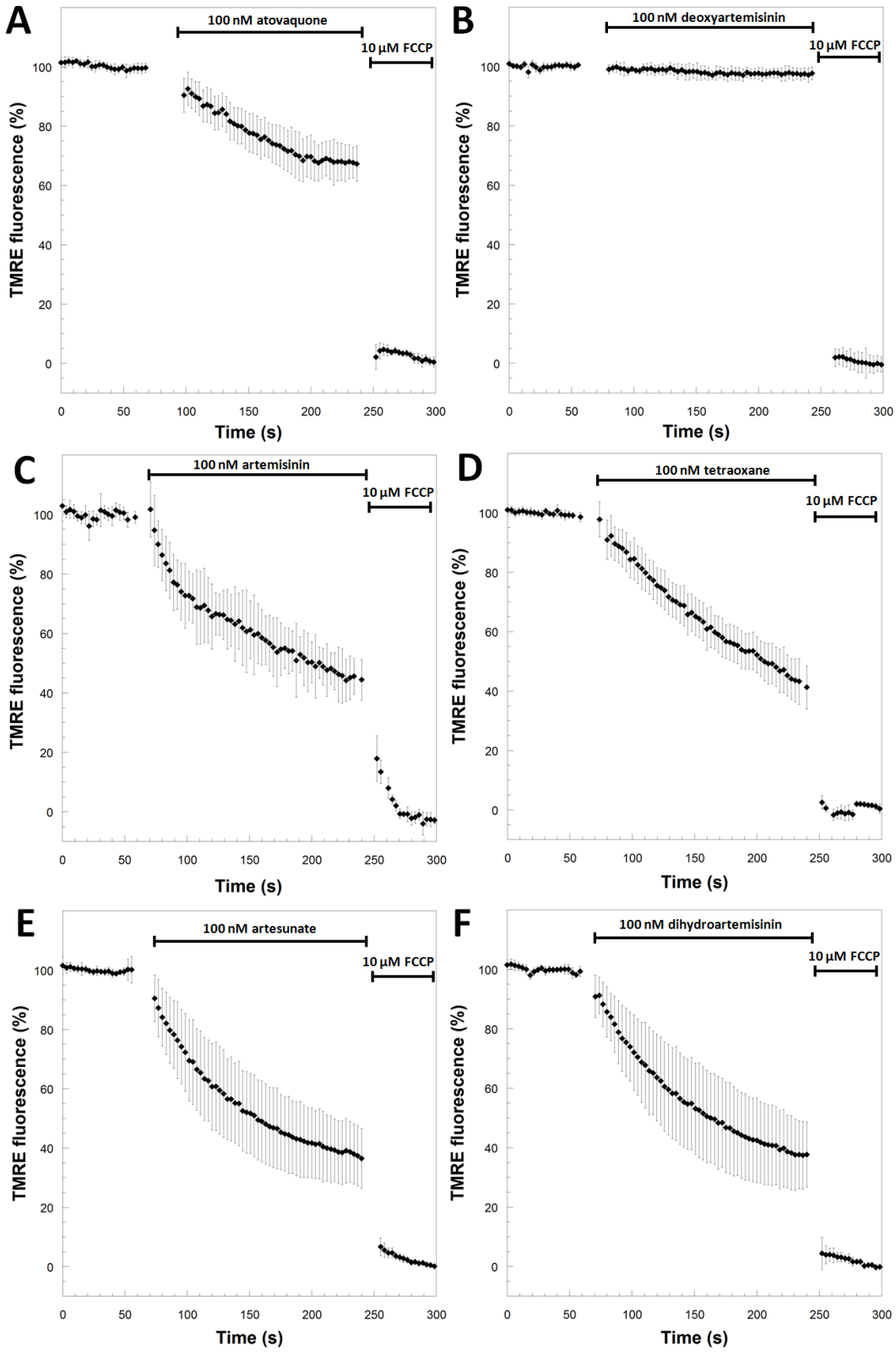

Figure 5.5. Effect of endoperoxide antimalarials on both plasma and mitochondrial membrane potential of *P. falciparum*. Time course of TMRE-dependent fluorescence of *P. falciparum*-infected erythrocytes after the addition of **(A)** 100 nM atovaquone, **(B)** 100 nM deoxyartemisinin, **(C)** 100 nM artemisinin, **(D)** 100 nM tetraoxane (compound RKA-182), **(E)** 100 nM artesunate **(F)** and 100 nM didhydroartemisinin. The data were normalized to 100% in untreated cells and to 0% in FCCP (10µM)-treated cells. Graphs show means ± standard errors from three independent experiments monitoring ≥ 7 single cells.

Because both plasma and mitochondrial membrane potentials participate to the TMRE accumulation in their respective lipid bilayer, their independent contribution to the global depolarization cannot be accurately quantified in this assay. However, pre-treatment with atovaquone or concanamycin A before addition of the inhibitor allows the contribution from each membrane to be monitored separately.

5.2.2. Depolarization of the mitochondrial membrane potential ($\Delta\Psi_m$) by artemisinin and tetraoxane.

To evaluate the impact of endoperoxides on the mitochondrial $\Delta\Psi_m$, cells were pre-treated with concanamycin A, a V-type H^+ ATPase inhibitor. Upon addition of concanamycin A (200 nM), the fluorescent intensity from the cytosol decreases approximately of 70 to 80% (Biagini et al., 2006), leaving a local and strong signal originating from the parasite mitochondrion **(Fig. 6.6 1b, 2b and 3b)**. The morphology of the mitochondrion differs in function of the stage in the parasite life cycle (see Chapter 1, section 1.2.1).

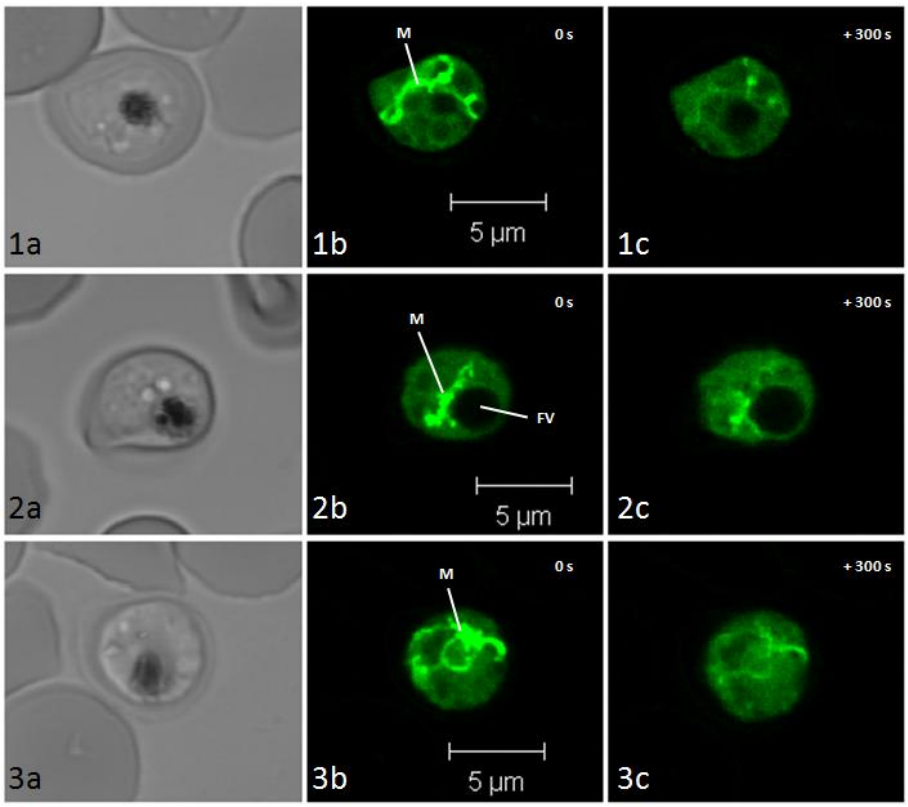

Figure 5.6. Effect of atovaquone, artemisinin and tetraoxane (RKA-182) on fluorescent mitochondria from *P. falciparum* trophozoites. The panel shows **(a)** bright-field fluorescence and TMRE fluorescence images of canconomycin pre-treated infected erythrocytes **(b)** before and **(c)** 300 seconds after induction with **(1)** 100 nM atovaquone, **(2)** 100 nM artemisinin and **(3)** 100 nM tetraoxane. The green in these images is a pseudocolor. TMRE was excited at 543 nm and emission was collected with a 560 nm long pass filter. 'M' label indicates the parasite mitochondrion and 'FV' the food vacuole.

To measure the mitochondrial-dependent fluorescence, concanamycin A-treated parasites were normalized to 100% and the baseline (0%) was set by FCCP. Known to widely collapse the mitochondrial membrane potential ($\Delta\Psi_m$) via the inhibition of the respiratory chain, atovaquone was shown to reduce quickly (~ 3 min) the TMRE fluorescence by 70% **(Fig. 5.7 A)**. For the same short period of time, addition of artemisinin and tetraoxane decreased the fluorescence by 60% and 50% respectively **(Fig. 5.7 B and C)**. In **Figure 5.6**, confocal microscopy pictures show a significant reduction of mitochondrially-derived fluorescence after 5 min of drug treatment (atovaquone, artemisinin or tetraoxane).

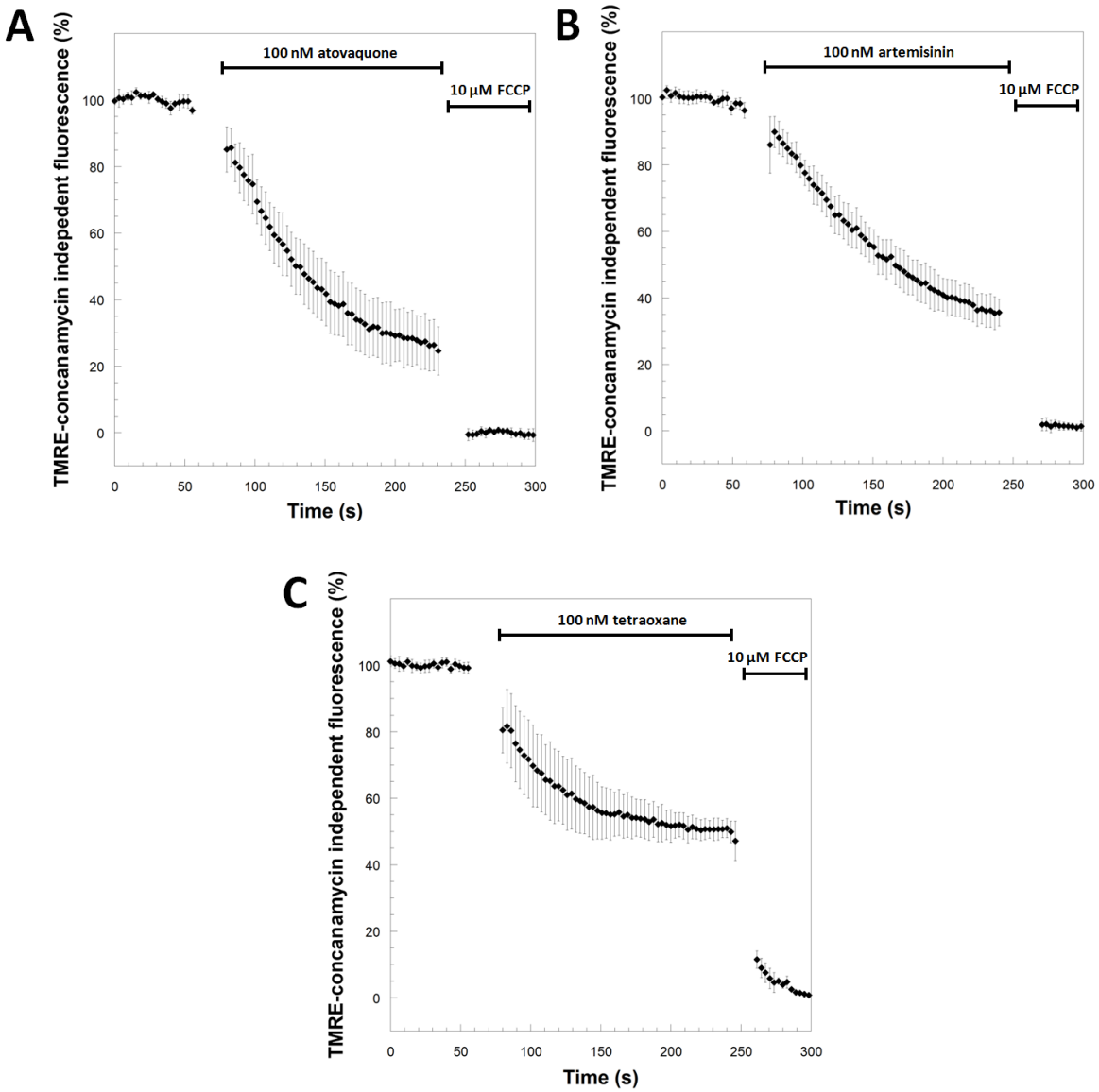

Figure 5.7. Effect of artemisinin and tetraoxane on mitochondrial membrane potential only. Plasma membrane potential is depolarized by treatment of *P. falciparum*-infected erythrocytes with 200 nM concanamycin A before induction of inhibitors. Time course of TMRE-plasma independent fluorescence is followed after addition of **(A)** 10 nM atovaquone, **(B)** 100 nM artemisinin and **(C)** 100 nM tetraoxane. Data were normalized to 100% in untreated cells and to 0% in FCCP (10µM)-treated cells. Graphs show means ± standard errors from three independent experiments monitoring ≥ 7 single cells.

5.2.3. Depolarization of the plasma membrane potential by artemisinin and tetraoxane.

The mitochondrial $\Delta\Psi_m$ was demonstrated to represent between 20% to 30% of the total cellular TMRE fluorescence, leaving a homogenous cytosolic signal originating from the plasma membrane only (Biagini et al., 2006). To evaluate the plasma-dependent fluorescence, parasites were pre-treated with 100 nM atovaquone for 5 min before addition of the endoperoxide inhibitor. Then, atovaquone-treated parasites were normalized to 100% and the baseline (0%) was set by FCCP. The vacuolar H^+ ATPase is involved in transforming the energy of ATP hydrolysis to generate the electrochemical potential at the surface of the malaria parasite through the transport of H^+ across the plasma membrane (Allen and Kirk, 2004). The inhibition by concanamycin A, a well known V-type ATPases inhibitor, was shown to reduce rapidly the plasma-dependent fluorescence by 60% **(Fig. 5.8 A)**. In a similar manner, artemisinin and tetraoxane were observed to decrease the fluorescent signal by 40 to 60% respectively **(Fig. 5.8 B and C)**.

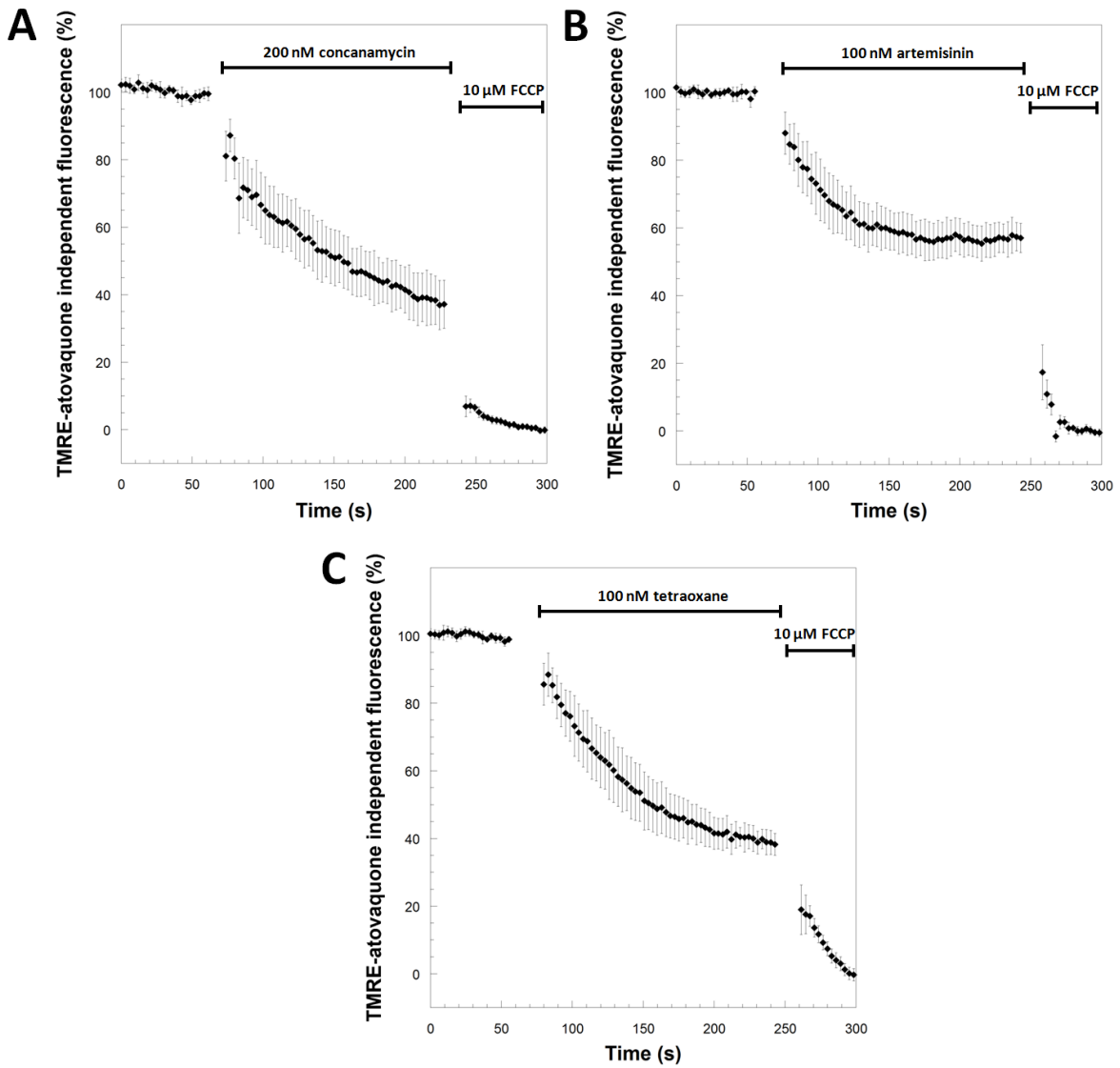

Figure 5.8. Effect of artemisinin and tetraoxane on plasma membrane potential only. Mitochondrial membrane potential is depolarized by treatment of *P. falciparum*-infected erythrocytes with 100 nM atovaquone before induction of inhibitors. Time course of TMRE-mitochondrial independent fluorescence is followed after addition of **(A)** 200 nM concanamycin A, **(B)** 100 nM artemisinin and **(C)** 100 nM tetraoxane. Data were normalized to 100% in untreated cells and to 0% in FCCP (10 µM)-treated cells. Graphs show means ± standard errors from three independent experiments monitoring ≥ 7 single cells.

5.2.4. Effect of Fe^{2+}-chelators desferrioxamine (DFO) and deferipone (DFP) on the membrane potential depolarization by artemisinin and tetraoxane.

The fixed-dose effect of iron chelators on membrane potential depolarization were observed to determine the involvement of free iron on the activity of endoperoxides by using desferrioxamine (DFO) and deferipone (DFP), two chelating agents selective for non-heme iron such as intracellular Fe^{2+} (Stocks et al., 2007).

Both iron-chelators have *in vitro* antimalarial activities with a 48h IC_{50}-dose-responsed against 3D7 *P. falciparum* growth of 17.3 ± 2 µM (DFO) and 111.8 ± 1.8 µM (DFP). However, under the short time period of this assay (< 6 min), 100 µM DFO and 100 µM DFP have not been observed to diminish the fluorescent signal coming from both membrane potentials. *P. falciparum*-infected erythrocytes were treated with 100 µM DFO and 100 µM DFP before and during induction of artemisinin (100 nM) or tetraoxane (100 nM) in order to study the impact of iron chelators on depolarization events. In presence of DFO and DFP, artemisinin was observed to reduce TMRE fluorescence only by 15 and 35%, respectively within 3 min after induction, whereas the drug diminished by 60% the fluorescent signal in absence of iron-chelators **(Fig. 5.9 A)**. In a similar manner, tetraoxane was monitored to decrease by 15 and 40% the TMRE fluorescence from pre-treated parasites with DFO and DFP respectively, while the inhibitor diminished by 55% the TMRE signal from untreated parasites **(Fig. 5.9 B)**. DFO presents a high antagonistic effect inhibiting by 75 and 73% the collapse of transmembrane potential induced by artemisinin and tetraoxane, respectively. To a lesser extent, DFP prevents by 41 and 27% the action of artemisinin and tetraoxane respectively, on the membrane potential.

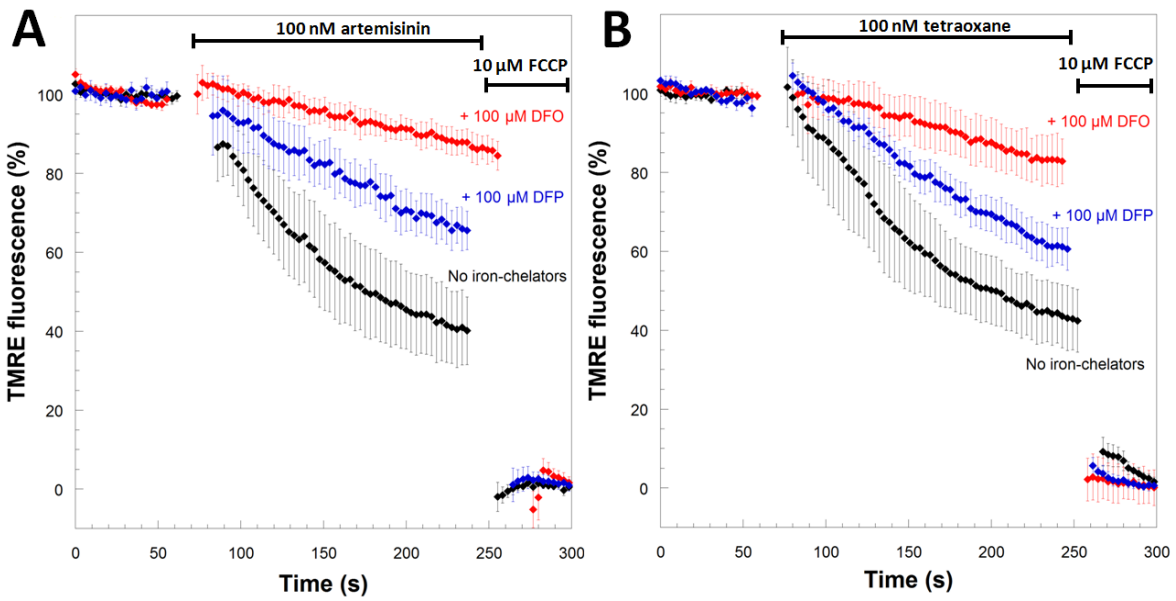

Figure 5.9. Effect of artemisinin and tetraoxane on membrane potential in presence of iron-chelators. Time course of TMRE-dependent fluorescence of *P. falciparum*-infected erythrocytes after addition of **(A)** 100 nM artemisinin and **(B)** 100 nM tetraoxane. Cells are not treated (○) or subjected to iron-chelator treatment with 100 µM desferrioxamine (●) and 100 µM deferiprone (♦). Data were normalized to 100% in untreated cells and to 0% in FCCP (10 µM)-treated cells. Graphs show means ± standard errors from three independent experiments monitoring ≥ 7 single cells.

5.2.5. Effect of the superoxide scavenger Tiron on the membrane potential depolarization induced by artemisinin and tetraoxane.

To gain further insights into the mechanism of action of artemisinin, the contribution of oxidative stress to the depolarizing activity of endoperoxides was investigated by treating malaria parasites with Tiron, a cell membrane permeable superoxide scavenger (Greenstock and Miller, 1975). In a similar manner to iron-chelators, parasite-infected erythrocytes were incubated with 100 µM Tiron before and during induction with artemisinin and tetraoxane. It was noted that no reduction of TMRE fluorescence was observed during treatment with the superoxide scavenger only. In the presence of Tiron, artemisinin and tetraoxane were monitored to decrease by 35 and 25% the fluorescent signal respectively, whereas in the absence of the scavenger, a reduction of 55% to 70% was observed **(Fig. 5.10)**. Therefore, in our in vitro system, ROS scavenging by Tiron significantly reduced the endoperoxide-induced depolarisation by 50 to 55%.

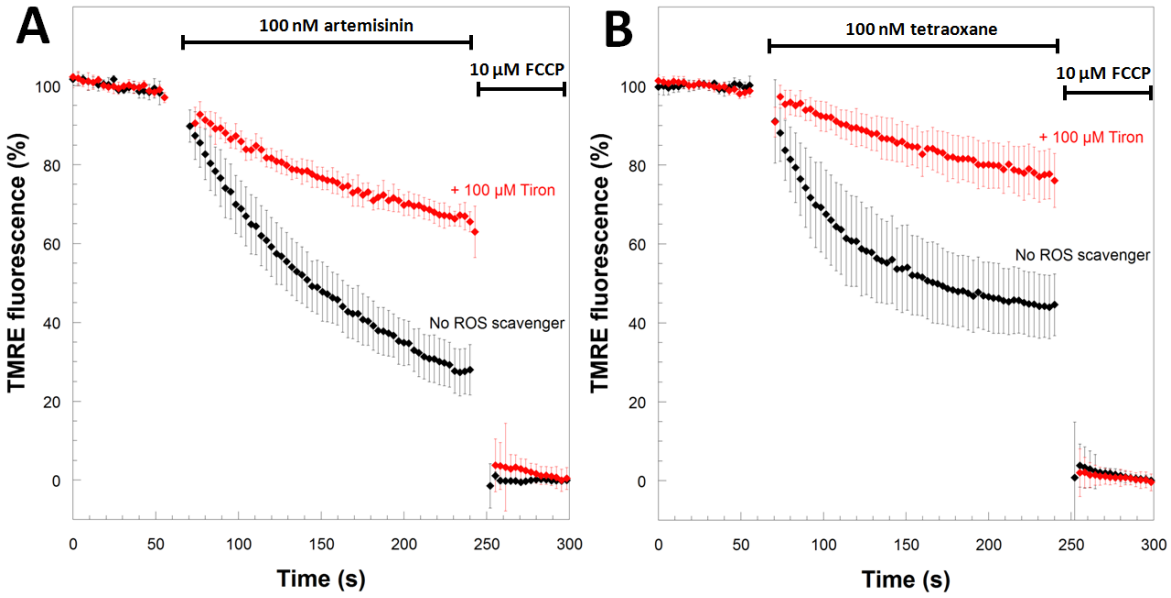

Figure 5.10. Effect of artemisinin and tetraoxane on membrane potential in presence of ROS scavenger. Time course of TMRE-dependent fluorescence of *P. falciparum*-infected erythrocytes after addition of **(A)** 100 nM artemisinin and **(B)** 100 nM tetraoxane. Cells are not treated (○) or subjected to ROS scavenger treatment with 100 µM Tiron (●). Data were normalized to 100% in untreated cells and to 0% in FCCP (10µM)-treated cells. Graphs show means ± standard errors from three independent experiments monitoring ≥ 7 single cells.

5.2.6. Direct inhibitory effect of endoperoxides on the respiratory chain components

Because previous studies have reported the involvement of the ETC in the activation of artemisinin (Li et al., 2005), here, the direct inhibitory activities of endoperoxides on major components of the ETC were investigated. Activities from three main ETC enzymes (*Pf*NDH2, bc_1 complex and cytochrome *c* oxidase) were monitored spectrophotometrically. Because *Pf*DNH2

was demonstrated to be the main provider of electrons among all dehydrogenases (as described in Chapter 4), effects of artemisinin and its derivates on its enzyme activity were determined on recombinant *Pf*NDH2. Free parasite extracts were used to evaluate the inhibitory effect on the bc_1 protein (complex III) and cytochrome *c* oxidase (complex IV), essential for downstream generation of the electrochemical membrane potential. The results indicate that at up to 1 µM (final concentration) of endoperoxides, relatively weak inhibition of the individual respiratory components was observed **(Table 5.1)**. The maximum inhibition values obtained were 17.1% of *Pf*NDH2 activity by artemisinin, 23.2% of bc_1 activity by tetraoxane and between 18.4% to 23.0% of complex IV activity for all endoperoxides. The inhibitory effects of endoperoxides are widely inferior to those obtained with HDQ, atovaquone and cyanide which are specific inhibitors of *Pf*NDH2, bc_1 complex and cytochrome *c* oxidase respectively.

Table 5.1. Inhibitory profiles of endoperoxide compounds on three majors components of the electron transport chain of *Plasmodium falciparum* (3D7 strain). Specific inhibitors of *Pf*NDH2 (HDQ), bc_1 protein (atovaquone) and complex IV (cyanide) are used as positive controls. Direct activity assays have been performed on recombinant *Pf*NDH2 enzymes whereas bc_1 protein and Complex IV have been assayed with free parasites extract.

Inhibitor	% inhibition of		
	***Pf*NDH2**	**bc_1 protein**	**Complex IV**
Artemisinin (1 µM)	17.1 ± 4.2	3.2 ± 3.7	18.4 ± 4.3
Tetraoxane (1 µM)	12.3 ± 4.9	23.2 ± 4.2	19.1 ± 2.0
Dihydroartemisinin (1µM)	5 ± 4.3	6.7 ± 4.1	21.1 ± 7.9
Artesunate (1 µM)	3.7 ± 2.9	2.3 ± 0.4	21.1 ± 3.9
Artemether (1 µM)	4.1 ± 3.3	1.8 ± 1.9	23.0 ± 2.0
HDQ (100 nM)	88.1 ± 0.5	N.D.	N.D.
Atovaquone (50 nM)	N.D.	89.0 ± 1.0	N.D.
Cyanide (15 mM)	N.D.	N.D.	100 ± 0.0

Inhibitor concentration used are indicated in bracket. Values are means ± SE. n=3.

5.3. Discussion

5.3.1. Endoperoxides induce a rapid depolarization of both plasma and mitochondrial membrane potentials

In this work, a robust assay has been used for the real-time single-cell measurement of plasma ($\Delta\psi_p$) and mitochondrial ($\Delta\psi_m$) membrane potentials in *P. falciparum* infected erythrocytes. It has been proposed that both membrane potentials are the two major components driving the accumulation of cationic fluorescent dyes like rhodamine 123 or TMRE (Biagini et al., 2006; Izumo et al., 1988). First, by monitoring a global membrane potential, the selective mitochondrial inhibitor atovaquone (100 nM) was shown to collapse only the

contribution attributed to the organelle, in line with a previous study (Biagini et al., 2006). With therapeutically relevant concentrations (100 nM), different trioxanes (artemisinin, artesunate and dihydroartemisinin) and a tetraoxane (drug-development candidate RKA-182) display a two-fold higher depolarization activity than atovaquone on the overall membrane electrochemical potential. This observation indicated a probable dual action of the drug on mitochondrial and plasma membranes of the malaria parasite **(Fig. 5.5)**. To confirm this hypothesis, the relative contributions of plasma and mitochondrial membrane potentials were monitored using selective pre-treatments of parasites (Biagini et al., 2006).

Pre-treatment of parasite-infected erythrocytes with 100 nM atovaquone enables the removal of the fluorescent signal emitted by the mitochondrial membrane potential without affecting the plasma membrane counterpart. The **Figure 5.8** shows that two structurally different endoperoxides, artemisinin and tetraoxane, were able to mimic the action of the V-type ATPase inhibitor concanamycin A, by collapsing rapidly and partially the plasma membrane potential. Although the inhibitory effect of endoperoxides on V-type ATPases remains to be investigated, an indirect mode of action via the oxidative damage of cell membranes seems most plausible (O'Neill and Posner, 2004). In line with this, ROS generation may trigger the depolarization of the plasma membrane ($\Delta\psi_p$) whose the maintenance has been linked to the uptake of K^+, inorganic phosphate and choline (Allen and Kirk, 2004; Lehane et al., 2004; Saliba et al., 2006). Thus, the collapse of the electrochemical gradient can stop the incorporation of these ions and nutrients inside the cytosol but also deregulate the pH gradient maintained across the plasma membrane provoking a cascade of reactions affecting rapidly the physiological integrity of the parasite. For instance, inhibition of the V-type ATPase activity was reported to drop the neutral cytosolic pH (around 7.3) by 0.4 pH unit in less than 3 min and 0.5 to 0.6 units within 20 min (Saliba and Kirk, 1999; van Schalkwyk et al., 2010). It has also been revealed that pH regulation inhibitors prevent the parasite proliferation in 30 min to 4 h depending of their concentration (van Schalkwyk et al., 2010). Therefore, the inability of the parasite to maintain its cytosolic pH has been established to cause rapid parasite death. However, further investigations are necessary to define the exact mechanisms linking the plasma membrane depolarization induced by endoperoxides to the parasite physiological disturbance.

By pre-treating cells with concanamycin A, the fluorescent contribution of the plasma membrane can be drastically reduced to monitor the single mitochondrial membrane potential ($\Delta\psi_m$). It also allows to reveal the shape and size of the mitochondrion **(Fig. 5.6)**. The **Figure 5.7** reports that artemisinin and tetraoxane depolarize rapidly the mitochondrial $\Delta\psi_m$ in the same manner as atovaquone. This result supports the hypothesis of a role of endoperoxide compounds

disturbing the mitochondrial functions of the malaria parasite by a fast collapse of its membrane potential via formation of radical oxygen species. A strong link between loss of mitochondrial membrane potential and parasite death has been demonstrated by the mode of action of bc_1 complex inhibitors such as atovaquone or antimycin A (Biagini et al., 2008).

5.3.2. The endoperoxide bridge is the essential pharmacophore for drug activity

In line with previous studies (Brossi et al., 1988; Kaiser et al., 2007; Wang et al., 2010), the presented results confirm the inefficiency of deoxyartemisinin to inhibit parasite growth and demonstrate its inability to collapse both plasma and mitochondrial membrane potentials **(Fig. 5.5 B)**. The endoperoxide bridge is deduced to be the key pharmacophore for the membrane depolarization activity of this class of compounds. Additionally, the analogous disrupting effects of artemisinin and tetraoxane on membrane potentials despite their important structural differences highlight the role of their only common feature: the endoperoxide bond.

5.3.3. Non heme iron Fe^{2+} is involved in artemisinin-induced membrane depolarization activity.

The reductive cleavage of the endoperoxide bridge is widely accepted to be due to a cellular source of ferrous iron. However, its origin from either hemin (ferrous heme) and/or exogenous non-heme iron (II) is still not well established and remains under debate (O'Neill et al., 2010b). Different iron chelators, selective for non-heme free iron, have been previously observed to strongly antagonize the antimalarial activity of this class of drugs *in vitro* and to prevent the toxic effects of artemisinin in mice (Eckstein-Ludwig et al., 2003; Meshnick et al., 1993; Pradines et al., 2002). It was shown that two different iron-chelators, desferrioxamine (DFO) and deferiprone (DFP) reduce at different degrees the collapse of the plasma and mitochondrial membrane potential. Chelating ferric iron as part of 1:1 molecular complex, DFO displays the strongest antagonistic effect by decreasing 67% and 84% the depolarization effect induced by artemisinin and tetraoxane respectively. Despite being more lipophilic, DFP reports a weaker chelating activity which can be explained by a 1:2 molar ratio with Fe^{2+} and by its higher complex-formation affinity with Fe^{3+} (Manzoori et al., 2011). Inhibition by DFO or DFP demonstrates the involvement of non-heme iron Fe^{2+} in the process of depolarization induced by artemisinin. According to the mechanism proposed by O'Neill and Posner **(Fig. 5.3)**, Fe^{2+} can step in the pathway during the bioactivation of endoperoxide and mediates the Fenton reaction to generate hydroxyl radical ($^{\bullet}OH$) (O'Neill and Posner, 2004). Assays performed in this study cannot precise if free Fe^{2+} is only involved as cofactor for ROS generation or is also involved in endoperoxide

activation. However, recent work with fluorescent-tagged artemisinin showed that DFO and DFP inhibit the formation of stable adducts and their irreversible accumulation in the malaria parasite (Stocks et al., 2007). Stocks *et al.* concluded that non-heme chelatable-iron can mediate activation of endoperoxides confirming its involvement at both steps of the membrane potential depolarization pathway.

5.3.4. Hydroxyl radical generation is the final factor of global membrane depolarization

The partial inhibition of depolarization obtained with Tiron indicates clearly the implication of superoxide anions ($^{\bullet}O_2^-$) in a process of global membrane depolarization in *P. falciparum* **(Fig. 5.10)**. Superoxide anions are speculated to mediate the generation of hydroxyl radicals by regenerating Fe^{2+} from Fe^{3+} to accelerate Fenton chemistry. Involvement of superoxide and non-heme iron Fe^{2+} validates the pathway suggested by linking lipid peroxidation with membrane depolarization via generation of hydroxyl radicals. Due to their reactive nature, most of ROS are acting where they are produced (Brosché et al., 2010). Thus, effect of hydroxyl radicals on membrane-bound proteins (enzymes, receptors, pores, etc.) and lipids may be located near their site of formation via lipid peroxidation induced by artemisinin carbon-centred radicals (O'Neill and Posner, 2004). A large ROS formation, not controllable by anti-oxidant defences, has been demonstrated to collapse the plasma membrane potential in the protozoon *Giardia intestinalis* (Lloyd et al., 2000). The oxidative stress damaging mitochondrial membranes may also lead to a dissipation of proton gradient and consequent membrane depolarization (Chinopoulos et al., 1999; Rogalska et al., 2008; Sen et al., 2006).

A collapse of the mitochondrial electrochemical gradient ($\Delta\psi_m$) could also be explained by a direct inhibition of key enzymes constituting the respiratory chain such as complex I (by rotenone), III (by antimycin A) or IV (by cyanide) (Duchen and Biscoe, 1992; Moon et al., 2005; Wyatt and Buckler, 2004). In *P. falciparum*, bc_1 inhibition by atovaquone has been demonstrated to collapse the mitochondrial membrane potential (Biagini et al., 2006; Srivastava et al., 1997). However, endoperoxide compounds showed weak inhibitory effects (< 25% inhibition at 1µM) on the three main components of the *P. falciparum* ETC (Table 6.1). Because endoperoxides kill malaria parasites in a low nanomolar range, this class of compounds follow an indirect pathway via ROS generation to affect the mitochondrial membrane potential instead of targeting a specific component of the respiratory chain. Recently, artemisinins cytotoxicity in human cell lines has also been confirmed to be independent of the ETC functionality (Mercer et al., 2011).

In summary, this study confirms the effect of endoperoxide compounds on mitochondrial membrane potential and presents the first evidence of their impact on the cytoplasmic barrier of the malaria parasite. Artemisinin and its derivatives act as a generator of additional reactive oxygen species that overcome the oxidative defenses of the malaria parasite and cause a widespread and rapid membrane potential depolarization leading to mitochondrial dysfunction. Some further studies will be essential to clarify details of the depolarization mechanisms, to confirm the cytotoxic effect of plasma membrane depolarization and to determine the weight of this mode of action on parasite death.

Chapter 6

Reduced cytochrome bc_1 complex expression in the *Plasmodium falciparum* atovaquone-resistance field isolate TM90C2B

6.1. Introduction

In this chapter, the bc_1 protein expression is studied to investigate the stability of the enzyme in the *P. falciparum* atovaquone-resistance field isolate TM90C2B. This work has been recently published in "Cytochrome *b* Mutation Y268S Conferring Atovaquone Resistance Phenotype in Malaria Parasite Results in Reduced Parasite bc_1 Catalytic Turnover and Protein Expression" by Fisher *et al*., 2012.

6.1.1. Atovaquone, a bc_1 complex inhibitor

Atovaquone, a hydroxynapthoquinone, is a competitive inhibitor of ubiquinone, specially inhibiting *Plasmodium falciparum* (Fry and Pudney, 1992). Combined with proguanil in a fixed-dose tablet (Malarone™), atovaquone is a potent and effective antimalarial drug for the treatment of children and adults with uncomplicated *P. falciparum* malaria (Osei-Akoto et al., 2005; Painter et al., 2007). However, because of its expensive manufacturing and price, the drug is mainly used by international travellers and overseas-stationed military personnel from developed countries (Lalloo and Hill, 2008; Petersen, 2003).

Since the early stage of drug development, the bc_1 complex has been suspected to be the primary site of action of atovaquone in the parasite (Kessl et al., 2007). Because a crystal structure of the *P. falciparum* cytochrome bc_1 is not available, the details of the binding between atovaquone and the enzymatic complex has been studied on model organisms (*Bos taurus*, *Saccharomyces cerevisiae*, *Rhodobacter capsulatus and Rb sphaeroides*) and using molecular modelling. Site-directed mutagenesis of model organism cytochrome *b*, gene sequencing of atovaquone-resistant *Plasmodium* species or EPR spectroscopy of the Rieske [2Fe2S] cluster have demonstrated that atovaquone compete with quinol at the Q_o site of the cytochrome bc_1 (reviewed in Barton et al., 2010). As described in the Chapter 1 (section 1.2.4.3.6), the cytochrome bc_1 complex is a dimeric multi-subunit complex located in the inner membrane of the mitochondrion. This enzyme is a key element of the electron transport chain (ETC) by transferring electrons from ubiquinol, produced by different dehydrogenases, to cytochrome *c* (Crofts, 2004;

Hunte et al., 2003). This electron transfer is coupled to a vectorial translocation of protons across the inner membrane generating an electrochemical (and pH) gradient. The loss of bc_1 activity results in mitochondrial dysfunction due to the collapse of the membrane potential ($\Delta\Psi_m$) and is lethal to the malaria parasite (Biagini et al., 2006; Srivastava et al., 1997). In the erythrocyte stages of the malaria parasite, one of the essential functions of the bc_1 is the maintenance of the Q cycle in order to provide ubiquinone to act as electron acceptor for dihydroorotate dehydrogenase (DHODH). The formation of orotate by DHODH for the pyrimidine biosynthesis has been demonstrated to be an essential mitochondrial function for the malaria parasite by the generation of an atovaquone-resistant phenotype in transgenic *P. falciparum* parasites expressing ubiquinone-independent yeast DHODH (Painter et al., 2010). In line with this, inhibition of the bc_1 complex by atovaquone results in an increase in carbamoyl-aspartate and a reduction in UTP, CTP and dTTP (Hammond et al., 1985; Seymour et al., 1997).

6.1.2. Cytochrome *b* mutation Y268S conferring the atovaquone resistance phenotype

Different resistance mutations associated with atovaquone have been detected in isolates of *Plasmodium* species (Kessl et al., 2007). However, a common mutation in *P. falciparum* atovaquone-resistant isolates following Malarone™ treatment failure have been observed in infected patients returning from Thailand or African countries (David et al., 2003; Farnert et al., 2003; Korsinczky et al., 2000; Wichmann et al., 2004). This atovaquone-resistance is associated with a point mutation at position 268 in cytochrome *b* exchanging tyrosine for serine (Y268S), or less frequently, asparagine (Y268N) (Berry et al., 2006; Fisher and Meunier, 2008; Fivelman et al., 2002; Musset et al., 2006). The *P. falciparum* strain TM90C2B used in this work, is a field isolate associated to this mutation and was detected during a clinical phase 2 study to determine atovaquone efficacy in Thailand **(Fig. 6.1)** (Looareesuwan et al., 1996). Highly conserved across all species, the tyrosine 268, is located within the "ef" helix component of the Q_o site. Its side chain participates in a stabilizing hydrophobic interaction with bound ubiquinol (Barton et al., 2010). Compared with parasite sensitive strains (IC_{50} = 0.8 ±0.1 nM), the resultant atovaquone-resistant phenotype displays a 1000-fold higher growth IC_{50} (Fisher et al., 2012).

Figure 6.1. Sequence alignments of the cytochrome *b* proteins from human, bovine, yeast and *P. falciparum* sensitive- (Pf_3D7) and resistant-atovaquone (Pf_TM90C2B) strains around the Q_o site. In red is highlighted the mutated Tyrosine 268 in *P. falciparum* (at position 279 in yeast). Below the alignment, □ indicates residues interacting with atovaquone and ● those associated with atovaquone-resistance mutations in *Plasmodium* species.

Displaying a high degree of sequence identity with its *P. falciparum* homologue, the *S. cerevisiae* cytochrome *b* were used as a model to study the molecular aspect of the atovaquone resistance (Fisher and Meunier, 2005; Kessl et al., 2007; Mather et al., 2005). Because atovaquone is also an inhibitor of the yeast bc_1 complex with a K_i of 9 nM (Kessl et al., 2003), their interaction were studied by using molecular modelling based on the crystal structure of *S. cerevisiae* cytochrome bc_1 (Kessl et al., 2007). The presence of a similar stable interaction between Tyr^{268} of cytochrome *b* (at position 279 in yeast) and atovaquone have been reported **(Fig. 6.2)**. To stabilize the binding of atovaquone to the Q_o site, additional interactions are believed to take place, namely hydrogen bonding between the His^{181} of the Rieske subunit and the Glu^{272} of the cytochrome *b* via a bridging water molecule. A hydrophobic pocket is formed from the side chain of Phe^{121} (transmembrane helix C) and Phe^{278} (ef loop) (Fisher et al., 2012). A hydrophobic interaction is predicted with the side chain of Leu^{275}. The introduction of the Y268S mutation in yeast (Y279S) results in an increase in IC_{50} for atovaquone inhibition of bc_1 enzymatic activity from 60 nM to 4000 nM (Fisher and Meunier, 2005). By using mutant of bc_1 from the bacterium *Rhodobacter spharoides,* Crofts *et al*. reported that a large or aromatic hydrophobic side chain residue like tyrosine is essential at the position 268 for an efficient catalytic activity (Crofts et al., 2000).

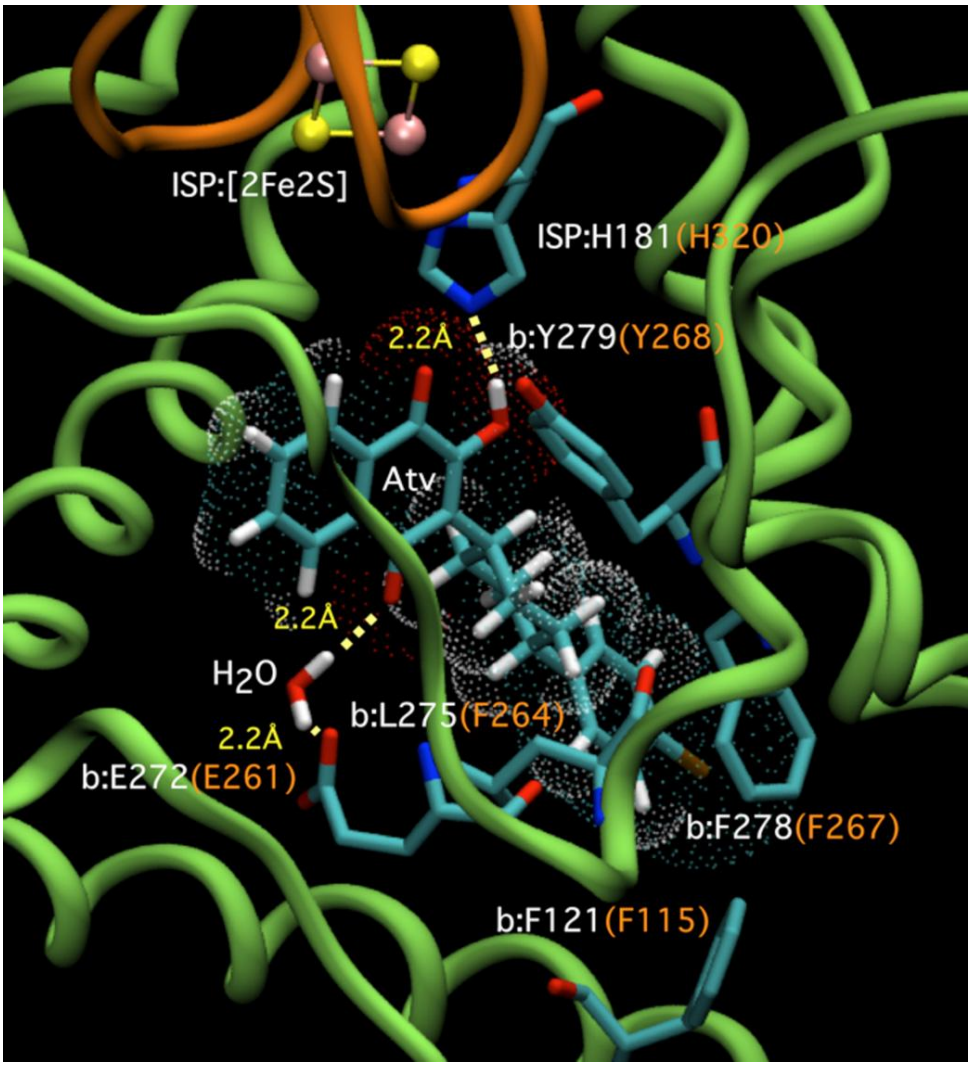

Figure 6.2. Molecular model of atovaquone (Atv) docked into the Q_o site of yeast cytochrome bc_1 complex (Fisher et al., 2012). Yeast residues are labeled in *white*, with the corresponding *P. falciparum* residues labeled in *orange*. The cytochrome *b* polypeptide backbone is represented in *green*, with the Rieske protein backbone in *brown*. The [2Fe-2S] cluster of the Rieske protein is represented in CPK form (sulfur, *yellow*; iron, *pink*). Hydrogen bonds are indicated by *yellow dotted lines*. A 1.4 Å radius CPK dotted surface has been added around the docked atovaquone molecule to aid visual clarity. The Protein Database (PDB) accession number used for the cytochrome bc_1 complex structure is 3CX5.

6.1.3. Effect of the mutation Y268S on the parasite bc_1 enzyme

Although the steady-state turnover activity of the yeast Y279S mutant has previously been measured with a reduction of 70% in comparison with the wild-strain, the effect of atovaquone resistant mutation Y268S on the parasite bc_1 enzyme has just recently been elucidated (Fisher et al., 2012).

First, growth inhibition assays confirmed the phenotypic profiles of the wild type (3D7) and atovaquone-resistant strains (TM90C2B and 3D7-yDHODH·GFP) to therapeutic drugs and various specific electron transport inhibitors **(Table 6.1)**. As expected, TM90C2B with the Y268S mutation in bc_1 displayed high levels of resistant to atovaquone (~12,000 fold). TM90C2B was also

shown to have an increased resistance to other bc_1 inhibitors including the Q_o site inhibitors myxothiazol (~20-fold) and stigmatellin (~5-fold), as well as the Q_i site inhibitor antimycin (≈20-fold). The Q_i site being located at the opposite side of the inner mitochondrial membrane within cytochrome *b* (separated by ~25 Å with the Q_o site), the increase in IC_{50} for antimycin in TM90C2B compared with the control 3D7 strain is at first sight surprising. However, regulatory interactions between the Q_o and Q_i sites have been observed in yeast bc_1 in which the binding of stigmatellin affected the interaction of antimycin in a complex manner, with one half of the (dimeric) enzyme binding antimycin in a slow, concentration-independent way. Antimycin was observed to bind rapidly and in a concentration-dependent manner in the presence of myxothiazol (a "b-proximal" Q_o site inhibitor) (Covian and Trumpower, 2006). The structural mechanism for this apparent communication pathway between the quinone-binding sites within cytochrome *b* remains to be determined. The other atovaquone-resistant strain 3D7-yDHODH·GFP was also highly resistant to atovaquone and other bc_1-targeting inhibitors (antimycin and stigmatellin), in line with the original work performed by Painter *et al.* (Painter et al., 2007).

Table 6.1. Growth inhibition profiles of *P. falciparum* 3D7, TM90C2B and 3D7-yDHODH·GFP parasites (Fisher et al., 2012).

Drug	Target	IC_{50} (nM)		
		3D7	TM90C2B	3D7-yDHODH·GFP
Artesunate		1.6 ± 0.4	0.45 ± 0.09	1.1 ± 0.13
Chloroquine		11.4 ± 0.4	70.6 ± 9.6	10.4 ± 0.4
Atovaquone	bc_1 (Q_o)	0.8 ± 0.1	12,418 ± 1,6 55	5,823 ± 2,254
Stigmatellin	bc_1 (Q_o)	23 ± 4.2	106.95 ± 13.66	4,145 ± 425
Myxothiazol	bc_1 (Q_o)	33± 6	564.2 ± 11.7	ND
Antimycin	bc_1 (Q_i)	13± 2	300.7 ± 34.67	ND

Data are expressed as mean ± S.E., acquired from multiple replicates performed on at least 3 independent occasions. IC_{50} values were calculated by fitting of four-parameter logistic curves (Kaleidagraph software). ND, Not Determined.

To determine the impact of Y268S mutation on the catalytic activity of *P. falciparum* bc_1, steady-state kinetics were performed on both wild type (3D7) and atovaquone-resistant (TM90C2B) strains. First, TM902CB bc_1 displayed a 100-fold decrease in IC_{50} value against atovaquone (600 ± 90 nM) in comparison with the enzyme from the sensitive strain 3D7 (6 ± 1 nM) **(Fig. 6.3)** (Fisher et al., 2012).

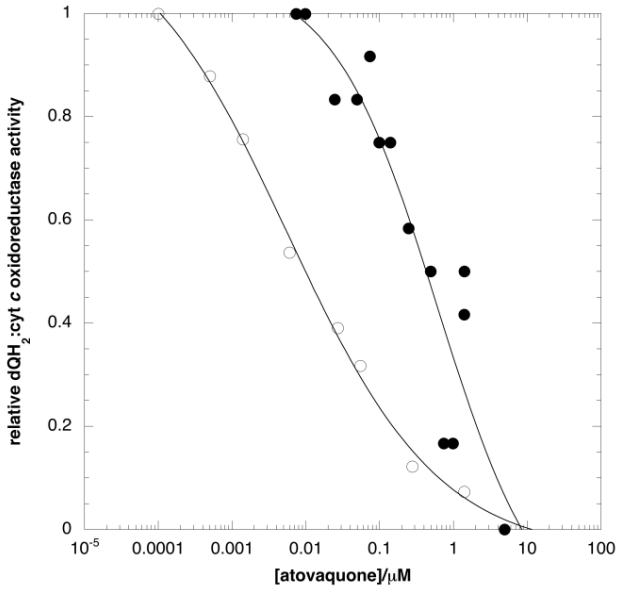

P. falciparum strain	Atovaquone (nM)	
	IC_{50}	K_i
3D7	6 ± 1	0.6
TM90C2B	600 ± 90	162

Values are mean ± standard errors from independent experiment. The K_i values for atovaquone inhibition were calculated using the Cheng-Prusoff equation (Cheng and Prusoff, 1973).

Figure 6.3. 'Cell-free extract' cytochome bc_1 complex inhibition by atovaquone in *P. falciparum* sensitive- (3D7) and resistant-atovaquone strains (TM902CB) (Fisher et al., 2012). Inhibition of steady-state decylubiquinol:cytochrome *c* oxidoreductase activity of *P. falciparum* 3D7 (○) and TM90C2B (●) bc_1 in crude cell-free extracts by atovaquone.

Steady-state studies measured a decrease in V_{max} in crude preparations of TM90C2B bc_1 (60.2 ± 3.2 nmol cyt *c* reduced/min/mg protein) compared with the control 3D7 strain (97.4 ± 5.1 nmol cyt *c* reduced/min/mg protein) **(Fig. 6.4)** (Fisher et al., 2012). A three-fold increase in K_m observed for decylubiquinol in TM90C2B bc_1 were notified in comparison with the enzyme in 3D7. This increase in K_m for decylubiquinol coupled with the decrease in V_{max} observed in TM90C2B bc_1 suggests that the binding and/or positioning of the substrate ubiquinol within the Q_o site is impaired in the atovaquone-resistant strain. A similar observation has been made for the yeast Y279C and Y279S mutants (turnover numbers of 47 and 30 s^{-1}, respectively, compared with the wild type value of 80 s^{-1}) (Fisher et al., 2004b; Fisher and Meunier, 2005; Wibrand et al., 2001), although it should be noted that more deleterious effects on the yeast enzyme activity have been noted in Y279S preparations in other laboratories (Kessl et al., 2005).

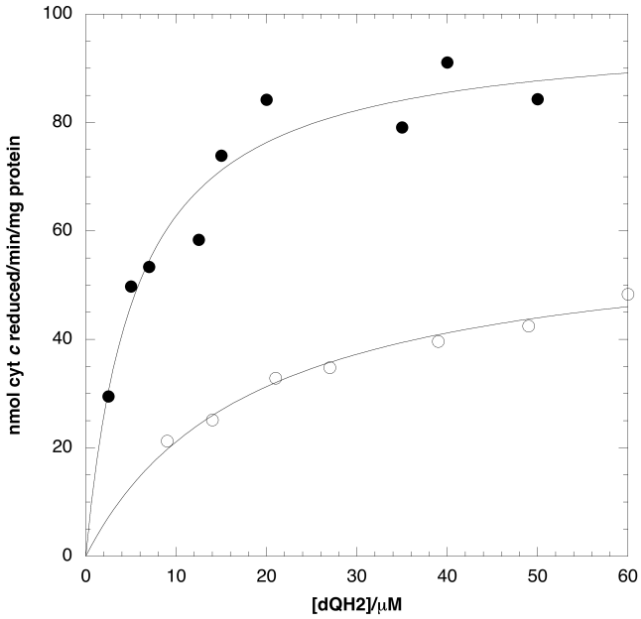

P. falciparum strain	V_{max} (nmol cyt *c* reduced /min/mg protein)	K_m (dQH2, μM)
3D7	97.4 ± 5.1	5.5 ± 1.1
TM90C2B	60.2 ± 3.2	18.5 ± 2.6

Values are mean ± standard errors from independent experiment.

Figure 6.4. 'Cell-free extract' steady-state cytochome bc_1 complex activity in *P. falciparum* sensitive- (3D7) and resistant-atovaquone strains (TM902CB) (Fisher et al., 2012). Steady-state decylubiquinol:cytochrome *c* oxidoreductase activity of *P. falciparum* 3D7 (●) and TM90C2B (○) bc_1 in crude cell-free extracts.

6.1.4. Comparison of bc_1 gene expression in sensitive and resistant-atovaquone strains

Analysis of expression levels of genes composing the respiratory chain from the TM902CB strain revealed significant differences with the 3D7 atovaquone-sensitive strain. Then a ~2 fold increase in expression of some bc_1 complex genes including cytochromes *b*, c_1, and the Rieske (ISP) subunit of bc_1 were observed in the atovaquone-resistant strain **(Fig. 6.5)** (Fisher et al., 2012). Additionally a similar overexpression were reported for cytochrome *c* and two subunits of the cytochrome *c* oxidase (subunit 1 and 2).

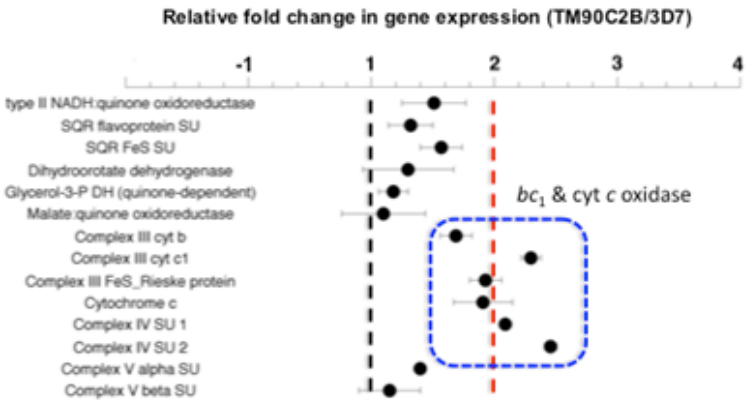

Figure 6.5. Fold changes in gene expression of electron transport chain components between *P. falciparum* sensitive- (3D7) and resistant-atovaquone (TM90C2B) strains (Fisher et al., 2012). Dashed blue box indicates genes encoding for components of mitochondrial Complex III and IV.

Point mutations of mitochondrial genes leading to residue substitutions impairs in some cases the stability of assembled respiratory chain complexes in mice model (Edgar et al., 2009). A protein deficiency due to instability or non-assembly can upregulate the tRNAs level of genes concerned via a compensatory mechanism (Ylikallio and Suomalainen, 2012).

In this chapter, the effect of the Y268S mutation on the stability of *P. falciparum* bc_1 has been investigated. First, a new specific polyclonal antibody against the Rieske (ISP) subunit of the *P. falciparum* cytochrome bc_1 was raised and characterized via immunoprecipitation and NanoLC/MS-MS. Furthermore, using Western Blot analyses, protein expression levels were compared between atovaquone sensitive and resistant *P. falciparum* and yeast strains. The results are discussed in the context of the impact of the Y268S mutation on the ISP stability and bc_1 complex assembly.

6.2. Material and methods

6.2.1. Synthesis of an anti-bc_1 polyclonal antibody

The peptide ^{322}SHYDNSGRIRQGPA^{335} of the ubiquinol-cytochrome *c* reductase Rieske iron-sulfur subunit (Swissprot accession # Q8IL75) of the *Plasmodium falciparum* bc_1 protein was selected **(Fig. 6.6)**, synthesized, and used for immunization in the rabbit and generation of an affinity-purified polyclonal antibody (GenScript Corp., Piscataway, NJ). The rabbit anti-Pfbc1 polyclonal antibodies were lyophilized in phosphate-buffered saline (pH 7.4) with 0.02% sodium azide as preservative. Lyophilized antibodies were reconstituted with MilliQ water, and aliquots were stored at -20 °C until use.

```
Pf_3D7   293 LVNIGICTHLGCVPA-QGGNYSGYFCPCHGSHYDNSGRIRQGPAPSNLEVPPYEFVDENTIKIG 355 (40.9 kDa)

Yeast    153 LIMLGICTHLGCVPIGEAGDFGGWFCPCHGSHYDISGRIRKGPAPLNLEIPAYEFDGDKVIVG- 215 (23.3 kDa)
Bovine   211 VILIGVCTHLGCVPIANAGDFGGYYCPCHGSHYDASGRIRKGPAPLNLEVPSYEFTSDDMVIVG 274 (29.5 kDa)
Human    220 VILIGVCTHLGCVPIANAGDFGGYYCPCHGSHYDASGRIRLGPATLNLEVPTYEFTSDDMVIVG 283 (30.8 kDa)
                * ********    *   *  ********* ***** ***   *** * ***
```

Figure 6.6. Sequence alignments of C-terminal ubiquinol-cytochrome *c* reductase Rieske iron-sulfur (ISP subunit) from human, bovine, yeast and *P. falciparum* 3D7 strain (Pf_3D7). In red is highlighted the peptide chosen in *P. falciparum* for the antibody synthesis. Below the alignment, * indicates conserved residues across all species.

6.2.2. Immunoprecipitation of parasite membrane proteins

For immunoprecipitation studies, cell-free parasite membrane proteins were boiled (5 min at 95 °C) in denaturing lysis buffer (50mMTris-HCl, 5mMEDTA, 2% (w/v) SDS, 10mM DTT) and diluted (10-fold) with nondenaturing lysis buffer (50 mM Tris-HCl, 150 mM NaCl, 1 mM EDTA, 1% (v/v) Triton X-100, pH 7.5). Following centrifugation (17,000 x *g* for 30 min), denatured proteins were collected in the supernatant and incubated overnight with 2 µg of anti-bc_1 antibody, rotating

at 4°C, followed by 50 µl of protein A-Sepharose slurry for 3 h at 4 °C. Immunoprecipitates were washed, gently eluated with an acidic buffer (pH 2.8), and then separated by 10% (w/v) SDS-PAGE gel electrophoresis before proceeding to immunoblotting, in gel-trypsin digestion and mass spectrometry.

6.3. Results

6.3.1. Characterization of the anti-Rieske subunit antibody

To measure bc_1 protein expression in the parasite, a custom polyclonal antibody against the Rieske subunit of the *P. falciparum* bc_1 complex was raised using a commercial supplier (GenScript Corp., USA). Due to its high conservation across species, the peptide ^{322}SHYDNSGRIRQGPA^{335} located near the C-terminal of the *P. falciparum* Rieske subunit was chosen for antibody generation. The anti-bc_1 polyclonal antibody was raised by immunizing rabbits with the specific peptide (as peptide–KLH conjugate) and purified by affinity.

To validate this customized antibody by analysis of its antigens with NanoLC-MS/MS, an immunoprecipitation experiment was performed on the membrane proteins obtained from 3D7 free-parasite extracts. The result of the immunocapture (separated by 10% SDS-PAGE) was observed by Western blot and silver staining **(Fig. 6.7)**. The immunoblot revealed a protein captured at approxiamtely 41 kDa, consistent with the size of the Rieske subunit in the malaria parasite. The band corresponding to the protein was excised from the silver-stained gel, digested with trypsin, and analyzed by NanoLC-MS/MS to obtain the peptide sequence data. The Rieske subunit was identified by 28 peptide mass fingerprints with sequence coverage of 60.0% **(Table 6.2)**. An example of the NanoLC-MS/MS fragmentation pattern of the peptide ^{101}YAHYNQTAEPVPR^{114} is shown in **Figure 6.8**. Immunofluorescence localization of the bc_1 complex inside the parasite-infected erythrocytes has been tempted by using the anti-Rieske antibody but results showed that it is unable to bind the subunit folded and can be used in denatured conditions only. Attempts to generate polyclonal antibodies specific to *P. falciparum* cytochrome *b* were unsuccessful.

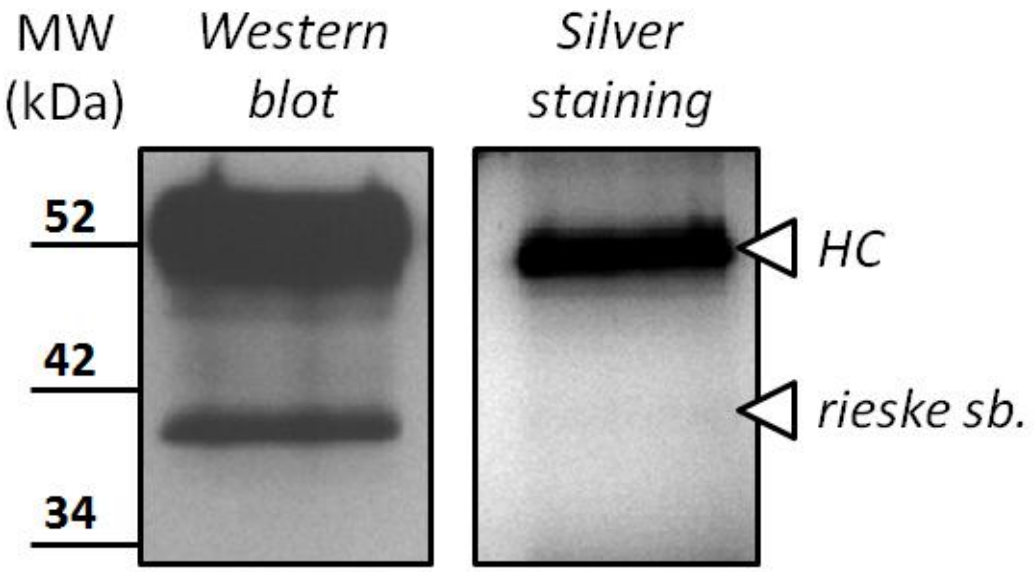

Figure 6.7. Western Blot and silver staining of the Rieske subunit (41 kDa) immunocapture from 3D7 free parasites. HC indicate the heavy chain (50 kDa) of the polyclonal antibody used for the immunoprecipitation. Western blot was performed with customized anti-bc_1 polyclonal antibodies (1/500 dilution).

Table 6.2. List of 10 first hits obtained by NanoLC-MS/MS analysis and Sequest algorithm search of the immunoprecipitated 41 kDa band. In yellow is highlighted the most significant hit with the highest score.

Hits	Accession	Coverage	# Peptides	# AAs	MW [kDa]	calc. pI	Score	Description
1	**PF14_0373**	**60.00%**	**28**[a]	**355**	**41.0**	**7.58**	**53.93**	**organism=Plasmodium_falciparum_3D7 | product=ubiquinol-cytochrome c reductase iron-sulfur subunit, putative | location=Pf3D7_14:1600876-1601943(-) | length=355**
2	PF10_0379	25.07%	14	359	41.7	6.87	11.41	organism=Plasmodium_falciparum_3D7 | product=phospholipase, putative | location=Pf3D7_10:1562808-1563887(+) | length=359
3	PFB0480w	7.96%	3	314	37.1	7.53	6.71	organism=Plasmodium_falciparum_3D7 | product=syntaxin, Qa-SNARE family | location=Pf3D7_02:436050-436994(+) | length=314
4	MAL13P1.339	13.08%	8	367	44.6	9.23	5.46	organism=Plasmodium_falciparum_3D7 | product=conserved Plasmodium protein, unknown function | location=Pf3D7_13:2679915-2681301(+) | length=367
5	PF13_0004	15.45%	11	343	38.4	9.28	5.33	organism=Plasmodium_falciparum_3D7 | product=rifin | location=Pf3D7_13:47686-48872(+) | length=343
6	MAL7P1.118	8.19%	8	403	47.0	8.69	5.30	organism=Plasmodium_falciparum_3D7 | product=PelOta protein homologue, putative | location=Pf3D7_07:999399-1000610(+) | length=403
7	PFF0025w	17.20%	6	372	41.5	9.01	4.79	organism=Plasmodium_falciparum_3D7 | product=rifin | location=Pf3D7_06:26557-27830(+) | length=372
8	PFI0035c	22.31%	9	381	42.1	9.06	4.51	organism=Plasmodium_falciparum_3D7 | product=rifin | location=Pf3D7_09:49612-50971(-) | length=381
9	PF14_0266	6.93%	8	433	51.4	8.21	4.11	organism=Plasmodium_falciparum_3D7 | product=conserved protein, unknown function | location=Pf3D7_14:1129412-1130713(-) | length=433
10	MAL13P1.43	22.50%	11	360	42.3	8.03	3.98	organism=Plasmodium_falciparum_3D7 | product=conserved Plasmodium protein, unknown function | location=Pf3D7_13:416120-417202(-) | length=360

[a] The list of 28 peptides identified are indicated in **Appendix 2**.

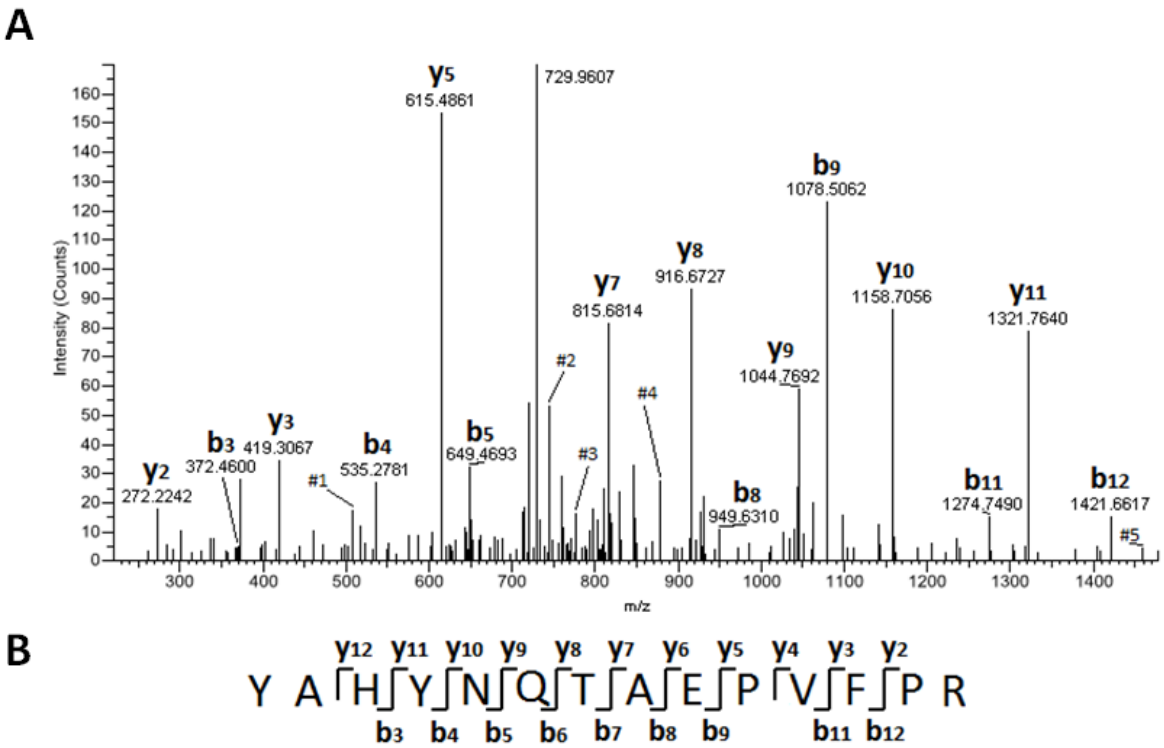

Figure 6.8. (A) Fragmentation spectra of the precursor ion with m/z = 846.90 Da (charge of +2) identified as peptide YAHYNQTAEPVPR (residues 101-114 of Rieske subunit). #1 = y4 (517.3738); #2 = y6 (744.0631); #3 = b6 (777.4517); #4 = b7 (878.6395); #5 = y12 (1459.2450). **(B) Peptide sequence consensus obtained after matching of y- and b-fragment ions.**

6.3.2. Cytochrome bc_1 protein expression in sensitive- and resistant-atovaquone parasites

Using the characterized anti-ISP antibody, the extent to which the Y268S mutation affected protein expression was determined by performing Western blots of cell-free extracts prepared from TM90C2B compared with the atovaquone-sensitive 3D7 strain. As shown in **Figure 6.9**, a decrease in ISP content was observed in Western blots prepared from TM90C2B compared with the 3D7 control strain. This experiment was performed on three separate occasions using different membrane preparations. For all experiments, aldolase was used to control for any potential differences in protein loading **(Fig. 6.9)**.

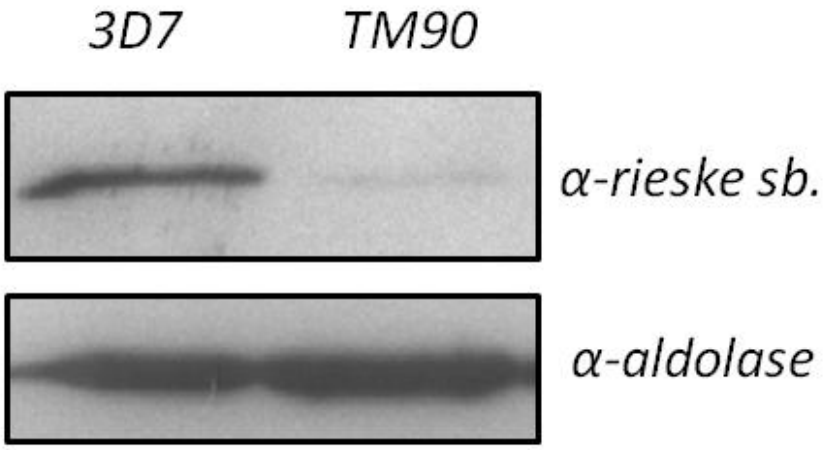

Figure 6.9. **Immunoblot analysis of the 3D7 and TM90C2B membrane proteins fractions with the customized anti-Rieske antibody.** Aldolase is used as a loading control and detected from their respective soluble proteins fractions.

6.3.3. Cytochrome bc_1 protein expression in yeast wild type and Y279S mutant

Further Western blot analysis was carried out to observe the same mutation effect on yeast model. In contrast to the parasite data, no such loss in the ISP signal was observed using crude mitochondrial membranes prepared from yeast containing the Y279S cytochrome *b* mutation, relative to wild type control (WT) **(Fig. 6.10 A)**. An identical SDS-Page stained with coomassie blue were performed as a loading control **(Fig. 6.10 B)**. Bovine mitochondrial membrane preparation were used as a positive control.

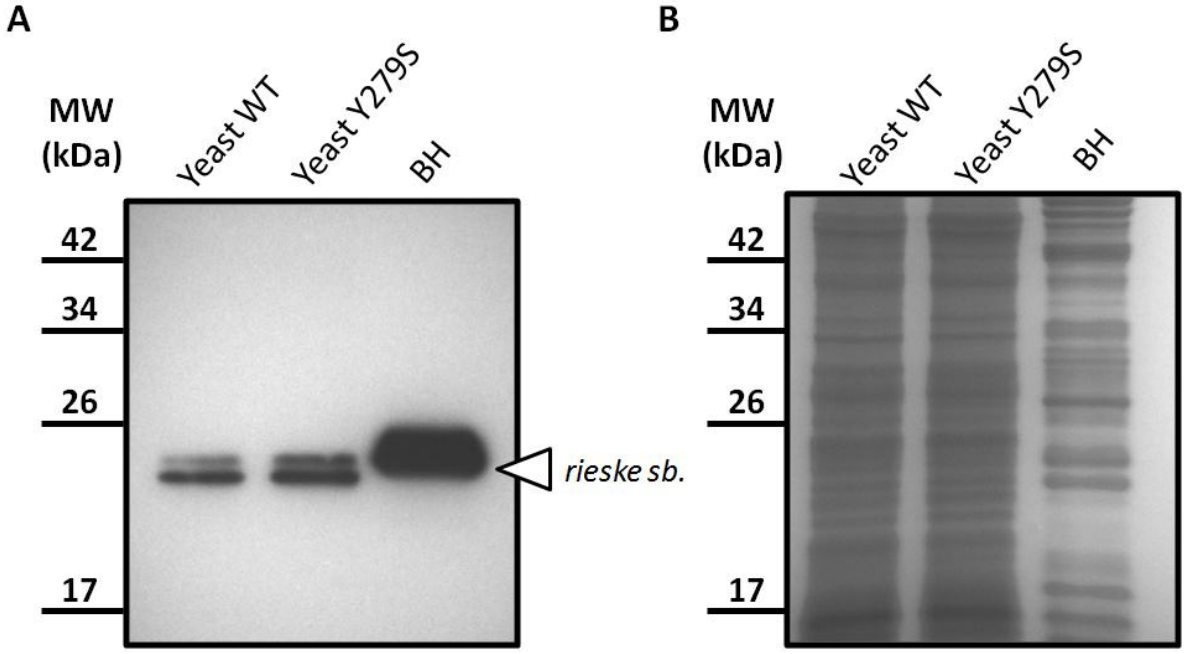

Figure 6.10. (A) Immunoblot analysis of the yeast wild type and Y279S membrane proteins fractions with the customized anti-Rieske antibody. WT indicates Wild Type strain and BH the Bovine mitochondrial membrane preparation. **(B) Coomassie blue staining of an identical SDS-PAGE with similar protein loading.**

6.4. Discussion

In this study the effect of the Y268S mutation in TM90C2B parasites was investigated at the bc_1 expression level and compared to the wild type strain 3D7. This mutation causes a 3-fold increase in *Km* observed for decylubiquinol in TM90C2B bc_1 coupled with the decrease in *Vmax* (Fisher et al., 2012). It suggests that the binding and/or positioning of the substrate ubiquinol within the Qo site is impaired in TM90C2B compared with the wild type, consistent with mutation studies of this residue in yeast model (Fisher and Meunier, 2005). To investigate if the loss of bc_1 activity in the resistant strain is linked to a change of its expression at a proteomic level, a specific polyclonal antibody was raised and further characterization revealed it to be specific to the *P. falciparum* Rieske subunit (a component of the bc_1 complex) via immunoprecipitation and NanoLC-MS/MS analysis. The choice of a conserved peptide as antigen allocates a cross-species feature to the polyclonal antibody able to bind the protein from yeast and beef.

Western blot analysis of the Rieske subunit (ISP) content in free parasite extracts from resistant-atovaquone strain TM90C2B revealed a decreased level of the bc_1 subunit in comparison with the sensitive strain 3D7 **(Fig. 6.9)**. Although a ~2-fold increasing at the gene expression level has been observed in the resistant strain **(Fig. 6.6)**, a reduced quantity of Rieske in TM90C2B membranes might be due to a protein instability. However, a similar procedure showed no distinguishable difference in ISP expression between yeast mutant (Y279S) and wild type (WT) **(Fig. 6.10)**. In line with this, no loss of ISP content was observed in the yeast Y279A and Y279C mutants, although the Y279W mutation was found to be structurally destabilizing (Fisher et al., 2004b; Kessl et al., 2005). These data further highlight the differences between parasite and yeast cytochrome *b* and the need for performing biochemical analyses on parasite material irrespective of the technical difficulties.

The instability of Rieske subunit has been previously suggested to be a cause of loss (or decrease) of bc_1 activity. Early, some replacement of aromatic residues to non-aromatic in yeast mutant exhibited a reduced ISP level and cytochrome bc_1 activity (Snyder et al., 1999). Mutations in the hinge region of the bacterium *Rhodobacter sphaeroides* bc_1 complex reduced the flexibility of the neck region, increasing the sensitivity of the enzyme to detergent and leading to a destabilization of ISP and a loss of activity (Tian et al., 1998). Multiple-alanine substitutions of the extra fragment of the ISP in *Rhodobacter sphaeroides* decreased (or removed) the bc_1 activity because of an instable mutant ISP protein despite an unaffected mutant mRNA (Xiao et al., 2004). A specific mutations in yeast ISP increase its sensitivity to proteolytic cleavage, destabilizing the bc_1 complex and resulting in a lower QH2-cytochrome c reductase activity (Fisher et al., 2004a).

The apparent instability of the ISP in TM90C2B as revealed by Western blotting suggests a weakened interaction between this subunit and cytochrome *b.* This instability of the Rieske subunit may be due to perturbation of the ef helix and surrounding protein structure at the Q_o site caused by the introduced serinyl side chain. A potential consequence of structural perturbation around the Q_o site would be a perturbation of the docking or positioning of the ISP ecto-domain at Q_o, weakening the hydrogen bonding association and/or an increase in the electron transfer distance between bound ubiquinol and the ISP [2Fe-2S] cluster, or lowering the occupancy of bound ubiquinol. Such perturbations have been observed in Q_o site mutants of the yeast bc_1 complex (Brasseur et al., 2001; Brasseur et al., 2004; Fisher et al., 2004b). The differences in bc_1 complex integrity observed in TM90C2B and the yeast Y279S mutant may arise from the potentially unusual structure of the Q_o site and ISP docking surface in Apicomplexa (*i.e.* the four residue deletion in the N-terminal region of the cd2 helix (Biagini et al., 2008)). This potential structural perturbation affecting electron transfer may also account for the apparent increased tolerance (~20-fold) that the TM902CB parasite has for heme-proximal Q_o inhibitors as well as Q_i inhibitors. It will be important to further understand this phenomenon because the TM902CB strain is widely used to assess the suitability of novel bc_1 inhibitors (Cross et al., 2011), and an apparent cross-resistance of novel chemotypes may be mistakenly interpreted as deriving from atovaquone-like binding.

In conclusion, this study gives the first description of the effect of the Y268S mutation on parasite bc_1 catalytic turnover and stability. Results obtained indicate that the reduced enzyme activity affects protein stability and should incur a fitness penalty to the parasite, features that were not fully discernable using the yeast model alone.

Chapter 7

Import and processing of mitochondrial proteins in *Plasmodium falciparum* and other apicomplexan parasites

7.1. Introduction

Apicomplexan parasites are causative agents of various diseases including human malaria, toxoplasmosis or cryptosporidiosis. The mitochondrion of apicomplexan species is an essential organelle and differs from the mitochondria in other eukaryotes. In the malaria parasite *P. falciparum*, the maintenance of a mitochondrial integrity is required for different functions such as [Fe-S] cluster assembly and heme and pyrimidine biosynthesis, which have become attractive targets for antimalarial drugs (Bonday et al., 1997; Lange et al., 2000; Painter et al., 2007). Apicomplexan mitochondrial genomes (mtDNAs) are extremely reduced by encoding only three components of the mitochondrial electron transport chain (ETC): the cytochrome *c* oxidase subunits I and III (Cox1 and Cox3) and the cytochrome *b* (Cytb) (reviewed in Gray et al., 2004; Vaidya and Mather, 2009). Among apicomplexan parasites, the human pathogen *Cryptosporidium* does not have a mtDNA and thus the organelle is completely dependent on nuclear-encoded proteins (Henriquez et al., 2005). Consequently, the great majority of mitochondrial proteins are imported post-translationally from the cytosol into the organelle. Those mitochondrial precursors contain N-terminal or internal targeting peptides recognized by surface receptors which induce their translocation. In *P. falciparum*, proteins targeting the mitochondrion have been predicted to represent around 7% (~380 proteins) of the total nuclear-encoded proteins (Bender et al., 2003).

The protein uptake into mitochondria has been demonstrated to be crucial for cell viability and at least four different pathways have been identified depending on the final destination of these precursors: the presequence pathway to the inner membrane or matrix, carrier pathway to the inner membrane, β-barrel pathway to the outer membrane and the intermembrane space assembly (reviewed in Chacinska et al., 2009; Neupert and Herrmann, 2007; Schmidt et al., 2010). To be sorted into mitochondrial membranes or transported across, mitochondrial precursors are assisted by multi-subunits membrane bound translocases and soluble chaperones located in the cytosol, intermembrane space and matrix. After import into the mitochondria, precursors are proteolytically processed by proteases to become functional. The proteolytic machinery is distributed in different mitochondrial compartments and cleaves

presequences or additional peptides to ensure the maturation, localization and assembly of mitochondrial proteins (recently reviewed in Mossmann et al., 2011).

In the last 10 years, our understanding of the mitochondrial proteins import machinery has been accelerated with the identification of new components through the use of genetic approaches in model organisms such as baker's yeast *Saccharomyces cerevisiae* or fungi *Neurospora crassa* (Neupert and Herrmann, 2007). The sequencing of all apicomplexan genomes allowed a first description of the mitochondrial protein import apparatus in *Plasmodium falciparum* or *Toxoplasma gondii* based on yeast and plant homologues (Sheiner and Soldati-Favre, 2008; van Dooren et al., 2006). However, the description of the apicomplexan model is still fragmented and no general overview has been proposed.

This work presents an updated picture of the whole protein import and processing machinery in apicomplexa, as well as, reveals novel putative components in this pathway. Hereby, all pathways and components in *Plasmodium falciparum* are described in detail and five different apicomplexan species homologues (*Toxoplasma gondii*, *Cryptosporidium muris*, *Theileria parva*, *Babesia bovis* and *Neospora caninum*) have been determined. The comparison with yeast, mammalians or plants exhibits certain similarities but also major distinctions that highlight an apicomplexan model distinct to other organisms.

7.2. Mitochondrial targeting signals

Mitochondrial precursors are synthesized in the cytosol and target this organelle though specific signal peptides encoded in their amino acid sequences. There are two main groups of targeting signals using different importation pathways. The most common signal is the cleavable N-terminus of mitochondrial leading peptides (Horwich et al., 1985; Hurt et al., 1984). The pre-sequence forms amphipathic α-helices with two faces, one which is hydrophilic and the other positively charged, these are recognized by import receptors of the mitochondrial outer and inner membranes (Neupert and Herrmann, 2007). Proteins with a pre-sequence are released into the matrix or inserted into the inner membrane if a hydrophobic sorting peptide follows the targeting signal **(Fig. 7.1)**.

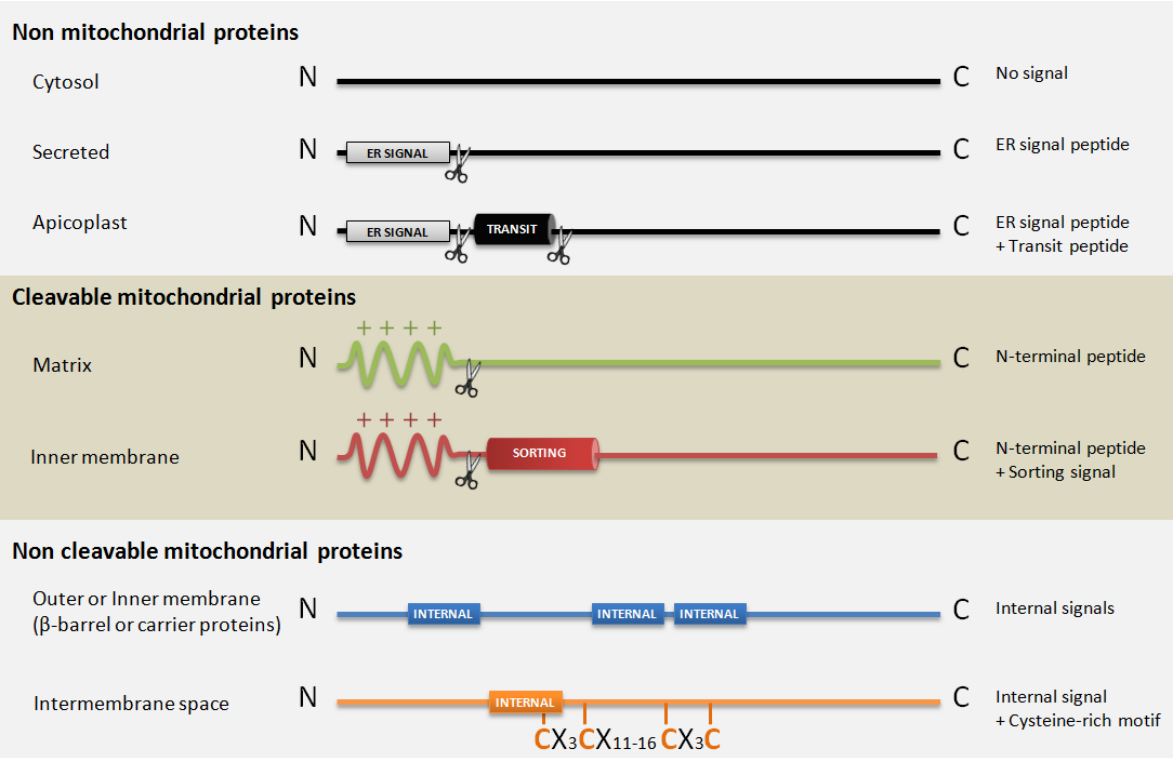

Figure 7.1. Signal profiles of proteins targeting mitochondrial compartments or other apicomplexan cellular locations. Extracellular and apicoplastical proteins display an N-terminal signal peptide that targets the endoplasmic reticulum (ER) where it is cleaved. Then proteins traffic via a secretory pathway but are not secreted if a transit peptide is exposed. In this case these proteins are transferred to the apicoplast where they become mature after processing of their transit sequence (Waller et al., 1998; Yung et al., 2001). N-terminal pre-sequences designated for the mitochondrion are cleaved by the mitochondrial processing peptidase (MPP) located inside the matrix.

Among apicomplexans, the properties of mitochondrial N-terminal signal peptides have only been studied in *Plasmodium falciparum* leading to the development of two bioinformatic tools for predicting mitochondrial proteins in malaria parasites: PlasMit in 2003 (gecco.org.chemie.uni-frankfurt.de/plasmit) followed by PFMpred in 2009 (www.imtech.res.in/raghava/pfmpred) (Bender et al., 2003; Verma et al., 2010). In *Plasmodium* species, the length of targeting peptides can vary between 23 to 169 amino acids, with an average of 48 residues, and presents specific features compared to the N-terminal signals of apicoplast or secretory proteins. They display the highest content of positively charged residues and the lowest amount of hydrophobic amino acids, as well as a distinct abundance of glutamic acid (E), isoleucine (I) and tyrosine (T). For the rest of apicomplexans, two other *in silico* methods are commonly used for mitochondrial signal prediction, TargetP (www.cbs.dtu.dk/services/TargetP) and MitoProt II (ihg.gsf.de/ihg/mitoprot.html) developed for eukaryotic proteins, but the use of *Plasmodium* dedicated algorithms can also be possible (Cai et al., 2005; Zhou et al., 2005).

The second group contains proteins with internal targeting signals, these are uncleavable and remain as part of the mature proteins (Brix et al., 1999; Egan et al., 1999; Schmidt et al., 2010). These include β-barrel proteins of the outer membrane, hydrophobic carrier proteins of the inner membrane and intermembrane space (IMS) proteins. For β-barrel and carrier proteins, several internal signals can be exposed at different positions within their amino acid sequence, while only one internal signal peptide coupled to a cysteine-rich motif is needed to target the intermembrane space. The nature of these internal signals remains unclear and is difficult to identify. Furthermore, to date, there are no bioinformatic tools able to predict their localization in amino acid sequences.

7.3. *In silico* identification of protein import and processing machinery components in Apicomplexan

Sequencing of apicomplexan genomes (for *Plasmodium*, *Cryptosporidium*, *Theileri and Babesia* species) or large-scale expressed sequence tag (EST) (for *Toxoplasma* or *Neospora* species) have become a widely used technique in order to get a deeper understanding of many of their biological processes (Abrahamsen et al., 2004; Ajioka et al., 1998; Brayton et al., 2007; Carlton et al., 2002; Gardner et al., 2005; Gardner et al., 2002; Pain et al., 2005; Xu et al., 2004). The apparatus of protein translocation into the mitochondria and their subsequent processing has been mainly studied in *P. falciparum* and *T. gondii* through the identification of their putative components by homology searching of model organisms such as yeast, mammalian or plant mitochondrial (Dowse and Soldati, 2005; Gangwar et al., 2009; Maćašev et al., 2004; Sheiner and Soldati-Favre, 2008; van Dooren et al., 2006; van Dooren et al., 2002). However, our knowledge of those machineries in malaria parasite remains unclear in some areas mainly due to a lack of certain components. This can be explained by either their absence in the nuclear genome or their high divergence which makes their identification more difficult. Recently Dolezal *et al.* identified Sam50, a component of the outer membrane SAM complex, in different apicomplexan species by using a Hidden Markov Model approach (Dolezal et al., 2006). Compared to BLAST algorithms, profile Hidden Markov Models (HMMs) enhances the sensitivity for protein homology identification (Hofmann, 2000). New putative genes involved into the translocation and processing machineries of *P. falciparum* and five other apicomplexan species have been identified in this study by employing HMMER (hmmer.janelia.org), a sequence homology search software based on profile HMMs (Finn et al., 2011).

7.4. Protein import into apicomplexan mitochondria

Based on component homologues from yeast (*Saccharomyces cerevisiae*), mammalian (*Homo sapiens*) and plant (*Arabidopsis thaliana*) models, an *in silico* inventory of the apicomplexan mitochondrial protein import apparatus was established **(Table 7.1)**.

Table 7.1. Components of the mitochondrial importation machinery in apicomplexan species and comparison with fungi, mammalian and plant representatives. *Pf* indicates *Plasmodium falciparum, Tg: Toxoplasma gondii, Cm: Cryptosporidium muris, Tp: Theileria parva, Bb: Babesia bovi* and *Nc: Neospora caninum. Saccharomyces cereviae* (*Sc*), *Homo sapiens* (*Hs*) *and Arabidopsis thaliana* (*At*) represent fungi, mammalian and plant kingdoms respectively. '•' indicates novel candidate genes. '■' indicates components demonstrated essential for yeast viability. Uniprot accession number of each component are available in **Appendix 3**.

	Protein	Function	*Pf*	*Tg*	*Cm*	*Tp*	*Bb*	*Nc*	*Sc*	*Hs*	*At*
Cytosolic chaperones and factors	cHsp70	Bind precursors and maintain them soluble and unfolded (import-competent conformation)									
	Hsp90										
	MSF	Bind precursor/chaperone complexes to maintain preproteins in import-competent conformation									
	AIP		•								
	NAC	Bind nascent polypeptides and assist their mitochondrial importing									
	RAC (*h*DnaJ)										
	RAC (cHSP70)										
TOM complex	Tom40	Channel of the translocation complex							■		
	Tom22	Receptor of preproteins (cytosol side) and Tim50 (IMS side)									
	mtOM64 (TOM70)	Initial receptor for internal signals proteins, functional homolog of TOM70									
	Tom20	Initial receptor for N-terminal signal proteins									
	Tom7	Delays TOM complex assembly	•								
	Tom6	Favours TOM complex assembly									
	Tom5	Guides preproteins from receptors to Tom40 channel									
SAM complex	Sam50	Main component of the insertion in the outer membrane							■		
	Sam37	Stabilizes SAM complex and/or promotes release of β-barrel proteins in the outer membrane									
	Sam35	Receptor of β-barrel proteins							■		
	Mdm10	Assists β-barrel proteins assembly									
Tiny TIMs	Tim8	Transfer of internal signals proteins to SAM or TIM22 complexes through the IMS Assembly in chaperone complexes Tim8-Tim13 and Tim9-Tim10									
	Tim13										
	Tim9								■		
	Tim10								■		
MIA pathway	Mia40	Transfers disulfide bonds to IMS proteins							■		
	Erv1	Generates disulphide bonds and transfers them to Mia40							■		
	Cytochrome c	Oxidizes reduced Erv1							■		
TIM22 complex	Tim22	Twin-pore channel of the translocation complex							■		
	Tim12	Guides carrier proteins to the complex by forming a complex with Tim9-Tim10							■		
	Tim18	Receptor of Tim9-Tim10-Tim12 complex									
	Tim54	Assists TIM22 complex assembly									

TIM23 complex + PAM motor	Tim23	Channel of the translocation complex								▪		
	Tim50	Receptor of precursors and regulator of channel opening								▪		
	Tim21	Modulates TIM23 assembly with PAM motor										
	Tim17	Assists sorting of preproteins into the inner membrane								▪		
	mtHsp70	Mitochondrial chaperone transferring precursors to the matrix								▪		
	Pam18 (Tim14)	Stimulates transfer activity of mtHsp70								▪		
	Pam16 (Tim16)	Regulates transfer activity of mtHSp70								▪		
	Pam17	Involves in the association of TIM23 complex with PAM motor										
	Tim44	Membrane-bound receptor of mtHsp70 which guides preproteins to the matrix								▪		
	GrpE	Assists mtHsp70 in its transfer activity								▪		
Oxa1 complex	mtDNA	Mitochondrial genome	yes	yes	no	yes	yes	yes		yes	yes	yes
	Oxa1	Core of the insertion into the inner membrane										
	Letm1/Mdm38	Receptor of ribosomes and assists mitochondrial encoded proteins translation	●	●	●	●	●	●		▪		
	Mba1	Promotes interaction with mitochondrial ribosomes										

7.4.1. Cytosolic chaperones and factors

All proteins required for mitochondrial functions, except for three (Cox1, Cox2 and Cytb), are encoded in the nuclear chromosomes. They are imported into the mitochondria after translation in the cytosol as precursor proteins with a pre- or internal sequence signals. However, the emerging polypeptide chain is prone to potential aggregation with other unfolded proteins by exposure of their hydrophobic domains. Cytosolic chaperones heat shock protein 70 and 90 (Hsp70 and Hsp90) are essential to maintain these preproteins soluble through the interaction with their hydrophobic segments and subsequent guidance into the mitochondrial surface **(Fig. 7.2)** (Deshaies et al., 1988; Murakami et al., 1988; Young et al., 2003). Hsp70 and Hsp90 amino acid sequences are highly conserved between species and several homologues were identified in every apicomplexans. However, only one cytosolic Hsp70 and Hsp90 is able to bind preproteins through their N-terminal ATPase domain which is followed by a peptide binding domain and terminated by the COOH-terminal sequence EEVD (Freeman et al., 1995).

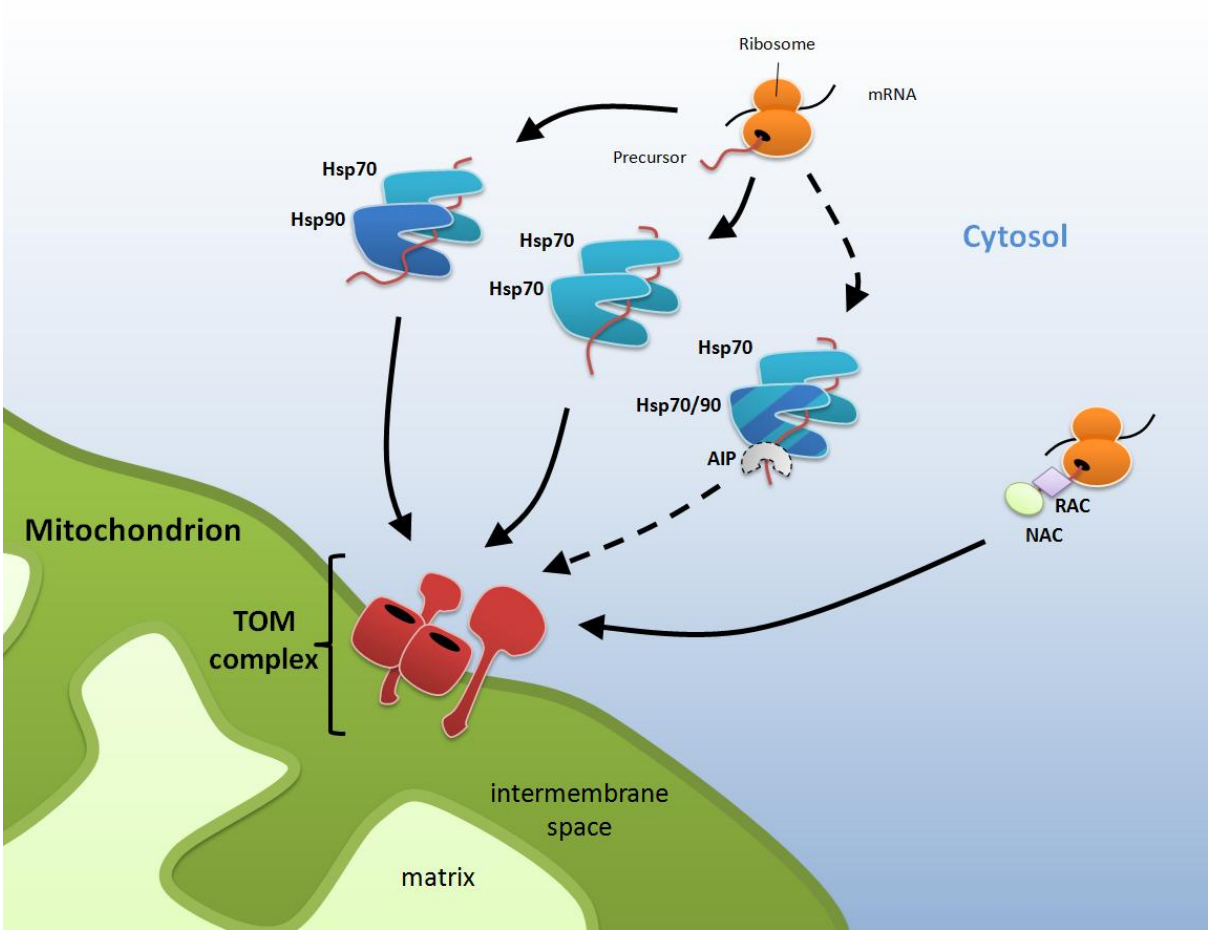

Figure 7.2. Transport of mitochondrial precursors at the organelle's surface in *P. falciparum*. Black dotted arrow indicates a novel pathway involving the new putative component AIP. OM indicates the mitochondrial outer membrane, IMS: the intermembrane space, IM: the inner membrane and M: the matrix.

In mammalian or yeast, additional factors can facilitate the formation of precursor/chaperone complexes or their interaction with outer membrane receptors such as the mitochondrial import stimulation factor (MSF) or the aryl hydrocarbon receptor-interacting protein (AIP) (Hachiya et al., 1993; Yano et al., 2003). In mammalian cytosol, MSF is composed of two subunits MSFL and MSFS (isoforms ε and ζ of 14-3-3 proteins respectively) and can act alone or in complex with Hsp70 to maintain or restore precursors in a import-competent conformation (Alam et al., 1994; Hachiya et al., 1994). In apicomplexan species, only one or two putative 14-3-3 proteins show over 30 % of similarities with human homologues (from 37% to 62% identities with the seven human ε, ζ, σ, η, ϑ, γ and β isoforms, **Table 7.2**). Due to the high degree of sequence conservation of these mammalian 14-3-3 proteins, apicomplexan homologues could not be assigned with confidence to a specific isoform. However, only an ε isoform has been clearly identified in *Cryptosporidium* (Brokx et al., 2011) and therefore, the presence of an MSP-supported import in apicomplexa cannot be established.

Table 7.2. Similarities between putative 14-3-3 proteins from Apicomplexan species and the seven human isoforms (ε, ζ, σ, η, ϑ, γ and β). Percentage identities have been determined by using ClustalW2 (www.ebi.ac.uk/Tools/msa/clustalw2) and highlighted in grey if over 30 % sequence identity is observed. Protein sequences are indicated by their Uniprot accession number. [1] B6AAH7 has been identified as a 14-3-3 ε isoform in *Cryptosporidium* (Brokx et al., 2011).

Apicomplexan species	Putative 14-3-3 proteins	Human isoforms						
		ε (MSFL) (*P62258*)	**ζ (MSFS) (*P63104*)**	σ (*P31947*)	η (*Q04917*)	ϑ (*P27348*)	γ (*P61981*)	β (*P31946*)
P. falciparum (str. 3D7)	*C0H4V6*	**60%**	**59%**	52%	56%	56%	56%	57%
	C0H5K0	**21%**	**22%**	21%	20%	23%	21%	20%
T. gondii (str. GT1)	*B9Q0N7*	**60%**	**60%**	55%	55%	56%	57%	58%
	B9PHG0	**44%**	**44%**	43%	44%	44%	45%	46%
	B9PHN5	**25%**	**21%**	24%	22%	21%	24%	21%
C. muris (str.RN66)	*B6AAH7*	**62%**[1]	**57%**	55%	55%	55%	55%	58%
	B6AI61	**23%**	**24%**	23%	25%	27%	24%	25%
	B6AFS7	**24%**	**23%**	21%	24%	23%	24%	24%
T. parva (str. Muguga)	*Q4N4N3*	**57%**	**58%**	53%	55%	55%	56%	58%
B. bovis (str.T2Bo)	*A7AUI2*	**55%**	**57%**	52%	54%	55%	54%	56%
N. caninum (str. Liverpool)	*F0VG50*	**60%**	**60%**	55%	55%	56%	57%	58%
	F0VJK0	**37%**	**38%**	39%	38%	40%	38%	39%
	F0VLI4	**18%**	**17%**	16%	12%	17%	14%	17%
	F0VJH0	**20%**	**22%**	22%	20%	20%	21%	23%

AIP (also termed FKBP37 or ARA9) is a 38 kDa peptidyl-prolyl cis/trans isomerase which has abilities to interact with Hsp70 and therefore mediate the binding between preproteins and the mitochondrial receptor Tom20 (Yano et al., 2003). A putative AIP homologue was identified only in *P. falciparum* with 19 % sequence identity with its human homologue, but exhibiting asimilar domain architecture with a N-terminal peptidylprolyl cis-trans isomerase domain (or FKBD domain) followed by three tetratricopeptide repeats (TPR) motifs **(Fig. 7.3)**. The putative *P. falciparum* AIP has been previously characterised as a 35 kDa FKBP family chaperone (referred as *Pf*PKBP35) with rotamase and protein folding activities (Kumar et al., 2005; Monaghan and Bell, 2005). It has been structurally demonstrated that TPR motifs of *Pf*PKBP35 can be associated with the C-terminal pentapeptide of the *P. falciparum* cytosolic Hsp90 (PlasmoDB accession number PF07_0029) and may also interact with the cytosolic *Pf*Hsp70 (Pf08_0054) which emphases a possible involvement of *Pf*PKB35 in the importation of precursors into mitochondria (Alag et al., 2009; Kumar et al., 2005).

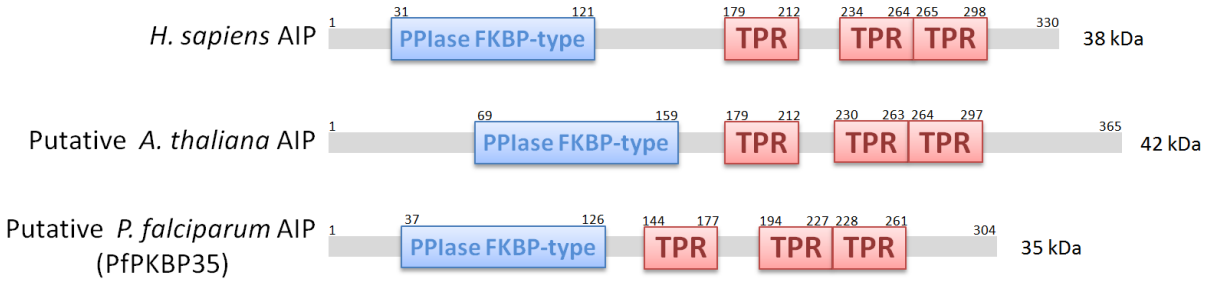

Figure 7.3. Schematic representation of domains contained in human AIP and putative homologues in plant and malaria parasite. The 42 kDa peptidyl-prolyl isomerase has been suggested to be a *Arabidopsis thaliana* homologue of AIP by displaying 27 % of sequence identities (45 % similarity) to the human AIP (Glaser and Whelan, 2007). Sequences used were AIP in *Homo sapiens* (Uniprot accession **#** O00170), a putative AIP in *Arabidopsis thaliana* (Q9LDC0) and *Plasmodium falciparum* PKBP35 (Q8I4V8). Tetratricopeptide repeat motifs indicated by red 'TPR' boxes were predicted with SMART (smart.embl.de).

The preprotein import can also be initiated through the presence of two ribosome-associated factors, both identified in apicomplexans: the nascent-associated polypeptide complex (NAC) and the ribosome-associated complex (RAC) (Beddoe and Lithgow, 2002; Gautschi et al., 2001; Wiedmann et al., 1994). NAC is a heterodimer protein while RAC is constituted by a DnaJ homologue and one of the cytosolic Hsp70s (Gautschi et al., 2002; Otto et al., 2005). Both complexes contact the ribosome near the tunnel exit and interact with the nascent polypeptide in order to control protein folding, preventing aggregation and degradation or initiating the importation to the mitochondrial compartment (Beddoe and Lithgow, 2002; Koplin et al., 2010; Wang et al., 1995). Further studies are necessary to clarify if a co-translational import exists in apicomplexa via mitochondrion-bound polysomes, as it has previously been observed in yeast (Marc et al., 2002).

7.4.2. Mitochondrial outer membrane

All imported proteins have to traffic through the Translocase of the Outer Membrane complex (TOM) **(Fig. 7.4)**. Although TOM complex can be composed of six to seven subunits in fungi, animal or plant species, only the subunit Tom40 is conserved among all apicomplexans. Tom40, a β-barrel protein, is the central pore for translocation of proteins into the intermembrane space (Maćašev et al., 2004). The subunit Tom22 is, on the other hand, a receptor present at the surface of the mitochondria which recognizes presequence proteins through the binding of the positively charged surface of the amphipathic α-helices formed by the N-terminal signal (Maćašev et al., 2004). Except for *T. gondii*, apicomplexan parasites conserve a functional but truncated form of Tom22 (referred as Tom22') whereby the N-terminal cytosolic receptor domain is absent.

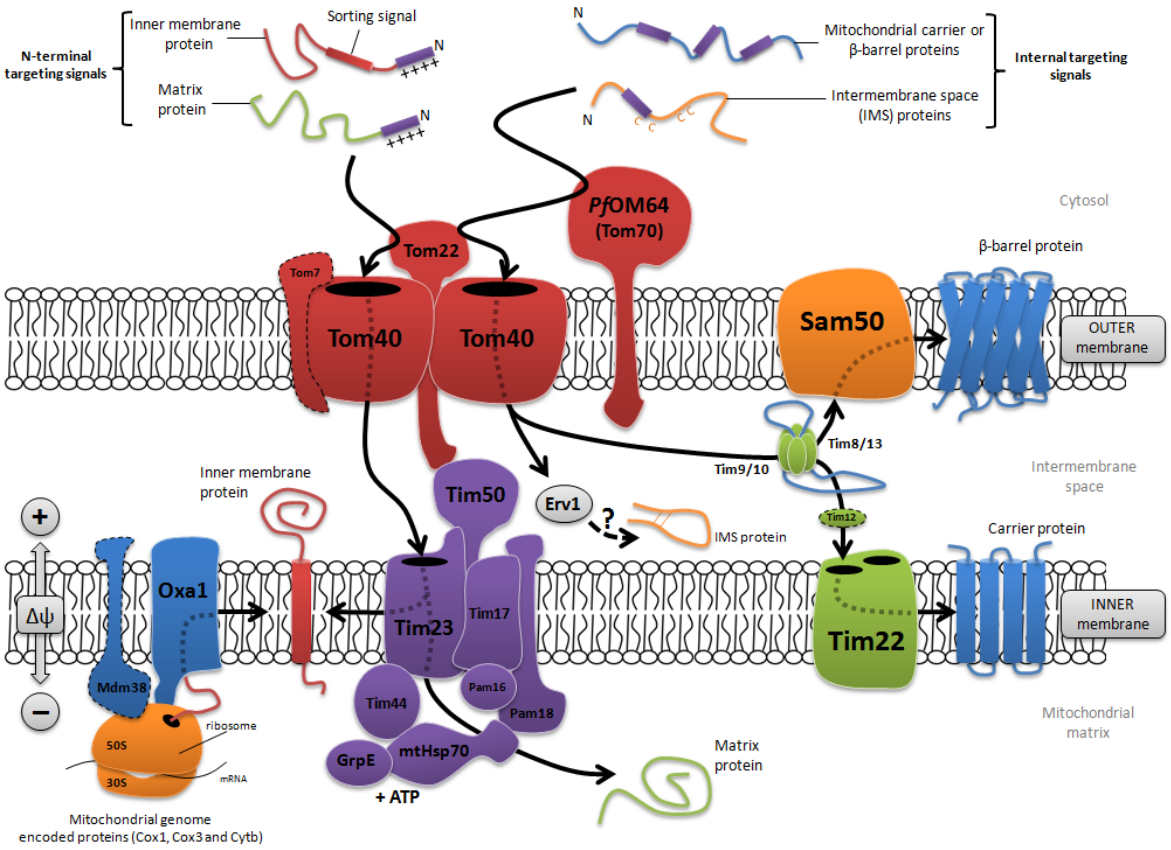

Figure 7.4. Schematic view of protein import routes in *Plasmodium falciparum*. Black dotted lines indicate the new putative components (Tom7, Tim12 and Mdm38).

The receptor Tom70 promotes the recruitment of proteins owning hydrophobic internal targeting peptides. However, no fungi or mammalian Tom70 homologues with significant sequence similarities could be identified in apicomplexan genomes. Although also absent in plants, an alternative Tom70 has been detected in *Arabidopsis thaliana,* this 64 kDa mitochondrial outer membrane protein (mtOM64) displays high sequence homology with a chloroplast protein import receptor from *Pisum sativum* (the translocase of the outer chloroplast envelope 64 - toc64) (Chew et al., 2004; Qbadou et al., 2006). Located on the mitochondrial surface, mtOM64 has proven to be rate-limiting for the import of a plant specific subunit of the mitochondrial ATP synthase, highlighting its possible role in the initial stages of the import process (Lister et al., 2007). Furthermore, recently it has been speculated that the gene PFL2015w (PlasmoDB accession number) could be a putative mitochondrial OM64 receptor in *Plasmodium falciparum* (Sheiner and Soldati-Favre, 2008). This 80 kDa protein possesses both mtOM64/toc64 features: three tetratricopeptide repeat (TPR) motifs on its C-terminal section and a short N-terminal transmembrane domain **(Fig. 7.5)** (Wu and Sha, 2006). The three predicted TPR motifs of the *P. falciparum* OM64 homologue (*Pf*OM64) are located at a similar position than that of mtOM64 or toc64 TPR domains, which are exposed on the cytosolic part of the protein and may mediate the

association of chaperones affiliated preproteins (Young et al., 2003). Furthermore, *Pf*OM64 has an N-terminal transmembrane domain essential to anchor the mitochondrial outer membrane. However, orthologues of the putative *Pf*OM64 have not been detected in other apicomplexan species. *T. gondii* seems to be devoid of both Tom70 and Tom20 receptors. Therefore, a minimised TOM complex without conventional receptors may be possible in apicomplexan parasites unless highly divergent homologues or apicomplexa-specific receptors have not been yet identified.

Figure 7.5. Schematic representation of domains contained in plant toc64, mtOM64 and putative homologue in *P. falciparum*. Sequences used were toc64 in *Pisum sativum* (Uniprot accession # Q9MUK5), mitochondrial OM64 in *Arabidopsis thaliana* (F4KCL7) and the putative *Plasmodium falciparum* OM64 (Q8I510). Transmembrane helix indicated by green 'TM' boxes were predicted by using THMMH algorithm (www.cbs.dtu.dk/services/TMHMM). Tetratricopeptide repeat motifs indicated by red 'TPR' boxes were predicted with SMART (smart.embl.de).

Tom5, Tom6 and Tom7 constitute a set of small proteins associated with Tom40 and stimulating the formation of the mature TOM complex. Tom7 regulates the oligomeric assembly of the TOM complex nevertheless it could not be identified in apicomplexan genomes due to low sequence conservation across species (Johnston et al., 2002). However, the amino acid motif $aGax_1Px_5G$ (with "a" for aromatic residues) was identified as a conserved pattern within Tom7 homologues and having an essential role in targeting the mitochondrial outer membrane (Allen et al., 2002; Johnston et al., 2002). Consequently, encoded proteins below the 10 kDa size range and displaying the Tom7 motif were searched in apicomplexa. An 8 kDa putative Tom7 gene was identified in the *P. falciparum* genome only, displaying the $aGax_1Px_5G$ pattern and a single transmembrane domain for anchoring the lipid bilayer **(Fig. 7.6)**. Tom7, together with Tom40 and Tom22, are the only three TOM components commonly found in earlier eukaryotes including protists (Dolezal et al., 2006) and may constitute the minimal functional translocon in malaria parasites. To date, no gene candidates for both Tom5 and Tom6 could be identified within the apicomplexan family which may lack all small Tom proteins or that may remain undetected

through conventional homology searching due to high divergence across species and absence of conserved motifs.

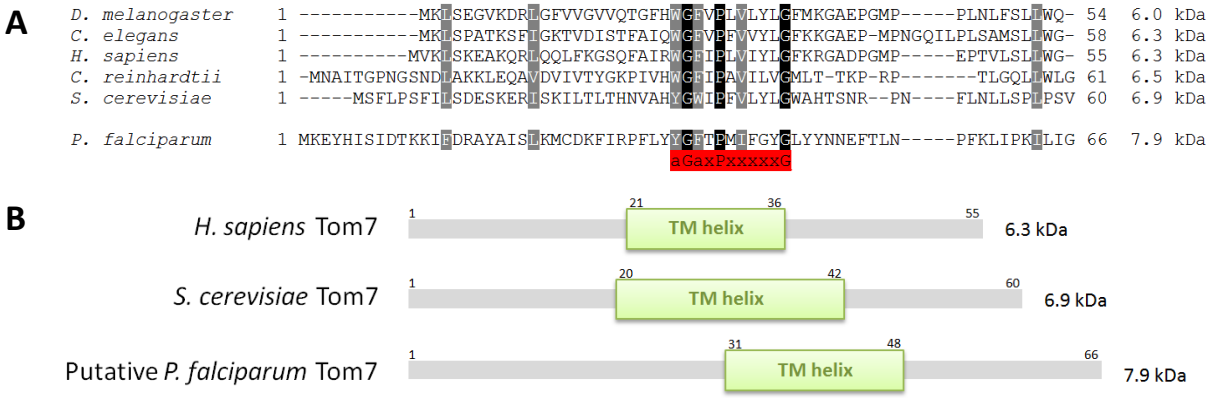

Figure 7.6. (A) Amino acid alignment of putative Tom7 in *Plasmodium* species along with Tom7 identified in other species. The sequences were aligned with ClustalW2 (www.ebi.ac.uk/Tools/msa/clustalw2). Residues are displayed with dark boxes for full conservation and grey boxes for strong similarities. In red is highlighted the Tom7 motif aGaxPxxxxxG conserved. **(B) Transmembrane helix are indicated by green 'TM helix' boxes were predicted using THMMH algorithm (www.cbs.dtu.dk/services/TMHMM).** The Tom7 sequences used were from *Homo sapiens* (Uniprot accession # 9P0U1), *Drosophila melanogaster* (Q7K036), *Saccharomyces cerevisiae* (P53507), *Chlamydomonas reinhardtii* (A8IG88), *Caenorhabditis elegans* (P34660) and the *Plasmodium falciparum* candidate **(**GeneDB accession # PF3D7_0823700).

The outer membrane contains two types of anchored proteins, α-helical proteins and β-barrel proteins, which use different ways of insertion. Along with the TOM complex, the additional Sorting and Assembly Machinery (SAM complex) are necessary for adequate import, folding and insertion into the outer membrane of β-barrel proteins such as porins or Tom40 (Kozjak et al., 2003; Wiedemann et al., 2003). In the yeast model, β-barrel proteins are translocated through the TOM complex and transferred to a four subunits-SAM complex via small intermembrane space chaperones Tim9-Tim10 or Tim8-Tim13 (Hoppins and Nargang, 2004; Wiedemann et al., 2004). Only the core component Sam50 was identified among apicomplexan species (Dolezal et al., 2006), whereas other subunits of the complex such as Sam35, Sam37 and Mdm10 seem absent. With only a single subunit conserved the insertion of α-helical via the SAM complex remains to be clarified in apicomplexa.

7.4.3. Mitochondrial intermembrane space

The mitochondrial intermembrane space (IMS) contains a variety of small proteins, less than 20 kDa, with characteristic cysteine-rich motifs Cx_3C, Cx_9C or Cx_2C (Gabriel et al., 2007). The four "Tiny TIMs" members (Tim 8, Tim9, Tim10 and Tim13) are ~10 kDa homologous proteins conserving the cysteine-rich motif $Cx_3Cx_{11\text{-}16}Cx_3C$ (where x is not a cysteine) and assembled in two types of hexamers: $Tim8_3$-$Tim10_3$ and $Tim9_3$-$Tim10_3$. Both hexameric chaperones are involved in

protein transfer of carrier and β-barrel proteins through the IMS previously released by the TOM complex and designated to the SAM and TIM22 complexes respectively (Curran et al., 2002; Hoppins and Nargang, 2004; Koehler et al., 1998b; Wiedemann et al., 2004). All Tiny TIMs members family have been previously identified in *P. falciparum* and *T. gondii* (Gentle et al., 2007; Sheiner and Soldati-Favre, 2008; van Dooren et al., 2006). A full set of Tiny Tims has also been identified in *N. caninum* but no Tim13 homologues could be found in *C. muris, T. parva* and *B. bovis* suggesting a unique functional small Tim complex. In accordance to these results, Tim9-Tim10 complex has proven to be essential and the main IMS chaperone in yeast whereas Tim8-Tim13 can be unnecessary in cell growth (Koehler et al., 1999).

Precursors of small intermembrane space proteins (IMS proteins) are translocated via the TOM complex in a reduced and unfolded conformation. In most of eukaryotes, the reducing and folding of IMS proteins through disulphide bond exchange are mediated by two components: the mitochondrial intermembrane space assembly protein Mia40 (Mitochondrial intermembrane space import and assembly protein 40) and the sulphydryl oxidase Erv1 (Essential for respiration and viability 1). In *P. falciparum*, a Erv1 homologue has been identified however, Mia40 seems to be lacking in the human malaria parasite (Senkevich et al., 2000). Although Erv1 orthologues were detected in other apicomplexans, no Mia40 homologues could be detected due to limitations in gene prediction or possibly due to these organisms using another model of cysteine-rich proteins folding. Inactivation of *A. thaliana* Mia40 does not affect the import and/or assembly of small Tim proteins into plant mitochondria while Erv1 plays an essential role (Carrie et al., 2010). Additionally, a Mia40-independent pathway has been suggested in *Trypanosoma* parasites where IMS proteins require only Erv1 for a disulphide bond exchange (Allen et al., 2008). This model can also be applied to apicomplexans **(Fig. 7.7).** Erv1 acts as a disulphide bonds carrier to the IMS proteins through the formation of a transient disulphide bond prior to its transfer. Erv1 oxidation is mediated by cytochrome *c* which generates the disulphide bond by transferring the electrons from Erv1 to O_2 via the cytochrome *c* oxidase (complex IV) of the respiratory chain (Allen et al., 2005). *Cryptosporidium* species lack the cytochrome *c* oxidase and it was then proposed that Erv1 could be oxidised through the low-affinity physiological oxidant O_2 that may be facilitated by an enzyme alternative oxidase (AOX) which promotes electron transfer to O_2 (Allen et al., 2008). To transfer several disulphide bonds, Erv1 shuttle between the protein precursor and the source of oxidation until the mature form of the IMS protein is reached.

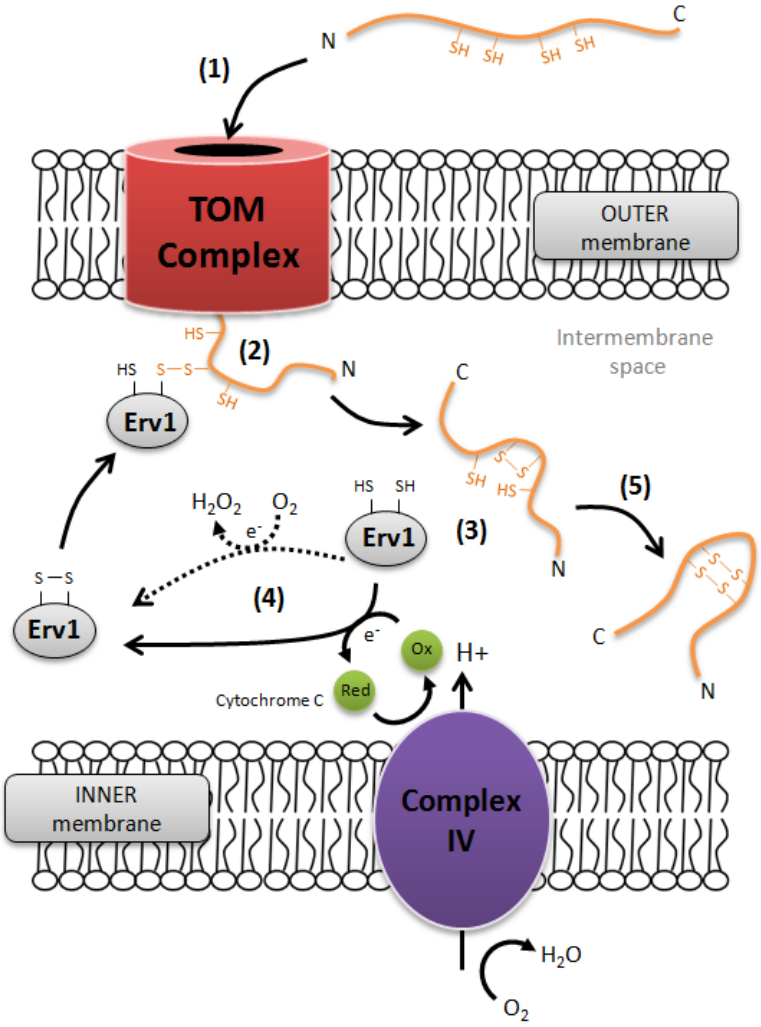

Figure 7.7. Mia40-independent oxidative folding of intermembrane space proteins in apicomplexan (adapted from Allen et al., 2008). (1) The IMS protein is translocated across the outer membrane via the TOM complex. (2) Erv1 binds the IMS protein forming a transient disulphide bond (S-S). (3) Erv1 becomes reduced by transferring the disulphide bond to the unfolded IMS protein. (4) Erv1 is oxidised though its interaction with cytochrome c. Electrons are transferred from reduced cytochrome c to O_2 via the cytochrome c oxidase (complex IV). An alternative pathway with the physiological oxidant O_2 and generating ROS (H_2O_2) have been hypothesised if the cytochrome c-dependent respiration is absent. (5) To transfer several disulphide bonds, the previous cycle is repeated with a shuttle of Erv1 between the IMS precursor and cytochrome c (or O_2) until the protein is entirely oxidized.

7.4.4. Mitochondrial inner membrane

The inner membrane is the host of three different translocase complexes: (i) the TIM23 complex which translocates inner membrane-sorted or matrix-targeted proteins with N-terminal presequences (coupled with the PAM machinery), (ii) the TIM22 complex inserting carrier proteins with internal targeting signals and (iii) Oxa1 that imports proteins synthesised in the mitochondrial matrix into the inner membrane **(Fig. 7.4)**.

Nearly all components of TIM23 complex and presequence translocase-associated motor (PAM) have clear homologues in apicomplexan species (van Dooren et al., 2006). Tim23, Tim50 and Tim17 form the core of the complex ($Tim23^{CORE}$) inserted in the inner membrane (Neupert and Herrmann, 2007). Furthermore, subunit Tim23 and its partner Tim17, form the translocation channel which transports α-helical presequence proteins across the inner membrane. The N-terminal section of the yeast Tim23 has been demonstrated to bind the outer membrane to improve the protein import efficiency into the mitochondria (Donzeau et al., 2000). However, Tim23 in apicomplexans may lack the outer membrane anchoring function due to a deletion of the first 28 to 52 residues in comparison with its yeast homologue. Moreover, the leucine zipper motif $^{61}Lx_6Lx_6L^{83}$, a motif identified only in yeast which facilitates a membrane potential-dependent Tim23 dimer formation, is not conserved in apicomplexan species (Bauer et al., 1996). Tim50 plays a triple role by (i) acting as a receptor for the precursors destined to the inner membrane or the matrix, (ii) interacting with the trans domain of Tom22 to enhance the protein transfer between TOM and TIM23 complexes and (iii) regulating the channel opening and closing to avoid ions leaking through the inner membrane and reduction of the membrane potential $\Delta\Psi_m$ (Maćašev et al., 2004; Meinecke et al., 2006; Yamamoto et al., 2002). Only the component Tim21 is still not identified in apicomplexans, but its role of preproteins sorting switch to the matrix or the inner membrane, have been demonstrated to be non-essential (Mokranjac et al., 2005; Wiedemann et al., 2007).

When preproteins are destined to the mitochondrial matrix, a PAM motor is coupled to the TIM23 complex. Five essential components of the PAM machinery (mtHsp70, Pam18, Pam16, Tim44 and GrpE) have been annotated in *P. falciparum* genome (Brehelin et al., 2010; Slapeta and Keithly, 2004; van Dooren et al., 2006). Their orthologues in other apicomplexans were easily identified and revealed a complete PAM motor in every species. Tim44 interacts with the emerging preprotein from the Tim23 channel and recruits the mitochondrial Hsp70 (mtHsp70) which drives the polypeptide chain into the matrix, a mechanism which requiries ATP hydrolysis (Kang et al., 1990; Liu et al., 2003; Schneider et al., 1994b). The nucleotide exchange factor GrpE stimulates the release of ADP from mtHsp70 to promote a new cycle of ATP binding and continue the presequence protein translocation (Neupert and Herrmann, 2007; Schneider et al., 1996). Furthermore, two membrane-bound co-chaperones Pam18 and Pam16 regulate the activity of mtHsp70. As a J-protein family member, Pam18 stimulates the ATP hydrolysis from its partner mtHsp70 (Mokranjac et al., 2003; Truscott et al., 2003). Additionally, Pam16, a J-like protein, acts as an antagonist by binding Pam18 and regulating its stimulating function (Kozany et al., 2004; Li et al., 2004). The Pam17 component is involved in the association between TIM23 complex and

PAM motor (Hutu et al., 2008; van der Laan et al., 2005). Only identified in yeast and *C. elegans*, Pam17 could not be detected in apicomplexan species.

The TIM22 complex inserts carrier proteins with non-cleavable mitochondrial targeting signals into the inner membrane. The carrier import pathway in apicomplexan differs from other known models as it has only two crucial components Tim22 and Tim12 (Gentle et al., 2007; van Dooren et al., 2006). The absence of yeast-specific components Tim18 and Tim54 suggests a minimised complex, with the twin-pore translocase Tim22 as the central element, releasing precursors into the lipid membrane in a functional form (Koehler et al., 2000; Rehling et al., 2003; Sirrenberg et al., 1996). All apicomplexans seem to have acquired a supplementary Tim12-type protein due to a recent gene duplication event from a Tiny TIMs member (Gentle et al., 2007). Tim12 has a crucial role, as it establishes a membrane bound complex with Tim9-Tim10 at the surface of Tim22 which guides carrier proteins to the pore (Koehler et al., 1998a; Koehler et al., 1999).

Oxa1 (also termed YidC in bacteria) facilitates the insertion into the inner membrane of mitochondrially coded membrane proteins and binds mitochondrial ribosomes to facilitate co-translational protein translocation (Hell et al., 2001; Kohler et al., 2009). Although *Trypanosoma* and *Leishmania* species display two Oxa1 homologues, only one has been detected in apicomplexan parasites which can mediate the insertion of the three mitochondrial encoded proteins (Cox1, Cox3 and Cytb) (Schneider et al., 2008; van Dooren et al., 2006). Interestingly, C*ryptosporidium* lost Oxa1 most likely due to the lack of mitochondrial genome (Henriquez et al., 2005). A Letm1-like protein, conserved across all apicomplexans, displays similarities with Letm1 in human or yeast (termed Mdm38) **(Fig. 7.8)**. Mdm38/Letm1 is a mitochondrial inner membrane receptor essential for respiratory chain biogenesis. Hereby Mdm38/Letm1 interacts with a large ribosomal subunit and therefore supporting the translation of mitochondrial proteins destined to the inner membrane (Lupo et al., 2011; Piao et al., 2009). A similar role can be speculated for the apicomplexan Letm1 through the promotion of the ribosomes recruitment near Oxa1 and supporting the translation of three mitochondrial-encoded ETC subunits. The yeast-specific component Mba1 which is known to cooperate with Oxa1 through favouring protein translation, doesn't seem to have homologues in apicomplexa (Ott et al., 2006).

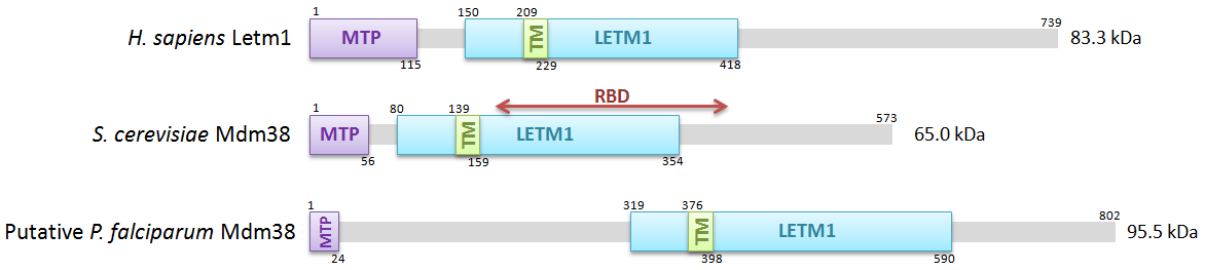

Figure 7.8. Schematic representation of domains contained in human Letm1, yeast Mdm38 and putative homologue in *P. falciparum*. Sequences used were LETM1 in *Homo sapiens* (Uniprot accession # O95202), Mdm38 in *Saccharomyces cerevisiae* (Q08179) and the putative *Plasmodium falciparum* Mdm38 (Q8I1R5). Transmembrane helixes indicated in green 'TM' boxes were predicted by using THMMH algorithm (www.cbs.dtu.dk/services/TMHMM). LETM1 domains indicated by blue boxes were predicted with InterPro (www.ebi.ac.uk/Tools/pfa/iprscan*). P. falciparum* mitochondrial transit peptide were predicted with PlasMit (gecco.org.chemie.uni-frankfurt.de/plasmit).The 'RBD' arrow indicates an essential ribosome binding site in yeast Mdm38 (Lupo et al., 2011).

7.5. Mitochondrial processing and protein stability

In mitochondria, a proteolytic machinery participates in the processing and stability of the imported preproteins. Several proteases have been identified in apicomplexan species which can be categorised according to their location in either the matrix or inner membrane **(Table 7.3)**.

Table 7.3. Components of the mitochondrial processing and stability machinery in apicomplexan species and comparison with fungi, mammalian and plant representatives. '•' indicates putative candidates. '▪' indicates components demonstrated essential for yeast viability. Uniprot accession number of apicomplexan components are available in **Appendix 4**.

	Protein	Function	*Pf*	*Tg*	*Cm*	*Tp*	*Bb*	*Nc*	*Sc*	*Hs*	*At*
Matrix processing	MPP (α subunit)	Cleaves N-terminal presequences of matrix and inner membrane proteins							▪		
	MPP (β subunit)								▪		
	MIP	Cleaves octapeptide in MPP downstream	•	•	•	•	•	•			
	Icp55	Cleaves a single amino acid in MPP downstream									
	FCN (PreP/Cym1)	Degrades presequence peptides									
	mtHsp60	Assist folding of matrix proteins									
	Hsp10										
Inner membrane processing	m-AAA	Cleaves matrix peptides of matrix proteins	•	•	•	•	•	•			
	i-AAA	Cleaves matrix peptides of inner membrane proteins	•	•		•	•	•			
	Atp23										
	Rom6	Cleaves transmembrane domain peptides				*Ta*					
	Imp1		•	•	•	•	•	•			
	Imp2										

Ta: *Theileria annulata*

7.5.1. Processing and stability of matrix preproteins

After their transfer into the matrix, most of the precursor proteins undergo a proteolytic cleavage of their N-terminal presequences by a mitochondrial processing peptidase (MPP) (reviewed in Gakh et al., 2002). Composed of two subunits (α-MPP and β-MPP), the soluble heterodimer is highly conserved across species including apicomplexans **(Table 7.3)** (van Dooren et al., 2006). The apicomplexan MPP contains an inverted zinc-binding motif ($Hx_2EHx_{71\text{-}77}E$) located on its β subunit which constitutes the catalytic binding site (Gakh et al., 2002; Taylor et al., 2001). The cleavage site near an arginine has been analysed in several species and categorised in four classes: R-none motif (X↓X-(S/X)), R-2 motif (R-X↓X), R-3 motif (R-X-(Y/F/L)↓(S/A/X)) and R-10 motif (R-X↓(F/L/I)-X2-(T/S/G)-X4↓X) (Gavel and von Heijne, 1990). Demonstrated to be essential for yeast viability, MPP cleaves matrix proteins entirely translocated and also preproteins in transit to the inner membrane **(Fig. 7.9)** (Gakh et al., 2002).

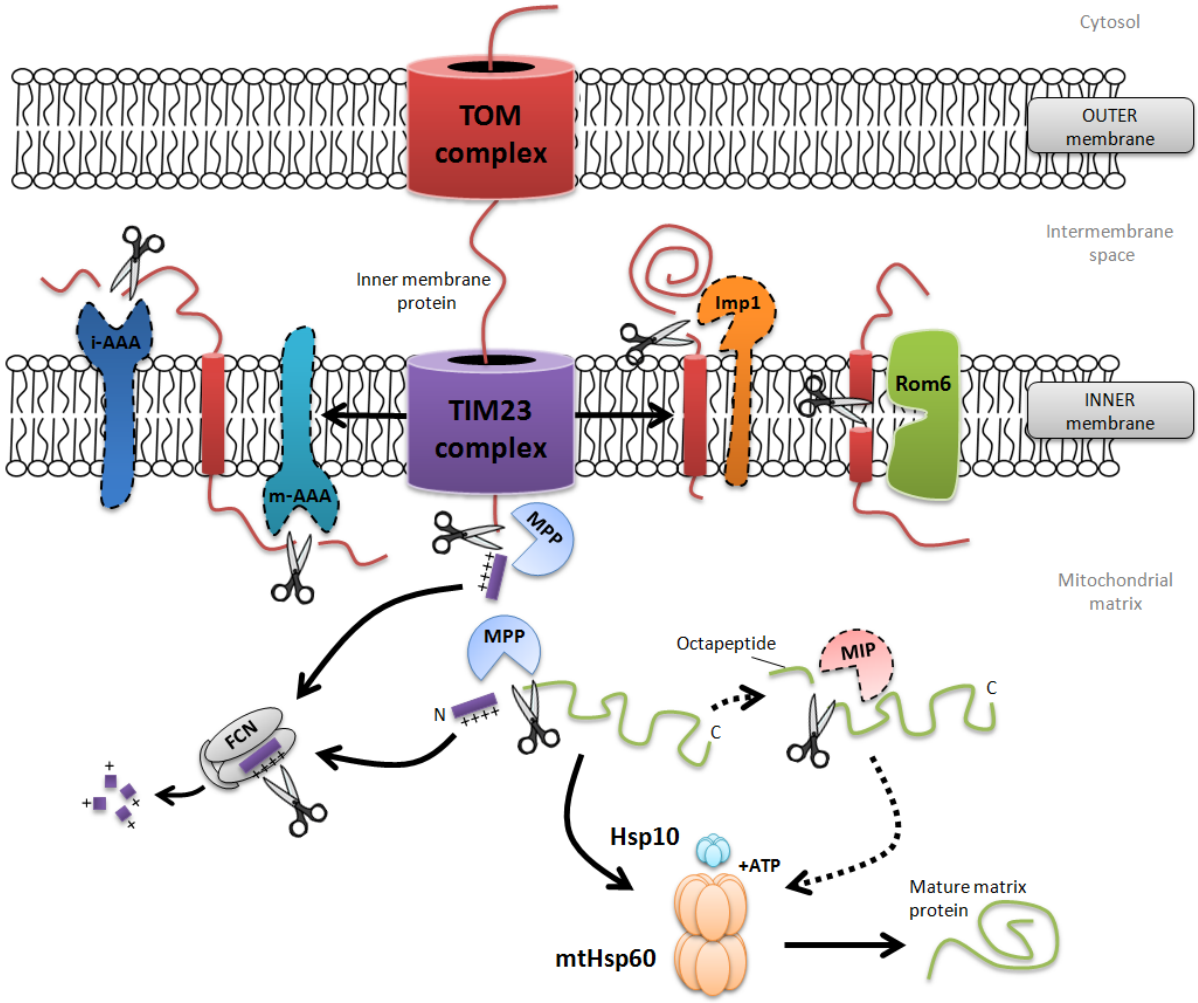

Figure 7.9. Schematic view of processing for inner membrane and matrix proteins in *Plasmodium falciparum*. Black dotted lines indicate new putative components (MIP, Imp1, i-AAA and m-AAA).

Following the MPP cleavage, two matrix proteases - the mitochondrial intermediate peptidase (MIP) and the yeast-specific Icp55 - have been shown to perform a second proteolytic event. MIP is a soluble monomeric metalloprotease known to cleave an octapeptide from the N-terminal of proteins previously processed by MPP (reviewed in Gakh et al., 2002). A yeast study (Chew et al., 1996) demonstrated that a deletion of MIP is not lethal but may cause a respiratory deficiency. Each apicomplexan genome contains a M3 family peptidase with the conserved zinc-binding motif HEx_2H essential to cleave N-termini. This cleavage is mainly performed at a R-3 motif site (Isaya et al., 1994). This protease has been shown to be the most significant MIP homologue in apicomplexa, according to the HMM searching performed in this study using human or yeast MIP as templates. Additionally, transit peptide analysis of the putative *P. falciparum* MIP predicted its localisation in the mitochondria. Further localisation studies of the MIP homologue in apicomplexans could confirm its involvement in mitochondrial processing. Recently, the novel protease Icp55, which cleaves a single amino acid from an intermediate generated by MPP, has been identified in yeast but seems absent in mammalian plant or apicomplexan genomes (Naamati et al., 2009; Vogtle et al., 2009).

Once cleaved, mitochondrial presequences and free peptides may cause mitochondrial damages by penetrating the lipid bilayer and subsequently reducing membrane potential and uncouple respiration (Lu and Beavis, 1997; Nicolay et al., 1994; Roise et al., 1986). Thus, both peptide sequences are degraded within the mitochondria by the matrix protease Cym1 in yeast (known as PreP in human and plants) (Alikhani et al., 2011; Bhushan et al., 2003; Falkevall et al., 2006; Kambacheld et al., 2005; Mzhavia et al., 1999; Stahl et al., 2002). No evident homologues of PreP/Cym1 aminopeptidases were identified in apicomplexan species. However, the *P. falciparum* falcilysin (FCN) has been speculated to be a possible substitute. FCN is a zinc metalloprotease member of the M16 family mainly involve in haemoglobin removal into the food vacuole through the degradation of 10-20 amino acid globin peptides (Eggleson et al., 1999; Goldberg, 2005). However, its localisation in mitochondria as well as in the apicoplast of the malaria parasite suggests an additional function, such as cleavage of targeting peptides in the *P. falciparum* mitochondrion (Ponpuak et al., 2007). It is important to mention that except for *C. muris*, all other apicomplexan parasites possess a FCN orthologue.

To reach their mature form, the folding process of matrix proteins can be spontaneous or assisted by two chaperones Hsp10 and Hsp60, early identified in human cells and rat liver (Hartman et al., 1992; Jindal et al., 1989). These chaperones are highly conserved across species and one Hsp10 and two Hsp60 homologues were found in apicomplexans. Their characterisation in *P. falciparum* revealed that only one Hsp60 is a mitochondrial resident (mtHsp60), the other

being affected to the apicoplast (apHsp60) (Sato et al., 2003; Sato and Wilson, 2004). *Pf*Hsp10 is only located in the mitochondrion, although its mammalian homologue can be found in other cell compartments (Sadacharan et al., 2001; Sato and Wilson, 2005). In mammals, Hsp60 forms a tetradecamer complex consisting of two ring barrels of seven subunits which form two defined cavities. If capped by a Hsp10 heptamer and associated with ATP, each cavity becomes a suitable environment for protein folding (Ranson et al., 1998; Rye et al., 1997).

7.5.2. Inner membrane processing machinery

AAA proteases (ATPases Associated with diverse cellular Activities, also termed Ftsh peptidases) are ATP-dependent metalloproteases anchored to the inner membrane participating in assembly, proteolytic maturation and degradation of misfolded or unassembled mitochondrial membrane proteins (Langer, 2000). Found in fungi, mammals or plants, m-AAA and i-AAA are two oligomeric complexes exposing their catalytic centre in the matrix or the intermembrane space respectively. The m-AAA protease is a hetero- or homo-hexamer constituted of one or two different subunits (Yta12 and Yta10 in *S. cerevisiae*, Ftsh10 and Ftsh3 in *A. thaliana*) (Arlt et al., 1996; Piechota et al., 2010). Only one component (Yme1) forms the i-AAA complex in yeast while two homologues have been found to constitute two independent i-AAA in plants (Ftsh4 and Ftsh11) (Leonhard et al., 1996; Urantowka et al., 2005). In *P. falciparum*, three metalloproteases (PlasmoDB accession number PF11_0203, PFL1925w and PF14_0616), belonging to the M41 family peptidase, have been identified and their domain analysis revealed certain m-AAA/i-AAA features: one or two transmembrane regions in their N-terminal followed by two domains, a P-loop ATPase and a peptidase M41 (with a zinc-binding motif HEx_2H in its active centre) **(Fig. 7.10 and 7.11)** (Gangwar et al., 2009). The *P. falciparum* AAA isoform PF11_0203 displays a high sequence similarity with Yta10/Ftsh3 and Yta12/Ftsh10 indicating its probable involvement in an m-AAA complex. Two other malaria parasite isoforms show higher identities with subunits of the i-AAA complex in yeast (Yme1) or plants (Ftsh4/Ftsh11). Identification of apicomplexan orthologues showed that each parasite has two subunits to compose i-AAA complexes and only one to form a homo-oligomeric m-AAA structure, except for *Cryptosporidium* species with no putative i-AAA components found.

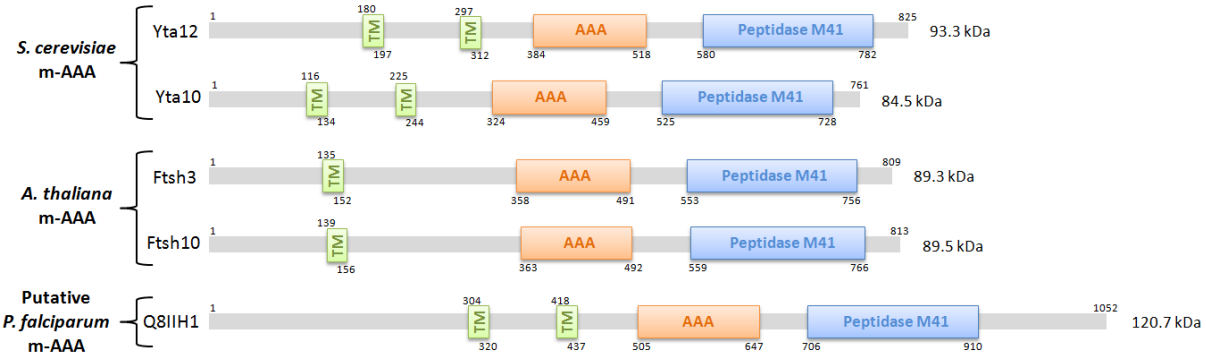

Figure 7.10. Schematic representation of domains contained in yeast, plant and putative *P. falciparum* m-AAA. Sequences used were m-AAA in *Saccharomyces cerevisiae* (Uniprot accession # P40341 for Yta12; P39925 for Yta10), in *Arabidopsis thaliana* **(**Q84WU8 for Ftsh3; Q8VZI8 for Ftsh10) and putative *Plasmodium falciparum* m-AAA (Q8IIH1 and Q8I526). Transmembrane helix, AAA domain and Peptidase M41 indicated in green 'TM' boxes, orange 'AAA' boxes and blue 'Peptidase M41' respectively as predicted by Pfam (pfam.sanger.ac.uk).

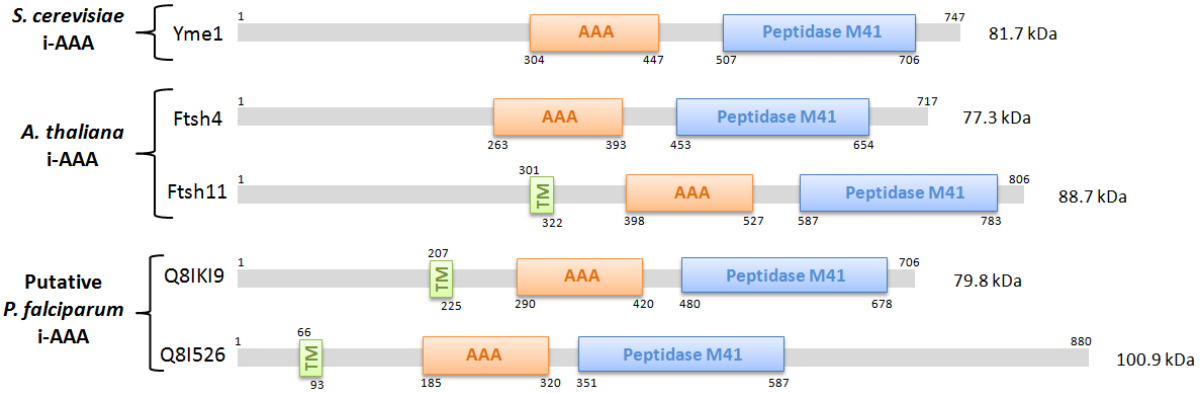

Figure 7.11. Schematic representation of domains contained in yeast, plant and putative *P. falciparum* i-AAA. Sequences used were i-AAA in *Saccharomyces cerevisiae* (Uniprot accession **#** P32795 for Yme1), in *Arabidopsis thaliana* (O80983 for Ftsh4; Q9FGM0 for Ftsh11) and the putative *Plasmodium falciparum* m-AAA (Q8IKI9). Transmembrane helix, AAA domain and Peptidase M41 indicated by green 'TM' boxes, orange 'AAA' boxes and blue 'Peptidase M41' respectively were predicted by Pfam (pfam.sanger.ac.uk).

Rhomboid-like proteins are a family of integral membrane serine proteases which assist protein assembly by cleaving transmembrane domains of inserted proteins. First characterised in the Golgi apparatus of *Drosophila melanogaster* (Urban et al., 2001), it has been established that rhomboids are ubiquitous and were classified according to their cell compartment localisation (Koonin et al., 2003). The only rhomboid located in mitochondria (Pcp1 in yeast) in all apicomplexan parasites has been named as Rom6 (Dowse and Soldati, 2005; M. Santos et al., 2012). Surprisingly, no Rom6 homologue has been found in *Theileria parva* despite its presence in *Theileria annulata*. Rom6 contains a putative catalytic dyad within their transmembrane domains indicating a proteolytic activity into the lipid bilayer (Lemberg et al., 2005). Located in the inner membrane, the yeast Pcp1 has been demonstrated to mediate a second cleavage of the

cytochrome c peroxidase Ccp1 and the dynamin-like GTPase Mgm1 while its mammalian homologue (PARL) is involved in processing of the mitochondrial protease Omi/HhtrA2 and kinase PINK1. (Esser et al., 2002; Herlan et al., 2003; Whitworth et al., 2008).

The mitochondrial inner membrane protease (IMP) is an hetero-oligomer composed of two catalytic subunits Imp1 and Imp2 (Schneider et al., 1994a). IMP cleaves the hydrophobic sorting signal from proteins which expose an active site in the IMS (Nunnari et al., 1993). Five mitochondrial proteins (Cox2, Cyb2, Mcr1, DIABLO and Gut2) are matured by Imp1 and only one by Imp2 (Cyc1) (Burri et al., 2005; Esser et al., 2004; Gasser et al., 1982; Haucke et al., 1997; Nunnari et al., 1993; Pratje et al., 1983). Both Imp subunits have a peptidase S26 domain and are classified in the type-I signal peptidase family of proteases which includes the bacterial signal peptidase I or the chloroplastic thylakoid processing peptidase (Dalbey, 1991). According to the bioinformatic search presented in this study, only one Imp1 homologue seems encoded in each apicomplexan genome. Furthermore, evolutionary analysis reveals that eukaryotic IMPs appear to be the nearest neighbour to the *P. falciparum* candidate (Wu et al., 2003). The presence of a single IMP subunit is not unusual, for example, Imp2 is the only component identified in the other protist *Trypanosoma* (Schneider et al., 2008).

Atp23 is a metalloprotease localized in the IMS which plays a unique role of processing and assisting the assembly of the subunit *a* (atp6) of the mitochondrial ATPase (Michon et al., 1988; Zeng et al., 2007). To date, Atp23 has been identified in fungi, mammals and/or plants but remains unknown in protists including apicomplexa. Atp6 is an essential subunit of the mitochondrial ATP synthase Fo sector but it is still undetected in apicomplexan species (Balabaskaran Nina et al., 2011).

7.6. Conclusion

As shown by the mode of action of atovaquone, the *P. falciparum* mitochondrion is a validated drug target as the mitochondrial protein import and processing machineries are expected to be indispensable for parasite survival. Throughout this chapter, an extensive evaluation of the current knowledge on the mitochondrial importation and processing in *P. falciparum* has been described. To date, studies on mitochondrial protein import in apicomplexa has been rather limited to bioinformatic analysis (Sheiner and Soldati-Favre, 2008; van Dooren et al., 2006). Comparative genomics have therefore given crucial insights into the importation and processing mechanisms in apicomplexan mitochondria as availability of experimental studies are scarce.

Although the mitochondrial protein import and processing is expected to be conserved among eukaryotes, the composition of those pathways is relatively heterogeneous between species (Eckers et al., 2012; Hewitt et al., 2011). In line with this, apicomplexan mitochondria display reduced machineries due to the lack of several components such as Tom20, Tom5, Tom6, Sam35, Mia40, Tim18, Tim54, etc. Thus, *several* major questions remain to be clarified, such as; how nuclear-encoded mitochondrial proteins are recognized without any TOM receptors in *T. gondii*? How the folding of IMS proteins can be functional without the essential component Mia40? How β-barrel proteins are recognized and incorporated into the outer membrane in the absence of Sam35? And how proteins can be embedded in the innner membrane without the receptor (Tim18) and assisting component (Tim54) of TIM22?

Future research studies should be directed towards finding missing components using novel bioinformatic algorithms as well as on the experimental study of the functionality of these restricted machineries. Subcellular localisation of components, *in vivo* protein import kinetics or the determination of essential genes by knockout analyses will aid to understand how apicomplexan parasites have adapted and minimized import and processing systems to perform an equivalent role to other more extensive pathways in mitochondria.

Chapter 8

Concluding remarks and perspectives

This chapter presents the main findings of this thesis and their contribution to our understanding of processes of the *Plasmodium* electron transport chain, the mode of action of endoperoxide compounds and parasite resistance to atovaquone. Limitations of the studies are also presented and potential future research directions are explored.

8.1. The *Plasmodium* complex II, a dehydrogenase which remains to be elucidated

In Chapters 3, the characterization of complex II components from *P. falciparum* was attempted towards understanding the observed catalytic properties measured in Chapter 4. This enzyme remains the only dehydrogenase of the electron transport chain which is neither clearly annotated nor well defined. Although the complex II has been established as a succinate:ubiquinol oxidoreductase (SQR) by previous studies, results in this thesis and recent new findings (Tanaka et al., 2012) argue that the enzyme could instead be a quinol:fumarate oxidoreductase (QFR). Indeed, the absence of SQR activity was demonstrated whereas a clear QFR activity inhibitable by malonate, a well known complex II inhibitor, was detected. Additionally, whereas most bacterial QFRs can use the low-potential menaquinone as an electron donor (Miyadera et al., 2003), the *Plasmodium* QFR has the unusual feature to have a single substrate with ubiquinone. This new insight into complex II activity is mainly due to a new type of enzymatic assay used. A direct measurement of dehydrogenase activity has been favoured instead of using linked assays which can be interfered with by nonspecific activities of competing enzymes able to reduce DCPIP or cytochrome *c*. However, direct measurement of quinone reduction may have a limit of detection when using free-cell parasite extract, which is rich in hemozoin, instead of clear mitochondrial enrichment. The possibility that dehydrogenase activities obtained could be underestimated should not be exclude and that SQR activity or menaquinone consumption could be below that limit of detection. Thus, the QFR identified may be reversible as observed in *Escherichia coli* or *Wolinella succinogenes*. Further work is required to examine the physiological role of this enzyme in the *Plasmodium* respiratory chain. It is crucial to understand why the *Plasmodium* complex II seems to favour fumarate respiration. The *Plasmodium* QFR could be part of an alternative metabolic pathway which remains yet to be determined.

With a bioinformatic approach based on specific fingerprints, gene candidates were identified for subunits SdhC and SdhD, and ATP synthase subunits *a* and *b*. These putative candidates present all structural properties and motif patterns required to achieve particular subunit functions. However, gene candidates obtained in this study are different to those proposed by Mogi *et al.* who used a similar *in silico* method (Mogi and Kita, 2009). The type of fingerprints, their cutoffs and the motif patterns chosen explain why this approach found different candidate genes. In light of this divergence, a proteomic validation is essential to confirm those bioinformatic predictions. Although the development of a complex II antibody has been successful, the identification of both anchor subunits from *P. falciparum* extract failed despite using gradient or non-gradient 2D BNE-SDS-Page gels. By comparison, with a mitochondrial bovine 2D pattern, it could be speculated that complex II in malaria parasites has a similar size of approximately 130 kDa, confirming the presence of both membrane anchor subunits. While 2D BNE/SDS-Page followed by mass spectrometry enabled the complex II characterization in several species, this approach revealed itself as extremely complex with malaria parasites. The low-level expression of complex II in blood stages and the difficulties to prepare a clean extract of isolated mitochondria were both important limitations for the proteomic method. In future, subunit identification might be achieved by an optimization strategy such as an improvement of mitochondrial extraction to obtain a higher yield and purity and/or to work with sexual stage parasites where expression of ETC enzymes may be more important than in blood stages. The capture of the complex II by immunoprecipitation and identification of its subunits by mass spectrometry will be the best alternative proteomic method when a specific antibody able to bind the *Plasmodium* enzyme in native conditions is available.

8.2. A conventional ATP synthase but a limited oxidative phosphorylation?

A recent study confirmed that the *Plasmodium* ATP synthase should be conventionally assembled as a large dimeric complex (Balabaskaran Nina et al., 2011). As previously mentioned, potential gene candidates for the missing ATP synthase subunits *a* and *b* were identified. However, specific anti-ATPα antibody could not be generated and thus attempt to validate the bioinformatic predictions via the proteomic approach. Thereby, many questions regarding the F_0 section remain: characterization of subunits *a* and *b*, number of *c*-subunits composing the rotational ring, presence of additional subunits (e.g. subunits *d* or F6)?

Oxidative phosphorylation is likely essential for parasite survival and relies on the electrochemical gradient. As mentioned in Chapter 4, only complex III and IV pump protons across the mitochondrial inner membrane to generate the membrane potential. Under conditions of

active ATP synthesis, the $H^+/2\ e^-$ ratio is 2 and 4 for complex III and IV respectively. The lack of conventional complex I results in a loss of 3 protons translocated per NADH oxidised (2 e-) (Wikstrom and Hummer, 2012). The protonmotive complex I is a large and complex enzyme whose synthesis requires considerable cellular resources and is also a source of cell-damaging ROS. It can be speculated that the parasite is better off without it if its energetic demands can be met in other ways (e.g. the glycolysis pathway).

However, the replacement of complex I by non-protonmotive *Pf*NDH2 has two possible consequences for *Plasmodium* oxidative phosphorylation. On one hand, the parasite ETC has to "work harder" to pump protons and generate an electrochemical gradient comparable to those observed in mammalian mitochondria possessing complex I. In that case, the respiratory chain tries to maximise the rate of ATP production. On the other hand, the protonmotive force may be lower in *Plasmodium* which has consequences for ATP synthesis. The difference in proton potential needed to maintain the ATP/ADP ratio required for parasite life is dependent on the number of protons translocated for each synthesized ATP molecule (termed H^+/ATP ratio) (Steigmiller et al., 2008). A straightforward interpretation of rotational ATP synthesis predicts that the H^+/ATP ratio coincides with the ratio of proton-binding subunits *c* to the three catalytic ADP-binding β-subunits, implying that for mammalian ATP synthases (with 10 subunits *c*) an H^+/ATP ratio of 3.3 is expected. If the protonmotive force is lower in *Plasmodium* parasites then the H^+/ATP ratio should be higher and the ATPase might be expected to have more *c*-subunits. Having a low electrochemical proton potential, thermoalkaliphilic bacteria present a large oligomeric *c* ring and thus a high stoichiometry of protons per ATP synthesized (Meier et al., 2007). The phosphate/oxygen ratio (also called the P/O ratio), which refers to the amount of ATP produced from two electrons donated by reduction of an oxygen atom, is dependent on the amount of H^+ pumped across the inner membrane and returned inward through the ATP synthase. Because the parasite produces plenty of ATP via the glycolysis pathway during the erythrocytic stage and does not need an optimal respiratory chain with respect to ATP synthesis, this P/O ratio could also be lower in *Plasmodium.* A limited rate of oxidative phosphorylation could not make significant contributions to the cytosolic energetic demands but could provide sufficient ATP for the local energy requirements of the mitochondrion.

8.3. ETC dehydrogenases: their contribution to the membrane potential

Although expression of dehydrogenases remains low in asexual stages, their basal activities are essential to maintain the electrochemical gradient across the inner membrane of the mitochondria. Data obtained suggests that *Pf*NDH2 is the main electron provider to the bc_1

complex whilst other dehydrogenases (i.e. DHODH, MQO and G3PDH) make minimal contributions in *in vitro* conditions. A similar experiment with cell-free extract from *P. berghei* parasites will confirm the situation *in vivo*. In absence of *Pf*NDH2 or complex II, recent studies showed that the electrochemical gradient can be maintained by the contribution of the others (Boysen and Matuschewski, 2011; Hino et al., 2012).

8.4. Possible strategies to inhibit the *Plasmodium* ETC

The development of atovaquone as an antimalarial drug validated the malaria parasite's mitochondrial electron transport chain (ETC) as an exploitable drug target. However, with the emergence of atovaquone resistance there is an urgent need for new antimalarial drugs with novel mechanisms of action. The differences between host and parasite mitochondria hold promising targets for development of malaria chemotherapy. Because the cytochrome bc_1 complex revealed itself as an excellent target, the development of a novel generation of quinolone inhibitors targeting the Q_o site remains a realistic strategy **(Fig. 8.1, strategy A)**. Thus, quinolone esters or acridinediones are new types of selective and potent inhibitors of the mitochondrial bc_1 complex (Biagini et al., 2008; Cowley et al., 2012). The generation of inhibitors that are active against two key enzymes in the respiratory pathway - *Pf*NDH2 and bc_1 complex - is a recently developed multi-target approach (Biagini et al., 2012) **(Fig. 8.1, strategy B)**. As mentioned previously, *Pf*NDH2 may be considerate as the main drug target through which to block electron transfer upstream of bc_1. This type of pharmacology should be an advantage both in potency across a wide range of malaria parasite strains and in protection against the rapid evolution of resistance. Specific inhibitors for both enzymes have been controlled by manipulation of the privileged quinolone core at the 2 or 3 position and displayed nanomolar activity against atovaquone-resistant *P. falciparum* parasites.

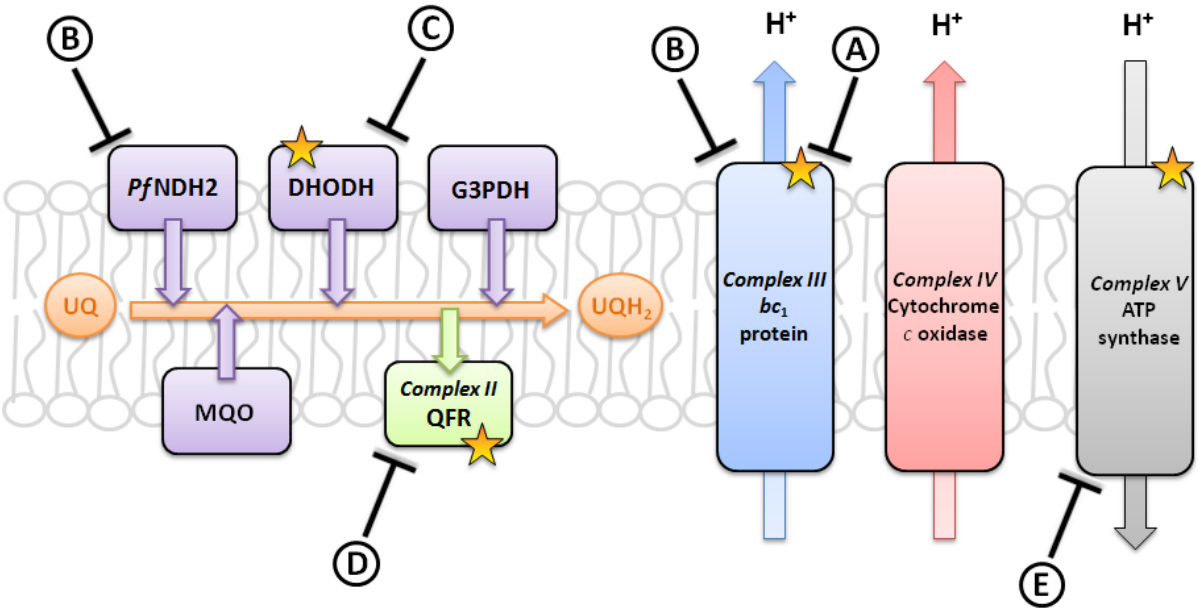

Figure 8.1. Chemotherapeutic strategies targeting the *Plasmodium* electron transport chain. The different enzymes targeted are indicated from strategy A to E. Yellow stars indicate enzymes which have been demonstrated to be essential for parasite development.

It is believed that in asexual parasites, one of the essential functions of the mitochondrion is to provide orotate for the biosynthesis of pyrimidine through the activity of dihydroorotate dehydrogenase (DHODH) **(Fig. 8.1, strategy C)**. Thus, several studies have chosen to target the dihydroorotate dehydrogenase with novel inhibitors (Baldwin et al., 2005; Booker et al., 2010; Coteron et al., 2011; Phillips et al., 2008; Skerlj et al., 2011). Complex II and ATP synthase have been recently demonstrated to be essential for the sexual stage development suggesting that they could be new targets for transmission blocking (Balabaskaran Nina et al., 2011; Hino et al., 2012) **(Fig. 8.1, strategies D and E)**. However, the development of *Plasmodium* complex II inhibitors will only be conceivable if the 3D structure of its ubiquinone-binding site is distinct from its mammalian counterpart. In line with this, previous work revealed that the mammalian complex II inhibitor Atpenin A5 lost its potency against the parasitic complex II, indicating a possible divergence of their respective ubiquinol binding site (Kawahara et al., 2009). In the same manner, the parasitic ATPase activity is highly insensitive to well-known complex V inhibitors such as oligomycin and azide, suggesting the possibility of an alternative F_0 structural section (Mather et al., 2010). In light of this divergence, further studies would be necessary to investigate the potential of *Plasmodium* complex II and V as therapeutic targets.

8.5. Global membrane depolarization via ROS generation: a new mode of action for artemisinins?

In Chapter 5, endoperoxide drugs are revealed to provoke a rapid collapse of both membrane potentials (and not only mitochondrial) essential for parasite survival. Addition of the iron chelator desferrioxamine or the superoxide scavenger Tiron drastically reduces the depolarization, highlighting the role of ferrous ions and oxidant stress in the artemisinins activation process and the membrane damaging activity.

Artemisinin-induced mitochondrial membrane depolarization has long been established as a possible cause of malaria parasite death (Li et al., 2005; Wang et al., 2010). In line with this, recent investigations confirm the initiation of human cell death by artesunate via mitochondrial membrane depolarization and ROS generation (Mercer et al., 2011). For *Leishmania* parasites, artemisinin has been demonstrated to cause induction of apoptosis associated with depolarization of the mitochondria (Sen et al., 2007). Therefore, an alternative cytotoxic mode of action of endoperoxides has been suggested whereby mitochondrial dysfunction is triggered by a collapse of electrochemical gradient via reactive oxygen species. Data obtained supports the theory previously proposed but globalises it to all parasite membranes. Indeed, the plasma membrane depolarization observed adjusts this mode of action to the global parasite lipid bilayers.

Mitochondrial depolarization has already been suspected to cause parasite death via a loss of its essential functions (Biagini et al., 2008; Srivastava et al., 1997). Although the damage of the plasma membrane seems cytotoxic, the role and impact of its depolarization on parasite death remains to be clearly established. Interestingly, oxidative stress was suggested to disrupt the plasma membrane potential of the parasitic protozoon *Giardia intestinalis* leading to its death (Lloyd et al., 2000). In line with the proposal of a global membrane disturbance induced by endoperoxide compounds, morphological observations of the food vacuole in malaria parasite showed early damage of its membrane in presence of artemisinin, which is suspected to alkylate its components (enzymes and lipids) (Bousejra-El Garah et al., 2011; del Pilar Crespo et al., 2008).

Those findings contribute to the understanding of the molecular mechanism of action of these drugs. To date, artemisinin and its derivatives might have several modes of action by directly inhibiting or alkylating specific proteins (e.g. *Pf*ATPase6 or *Pf*TCTP) and interfering with vital organelle functions (e.g. heme detoxification, mitochondrial and plasma membrane potentials) **(Fig. 8.2)** However, more studies are needed to clarify the contribution of these multiple targets to parasite killing depending on the artemisinin derivative, the *Plasmodium*

strain, and the parasite stage investigated. Recently, clinical isolates of malaria that possess a artemisinin-tolerant phenotype (delayed parasite clearance), but that are not resistant in vitro, have been reported. This alteration of artemisinin sensitivity has been associated with several genes (e.g. *Pf*Mdr1, *Pf*Crt and *Pf*ATPase6) but the difficulty for the parasite in developing a strong resistance is compatible with the hypothesis that several pathways are targeted by that class of compound. It can be supposed that the "inhibition pathway" could be the most susceptible to emerging resistances due to point mutations interfering with the non-covalent binding of artemisinin to specific proteins. However, the increased capacity of protein turnover and protein synthesis might also contribute to artemisinin resistance by withstanding the loss of active proteins caused by oxidative stress and/or protein alkylation effects of these drugs. In future, it will be interesting to measure the endoperoxide effects on global membrane potential from artemisinin-resistant strains in order to detect whether that pathway could be also source of emerging resistances.

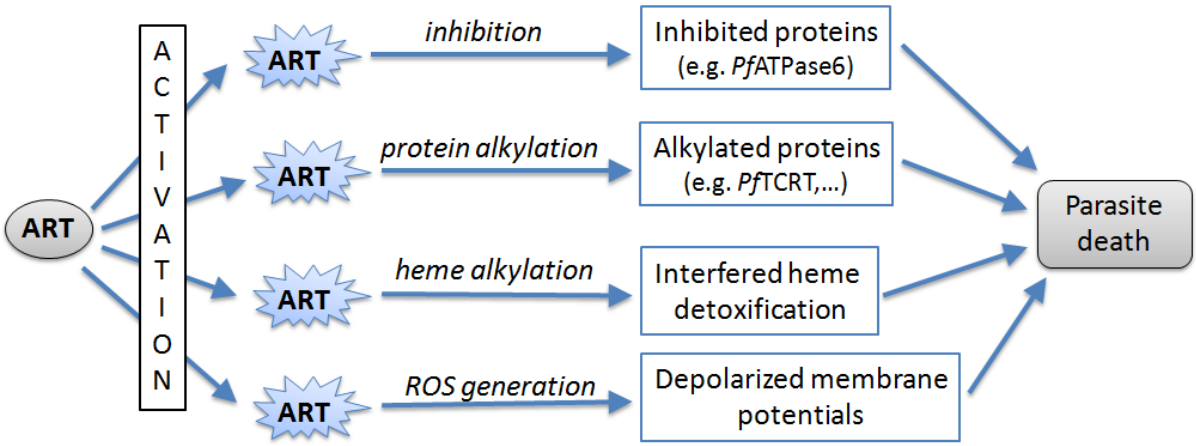

Figure 8.2. Proposed biological modes of action for artemisinin (ART) and its endoperoxide derivatives.

With several potential mechanisms of action slowing down the development of truly resistant strains, artemisinin and its derivatives remain powerful antimalarial drugs for combination treatments against uncomplicated malaria and widespread drug-resistant malaria.

8.6. An atovaquone resistance causing bc_1 instability and fitness penalty to the parasite

In Chapter 6, the point mutation harboured by the atovaquone-resistant strain TM90C2B was shown to affect both catalytic bc_1 turnover and substrate affinity, as well as atovaquone binding. Extensively studied in model organisms, the effect of this mutation has been analyzed in the parasite itself. Western blotting analysis indicated reduced levels of ISP protein in the TM90C2B strain compared to the bc_1 wild type 3D7 strain, suggestive of a weakened interaction

between this subunit and cytochrome *b*. The reduced enzyme turnover and the significant reduction in ISP content in parasite bc_1 carrying the Y268S mutation may result in a significant fitness cost (manifested as a slower growth rate) to the parasite. In line with this hypothesis, a fitness cost has been demonstrated for atovaquone-resistant K1 clones of *P. falciparum* containing the M133I/G280D double mutation within cytochrome *b* (Peters et al., 2002). However, analysis of the fold change in gene expression of the atovaquone-resistant strain TM90C2B compared with the atovaquone-sensitive 3D7 strain revealed some significant differences between the two strains (Fisher et al., 2012). An approximate 2-fold increase in expression of complex III and complex IV genes, including the ISP Rieske subunit, has been observed for the resistant strain. Thus, it is also hypothesized that the observed differential expression of these and other key genes may offset the fitness cost resulting from reduced bc_1 activity.

8.7. The unusual protein import in Apicomplexan mitochondria

In all eukaryotes, the biogenesis and proper functionality of the mitochondrion is dependent on the import and processing machinery for nuclear-encoded proteins. In apicomplexa, the limitation of the mitochondrial genome (only three genes encoded) highlights the importance of understanding the importation pathways and identification of all their components. Due to the complete sequencing of apicomplexan genomes, noticeable progress has been achieved toward the *in silico* identification of involved proteins. New putative components complete an apicomplexan map which exposes all main importation pathways known in yeast, animal or plant models. However, essential components such as Mia40 or Sam35 may be missing or not yet annotated due to limitations of homology searching. The absence of receptors Tom20 and Tom70 is another major difference compared to other eukaryotes. Despite the identification of a plant mtOM64 homologue in *P. falciparum* that might play a similar role than Tom70, the mechanism of precursor detection at the mitochondrial surface remains unclear in apicomplexa. The total absence of receptors in *Toxoplasma gondii* may lead to the hypothesis of apicomplexan-specific proteins able to detect presequences or internal sequences. The discovery of a putative Tom6 subunit by studying plant homologues demonstrates specific affinities with the *A. thaliana* model. Because apicomplexan parasites possess an apicoplast similar to chloroplast, they may have acquired plant-specific proteins. Additionally, some apicomplexan components display a clear diversification with eukaryotic homologues being truncated or with a greater amino acid length.

The identification of apicomplexan-specific subunits and the characterization of unusual homologue components will need experimental validation. Newly identified mitochondrial

proteases highlight the importance of remodelling mitochondrial proteins. Most studies on mitochondrial import and processing have been done in a baker's yeast model but the coverage of its mitochondrial proteome is not yet complete. The possible identification of new fungal components in future might give answers to the apicomplexan model gaps.

8.8. Future challenges for mitochondrial research in malaria

Today, the key role of malaria parasite mitochondria as drug target has been recognized due to extensive studies. Indeed, impressive progresses in the understanding of physiological processes in *Plasmodium* mitochondria have been made. However, important challenges remain to be raised:

(i) **Define the exact composition of the respiratory chain.** To date, the cataloguing of the ETC in *Plasmodium* species is still uncompleted. It is critical to know all subunits composing the respiratory chain for our understanding of the function and evolution of the ETC in general. For example, the functionality of the ATP synthase in blood stages of malaria parasites has been debated for decades only due to incapacity for annotating two membrane anchor subunits (Balabaskaran Nina et al., 2011). Direct purification and characterization of *Plasmodium* ETC complexes facilitates the discovery of lacking and novel subunits, providing a functional context for certain hypothetical proteins identified in proteomic or genomic studies like presented in this thesis.

(ii) **Study the essentiality of ETC enzymes in *P. falciparum***. To know if an enzyme is a "druggable" target, determine its impact on parasite survival is a key step. Recently, NDH2 and Complex II have been determined essential in sexual stages of the rodent malaria parasite (Boysen and Matuschewski, 2011; Hino et al., 2012). However, this conclusion has to be confirmed in its human counterpart. Therefore, those genes and other coding for ETC enzymes should be disrupted in the human malaria parasite *P. falciparum* and phenotypes of the disruptant should be observed in experimental infections in mosquitoes in order to investigate their role in parasite death.

(iii) **Determine the presence of supercomplexes.** In eukaryote mitochondria, the electron transport chain was shown to be organized in multiple supercomplexes (Schagger and Pfeiffer, 2000). For example, in yeast which lacks the conventional complex I as in malaria parasites, complex III exists as a free dimer or in supercomplexes with one or two complex IV monomers (Schagger and Pfeiffer, 2000). The main role of these supramolecular assemblies, called also "respirasomes", is thought to enhance the electron transfer and

regulation of these complexes (Dudkina et al., 2010). Except ATP synthase which was found to exist as a dimer (Balabaskaran Nina et al., 2011), little is known about supercomplex assembly in *Plasmodium* species which deserves further investigations in future. For example, it will be interesting to know if the cytochome bc_1 and cytochome *c* oxidase can operate as supercomplexes and if repercussions due to bc_1 mutations may exist. Threshold-effect studies (Rossignol *et al.,* 2003) or two dimensional gels coupled with LC-MS/MS analysis (Gomez et al., 2009; Wittig et al., 2006) can be attempted to demonstrate presence of mitochondrial supercomplexes in malaria parasites.

(iv) **Solve the crystal structure of ETC enzymes in *Plasmodium*.** Only two structures of ETC enzymes in *P. falciparum* are currently available (DHODH and G3PDH). To help the development of new antimalarial drugs targeting the respiratory chain, determine the structure of ETC enzymes appears to be an important step. Indeed, co-crystallization structures of *P. falciparum* DHODH with different inhibitors provide a good starting point for structure-based development of more potent drugs (Davies et al., 2009). In the same manner, resolution of the crystal structure for the *Plasmodium* bc_1, which rely only on the yeast model, and *Pf*NDH2 will be helpful for their respective drug discovery programs. To date, attempts to crystalize a recombinant *Pf*NDH2 failed (personal communication). Then, purification of those enzymes directly from parasites cell free extracts seems the best alternative even though this is particularly challenging as the *Plasmodium* parasite has only one mitochondrion. Therefore, the major obstacle is obviously the insufficient amount of starting materials which is required to start crystallisation of the protein. But, with time – maybe several years –, it should be possible to collect enough mitochondrial membrane for such a preparation.

(v) **Determine new drug targets in mitochondria.** Because many mitochondrial functions are critical for parasite survival as well as several mitochondrial proteins are enough divergent from their host counterparts, this organelle presents great opportunities for finding antimalarial drug targets. For example, the TCA cycle in malaria parasites has been revealed to be drastically different from the tricarboxylic acid metabolism in human mitochondria. Several of the TCA enzymes such as the malate:quinone oxidoreductase (MQO), absent in human, or the fumarate hydratase call for detail investigations to determine their properties as drug targets.

8.9. Conclusion

Although the malaria parasites appear to minimise the mitochondrial contributions to their physiology, the mitochondrion is nevertheless essential for their survival and a valid drug target. A better knowledge of the electron transport chain and its biochemical processes help us to understand how the existing drugs affect the parasite, but also to develop new drugs to target the disease. The several new insights presented in this thesis are a step towards achieving these objectives. Future research remains to be done to clarify knowledge gaps on certain enzymes and their roles in the metabolic pathways. Much existing works about *P. falciparum* mitochondria have been focused on the asexual stages due to the simplicity to obtain *in vitro* parasites, but the characterisation of other stages is likely to be rewarding. An important challenge remains to be taken up to complete this fascinating mitochondrial puzzle and develop new therapeutic methods against the parasite.

Appendix

Appendix 1. List of the 19 peptides covering the first hit identifying the *Escherichia coli* SdhA subunit.

Sequence	Protein Accession	Modifications	Probability	m/z [Da]	RT (min)
LGGNSLLDLVVFGR	P0AC43		65.36	730.41675	59.74
EFDAVVIGAGGAGmR	P0AC43	M14(Oxidation)	39.52	733.36273	36.26
ATVLATGGAGR	P0AC43		61.10	487.27557	19.74
IYQRPFGGQSK	P0AC43		14.71	640.83844	19.57
EFDAVVIGAGGAGmR	P0AC43	M14(Oxidation)	44.59	733.35651	36.00
VTGQALTVNEK	P0AC43		66.79	580.31848	21.28
ATVLATGGAGR	P0AC43		17.92	487.27603	19.23
VTGQALTVNEK	P0AC43		52.56	580.32086	21.07
NGEDPVAIR	P0AC43		33.37	485.74869	23.02
GEGGYLLNK	P0AC43		21.23	475.75095	25.54
NGEDPVAIR	P0AC43		23.83	485.75299	23.05
LPGILELSR	P0AC43		47.10	499.30646	41.89
NFGGEQAAR	P0AC43		8.31	475.22754	16.42
LPGILELSR	P0AC43		5.95	499.30945	42.39
LPGILELSR	P0AC43		19.93	499.30502	41.37
SImIEIR	P0AC43	M3(Oxidation)	2.07	439.24533	31.42
NGEDPVAIR	P0AC43		1.00	485.71313	22.33
SImIEIR	P0AC43	M3(Oxidation)	1.00	438.75085	30.99
HGERFMER	P0AC43		1.00	531.81787	48.96

Appendix 2. List of the 28 peptides covering the first hit identifying the *P. falciparum* Rieske subunit.

Sequence	Protein Accession	Modifications	Probability	m/z [Da]	RT (min)
YAHYNQTAEPVFPR	PF14_0373		77.00	846.90662	35.53
TDVWHNPKEPAIVSIGK	PF14_0373		23.63	631.00323	39.12
YAHYNQTAEPVFPR	PF14_0373		66.08	846.91394	35.02
YAHYNQTAEPVFPR	PF14_0373		28.91	564.94244	35.44
KVEDLSELVEPSNHPHQYEGIFAR	PF14_0373		48.58	699.34778	45.88
DLVAGGTTELDmR	PF14_0373	M12(Oxidation)	49.36	697.33398	37.99
NFRPAGYAENcPNPESINSDHHPDFR	PF14_0373	C11(Carbamidomethyl)	34.67	761.08417	36.55
VEDLSELVEPSNHPHQYEGIFAR	PF14_0373		38.28	667.32233	48.60
NLFDHAEDIK	PF14_0373		15.67	601.29681	37.27
YAHYNQTAEPVFPR	PF14_0373		8.09	564.94183	34.94
TVNPGEHVVIK	PF14_0373		26.68	596.83911	27.25
YAHYNQTAEPVFPR	PF14_0373		6.55	564.94177	35.97
IPPASEDPSYK	PF14_0373		8.83	602.29718	29.21
SVHFFWISK	PF14_0373		35.86	575.80487	47.66
IPPASEDPSYK	PF14_0373		42.21	602.29767	28.15
NLFDHAEDIK	PF14_0373		9.80	601.29956	37.86
IPPASEDPSYK	PF14_0373		31.06	602.29675	28.47
QGPAPSNLEVPPYEFVDENTIK	PF14_0373		1.00	1222.60071	52.86
IPPASEDPSYK	PF14_0373		35.96	602.29352	29.25
IPPASEDPSYK	PF14_0373		45.13	602.29761	28.66
TVNPGEHVVIK	PF14_0373		18.48	596.83600	27.77
TDVWHNPK	PF14_0373		26.70	498.74945	24.56
EPAIVSIGK	PF14_0373		1.00	457.27197	35.48
IPPASEDPSYK	PF14_0373		7.61	602.30524	27.66
IPPASEDPSYK	PF14_0373		1.00	602.29346	29.77
LWEIEEKQNVSHK	PF14_0373		1.00	547.67804	68.43
TIKPEWLVNIGIcTHLGcVPAQGGNYSGYFcPcHGSHYDNSGR	PF14_0373	C13(Carbamidomethyl) C18(Carbamidomethyl) C31(Carbamidomethyl) C33(Carbamidomethyl)	1.35	1220.39294	69.83
EPAIVSIGK	PF14_0373		1.00	457.26715	34.97

Appendix 3. Uniprot accession numbers of components of the mitochondrial importation machinery in different apicomplexan species (www.uniprot.org).

	Protein	*Plasmodium falciparum* (str.3D7)	*Toxoplasma Gondii* (str. GT1/ME49/VEG)	*Cryptosporidium muris* (str.RN66)	*Theileria parva* (str. Muguga)	*Babesia bovis* (str.T2Bo)	*Neospora Caninum* (str. Liverpool)
Cytosolic chaperones and factors	cHsp70	Q8IB24	Q9TW75 (GT1)	B6AE62	Q27031	Q9U545	F0VIP7
	Hsp90	Q8IC05	Q7Z1F7 (GT1)	B6AIL0	P24724	Q9NDI2	F0VBM9
	MSF	-	-	-	-	-	-
	AIP	Q8I4V8	-	-	-	-	-
	NAC	C6KT55	B9QF62 (VEG)	B6ACH0	Q4N187	A7APM3	F0VET4
	RAC (*h*DnaJ)	Q8I5N9	B9QFN4 (VEG)	B6AH49	Q4N2E7	A7AT73	F0VF74
	RAC (cHSP70)	Q8I2X4 Q8IB24 C0H5H0 PF3D7_0831700[1]	Q9U540 (GT1) Q9TW75 (GT1) B9PMT2 (GT1)	B6AHN5 B6AE62 B6AJW6	Q27031 Q4N3K7 Q4N8J2	A7AP56 Q9U545 A7AWL8	F0VN28 F0VIP7 F0VLQ7
TOM Complex	Tom40	C6KT11	B9PQE1 (GT1)	B6AI18	Q4N6X4	A7AQ94	F0VPX2
	Tom22'	Q8I3L8	-	B6AD33	Q4N6K1	A7AMW2	F0VH87
	OM64 (Tom70)	Q8I510	-	-	-	-	-
	Tom20	-	-	-	-	-	-
	Tom7	Q8IB71	-	-	-	-	-
	Tom6	-	-	-	-	-	-
	Tom5	-	-	-	-	-	-
SAM Complex	Sam50	PF3D7_0608310[1]	B6KIE3 (ME49)	B6AE29	Q4MYN3	A7AM13	F0VET2
	Sam37	-	-	-	-	-	
	Sam35	-	-	-	-	-	-
	Mdm10	-	-	-	-	-	-
Tiny TIMs	Tim8	Q8I500	B6KNU2 (GT1)	B6AJ50	Q4MYV5	A7AM86	F0V9J5
	Tim13	Q8ILN5	B9PG40 (GT1)	-	-	-	F0VIL7
	Tim9	Q8ID24	B9PGF1 (GT1)	B6AEM1	Q4N7M1	A7AS04	F0VIC8
	Tim10	Q8I5W2	B9PZS6 (GT1)	B6AAF8	Q4N7D5	A7ARS5	F0VL53
IMS machinery	Mia40	-	-	-	-	-	-
	Erv1	Q8I242	B9PVQ6 (GT1)	B6ACM3	Q4N5T5	A7AUU4	F0VBQ0
	Cytochrome c	Q8IM53	B9PQQ9	-	Q4N594	A7ANI1	F0VPL5
TIM22 complex	Tim22	C6KTB0	B9PMH5 (GT1)	B6AHV7	Q4MZU8	A7AVL2	F0VM00
	Tim12	Q8I472	B9PN09 (GT1)	B6ACI9	Q4N242	A7ASU8	F0VLJ2
	Tim18	-	-	-	-	-	-
	Tim54	-	-	-	-	-	-
TIM23 Complex + PAM motor	Tim23	Q8IDE0	B9PZG4 (GT1)	B6AD68	Q4N7T7	A7ASA5	F0VKW2
	Tim50	Q8IBI8	B9PSW6 (GT1)	B6AC38	Q4N713	A7AQ81	F0VCQ3
	Tim21	-	-	-	-	-	-
	Tim17	Q8ILB7	B9PK67 (GT1)	B6AJQ7	Q4N769	A7ARK7	F0VN60
	Pam18 (Tim14)	Q8IBK8	B9PUI0 (GT1)	B6ACF8	Q4N5D4	A7AP77	F0VFC7
	Pam16 (Tim16)	Q8I3X2	B9PRA9 (GT1)	B6AAU5	Q4N488	A7AVW7	F0VR30
	Pam17	-	-	-	-	-	-
	Tim44	Q8IIA9	B9PN05 (GT1)	B6AG36	Q4N770	A7ARK8	F0VLJ6
	mHSP70	Q8II24	B9PRL0 (GT1)	B6AIR7	Q4N486	A7AVW9	F0VRB1
	GrpE	Q8IIB6	B9Q1G8 (GT1)	B6ACF7	Q4N773	A7ARL1	F0VBE5
OXA complex	Oxa1	Q8IBB5	B9PK92	-	Q4MZ94	A7AVL5	F0VN78
	Mdm38	Q8I1R5	B9PU05	B6A9N6	Q4N224	A7ATX9	F0VBN1
	Mba1	-	-	-	-	-	-
	Ylh47	-	-	-	-	-	-

[1] GeneDB accession number (www.genedb.org).

Appendix 4. Uniprot accession numbers of components of the mitochondrial processing machinery in different apicomplexan species (www.uniprot.org).

	Protein	*Plasmodium falciparum* (str.3D7)	*Toxoplasma Gondii* (str. GT1)	*Cryptosporidium muris* (str.RN66)	*Theileria parva* (str. Muguga)	*Babesia bovis* (str.T2Bo)	*Neospora Caninum* (str. Liverpool)
Matrix processing	MPP (α subunit)	Q8MTV4	B9PUJ6	B6AFN5	Q4N5S2	A7AN14	F0VFD9
	MPP (β subunit)	Q8MTV6	B9PW21	B6ACH4	Q4N9G3	A7AV97	F0VKL8
	MIP	Q8IDW2	B9PFS9	B6AH36	Q4N8F6	A7AMP2	F0VIX1
	Icp55	-	-	-	-	-	-
	FCN	Q9U7N7	B9PN15	-	Q4N5N0	A7AU33	F0VLI5
	mtHsp60	Q8IJN9	B9PPQ1	B6AJJ0	Q4N3C1	A7AR66	F0VQU9
	Hsp10	Q8I5Q3	B6KCB9	B6AFS0	Q4N9C4	A7AWV1	F0VG09
Inner membrane processing	m-AAA	Q8IIH1	B9PUJ9	B6AIA1	Q4N560	A7ANF2	F0VFE8
	i-AAA	Q8IKI9 Q8I526	B9Q2U6 B9PKW2	-	Q4N3I7 Q4N6P8	A7ASY6 A7ASM0	F0VQP5 F0VGU4
	Atp23	-	-	-	-	-	-
	Rom6	Q8IDP3	Q2PP52	B6ADY7	Q4UH21 *(T. annulata)*	A7AWM4	F0VQ63
	Imp1	Q8IEA9	B9PH52	B6AEI4	Q4N750	A7AWS9	F0VJQ1
	Imp2	-	-	-	-	-	-

References

Abrahamsen, M.S., Templeton, T.J., Enomoto, S., Abrahante, J.E., Zhu, G., Lancto, C.A., Deng, M., Liu, C., Widmer, G., Tzipori, S*., et al.* (2004). Complete genome sequence of the apicomplexan, Cryptosporidium parvum. Science *304*, 441-445.

Aggeler, R., Coons, J., Taylor, S.W., Ghosh, S.S., Garcia, J.J., Capaldi, R.A., and Marusich, M.F. (2002). A functionally active human F1F0 ATPase can be purified by immunocapture from heart tissue and fibroblast cell lines. Subunit structure and activity studies. J Biol Chem *277*, 33906-33912.

Agnandji, S.T., Lell, B., Soulanoudjingar, S.S., Fernandes, J.F., Abossolo, B.P., Conzelmann, C., Methogo, B.G., Doucka, Y., Flamen, A., Mordmuller, B*., et al.* (2011). First results of phase 3 trial of RTS,S/AS01 malaria vaccine in African children. N Engl J Med *365*, 1863-1875.

Aide, P., Dobaño, C., Sacarlal, J., Aponte, J.J., Mandomando, I., Guinovart, C., Bassat, Q., Renom, M., Puyol, L., Macete, E*., et al.* (2011). Four year immunogenicity of the RTS,S/AS02A malaria vaccine in Mozambican children during a phase IIb trial. Vaccine *29*, 6059-6067.

Aikawa, M. (1966). The fine structure of the erythrocytic stages of three avian malarial parasites, Plasmodium fallax, P. lophurae, and P. cathemerium. Am J Trop Med Hyg *15*, 449-471.

Aikawa, M., Hepler, P.K., Huff, C.G., and Sprinz, H. (1966). The feeding mechanism of avian malarial parasites. J Cell Biol *28*, 355-373.

Ajioka, J.W., Boothroyd, J.C., Brunk, B.P., Hehl, A., Hillier, L., Manger, I.D., Marra, M., Overton, G.C., Roos, D.S., Wan, K.L*., et al.* (1998). Gene discovery by EST sequencing in Toxoplasma gondii reveals sequences restricted to the Apicomplexa. Genome Res *8*, 18-28.

Alag, R., Bharatham, N., Dong, A., Hills, T., Harikishore, A., Widjaja, A.A., Shochat, S.G., Hui, R., and Yoon, H.S. (2009). Crystallographic structure of the tetratricopeptide repeat domain of Plasmodium falciparum FKBP35 and its molecular interaction with Hsp90 C-terminal pentapeptide. Protein Sci *18*, 2115-2124.

Alam, R., Hachiya, N., Sakaguchi, M., Kawabata, S., Iwanaga, S., Kitajima, M., Mihara, K., and Omura, T. (1994). cDNA cloning and characterization of mitochondrial import stimulation factor (MSF) purified from rat liver cytosol. J Biochem *116*, 416-425.

Aldritt, S.M., Joseph, J.T., and Wirth, D.F. (1989). Sequence identification of cytochrome b in Plasmodium gallinaceum. Mol Cell Biol *9*, 3614-3620.

Alikhani, N., Berglund, A.K., Engmann, T., Spanning, E., Vogtle, F.N., Pavlov, P., Meisinger, C., Langer, T., and Glaser, E. (2011). Targeting capacity and conservation of PreP homologues localization in mitochondria of different species. J Mol Biol *410*, 400-410.

Allen, J.W., Ferguson, S.J., and Ginger, M.L. (2008). Distinctive biochemistry in the trypanosome mitochondrial intermembrane space suggests a model for stepwise evolution of the MIA pathway for import of cysteine-rich proteins. FEBS Lett *582*, 2817-2825.

Allen, R., Egan, B., Gabriel, K., Beilharz, T., and Lithgow, T. (2002). A conserved proline residue is present in the transmembrane-spanning domain of Tom7 and other tail-anchored protein subunits of the TOM translocase. FEBS Lett *514*, 347-350.

Allen, R.J., and Kirk, K. (2004). The membrane potential of the intraerythrocytic malaria parasite Plasmodium falciparum. J Biol Chem *279*, 11264-11272.

Allen, S., Balabanidou, V., Sideris, D.P., Lisowsky, T., and Tokatlidis, K. (2005). Erv1 mediates the Mia40-dependent protein import pathway and provides a functional link to the respiratory chain by shuttling electrons to cytochrome c. J Mol Biol *353*, 937-944.

Alonso, P.L., Sacarlal, J., Aponte, J.J., Leach, A., Macete, E., Milman, J., Mandomando, I., Spiessens, B., Guinovart, C., Espasa, M*., et al.* (2004). Efficacy of the RTS,S/AS02A vaccine against Plasmodium falciparum infection and disease in young African children: randomised controlled trial. The Lancet *364*, 1411-1420.

Alonso, P.L., Smith, T., Schellenberg, J.R., Masanja, H., Mwankusye, S., Urassa, H., Bastos de Azevedo, I., Chongela, J., Kobero, S., Menendez, C.*, et al.* (1994). Randomised trial of efficacy of SPf66 vaccine against Plasmodium falciparum malaria in children in southern Tanzania. Lancet *344*, 1175-1181.

Alonso, P.L., Smith, T.A., Armstrong-Schellenberg, J.R., Kitua, A.Y., Masanja, H., Hayes, R., Hurt, N., Font, F., Menendez, C., Kilama, W.L.*, et al.* (1996). Duration of protection and age-dependence of the effects of the SPf66 malaria vaccine in African children exposed to intense transmission of Plasmodium falciparum. J Infect Dis *174*, 367-372.

Andriantsoanirina, V., Menard, D., Rabearimanana, S., Hubert, V., Bouchier, C., Tichit, M., Bras, J.L., and Durand, R. (2010). Association of microsatellite variations of Plasmodium falciparum Na+/H+ exchanger (Pfnhe-1) gene with reduced in vitro susceptibility to quinine: lack of confirmation in clinical isolates from Africa. Am J Trop Med Hyg *82*, 782-787.

Angevine, C.M., Herold, K.A., Vincent, O.D., and Fillingame, R.H. (2007). Aqueous access pathways in ATP synthase subunit a. Reactivity of cysteine substituted into transmembrane helices 1, 3, and 5. J Biol Chem *282*, 9001-9007.

Arakawa, T., Komesu, A., Otsuki, H., Sattabongkot, J., Udomsangpetch, R., Matsumoto, Y., Tsuji, N., Wu, Y., Torii, M., and Tsuboi, T. (2005). Nasal immunization with a malaria transmission-blocking vaccine candidate, Pfs25, induces complete protective immunity in mice against field isolates of Plasmodium falciparum. Infect Immun *73*, 7375-7380.

Arlt, H., Tauer, R., Feldmann, H., Neupert, W., and Langer, T. (1996). The YTA10-12 complex, an AAA protease with chaperone-like activity in the inner membrane of mitochondria. Cell *85*, 875-885.

Arnold, I., Pfeiffer, K., Neupert, W., Stuart, R.A., and Schagger, H. (1998). Yeast mitochondrial F1F0-ATP synthase exists as a dimer: identification of three dimer-specific subunits. EMBO J *17*, 7170-7178.

Asawamahasakda, W., Ittarat, I., Pu, Y.M., Ziffer, H., and Meshnick, S.R. (1994). Reaction of antimalarial endoperoxides with specific parasite proteins. Antimicrob Agents Chemother *38*, 1854-1858.

Atamna, H., and Ginsburg, H. (1993). Origin of reactive oxygen species in erythrocytes infected with Plasmodium falciparum. Mol Biochem Parasitol *61*, 231-241.

Balabaskaran Nina, P., Dudkina, N.V., Kane, L.A., van Eyk, J.E., Boekema, E.J., Mather, M.W., and Vaidya, A.B. (2010). Highly divergent mitochondrial ATP synthase complexes in Tetrahymena thermophila. PLoS Biol *8*, e1000418.

Balabaskaran Nina, P., Morrisey, J.M., Ganesan, S.M., Ke, H., Pershing, A.M., Mather, M.W., and Vaidya, A.B. (2011). ATP synthase complex of Plasmodium falciparum: dimeric assembly in mitochondrial membranes and resistance to genetic disruption. J Biol Chem *286*, 41312-41322.

Baldwin, J., Michnoff, C.H., Malmquist, N.A., White, J., Roth, M.G., Rathod, P.K., and Phillips, M.A. (2005). High-throughput screening for potent and selective inhibitors of Plasmodium falciparum dihydroorotate dehydrogenase. J Biol Chem *280*, 21847-21853.

Bannister, L.H., Hopkins, J.M., Fowler, R.E., Krishna, S., and Mitchell, G.H. (2000). A brief illustrated guide to the ultrastructure of Plasmodium falciparum asexual blood stages. Parasitol Today *16*, 427-433.

Bannister, L.H., and Mitchell, G.H. (2009). The malaria merozoite, forty years on. Parasitology *136*, 1435-1444.

Barham, H.M., Inglis, R., Chinje, E.C., and Stratford, I.J. (1996). Development and validation of a spectrophotometric assay for measuring the activity of NADH: cytochrome b5 reductase in human tumour cells. Br J Cancer *74*, 1188-1193.

Barnwell, J.W., and Galinski, M.R. (1998). Invasion of vertebrate cells: erythrocytes. Malaria: Parasite Biology, Pathogenesis and Protection, ASM Press, Washington, DC, 93-120.

Barton, V., Fisher, N., Biagini, G.A., Ward, S.A., and O'Neill, P.M. (2010). Inhibiting Plasmodium cytochrome bc1: a complex issue. Curr Opin Chem Biol *14*, 440-446.

Bauer, M.F., Sirrenberg, C., Neupert, W., and Brunner, M. (1996). Role of Tim23 as voltage sensor and presequence receptor in protein import into mitochondria. Cell *87*, 33-41.

Beck, H.P., Felger, I., Huber, W., Steiger, S., Smith, T., Weiss, N., Alonso, P., and Tanner, M. (1997). Analysis of multiple Plasmodium falciparum infections in Tanzanian children during the phase III trial of the malaria vaccine SPf66. J Infect Dis *175*, 921-926.

Beddoe, T., and Lithgow, T. (2002). Delivery of nascent polypeptides to the mitochondrial surface. Biochim Biophys Acta *1592*, 35-39.

Bejon, P., Lusingu, J., Olotu, A., Leach, A., Lievens, M., Vekemans, J., Mshamu, S., Lang, T., Gould, J., Dubois, M.C*., et al.* (2008). Efficacy of RTS,S/AS01E vaccine against malaria in children 5 to 17 months of age. N Engl J Med *359*, 2521-2532.

Bekker, M., Kramer, G., Hartog, A.F., Wagner, M.J., de Koster, C.G., Hellingwerf, K.J., and de Mattos, M.J. (2007). Changes in the redox state and composition of the quinone pool of Escherichia coli during aerobic batch-culture growth. Microbiology *153*, 1974-1980.

Bender, A., van Dooren, G.G., Ralph, S.A., McFadden, G.I., and Schneider, G. (2003). Properties and prediction of mitochondrial transit peptides from Plasmodium falciparum. Mol Biochem Parasitol *132*, 59-66.

Berman, P.A., and Adams, P.A. (1997). Artemisinin enhances heme-catalysed oxidation of lipid membranes. Free Radic Biol Med *22*, 1283-1288.

Berry, A., Senescau, A., Lelievre, J., Benoit-Vical, F., Fabre, R., Marchou, B., and Magnaval, J.F. (2006). Prevalence of Plasmodium falciparum cytochrome b gene mutations in isolates imported from Africa, and implications for atovaquone resistance. Trans R Soc Trop Med Hyg *100*, 986-988.

Bhisutthibhan, J., and Meshnick, S.R. (2001). Immunoprecipitation of [(3)H]dihydroartemisinin translationally controlled tumor protein (TCTP) adducts from Plasmodium falciparum-infected erythrocytes by using anti-TCTP antibodies. Antimicrob Agents Chemother *45*, 2397-2399.

Bhisutthibhan, J., Pan, X.Q., Hossler, P.A., Walker, D.J., Yowell, C.A., Carlton, J., Dame, J.B., and Meshnick, S.R. (1998). The Plasmodium falciparum translationally controlled tumor protein homolog and its reaction with the antimalarial drug artemisinin. J Biol Chem *273*, 16192-16198.

Bhushan, S., Lefebvre, B., Stahl, A., Wright, S.J., Bruce, B.D., Boutry, M., and Glaser, E. (2003). Dual targeting and function of a protease in mitochondria and chloroplasts. EMBO Rep *4*, 1073-1078.

Biagini, G.A., Fisher, N., Berry, N., Stocks, P.A., Meunier, B., Williams, D.P., Bonar-Law, R., Bray, P.G., Owen, A., O'Neill, P.M*., et al.* (2008). Acridinediones: Selective and Potent Inhibitors of the Malaria Parasite Mitochondrial bc1 Complex. Molecular Pharmacology *73*, 1347-1355.

Biagini, G.A., Fisher, N., Shone, A.E., Mubaraki, M.A., Srivastava, A., Hill, A., Antoine, T., Warman, A.J., Davies, J., Pidathala, C*., et al.* (2012). Generation of quinolone antimalarials targeting the Plasmodium falciparum mitochondrial respiratory chain for the treatment and prophylaxis of malaria. Proc Natl Acad Sci U S A.

Biagini, G.A., Pasini, E.M., Hughes, R., De Koning, H.P., Vial, H.J., O'Neill, P.M., Ward, S.A., and Bray, P.G. (2004). Characterization of the choline carrier of Plasmodium falciparum: a route for the selective delivery of novel antimalarial drugs. Blood *104*, 3372-3377.

Biagini, G.A., Viriyavejakul, P., O'Neill P, M., Bray, P.G., and Ward, S.A. (2006). Functional characterization and target validation of alternative complex I of Plasmodium falciparum mitochondria. Antimicrob Agents Chemother *50*, 1841-1851.

Bisetto, E., Picotti, P., Giorgio, V., Alverdi, V., Mavelli, I., and Lippe, G. (2008). Functional and stoichiometric analysis of subunit e in bovine heart mitochondrial F(0)F(1)ATP synthase. J Bioenerg Biomembr *40*, 257-267.

Bonday, Z.Q., Taketani, S., Gupta, P.D., and Padmanaban, G. (1997). Heme biosynthesis by the malarial parasite. Import of delta-aminolevulinate dehydrase from the host red cell. J Biol Chem *272*, 21839-21846.

Booker, M.L., Bastos, C.M., Kramer, M.L., Barker, R.H., Jr., Skerlj, R., Sidhu, A.B., Deng, X., Celatka, C., Cortese, J.F., Guerrero Bravo, J.E.*, et al.* (2010). Novel inhibitors of Plasmodium falciparum dihydroorotate dehydrogenase with anti-malarial activity in the mouse model. J Biol Chem *285*, 33054-33064.

Bosia, A., Ghigo, D., Turrini, F., Nissani, E., Pescarmona, G.P., and Ginsburg, H. (1993). Kinetic characterization of Na+/H+ antiport of Plasmodium falciparum membrane. J Cell Physiol *154*, 527-534.

Bousejra-El Garah, F., Wong, M.H., Amewu, R.K., Muangnoicharoen, S., Maggs, J.L., Stigliani, J.L., Park, B.K., Chadwick, J., Ward, S.A., and O'Neill, P.M. (2011). Comparison of the reactivity of antimalarial 1,2,4,5-tetraoxanes with 1,2,4-trioxolanes in the presence of ferrous iron salts, heme, and ferrous iron salts/phosphatidylcholine. J Med Chem *54*, 6443-6455.

Boyer, P.D. (1997). The ATP synthase--a splendid molecular machine. Annu Rev Biochem *66*, 717-749.

Boysen, K.E., and Matuschewski, K. (2011). Arrested oocyst maturation in Plasmodium parasites lacking type II NADH:ubiquinone dehydrogenase. J Biol Chem *286*, 32661-32671.

Bozdech, Z., Llinas, M., Pulliam, B.L., Wong, E.D., Zhu, J., and DeRisi, J.L. (2003). The transcriptome of the intraerythrocytic developmental cycle of Plasmodium falciparum. PLoS Biol *1*, E5.

Bradford, M.M. (1976). A rapid and sensitive method for the quantitation of microgram quantities of protein utilizing the principle of protein-dye binding. Anal Biochem *72*, 248-254.

Brasseur, G., Di Rago, J.P., Slonimski, P.P., and Lemesle-Meunier, D. (2001). Analysis of suppressor mutation reveals long distance interactions in the bc(1) complex of Saccharomyces cerevisiae. Biochim Biophys Acta *1506*, 89-102.

Brasseur, G., Lemesle-Meunier, D., Reinaud, F., and Meunier, B. (2004). QO site deficiency can be compensated by extragenic mutations in the hinge region of the iron-sulfur protein in the bc1 complex of Saccharomyces cerevisiae. J Biol Chem *279*, 24203-24211.

Bray, P.G., Mungthin, M., Hastings, I.M., Biagini, G.A., Saidu, D.K., Lakshmanan, V., Johnson, D.J., Hughes, R.H., Stocks, P.A., O'Neill, P.M.*, et al.* (2006). PfCRT and the trans-vacuolar proton electrochemical gradient: regulating the access of chloroquine to ferriprotoporphyrin IX. Mol Microbiol *62*, 238-251.

Brayton, K.A., Lau, A.O., Herndon, D.R., Hannick, L., Kappmeyer, L.S., Berens, S.J., Bidwell, S.L., Brown, W.C., Crabtree, J., Fadrosh, D.*, et al.* (2007). Genome sequence of Babesia bovis and comparative analysis of apicomplexan hemoprotozoa. PLoS Pathog *3*, 1401-1413.

Brehelin, L., Florent, I., Gascuel, O., and Marechal, E. (2010). Assessing functional annotation transfers with inter-species conserved coexpression: application to Plasmodium falciparum. BMC Genomics *11*, 35.

Briolant, S., Pelleau, S., Bogreau, H., Hovette, P., Zettor, A., Castello, J., Baret, E., Amalvict, R., Rogier, C., and Pradines, B. (2011). In vitro susceptibility to quinine and microsatellite variations of the Plasmodium falciparum Na+/H+ exchanger (Pfnhe-1) gene: the absence of association in clinical isolates from the Republic of Congo. Malar J *10*, 37.

Brix, J., Rudiger, S., Bukau, B., Schneider-Mergener, J., and Pfanner, N. (1999). Distribution of binding sequences for the mitochondrial import receptors Tom20, Tom22, and Tom70 in a presequence-carrying preprotein and a non-cleavable preprotein. J Biol Chem *274*, 16522-16530.

Brokx, S.J., Wernimont, A.K., Dong, A., Wasney, G.A., Lin, Y.H., Lew, J., Vedadi, M., Lee, W.H., and Hui, R. (2011). Characterization of 14-3-3 proteins from Cryptosporidium parvum. PLoS One *6*, e14827.

Brosché, M., Overmyer, K., Wrzaczek, M., Kangasjärvi, J., and Kangasjärvi, S. (2010). Stress Signaling III: Reactive Oxygen Species (ROS)

Abiotic Stress Adaptation in Plants. In, A. Pareek, S.K. Sopory, and H.J. Bohnert, eds. (Springer Netherlands), pp. 91-102.

Brossi, A., Venugopalan, B., Dominguez Gerpe, L., Yeh, H.J., Flippen-Anderson, J.L., Buchs, P., Luo, X.D., Milhous, W., and Peters, W. (1988). Arteether, a new antimalarial drug: synthesis and antimalarial properties. J Med Chem *31*, 645-650.

Brown, M.C., Joaquim, T.R., Chambers, R., Onisk, D.V., Yin, F., Moriango, J.M., Xu, Y., Fancy, D.A., Crowgey, E.L., He, Y.*, et al.* (2011). Impact of immunization technology and assay application on antibody performance--a systematic comparative evaluation. PLoS One *6*, e28718.

Burke, P.V., and Poyton, R.O. (1998). Structure/function of oxygen-regulated isoforms in cytochrome c oxidase. J Exp Biol *201*, 1163-1175.

Burri, L., Strahm, Y., Hawkins, C.J., Gentle, I.E., Puryer, M.A., Verhagen, A., Callus, B., Vaux, D., and Lithgow, T. (2005). Mature DIABLO/Smac is produced by the IMP protease complex on the mitochondrial inner membrane. Mol Biol Cell *16*, 2926-2933.

Bustamante, P.J., Woodruff, D.C., Oh, J., Keister, D.B., Muratova, O., and Williamson, K.C. (2000). Differential ability of specific regions of Plasmodium falciparum sexual-stage antigen, Pfs230, to induce malaria transmission-blocking immunity. Parasite Immunol *22*, 373-380.

Butler, A.R., Gilbert, B.C., Hulme, P., Irvine, L.R., Renton, L., and Whitwood, A.C. (1998). EPR evidence for the involvement of free radicals in the iron-catalysed decomposition of qinghaosu (artemisinin) and some derivatives; antimalarial action of some polycyclic endoperoxides. Free Radic Res *28*, 471-476.

Cai, X., Herschap, D., and Zhu, G. (2005). Functional characterization of an evolutionarily distinct phosphopantetheinyl transferase in the apicomplexan Cryptosporidium parvum. Eukaryot Cell *4*, 1211-1220.

Canfield, C.J., Pudney, M., and Gutteridge, W.E. (1995). Interactions of atovaquone with other antimalarial drugs against Plasmodium falciparum in vitro. Exp Parasitol *80*, 373-381.

Capaldi, R.A., and Aggeler, R. (2002). Mechanism of the F(1)F(0)-type ATP synthase, a biological rotary motor. Trends Biochem Sci *27*, 154-160.

Carlton, J.M., Angiuoli, S.V., Suh, B.B., Kooij, T.W., Pertea, M., Silva, J.C., Ermolaeva, M.D., Allen, J.E., Selengut, J.D., Koo, H.L.*, et al.* (2002). Genome sequence and comparative analysis of the model rodent malaria parasite Plasmodium yoelii yoelii. Nature *419*, 512-519.

Carrie, C., Giraud, E., Duncan, O., Xu, L., Wang, Y., Huang, S., Clifton, R., Murcha, M., Filipovska, A., Rackham, O.*, et al.* (2010). Conserved and novel functions for Arabidopsis thaliana MIA40 in assembly of proteins in mitochondria and peroxisomes. J Biol Chem *285*, 36138-36148.

Carter, R., Mendis, K.N., Miller, L.H., Molineaux, L., and Saul, A. (2000). Malaria transmission-blocking vaccines--how can their development be supported? Nat Med *6*, 241-244.

Cazelles, J., Robert, A., and Meunier, B. (2001). Alkylation of heme by artemisinin, an antimalarial drug. Comptes Rendus de l'Académie des Sciences - Series IIC - Chemistry *4*, 85-89.

Chacinska, A., Koehler, C.M., Milenkovic, D., Lithgow, T., and Pfanner, N. (2009). Importing mitochondrial proteins: machineries and mechanisms. Cell *138*, 628-644.

Charman, S.A., Arbe-Barnes, S., Bathurst, I.C., Brun, R., Campbell, M., Charman, W.N., Chiu, F.C., Chollet, J., Craft, J.C., Creek, D.J.*, et al.* (2011). Synthetic ozonide drug candidate OZ439 offers new hope for a single-dose cure of uncomplicated malaria. Proc Natl Acad Sci U S A *108*, 4400-4405.

Chavchich, M., Gerena, L., Peters, J., Chen, N., Cheng, Q., and Kyle, D.E. (2010). Role of pfmdr1 amplification and expression in induction of resistance to artemisinin derivatives in Plasmodium falciparum. Antimicrob Agents Chemother *54*, 2455-2464.

Chen, J.J., and Yu, B.P. (1994). Alterations in mitochondrial membrane fluidity by lipid peroxidation products. Free Radic Biol Med *17*, 411-418.

Chen, P.Q., Li, G.Q., Guo, X.B., He, K.R., Fu, Y.X., Fu, L.C., and Song, Y.Z. (1994). The infectivity of gametocytes of Plasmodium falciparum from patients treated with artemisinin. Chin Med J (Engl) *107*, 709-711.

Cheng, Y., and Prusoff, W.H. (1973). Relationship between the inhibition constant (K1) and the concentration of inhibitor which causes 50 per cent inhibition (I50) of an enzymatic reaction. Biochem Pharmacol *22*, 3099-3108.

Chew, A., Rollins, R.A., Sakati, W.R., and Isaya, G. (1996). Mutations in a putative zinc-binding domain inactivate the mitochondrial intermediate peptidase. Biochem Biophys Res Commun *226*, 822-829.

Chew, O., Lister, R., Qbadou, S., Heazlewood, J.L., Soll, J., Schleiff, E., Millar, A.H., and Whelan, J. (2004). A plant outer mitochondrial membrane protein with high amino acid sequence identity to a chloroplast protein import receptor. FEBS Lett *557*, 109-114.

Chinopoulos, C., Tretter, L., and Adam-Vizi, V. (1999). Depolarization of in situ mitochondria due to hydrogen peroxide-induced oxidative stress in nerve terminals: inhibition of alpha-ketoglutarate dehydrogenase. J Neurochem *73*, 220-228.

Chiodini, P.L., Conlon, C.P., Hutchinson, D.B., Farquhar, J.A., Hall, A.P., Peto, T.E., Birley, H., and Warrell, D.A. (1995). Evaluation of atovaquone in the treatment of patients with uncomplicated Plasmodium falciparum malaria. J Antimicrob Chemother *36*, 1073-1078.

Collins, M.D., and Jones, D. (1981). Distribution of isoprenoid quinone structural types in bacteria and their taxonomic implication. Microbiological Reviews *45*, 316-354.

Coteron, J.M., Marco, M., Esquivias, J., Deng, X., White, K.L., White, J., Koltun, M., El Mazouni, F., Kokkonda, S., Katneni, K.*, et al.* (2011). Structure-guided lead optimization of triazolopyrimidine-ring substituents identifies potent Plasmodium falciparum dihydroorotate dehydrogenase inhibitors with clinical candidate potential. J Med Chem *54*, 5540-5561.

Covian, R., and Trumpower, B.L. (2006). Regulatory interactions between ubiquinol oxidation and ubiquinone reduction sites in the dimeric cytochrome bc1 complex. J Biol Chem *281*, 30925-30932.

Cowley, R., Leung, S., Fisher, N., Al-Helal, M., Berry, N.G., Lawrenson, A.S., Sharma, R., Shone, A.E., Ward, S.A., Biagini, G.A.*, et al.* (2012). The development of quinolone esters as novel antimalarial agents targeting the Plasmodium falciparum bc1 protein complex. MedChemComm *3*, 39-44.

Cowman, A.F., and Crabb, B.S. (2006). Invasion of red blood cells by malaria parasites. Cell *124*, 755-766.

Cox, F.E. (2010). History of the discovery of the malaria parasites and their vectors. Parasit Vectors *3*, 5.

Creek, D.J., Charman, W.N., Chiu, F.C., Prankerd, R.J., Dong, Y., Vennerstrom, J.L., and Charman, S.A. (2008). Relationship between antimalarial activity and heme alkylation for spiro- and dispiro-1,2,4-trioxolane antimalarials. Antimicrob Agents Chemother *52*, 1291-1296.

Crofts, A.R. (2004). The cytochrome bc1 complex: function in the context of structure. Annu Rev Physiol *66*, 689-733.

Crofts, A.R., Guergova-Kuras, M., Kuras, R., Ugulava, N., Li, J., and Hong, S. (2000). Proton-coupled electron transfer at the Q(o) site: what type of mechanism can account for the high activation barrier? Biochim Biophys Acta *1459*, 456-466.

Cross, R.M., Maignan, J.R., Mutka, T.S., Luong, L., Sargent, J., Kyle, D.E., and Manetsch, R. (2011). Optimization of 1,2,3,4-tetrahydroacridin-9(10H)-ones as antimalarials utilizing structure-activity and structure-property relationships. J Med Chem *54*, 4399-4426.

Curran, S.P., Leuenberger, D., Schmidt, E., and Koehler, C.M. (2002). The role of the Tim8p-Tim13p complex in a conserved import pathway for mitochondrial polytopic inner membrane proteins. J Cell Biol *158*, 1017-1027.

Dahlstrom, S., Veiga, M.I., Martensson, A., Bjorkman, A., and Gil, J.P. (2009). Polymorphism in PfMRP1 (Plasmodium falciparum multidrug resistance protein 1) amino acid 1466 associated with resistance to sulfadoxine-pyrimethamine treatment. Antimicrob Agents Chemother *53*, 2553-2556.

Dalbey, R.E. (1991). Leader peptidase. Mol Microbiol *5*, 2855-2860.

David, K.P., Alifrangis, M., Salanti, A., Vestergaard, L.S., Ronn, A., and Bygbjerg, I.B. (2003). Atovaquone/proguanil resistance in Africa: a case report. Scand J Infect Dis *35*, 897-898.

Davies, M., Heikkila, T., McConkey, G.A., Fishwick, C.W., Parsons, M.R., and Johnson, A.P. (2009). Structure-based design, synthesis, and characterization of inhibitors of human and Plasmodium falciparum dihydroorotate dehydrogenases. J Med Chem *52*, 2683-2693.

de Souza, W. (2008). An introduction to the structural organization of parasitic protozoa. Curr Pharm Des *14*, 822-838.

Deckers-Hebestreit, G., Greie, J.-C., Stalz, W.-D., and Altendorf, K. (2000). The ATP synthase of Escherichia coli: structure and function of F0 subunits. Biochimica et Biophysica Acta (BBA) - Bioenergetics *1458*, 364-373.

del Pilar Crespo, M., Avery, T.D., Hanssen, E., Fox, E., Robinson, T.V., Valente, P., Taylor, D.K., and Tilley, L. (2008). Artemisinin and a series of novel endoperoxide antimalarials exert early effects on digestive vacuole morphology. Antimicrob Agents Chemother *52*, 98-109.

Deshaies, R.J., Koch, B.D., Werner-Washburne, M., Craig, E.A., and Schekman, R. (1988). A subfamily of stress proteins facilitates translocation of secretory and mitochondrial precursor polypeptides. Nature *332*, 800-805.

Devenish, R.J., Prescott, M., and Rodgers, A.J. (2008). The structure and function of mitochondrial F1F0-ATP synthases. Int Rev Cell Mol Biol *267*, 1-58.

Dickson, V.K., Silvester, J.A., Fearnley, I.M., Leslie, A.G., and Walker, J.E. (2006). On the structure of the stator of the mitochondrial ATP synthase. EMBO J *25*, 2911-2918.

Disbrow, G.L., Baege, A.C., Kierpiec, K.A., Yuan, H., Centeno, J.A., Thibodeaux, C.A., Hartmann, D., and Schlegel, R. (2005). Dihydroartemisinin is cytotoxic to papillomavirus-expressing epithelial cells in vitro and in vivo. Cancer Res *65*, 10854-10861.

Dolezal, P., Likic, V., Tachezy, J., and Lithgow, T. (2006). Evolution of the molecular machines for protein import into mitochondria. Science *313*, 314-318.

Dondorp, A.M., Nosten, F., Yi, P., Das, D., Phyo, A.P., Tarning, J., Lwin, K.M., Ariey, F., Hanpithakpong, W., Lee, S.J*., et al.* (2009). Artemisinin resistance in Plasmodium falciparum malaria. N Engl J Med *361*, 455-467.

Donzeau, M., Kaldi, K., Adam, A., Paschen, S., Wanner, G., Guiard, B., Bauer, M.F., Neupert, W., and Brunner, M. (2000). Tim23 links the inner and outer mitochondrial membranes. Cell *101*, 401-412.

Dorn, A., Stoffel, R., Matile, H., Bubendorf, A., and Ridley, R.G. (1995). Malarial haemozoin/beta-haematin supports haem polymerization in the absence of protein. Nature *374*, 269-271.

Dowse, T.J., and Soldati, D. (2005). Rhomboid-like proteins in Apicomplexa: phylogeny and nomenclature. Trends Parasitol *21*, 254-258.

Duchen, M.R., and Biscoe, T.J. (1992). Relative mitochondrial membrane potential and [Ca2+]i in type I cells isolated from the rabbit carotid body. J Physiol *450*, 33-61.

Dudkina, N.V., Kouril, R., Peters, K., Braun, H.P., and Boekema, E.J. (2010). Structure and function of mitochondrial supercomplexes. Biochim Biophys Acta *1797*, 664-670.

Eastman, R.T., and Fidock, D.A. (2009). Artemisinin-based combination therapies: a vital tool in efforts to eliminate malaria. Nat Rev Microbiol *7*, 864-874.

Eckers, E., Cyrklaff, M., Simpson, L., and Deponte, M. (2012). Mitochondrial protein import pathways are functionally conserved among eukaryotes despite compositional diversity of the import machineries. Biol Chem *393*, 513-524.

Eckstein-Ludwig, U., Webb, R.J., Van Goethem, I.D., East, J.M., Lee, A.G., Kimura, M., O'Neill, P.M., Bray, P.G., Ward, S.A., and Krishna, S. (2003). Artemisinins target the SERCA of Plasmodium falciparum. Nature *424*, 957-961.

Edgar, D., Shabalina, I., Camara, Y., Wredenberg, A., Calvaruso, M.A., Nijtmans, L., Nedergaard, J., Cannon, B., Larsson, N.G., and Trifunovic, A. (2009). Random point mutations with major effects on protein-coding genes are the driving force behind premature aging in mtDNA mutator mice. Cell Metab *10*, 131-138.

Egan, B., Beilharz, T., George, R., Isenmann, S., Gratzer, S., Wattenberg, B., and Lithgow, T. (1999). Targeting of tail-anchored proteins to yeast mitochondria in vivo. FEBS Lett *451*, 243-248.

Eggleson, K.K., Duffin, K.L., and Goldberg, D.E. (1999). Identification and characterization of falcilysin, a metallopeptidase involved in hemoglobin catabolism within the malaria parasite Plasmodium falciparum. J Biol Chem *274*, 32411-32417.

Ekland, E.H., and Fidock, D.A. (2008). In vitro evaluations of antimalarial drugs and their relevance to clinical outcomes. Int J Parasitol *38*, 743-747.

Ekvall, H. (2003). Malaria and anemia. Curr Opin Hematol *10*, 108-114.

Ellis, D.S., Li, Z.L., Gu, H.M., Peters, W., Robinson, B.L., Tovey, G., and Warhurst, D.C. (1985). The chemotherapy of rodent malaria, XXXIX. Ultrastructural changes following treatment with artemisinine of Plasmodium berghei infection in mice, with observations of the localization of [3H]-dihydroartemisinine in P. falciparum in vitro. Ann Trop Med Parasitol *79*, 367-374.

Esseiva, A.C., Naguleswaran, A., Hemphill, A., and Schneider, A. (2004). Mitochondrial tRNA import in Toxoplasma gondii. J Biol Chem *279*, 42363-42368.

Esser, K., Jan, P.S., Pratje, E., and Michaelis, G. (2004). The mitochondrial IMP peptidase of yeast: functional analysis of domains and identification of Gut2 as a new natural substrate. Mol Genet Genomics *271*, 616-626.

Esser, K., Tursun, B., Ingenhoven, M., Michaelis, G., and Pratje, E. (2002). A novel two-step mechanism for removal of a mitochondrial signal sequence involves the mAAA complex and the putative rhomboid protease Pcp1. J Mol Biol *323*, 835-843.

Eubel, H., Jansch, L., and Braun, H.P. (2003). New insights into the respiratory chain of plant mitochondria. Supercomplexes and a unique composition of complex II. Plant Physiol *133*, 274-286.

Falkevall, A., Alikhani, N., Bhushan, S., Pavlov, P.F., Busch, K., Johnson, K.A., Eneqvist, T., Tjernberg, L., Ankarcrona, M., and Glaser, E. (2006). Degradation of the amyloid beta-protein by the novel mitochondrial peptidasome, PreP. J Biol Chem *281*, 29096-29104.

Farkas, D.L., Wei, M.D., Febbroriello, P., Carson, J.H., and Loew, L.M. (1989). Simultaneous imaging of cell and mitochondrial membrane potentials. Biophys J *56*, 1053-1069.

Farnert, A., Lindberg, J., Gil, P., Swedberg, G., Berqvist, Y., Thapar, M.M., Lindegardh, N., Berezcky, S., and Bjorkman, A. (2003). Evidence of Plasmodium falciparum malaria resistant to atovaquone and proguanil hydrochloride: case reports. BMJ *326*, 628-629.

Feagin, J. (2000). Mitochondrial genome diversity in parasites. International Journal for Parasitology *30*, 371-390.

Feagin, J.E. (1992). The 6-kb element of Plasmodium falciparum encodes mitochondrial cytochrome genes. Mol Biochem Parasitol *52*, 145-148.

Feagin, J.E., and Drew, M.E. (1995). Plasmodium falciparum: alterations in organelle transcript abundance during the erythrocytic cycle. Exp Parasitol *80*, 430-440.

Feagin, J.E., Mericle, B.L., Werner, E., and Morris, M. (1997). Identification of additional rRNA fragments encoded by the Plasmodium falciparum 6 kb element. Nucleic Acids Res *25*, 438-446.

Feagin, J.E., Werner, E., Gardner, M.J., Williamson, D.H., and Wilson, R.J. (1992). Homologies between the contiguous and fragmented rRNAs of the two Plasmodium falciparum extrachromosomal DNAs are limited to core sequences. Nucleic Acids Res *20*, 879-887.

Feng, Y., Li, W., Li, J., Wang, J., Ge, J., Xu, D., Liu, Y., Wu, K., Zeng, Q., Wu, J.W.*, et al.* (2012). Structural insight into the type-II mitochondrial NADH dehydrogenases. Nature *491*, 478-482.

Fidock, D.A., Nomura, T., Talley, A.K., Cooper, R.A., Dzekunov, S.M., Ferdig, M.T., Ursos, L.M., Sidhu, A.B., Naude, B., Deitsch, K.W.*, et al.* (2000). Mutations in the P. falciparum digestive vacuole transmembrane protein PfCRT and evidence for their role in chloroquine resistance. Mol Cell *6*, 861-871.

Finn, R.D., Clements, J., and Eddy, S.R. (2011). HMMER web server: interactive sequence similarity searching. Nucleic Acids Res *39*, W29-37.

Fisher, N., Abd Majid, R., Antoine, T., Al-Helal, M., Warman, A.J., Johnson, D.J., Lawrenson, A.S., Ranson, H., O'Neill, P.M., Ward, S.A*., et al.* (2012). Cytochrome b mutation Y268S conferring the atovaquone resistance phenotype in the malaria parasite results in reduced parasite bc1 catalytic turnover and protein expression. J Biol Chem.

Fisher, N., Bourges, I., Hill, P., Brasseur, G., and Meunier, B. (2004a). Disruption of the interaction between the Rieske iron-sulfur protein and cytochrome b in the yeast bc1 complex owing to a human disease-associated mutation within cytochrome b. Eur J Biochem *271*, 1292-1298.

Fisher, N., Bray, P.G., Ward, S.A., and Biagini, G.A. (2007). The malaria parasite type II NADH:quinone oxidoreductase: an alternative enzyme for an alternative lifestyle. Trends Parasitol *23*, 305-310.

Fisher, N., Castleden, C.K., Bourges, I., Brasseur, G., Dujardin, G., and Meunier, B. (2004b). Human disease-related mutations in cytochrome b studied in yeast. J Biol Chem *279*, 12951-12958.

Fisher, N., and Meunier, B. (2005). Re-examination of inhibitor resistance conferred by Qo-site mutations in cytochrome b using yeast as a model system. Pest Manag Sci *61*, 973-978.

Fisher, N., and Meunier, B. (2008). Molecular basis of resistance to cytochrome bc1 inhibitors. FEMS Yeast Res *8*, 183-192.

Fisher, N., Warman, A.J., Ward, S.A., and Biagini, G.A. (2009). Chapter 17 Type II NADH: quinone oxidoreductases of Plasmodium falciparum and Mycobacterium tuberculosis kinetic and high-throughput assays. Methods Enzymol *456*, 303-320.

Fitch, C.D. (2004). Ferriprotoporphyrin IX, phospholipids, and the antimalarial actions of quinoline drugs. Life Sci *74*, 1957-1972.

Fivelman, Q.L., Butcher, G.A., Adagu, I.S., Warhurst, D.C., and Pasvol, G. (2002). Malarone treatment failure and in vitro confirmation of resistance of Plasmodium falciparum isolate from Lagos, Nigeria. Malar J *1*, 1.

Fivelman, Q.L., McRobert, L., Sharp, S., Taylor, C.J., Saeed, M., Swales, C.A., Sutherland, C.J., and Baker, D.A. (2007). Improved synchronous production of Plasmodium falciparum gametocytes in vitro. Molecular and Biochemical Parasitology *154*, 119-123.

Foote, S.J., Thompson, J.K., Cowman, A.F., and Kemp, D.J. (1989). Amplification of the multidrug resistance gene in some chloroquine-resistant isolates of P. falciparum. Cell *57*, 921-930.

Foth, B.J., Stimmler, L.M., Handman, E., Crabb, B.S., Hodder, A.N., and McFadden, G.I. (2005). The malaria parasite Plasmodium falciparum has only one pyruvate dehydrogenase complex, which is located in the apicoplast. Mol Microbiol *55*, 39-53.

Francis, S.E., Sullivan, D.J., Jr., and Goldberg, D.E. (1997). Hemoglobin metabolism in the malaria parasite Plasmodium falciparum. Annu Rev Microbiol *51*, 97-123.

Freeman, B.C., Myers, M.P., Schumacher, R., and Morimoto, R.I. (1995). Identification of a regulatory motif in Hsp70 that affects ATPase activity, substrate binding and interaction with HDJ-1. EMBO J *14*, 2281-2292.

Friesen, J., Borrmann, S., and Matuschewski, K. (2011). Induction of antimalaria immunity by pyrimethamine prophylaxis during exposure to sporozoites is curtailed by parasite resistance. Antimicrob Agents Chemother *55*, 2760-2767.

Fry, M., and Beesley, J.E. (1991). Mitochondria of mammalian Plasmodium spp. Parasitology *102 Pt 1*, 17-26.

Fry, M., and Pudney, M. (1992). Site of action of the antimalarial hydroxynaphthoquinone, 2-[trans-4-(4'-chlorophenyl) cyclohexyl]-3-hydroxy-1,4-naphthoquinone (566C80). Biochem Pharmacol *43*, 1545-1553.

Fry, M., Webb, E., and Pudney, M. (1990). Effect of mitochondrial inhibitors on adenosinetriphosphate levels in Plasmodium falciparum. Comp Biochem Physiol B *96*, 775-782.

Gabriel, K., Milenkovic, D., Chacinska, A., Muller, J., Guiard, B., Pfanner, N., and Meisinger, C. (2007). Novel mitochondrial intermembrane space proteins as substrates of the MIA import pathway. J Mol Biol *365*, 612-620.

Gakh, O., Cavadini, P., and Isaya, G. (2002). Mitochondrial processing peptidases. Biochim Biophys Acta *1592*, 63-77.

Gangwar, D., Kalita, M.K., Gupta, D., Chauhan, V.S., and Mohmmed, A. (2009). A systematic classification of Plasmodium falciparum P-loop NTPases: structural and functional correlation. Malar J *8*, 69.

Garah, F.B., Stigliani, J.L., Cosledan, F., Meunier, B., and Robert, A. (2009). Docking studies of structurally diverse antimalarial drugs targeting PfATP6: no correlation between in silico binding affinity and in vitro antimalarial activity. ChemMedChem *4*, 1469-1479.

Gardner, H.W. (1989). Oxygen radical chemistry of polyunsaturated fatty acids. Free Radic Biol Med *7*, 65-86.

Gardner, M.J., Bishop, R., Shah, T., de Villiers, E.P., Carlton, J.M., Hall, N., Ren, Q., Paulsen, I.T., Pain, A., Berriman, M.*, et al.* (2005). Genome sequence of Theileria parva, a bovine pathogen that transforms lymphocytes. Science *309*, 134-137.

Gardner, M.J., Hall, N., Fung, E., White, O., Berriman, M., Hyman, R.W., Carlton, J.M., Pain, A., Nelson, K.E., Bowman, S.*, et al.* (2002). Genome sequence of the human malaria parasite Plasmodium falciparum. Nature *419*, 498-511.

Gasser, S.M., Ohashi, A., Daum, G., Bohni, P.C., Gibson, J., Reid, G.A., Yonetani, T., and Schatz, G. (1982). Imported mitochondrial proteins cytochrome b2 and cytochrome c1 are processed in two steps. Proc Natl Acad Sci U S A *79*, 267-271.

Gautschi, M., Lilie, H., Funfschilling, U., Mun, A., Ross, S., Lithgow, T., Rucknagel, P., and Rospert, S. (2001). RAC, a stable ribosome-associated complex in yeast formed by the DnaK-DnaJ homologs Ssz1p and zuotin. Proc Natl Acad Sci U S A *98*, 3762-3767.

Gautschi, M., Mun, A., Ross, S., and Rospert, S. (2002). A functional chaperone triad on the yeast ribosome. Proc Natl Acad Sci U S A *99*, 4209-4214.

Gavel, Y., and von Heijne, G. (1990). Cleavage-site motifs in mitochondrial targeting peptides. Protein Eng *4*, 33-37.

Gazarini, M.L., and Garcia, C.R. (2004). The malaria parasite mitochondrion senses cytosolic Ca2+ fluctuations. Biochem Biophys Res Commun *321*, 138-144.

Gentle, I.E., Perry, A.J., Alcock, F.H., Likic, V.A., Dolezal, P., Ng, E.T., Purcell, A.W., McConnville, M., Naderer, T., Chanez, A.L.*, et al.* (2007). Conserved motifs reveal details of ancestry and structure in the small TIM chaperones of the mitochondrial intermembrane space. Mol Biol Evol *24*, 1149-1160.

Genton, B., Betuela, I., Felger, I., Al-Yaman, F., Anders, R.F., Saul, A., Rare, L., Baisor, M., Lorry, K., Brown, G.V.*, et al.* (2002). A recombinant blood-stage malaria vaccine reduces Plasmodium falciparum density and exerts selective pressure on parasite populations in a phase 1-2b trial in Papua New Guinea. J Infect Dis *185*, 820-827.

Ginger, M.L. (2006). Niche metabolism in parasitic protozoa. Philos Trans R Soc Lond B Biol Sci *361*, 101-118.

Girard, M.P., Reed, Z.H., Friede, M., and Kieny, M.P. (2007). A review of human vaccine research and development: malaria. Vaccine *25*, 1567-1580.

Glaser, E., and Whelan, J. (2007). Import of Nuclear-Encoded Mitochondrial Proteins. In Annual Plant Reviews Volume 31: Plant Mitochondria (John Wiley & Sons, Inc.), pp. 97-140.

Goldberg, D.E. (2005). Hemoglobin degradation. Curr Top Microbiol Immunol *295*, 275-291.

Golenser, J., Domb, A., Leshem, B., Kremsner, P., and Luty, A. (2003). Iron chelators as drugs against malaria pose a potential risk. Redox Rep *8*, 268-271.

Golenser, J., Waknine, J.H., Krugliak, M., Hunt, N.H., and Grau, G.E. (2006). Current perspectives on the mechanism of action of artemisinins. Int J Parasitol *36*, 1427-1441.

Gomez, L.A., Monette, J.S., Chavez, J.D., Maier, C.S., and Hagen, T.M. (2009). Supercomplexes of the mitochondrial electron transport chain decline in the aging rat heart. Arch Biochem Biophys *490*, 30-35.

Gosoniu, L., Vounatsou, P., Tami, A., Nathan, R., Grundmann, H., and Lengeler, C. (2008). Spatial effects of mosquito bednets on child mortality. BMC Public Health *8*, 356.

Graham, S.M., Molyneux, E.M., Walsh, A.L., Cheesbrough, J.S., Molyneux, M.E., and Hart, C.A. (2000). Nontyphoidal Salmonella infections of children in tropical Africa. Pediatr Infect Dis J *19*, 1189-1196.

Grassi, G. (1900). Studi di uno Zoologo Sulla Malaria.

Gravitz, L. (2012). Vector control: The last bite. Nature *484*, S26-S27.

Gray, M.W., Lang, B.F., and Burger, G. (2004). Mitochondria of protists. Annu Rev Genet *38*, 477-524.

Greenstock, C.L., and Miller, R.W. (1975). The oxidation of tiron by superoxide anion. Kinetics of the reaction in aqueous solution in chloroplasts. Biochim Biophys Acta *396*, 11-16.

Greenwood, B.M., Fidock, D.A., Kyle, D.E., Kappe, S.H., Alonso, P.L., Collins, F.H., and Duffy, P.E. (2008). Malaria: progress, perils, and prospects for eradication. J Clin Invest *118*, 1266-1276.

Gregson, A., and Plowe, C.V. (2005). Mechanisms of Resistance of Malaria Parasites to Antifolates. Pharmacological Reviews *57*, 117-145.

Gu, H.M., Warhurst, D.C., and Peters, W. (1984). Uptake of [3H] dihydroartemisinine by erythrocytes infected with Plasmodium falciparum in vitro. Trans R Soc Trop Med Hyg *78*, 265-270.

Guest, J.R. (1981). Partial replacement of succinate dehydrogenase function by phage- and plasmid-specified fumarate reductase in Escherichia coli. J Gen Microbiol *122*, 171-179.

Gujjar, R., El Mazouni, F., White, K.L., White, J., Creason, S., Shackleford, D.M., Deng, X., Charman, W.N., Bathurst, I., Burrows, J.*, et al.* (2011). Lead optimization of aryl and aralkyl amine-based triazolopyrimidine inhibitors of Plasmodium falciparum dihydroorotate dehydrogenase with antimalarial activity in mice. J Med Chem *54*, 3935-3949.

Gutman, J., Kachur, S.P., Slutsker, L., Nzila, A., and Mutabingwa, T. (2012). Combination of probenecid-sulphadoxine-pyrimethamine for intermittent preventive treatment in pregnancy. Malar J *11*, 39.

Gutteridge, J.M., and Bannister, J.V. (1986). Copper + zinc and manganese superoxide dismutases inhibit deoxyribose degradation by the superoxide-driven Fenton reaction at two different stages. Implications for the redox states of copper and manganese. Biochem J *234*, 225-228.

Gutteridge, W.E., Dave, D., and Richards, W.H. (1979). Conversion of dihydroorotate to orotate in parasitic protozoa. Biochim Biophys Acta *582*, 390-401.

Hachiya, N., Alam, R., Sakasegawa, Y., Sakaguchi, M., Mihara, K., and Omura, T. (1993). A mitochondrial import factor purified from rat liver cytosol is an ATP-dependent conformational modulator for precursor proteins. EMBO J *12*, 1579-1586.

Hachiya, N., Komiya, T., Alam, R., Iwahashi, J., Sakaguchi, M., Omura, T., and Mihara, K. (1994). MSF, a novel cytoplasmic chaperone which functions in precursor targeting to mitochondria. EMBO J *13*, 5146-5154.

Hagerhall, C. (1997). Succinate: quinone oxidoreductases. Variations on a conserved theme. Biochim Biophys Acta *1320*, 107-141.

Hammond, D.J., Burchell, J.R., and Pudney, M. (1985). Inhibition of pyrimidine biosynthesis de novo in Plasmodium falciparum by 2-(4-t-butylcyclohexyl)-3-hydroxy-1,4-naphthoquinone in vitro. Mol Biochem Parasitol *14*, 97-109.

Hanssen, E., McMillan, P.J., and Tilley, L. (2010). Cellular architecture of Plasmodium falciparum-infected erythrocytes. Int J Parasitol *40*, 1127-1135.

Hartgers, F.C., and Yazdanbakhsh, M. (2006). Co-infection of helminths and malaria: modulation of the immune responses to malaria. Parasite Immunol *28*, 497-506.

Hartman, D.J., Hoogenraad, N.J., Condron, R., and Hoj, P.B. (1992). Identification of a mammalian 10-kDa heat shock protein, a mitochondrial chaperonin 10 homologue essential for assisted folding of trimeric ornithine transcarbamoylase in vitro. Proc Natl Acad Sci U S A *89*, 3394-3398.

Hartwig, C.L., Rosenthal, A.S., D'Angelo, J., Griffin, C.E., Posner, G.H., and Cooper, R.A. (2009). Accumulation of artemisinin trioxane derivatives within neutral lipids of Plasmodium falciparum malaria parasites is endoperoxide-dependent. Biochem Pharmacol *77*, 322-336.

Hatch, L.P., Cox, G.B., and Howitt, S.M. (1995). The essential arginine residue at position 210 in the alpha subunit of the Escherichia coli ATP synthase can be transferred to position 252 with partial retention of activity. J Biol Chem *270*, 29407-29412.

Haucke, V., Ocana, C.S., Honlinger, A., Tokatlidis, K., Pfanner, N., and Schatz, G. (1997). Analysis of the sorting signals directing NADH-cytochrome b5 reductase to two locations within yeast mitochondria. Mol Cell Biol *17*, 4024-4032.

Hawking, F., Wilson, M.E., and Gammage, K. (1971). Evidence for cyclic development and short-lived maturity in the gametocytes of Plasmodium falciparum. Transactions of the Royal Society of Tropical Medicine and Hygiene *65*, 549-559.

Hay, S.I., Guerra, C.A., Gething, P.W., Patil, A.P., Tatem, A.J., Noor, A.M., Kabaria, C.W., Manh, B.H., Elyazar, I.R., Brooker, S*., et al.* (2009). A world malaria map: Plasmodium falciparum endemicity in 2007. PLoS Med *6*, e1000048.

Hayashi, M., Yamada, H., Mitamura, T., Horii, T., Yamamoto, A., and Moriyama, Y. (2000). Vacuolar H(+)-ATPase localized in plasma membranes of malaria parasite cells, Plasmodium falciparum, is involved in regional acidification of parasitized erythrocytes. J Biol Chem *275*, 34353-34358.

Haynes, R.K., Chan, W.C., Lung, C.M., Uhlemann, A.C., Eckstein, U., Taramelli, D., Parapini, S., Monti, D., and Krishna, S. (2007). The Fe2+-mediated decomposition, PfATP6 binding, and antimalarial activities of artemisone and other artemisinins: the unlikelihood of C-centered radicals as bioactive intermediates. ChemMedChem *2*, 1480-1497.

Haynes, R.K., Chan, W.C., Wong, H.N., Li, K.Y., Wu, W.K., Fan, K.M., Sung, H.H., Williams, I.D., Prosperi, D., Melato, S*., et al.* (2010). Facile oxidation of leucomethylene blue and dihydroflavins by artemisinins: relationship with flavoenzyme function and antimalarial mechanism of action. ChemMedChem *5*, 1282-1299.

Haynes, R.K., Ho, W.Y., Chan, H.W., Fugmann, B., Stetter, J., Croft, S.L., Vivas, L., Peters, W., and Robinson, B.L. (2004). Highly antimalaria-active artemisinin derivatives: biological activity does not correlate with chemical reactivity. Angew Chem Int Ed Engl *43*, 1381-1385.

Haynes, R.K., and Krishna, S. (2004). Artemisinins: activities and actions. Microbes and Infection *6*, 1339-1346.

Haynes, R.K., Monti, D., Taramelli, D., Basilico, N., Parapini, S., and Olliaro, P. (2003). Artemisinin antimalarials do not inhibit hemozoin formation. Antimicrob Agents Chemother *47*, 1175.

Haynes, R.K., Pai, H.H.-O., and Voerste, A. (1999). Ring opening of artemisinin (qinghaosu) and dihydroartemisinin and interception of the open hydroperoxides with Formation of N-oxides — a chemical model for antimalarial mode of action. Tetrahedron Letters *40*, 4715-4718.

Heinemeyer, J., Braun, H.P., Boekema, E.J., and Kouril, R. (2007). A structural model of the cytochrome C reductase/oxidase supercomplex from yeast mitochondria. J Biol Chem *282*, 12240-12248.

Hell, K., Neupert, W., and Stuart, R.A. (2001). Oxa1p acts as a general membrane insertion machinery for proteins encoded by mitochondrial DNA. EMBO J *20*, 1281-1288.

Henriquez, F.L., Richards, T.A., Roberts, F., McLeod, R., and Roberts, C.W. (2005). The unusual mitochondrial compartment of Cryptosporidium parvum. Trends Parasitol *21*, 68-74.

Henry, M., Briolant, S., Zettor, A., Pelleau, S., Baragatti, M., Baret, E., Mosnier, J., Amalvict, R., Fusai, T., Rogier, C*., et al.* (2009). Plasmodium falciparum Na+/H+ exchanger 1 transporter

is involved in reduced susceptibility to quinine. Antimicrob Agents Chemother *53*, 1926-1930.

Herlan, M., Vogel, F., Bornhovd, C., Neupert, W., and Reichert, A.S. (2003). Processing of Mgm1 by the rhomboid-type protease Pcp1 is required for maintenance of mitochondrial morphology and of mitochondrial DNA. J Biol Chem *278*, 27781-27788.

Hermsen, C.C., Verhage, D.F., Telgt, D.S., Teelen, K., Bousema, J.T., Roestenberg, M., Bolad, A., Berzins, K., Corradin, G., Leroy, O*., et al.* (2007). Glutamate-rich protein (GLURP) induces antibodies that inhibit in vitro growth of Plasmodium falciparum in a phase 1 malaria vaccine trial. Vaccine *25*, 2930-2940.

Hewitt, V., Alcock, F., and Lithgow, T. (2011). Minor modifications and major adaptations: the evolution of molecular machines driving mitochondrial protein import. Biochim Biophys Acta *1808*, 947-954.

Hikosaka, K., Watanabe, Y., Kobayashi, F., Waki, S., Kita, K., and Tanabe, K. (2011). Highly conserved gene arrangement of the mitochondrial genomes of 23 Plasmodium species. Parasitol Int *60*, 175-180.

Hino, A., Hirai, M., Tanaka, T.Q., Watanabe, Y.I., Matsuoka, H., and Kita, K. (2012). Critical roles of the mitochondrial complex II in oocyst formation of rodent malaria parasite Plasmodium berghei. J Biochem.

Hisaeda, H., Stowers, A.W., Tsuboi, T., Collins, W.E., Sattabongkot, J.S., Suwanabun, N., Torii, M., and Kaslow, D.C. (2000). Antibodies to malaria vaccine candidates Pvs25 and Pvs28 completely block the ability of Plasmodium vivax to infect mosquitoes. Infect Immun *68*, 6618-6623.

Hofmann, K. (2000). Sensitive protein comparisons with profiles and hidden Markov models. Brief Bioinform *1*, 167-178.

Hoppins, S.C., and Nargang, F.E. (2004). The Tim8-Tim13 complex of Neurospora crassa functions in the assembly of proteins into both mitochondrial membranes. J Biol Chem *279*, 12396-12405.

Horsefield, R., Iwata, S., and Byrne, B. (2004). Complex II from a structural perspective. Curr Protein Pept Sci *5*, 107-118.

Horsefield, R., Yankovskaya, V., Sexton, G., Whittingham, W., Shiomi, K., Omura, S., Byrne, B., Cecchini, G., and Iwata, S. (2006). Structural and computational analysis of the quinone-binding site of complex II (succinate-ubiquinone oxidoreductase): a mechanism of electron transfer and proton conduction during ubiquinone reduction. J Biol Chem *281*, 7309-7316.

Horwich, A.L., Kalousek, F., Mellman, I., and Rosenberg, L.E. (1985). A leader peptide is sufficient to direct mitochondrial import of a chimeric protein. EMBO J *4*, 1129-1135.

Howells, R.E. (1970). Cytochrome oxidase activity in a normal and some drug-resistant strains of Plasmodium berghei--a cytochemical study. II. Sporogonic stages of a drug-sensitive srain. Ann Trop Med Parasitol *64*, 223-225.

Howells, R.E., Peters, W., and Fullard, J. (1969). Cytochrome oxidase activity in a normal and some drug-resistant strains of Plasmodium berghei--a cytochemical study. I. Asexual erythrocytic stages. Mil Med *134*, 893-915.

Huang, L.-s., Sun, G., Cobessi, D., Wang, A.C., Shen, J.T., Tung, E.Y., Anderson, V.E., and Berry, E.A. (2006). 3-Nitropropionic Acid Is a Suicide Inhibitor of Mitochondrial Respiration That, upon Oxidation by Complex II, Forms a Covalent Adduct with a Catalytic Base Arginine in the Active Site of the Enzyme. Journal of Biological Chemistry *281*, 5965-5972.

Hudson, A.T., Dickins, M., Ginger, C.D., Gutteridge, W.E., Holdich, T., Hutchinson, D.B., Pudney, M., Randall, A.W., and Latter, V.S. (1991). 566C80: a potent broad spectrum anti-infective agent with activity against malaria and opportunistic infections in AIDS patients. Drugs Exp Clin Res *17*, 427-435.

Hudson, A.T., Randall, A.W., Fry, M., Ginger, C.D., Hill, B., Latter, V.S., McHardy, N., and Williams, R.B. (1985). Novel anti-malarial hydroxynaphthoquinones with potent broad spectrum anti-protozoal activity. Parasitology *90 (Pt 1)*, 45-55.

Hunte, C., Palsdottir, H., and Trumpower, B.L. (2003). Protonmotive pathways and mechanisms in the cytochrome bc1 complex. FEBS Lett *545*, 39-46.

Hurt, D.E., Widom, J., and Clardy, J. (2006). Structure of Plasmodium falciparum dihydroorotate dehydrogenase with a bound inhibitor. Acta Crystallogr D Biol Crystallogr *62*, 312-323.

Hurt, E.C., Pesold-Hurt, B., and Schatz, G. (1984). The cleavable prepiece of an imported mitochondrial protein is sufficient to direct cytosolic dihydrofolate reductase into the mitochondrial matrix. FEBS Lett *178*, 306-310.

Hutu, D.P., Guiard, B., Chacinska, A., Becker, D., Pfanner, N., Rehling, P., and van der Laan, M. (2008). Mitochondrial protein import motor: differential role of Tim44 in the recruitment of Pam17 and J-complex to the presequence translocase. Mol Biol Cell *19*, 2642-2649.

Hyde, J.E. (2007a). Drug-resistant malaria - an insight. FEBS J *274*, 4688-4698.

Hyde, J.E. (2007b). Targeting purine and pyrimidine metabolism in human apicomplexan parasites. Curr Drug Targets *8*, 31-47.

Isaya, G., Miklos, D., and Rollins, R.A. (1994). MIP1, a new yeast gene homologous to the rat mitochondrial intermediate peptidase gene, is required for oxidative metabolism in Saccharomyces cerevisiae. Mol Cell Biol *14*, 5603-5616.

Ishmukhametov, R.R., Pond, J.B., Al-Huqail, A., Galkin, M.A., and Vik, S.B. (2008). ATP synthesis without R210 of subunit a in the Escherichia coli ATP synthase. Biochim Biophys Acta *1777*, 32-38.

Ittarat, I., Asawamahasakda, W., and Meshnick, S.R. (1994). The effects of antimalarials on the Plasmodium falciparum dihydroorotate dehydrogenase. Exp Parasitol *79*, 50-56.

Iwata, S., Lee, J.W., Okada, K., Lee, J.K., Iwata, M., Rasmussen, B., Link, T.A., Ramaswamy, S., and Jap, B.K. (1998). Complete structure of the 11-subunit bovine mitochondrial cytochrome bc1 complex. Science *281*, 64-71.

Izumo, A., Tanabe, K., and Kato, M. (1988). The plasma membrane and mitochondrial membrane potentials of Plasmodium yoelii. Comp Biochem Physiol B *91*, 735-739.

Jambou, R., Legrand, E., Niang, M., Khim, N., Lim, P., Volney, B., Ekala, M.T., Bouchier, C., Esterre, P., Fandeur, T.*, et al.* (2005). Resistance of Plasmodium falciparum field isolates to in-vitro artemether and point mutations of the SERCA-type PfATPase6. Lancet *366*, 1960-1963.

Jensen, M.D., Conley, M., and Helstowski, L.D. (1983). Culture of Plasmodium falciparum: the role of pH, glucose, and lactate. J Parasitol *69*, 1060-1067.

Jiang, J.B., Jacobs, G., Liang, D.S., and Aikawa, M. (1985). Qinghaosu-induced changes in the morphology of Plasmodium inui. Am J Trop Med Hyg *34*, 424-428.

Jindal, S., Dudani, A.K., Singh, B., Harley, C.B., and Gupta, R.S. (1989). Primary structure of a human mitochondrial protein homologous to the bacterial and plant chaperonins and to the 65-kilodalton mycobacterial antigen. Mol Cell Biol *9*, 2279-2283.

Johnston, A.J., Hoogenraad, J., Dougan, D.A., Truscott, K.N., Yano, M., Mori, M., Hoogenraad, N.J., and Ryan, M.T. (2002). Insertion and assembly of human tom7 into the preprotein translocase complex of the outer mitochondrial membrane. J Biol Chem *277*, 42197-42204.

Juhnke, H.D., Hiltscher, H., Nasiri, H.R., Schwalbe, H., and Lancaster, C.R. (2009). Production, characterization and determination of the real catalytic properties of the putative 'succinate dehydrogenase' from Wolinella succinogenes. Mol Microbiol *71*, 1088-1101.

Kaiser, M., Wittlin, S., Nehrbass-Stuedli, A., Dong, Y., Wang, X., Hemphill, A., Matile, H., Brun, R., and Vennerstrom, J.L. (2007). Peroxide bond-dependent antiplasmodial specificity of artemisinin and OZ277 (RBx11160). Antimicrob Agents Chemother *51*, 2991-2993.

Kambacheld, M., Augustin, S., Tatsuta, T., Muller, S., and Langer, T. (2005). Role of the novel metallopeptidase Mop112 and saccharolysin for the complete degradation of proteins residing in different subcompartments of mitochondria. J Biol Chem *280*, 20132-20139.

Kamchonwongpaisan, S., Chandra-ngam, G., Avery, M.A., and Yuthavong, Y. (1994). Resistance to artemisinin of malaria parasites (Plasmodium falciparum) infecting alpha-thalassemic erythrocytes in vitro. Competition in drug accumulation with uninfected erythrocytes. J Clin Invest *93*, 467-473.

Kamchonwongpaisan, S., and Meshnick, S.R. (1996). The mode of action of the antimalarial artemisinin and its derivatives. Gen Pharmacol *27*, 587-592.

Kang, P.J., Ostermann, J., Shilling, J., Neupert, W., Craig, E.A., and Pfanner, N. (1990). Requirement for hsp70 in the mitochondrial matrix for translocation and folding of precursor proteins. Nature *348*, 137-143.

Kannan, R., Sahal, D., and Chauhan, V.S. (2002). Heme-artemisinin adducts are crucial mediators of the ability of artemisinin to inhibit heme polymerization. Chem Biol *9*, 321-332.

Karunajeewa, H. (2012). Artemisinins: Artemisinin, Dihydroartemisinin, Artemether and Artesunate.

Kawahara, K., Mogi, T., Tanaka, T.Q., Hata, M., Miyoshi, H., and Kita, K. (2009). Mitochondrial dehydrogenases in the aerobic respiratory chain of the rodent malaria parasite Plasmodium yoelii yoelii. J Biochem *145*, 229-237.

Kawai, S., Kano, S., and Suzuki, M. (1993). Morphologic effects of artemether on Plasmodium falciparum in Aotus trivirgatus. Am J Trop Med Hyg *49*, 812-818.

Kerscher, S.J. (2000). Diversity and origin of alternative NADH:ubiquinone oxidoreductases. Biochim Biophys Acta *1459*, 274-283.

Kessl, J.J., Ha, K.H., Merritt, A.K., Lange, B.B., Hill, P., Meunier, B., Meshnick, S.R., and Trumpower, B.L. (2005). Cytochrome b mutations that modify the ubiquinol-binding pocket of the cytochrome bc1 complex and confer anti-malarial drug resistance in Saccharomyces cerevisiae. J Biol Chem *280*, 17142-17148.

Kessl, J.J., Lange, B.B., Merbitz-Zahradnik, T., Zwicker, K., Hill, P., Meunier, B., Palsdottir, H., Hunte, C., Meshnick, S., and Trumpower, B.L. (2003). Molecular basis for atovaquone binding to the cytochrome bc1 complex. J Biol Chem *278*, 31312-31318.

Kessl, J.J., Meshnick, S.R., and Trumpower, B.L. (2007). Modeling the molecular basis of atovaquone resistance in parasites and pathogenic fungi. Trends Parasitol *23*, 494-501.

Kita, K., Miyadera, H., Saruta, F., and Miyoshi, H. (2001). Parasite Mitochondria as a Target for Chemotherapy. Journal of Health Science *47*, 219-239.

Klayman, D.L. (1985). Qinghaosu (artemisinin): an antimalarial drug from China. Science *228*, 1049-1055.

Klodmann, J., Sunderhaus, S., Nimtz, M., Jansch, L., and Braun, H.P. (2010). Internal architecture of mitochondrial complex I from Arabidopsis thaliana. Plant Cell *22*, 797-810.

Koehler, C.M., Jarosch, E., Tokatlidis, K., Schmid, K., Schweyen, R.J., and Schatz, G. (1998a). Import of mitochondrial carriers mediated by essential proteins of the intermembrane space. Science *279*, 369-373.

Koehler, C.M., Leuenberger, D., Merchant, S., Renold, A., Junne, T., and Schatz, G. (1999). Human deafness dystonia syndrome is a mitochondrial disease. Proc Natl Acad Sci U S A *96*, 2141-2146.

Koehler, C.M., Merchant, S., Oppliger, W., Schmid, K., Jarosch, E., Dolfini, L., Junne, T., Schatz, G., and Tokatlidis, K. (1998b). Tim9p, an essential partner subunit of Tim10p for the import of mitochondrial carrier proteins. EMBO J *17*, 6477-6486.

Koehler, C.M., Murphy, M.P., Bally, N.A., Leuenberger, D., Oppliger, W., Dolfini, L., Junne, T., Schatz, G., and Or, E. (2000). Tim18p, a new subunit of the TIM22 complex that mediates insertion of imported proteins into the yeast mitochondrial inner membrane. Mol Cell Biol *20*, 1187-1193.

Kohler, R., Boehringer, D., Greber, B., Bingel-Erlenmeyer, R., Collinson, I., Schaffitzel, C., and Ban, N. (2009). YidC and Oxa1 form dimeric insertion pores on the translating ribosome. Mol Cell *34*, 344-353.

Koonin, E.V., Makarova, K.S., Rogozin, I.B., Davidovic, L., Letellier, M.C., and Pellegrini, L. (2003). The rhomboids: a nearly ubiquitous family of intramembrane serine proteases that probably evolved by multiple ancient horizontal gene transfers. Genome Biol *4*, R19.

Koplin, A., Preissler, S., Ilina, Y., Koch, M., Scior, A., Erhardt, M., and Deuerling, E. (2010). A dual function for chaperones SSB-RAC and the NAC nascent polypeptide-associated complex on ribosomes. J Cell Biol *189*, 57-68.

Korenromp, E.L., Williams, B.G., de Vlas, S.J., Gouws, E., Gilks, C.F., Ghys, P.D., and Nahlen, B.L. (2005). Malaria attributable to the HIV-1 epidemic, sub-Saharan Africa. Emerg Infect Dis *11*, 1410-1419.

Korsinczky, M., Chen, N., Kotecka, B., Saul, A., Rieckmann, K., and Cheng, Q. (2000). Mutations in Plasmodium falciparum cytochrome b that are associated with atovaquone resistance are located at a putative drug-binding site. Antimicrob Agents Chemother *44*, 2100-2108.

Kozany, C., Mokranjac, D., Sichting, M., Neupert, W., and Hell, K. (2004). The J domain-related cochaperone Tim16 is a constituent of the mitochondrial TIM23 preprotein translocase. Nat Struct Mol Biol *11*, 234-241.

Kozjak, V., Wiedemann, N., Milenkovic, D., Lohaus, C., Meyer, H.E., Guiard, B., Meisinger, C., and Pfanner, N. (2003). An essential role of Sam50 in the protein sorting and assembly machinery of the mitochondrial outer membrane. J Biol Chem *278*, 48520-48523.

Kremsner, P.G., and Krishna, S. (2004). Antimalarial combinations. Lancet *364*, 285-294.

Krishna, S., and Staines, H. (2012). Non-Antifolate Antibiotics: Clindamycin, Doxycycline, Azithromycin and Fosmidomycin.

Krotoski, W.A., Collins, W.E., Bray, R.S., Garnham, P.C., Cogswell, F.B., Gwadz, R.W., Killick-Kendrick, R., Wolf, R., Sinden, R., Koontz, L.C*., et al.* (1982). Demonstration of hypnozoites in sporozoite-transmitted Plasmodium vivax infection. Am J Trop Med Hyg *31*, 1291-1293.

Krungkrai, J. (1995). Purification, characterization and localization of mitochondrial dihydroorotate dehydrogenase in Plasmodium falciparum, human malaria parasite. Biochim Biophys Acta *1243*, 351-360.

Krungkrai, J., Burat, D., Kudan, S., Krungkrai, S., and Prapunwattana, P. (1999). Mitochondrial oxygen consumption in asexual and sexual blood stages of the human malarial parasite, Plasmodium falciparum. Southeast Asian J Trop Med Public Health *30*, 636-642.

Krungkrai, J., Krungkrai, S.R., and Bhumiratana, A. (1993). Plasmodium berghei: partial purification and characterization of the mitochondrial cytochrome c oxidase. Exp Parasitol *77*, 136-146.

Krungkrai, J., Krungkrai, S.R., and Phakanont, K. (1992). Antimalarial activity of orotate analogs that inhibit dihydroorotase and dihydroorotate dehydrogenase. Biochem Pharmacol *43*, 1295-1301.

Krungkrai, J., Krungkrai, S.R., Suraveratum, N., and Prapunwattana, P. (1997). Mitochondrial ubiquinol-cytochrome c reductase and cytochrome c oxidase: chemotherapeutic targets in malarial parasites. Biochem Mol Biol Int *42*, 1007-1014.

Krungkrai, J., Prapunwattana, P., and Krungkrai, S.R. (2000). Ultrastructure and function of mitochondria in gametocytic stage of Plasmodium falciparum. Parasite *7*, 19-26.

Krungkrai, S.R., and Yuthavong, Y. (1987). The antimalarial action on Plasmodium falciparum of qinghaosu and artesunate in combination with agents which modulate oxidant stress. Trans R Soc Trop Med Hyg *81*, 710-714.

Kublin, J.G., Dzinjalamala, F.K., Kamwendo, D.D., Malkin, E.M., Cortese, J.F., Martino, L.M., Mukadam, R.A., Rogerson, S.J., Lescano, A.G., Molyneux, M.E*., et al.* (2002). Molecular markers for failure of sulfadoxine-pyrimethamine and chlorproguanil-dapsone treatment of Plasmodium falciparum malaria. J Infect Dis *185*, 380-388.

Kuboyama, M., Yong, F.C., and King, T.E. (1972). Studies on cytochrome oxidase. 8. Preparation and some properties of cardiac cytochrome oxidase. J Biol Chem *247*, 6375-6383.

Kumar, R., Adams, B., Musiyenko, A., Shulyayeva, O., and Barik, S. (2005). The FK506-binding protein of the malaria parasite, Plasmodium falciparum, is a FK506-sensitive chaperone

with FK506-independent calcineurin-inhibitory activity. Mol Biochem Parasitol *141*, 163-173.

Kwiatkowski, D.P. (2005). How malaria has affected the human genome and what human genetics can teach us about malaria. Am J Hum Genet *77*, 171-192.

Laemmli, U.K. (1970). Cleavage of structural proteins during the assembly of the head of bacteriophage T4. Nature *227*, 680-685.

Laishram, D.D., Sutton, P.L., Nanda, N., Sharma, V.L., Sobti, R.C., Carlton, J.M., and Joshi, H. (2012). The complexities of malaria disease manifestations with a focus on asymptomatic malaria. Malar J *11*, 29.

Lakshmanan, V., Bray, P.G., Verdier-Pinard, D., Johnson, D.J., Horrocks, P., Muhle, R.A., Alakpa, G.E., Hughes, R.H., Ward, S.A., Krogstad, D.J*., et al.* (2005). A critical role for PfCRT K76T in Plasmodium falciparum verapamil-reversible chloroquine resistance. EMBO J *24*, 2294-2305.

Lalloo, D.G., and Hill, D.R. (2008). Preventing malaria in travellers. BMJ *336*, 1362-1366.

Lambros, C., and Vanderberg, J.P. (1979). Synchronization of Plasmodium falciparum erythrocytic stages in culture. J Parasitol *65*, 418-420.

Lange, C., and Hunte, C. (2002). Crystal structure of the yeast cytochrome bc1 complex with its bound substrate cytochrome c. Proc Natl Acad Sci U S A *99*, 2800-2805.

Lange, H., Kaut, A., Kispal, G., and Lill, R. (2000). A mitochondrial ferredoxin is essential for biogenesis of cellular iron-sulfur proteins. Proc Natl Acad Sci U S A *97*, 1050-1055.

Langer, T. (2000). AAA proteases: cellular machines for degrading membrane proteins. Trends Biochem Sci *25*, 247-251.

Langreth, S.G., Jensen, J.B., Reese, R.T., and Trager, W. (1978). Fine structure of human malaria in vitro. J Protozool *25*, 443-452.

Laveran, A. (1881). Un nouveau parasite trouvé dans le sang de malades atteints de fièvre palustre. Origine parasitaire des accidents de l'impaludisme. Bull Mém Soc Méd Hôpitaux Paris *17*, 158-164.

Ledesma, A., de Lacoba, M.G., and Rial, E. (2002). The mitochondrial uncoupling proteins. Genome Biol *3*, REVIEWS3015.

Lehane, A.M., Saliba, K.J., Allen, R.J., and Kirk, K. (2004). Choline uptake into the malaria parasite is energized by the membrane potential. Biochem Biophys Res Commun *320*, 311-317.

Lemberg, M.K., Menendez, J., Misik, A., Garcia, M., Koth, C.M., and Freeman, M. (2005). Mechanism of intramembrane proteolysis investigated with purified rhomboid proteases. EMBO J *24*, 464-472.

Lengeler, C. (2000). Insecticide-treated bednets and curtains for preventing malaria. Cochrane Database Syst Rev, CD000363.

Leonhard, K., Herrmann, J.M., Stuart, R.A., Mannhaupt, G., Neupert, W., and Langer, T. (1996). AAA proteases with catalytic sites on opposite membrane surfaces comprise a proteolytic system for the ATP-dependent degradation of inner membrane proteins in mitochondria. EMBO J *15*, 4218-4229.

Leung, S.C., Gibbons, P., Amewu, R., Nixon, G.L., Pidathala, C., Hong, W.D., Pacorel, B., Berry, N.G., Sharma, R., Stocks, P.A*., et al.* (2012). Identification, design and biological evaluation of heterocyclic quinolones targeting Plasmodium falciparum type II NADH:quinone oxidoreductase (PfNDH2). J Med Chem *55*, 1844-1857.

Li, W., Mo, W., Shen, D., Sun, L., Wang, J., Lu, S., Gitschier, J.M., and Zhou, B. (2005). Yeast model uncovers dual roles of mitochondria in action of artemisinin. PLoS Genet *1*, e36.

Li, Y., Dudek, J., Guiard, B., Pfanner, N., Rehling, P., and Voos, W. (2004). The presequence translocase-associated protein import motor of mitochondria. Pam16 functions in an antagonistic manner to Pam18. J Biol Chem *279*, 38047-38054.

Lingelbach, K., and Joiner, K.A. (1998). The parasitophorous vacuole membrane surrounding Plasmodium and Toxoplasma: an unusual compartment in infected cells. J Cell Sci *111 (Pt 11)*, 1467-1475.

Lister, R., Carrie, C., Duncan, O., Ho, L.H., Howell, K.A., Murcha, M.W., and Whelan, J. (2007). Functional definition of outer membrane proteins involved in preprotein import into mitochondria. Plant Cell *19*, 3739-3759.

Liu, Q., D'Silva, P., Walter, W., Marszalek, J., and Craig, E.A. (2003). Regulated cycling of mitochondrial Hsp70 at the protein import channel. Science *300*, 139-141.

Lloyd, D., Harris, J.C., Maroulis, S., Biagini, G.A., Wadley, R.B., Turner, M.P., and Edwards, M.R. (2000). The microaerophilic flagellate Giardia intestinalis: oxygen and its reaction products collapse membrane potential and cause cytotoxicity. Microbiology *146 Pt 12*, 3109-3118.

Loew, L.M. (1998). Measuring membrane potential in single cells with confocal microscopy. In Cell Biology: A Laboratory Handbook, Vol 3 J E Celis, editor Academic Press, San Diego, 375-379.

Loew, L.M., Tuft, R.A., Carrington, W., and Fay, F.S. (1993). Imaging in five dimensions: time-dependent membrane potentials in individual mitochondria. Biophys J *65*, 2396-2407.

Looareesuwan, S., Bunnag, D., and Harinasuta, T. (1990). The Textbook of Tropical Medicine. Ruamthasa Publishers *39-44*.

Looareesuwan, S., Viravan, C., Webster, H.K., Kyle, D.E., Hutchinson, D.B., and Canfield, C.J. (1996). Clinical studies of atovaquone, alone or in combination with other antimalarial drugs, for treatment of acute uncomplicated malaria in Thailand. Am J Trop Med Hyg *54*, 62-66.

Looareesuwan, S., Wilairatana, P., Chalermarut, K., Rattanapong, Y., Canfield, C.J., and Hutchinson, D.B. (1999). Efficacy and safety of atovaquone/proguanil compared with mefloquine for treatment of acute Plasmodium falciparum malaria in Thailand. Am J Trop Med Hyg *60*, 526-532.

Lu, Y., and Beavis, A.D. (1997). Effect of leader peptides on the permeability of mitochondria. J Biol Chem *272*, 13555-13561.

Lupo, D., Vollmer, C., Deckers, M., Mick, D.U., Tews, I., Sinning, I., and Rehling, P. (2011). Mdm38 is a 14-3-3-like receptor and associates with the protein synthesis machinery at the inner mitochondrial membrane. Traffic *12*, 1457-1466.

M. Santos, J., Graindorge, A., and Soldati-Favre, D. (2012). New insights into parasite rhomboid proteases. Molecular and Biochemical Parasitology *182*, 27-36.

Maćašev, D., Whelan, J., Newbigin, E., Silva-Filho, M.C., Mulhern, T.D., and Lithgow, T. (2004). Tom22', an 8-kDa trans-Site Receptor in Plants and Protozoans, Is a Conserved Feature of the TOM Complex That Appeared Early in the Evolution of Eukaryotes. Molecular Biology and Evolution *21*, 1557-1564.

Maeno, Y., Toyoshima, T., Fujioka, H., Ito, Y., Meshnick, S.R., Benakis, A., Milhous, W.K., and Aikawa, M. (1993). Morphologic effects of artemisinin in Plasmodium falciparum. Am J Trop Med Hyg *49*, 485-491.

Maier, A.G., Cooke, B.M., Cowman, A.F., and Tilley, L. (2009). Malaria parasite proteins that remodel the host erythrocyte. Nat Rev Microbiol *7*, 341-354.

Maklashina, E., Berthold, D.A., and Cecchini, G. (1998). Anaerobic expression of Escherichia coli succinate dehydrogenase: functional replacement of fumarate reductase in the respiratory chain during anaerobic growth. J Bacteriol *180*, 5989-5996.

Malkin, E.M., Diemert, D.J., McArthur, J.H., Perreault, J.R., Miles, A.P., Giersing, B.K., Mullen, G.E., Orcutt, A., Muratova, O., Awkal, M*., et al.* (2005a). Phase 1 clinical trial of apical membrane antigen 1: an asexual blood-stage vaccine for Plasmodium falciparum malaria. Infect Immun *73*, 3677-3685.

Malkin, E.M., Durbin, A.P., Diemert, D.J., Sattabongkot, J., Wu, Y., Miura, K., Long, C.A., Lambert, L., Miles, A.P., Wang, J*., et al.* (2005b). Phase 1 vaccine trial of Pvs25H: a transmission blocking vaccine for Plasmodium vivax malaria. Vaccine *23*, 3131-3138.

Malmquist, N.A., Gujjar, R., Rathod, P.K., and Phillips, M.A. (2008). Analysis of flavin oxidation and electron-transfer inhibition in Plasmodium falciparum dihydroorotate dehydrogenase. Biochemistry *47*, 2466-2475.

Manzoori, J.L., Amjadi, M., Soleymani, J., Tamizi, E., Rezamand, A., and Jouyban, A. (2011). Determination of deferiprone in urine and serum using a terbium-sensitized luminescence method. Luminescence.

Marc, P., Margeot, A., Devaux, F., Blugeon, C., Corral-Debrinski, M., and Jacq, C. (2002). Genome-wide analysis of mRNAs targeted to yeast mitochondria. EMBO Rep *3*, 159-164.

Marshansky, V.N., Novgorodov, S.A., and Yaguzhinsky, L.S. (1983). The role of lipid peroxidation in the induction of cation transport in rat liver mitochondria. The antioxidant effect of oligomycin and dicyclohexylcarbodiimide. FEBS Lett *158*, 27-30.

Martin, R.E., and Kirk, K. (2004). The malaria parasite's chloroquine resistance transporter is a member of the drug/metabolite transporter superfamily. Mol Biol Evol *21*, 1938-1949.

Martin, R.E., Marchetti, R.V., Cowan, A.I., Howitt, S.M., Broer, S., and Kirk, K. (2009). Chloroquine transport via the malaria parasite's chloroquine resistance transporter. Science *325*, 1680-1682.

Massey, V., and Singer, T.P. (1957). Studies on succinic dehydrogenase. III. The fumaric reductase activity of succinic dehydrogenase. J Biol Chem *228*, 263-274.

Mather, M.W., Darrouzet, E., Valkova-Valchanova, M., Cooley, J.W., McIntosh, M.T., Daldal, F., and Vaidya, A.B. (2005). Uncovering the molecular mode of action of the antimalarial drug atovaquone using a bacterial system. J Biol Chem *280*, 27458-27465.

Mather, M.W., Henry, K.W., and Vaidya, A.B. (2007). Mitochondrial drug targets in apicomplexan parasites. Curr Drug Targets *8*, 49-60.

Mather, M.W., Morrisey, J.M., and Vaidya, A.B. (2010). Hemozoin-free Plasmodium falciparum mitochondria for physiological and drug susceptibility studies. Molecular and Biochemical Parasitology *174*, 150-153.

Mather, M.W., and Vaidya, A.B. (2008). Mitochondria in malaria and related parasites: ancient, diverse and streamlined. Journal of Bioenergetics and Biomembranes *40*, 425-433.

Matsoso, L.G., Kana, B.D., Crellin, P.K., Lea-Smith, D.J., Pelosi, A., Powell, D., Dawes, S.S., Rubin, H., Coppel, R.L., and Mizrahi, V. (2005). Function of the cytochrome bc1-aa3 branch of the respiratory network in mycobacteria and network adaptation occurring in response to its disruption. J Bacteriol *187*, 6300-6308.

Mattevi, A., Obmolova, G., Sokatch, J.R., Betzel, C., and Hol, W.G. (1992). The refined crystal structure of Pseudomonas putida lipoamide dehydrogenase complexed with NAD+ at 2.45 A resolution. Proteins *13*, 336-351.

McFadden, G.I. (2011). The apicoplast. Protoplasma *248*, 641-650.

Meier, T., Morgner, N., Matthies, D., Pogoryelov, D., Keis, S., Cook, G.M., Dimroth, P., and Brutschy, B. (2007). A tridecameric c ring of the adenosine triphosphate (ATP) synthase from the thermoalkaliphilic Bacillus sp. strain TA2.A1 facilitates ATP synthesis at low electrochemical proton potential. Mol Microbiol *65*, 1181-1192.

Meinecke, M., Wagner, R., Kovermann, P., Guiard, B., Mick, D.U., Hutu, D.P., Voos, W., Truscott, K.N., Chacinska, A., Pfanner, N*., et al.* (2006). Tim50 maintains the permeability barrier of the mitochondrial inner membrane. Science *312*, 1523-1526.

Mendis, K.N., and Carter, R. (1995). Clinical disease and pathogenesis in malaria. Parasitol Today *11*, PTI1-16.

Mercer, A.E., Copple, I.M., Maggs, J.L., O'Neill, P.M., and Park, B.K. (2011). The role of heme and the mitochondrion in the chemical and molecular mechanisms of mammalian cell death induced by the artemisinin antimalarials. J Biol Chem *286*, 987-996.

Mercer, A.E., Maggs, J.L., Sun, X.M., Cohen, G.M., Chadwick, J., O'Neill, P.M., and Park, B.K. (2007). Evidence for the involvement of carbon-centered radicals in the induction of apoptotic cell death by artemisinin compounds. J Biol Chem *282*, 9372-9382.

Meshnick, S.R., Taylor, T.E., and Kamchonwongpaisan, S. (1996). Artemisinin and the antimalarial endoperoxides: from herbal remedy to targeted chemotherapy. Microbiol Rev *60*, 301-315.

Meshnick, S.R., Thomas, A., Ranz, A., Xu, C.M., and Pan, H.Z. (1991). Artemisinin (qinghaosu): the role of intracellular hemin in its mechanism of antimalarial action. Mol Biochem Parasitol *49*, 181-189.

Meshnick, S.R., Yang, Y.Z., Lima, V., Kuypers, F., Kamchonwongpaisan, S., and Yuthavong, Y. (1993). Iron-dependent free radical generation from the antimalarial agent artemisinin (qinghaosu). Antimicrob Agents Chemother *37*, 1108-1114.

Mi-Ichi, F., Takeo, S., Takashima, E., Kobayashi, T., Kim, H.S., Wataya, Y., Matsuda, A., Torrii, M., Tsuboi, T., and Kita, K. (2003). Unique properties of respiratory chain in Plasmodium falciparum mitochondria. Adv Exp Med Biol *531*, 117-133.

Michon, T., Galante, M., and Velours, J. (1988). NH2-terminal sequence of the isolated yeast ATP synthase subunit 6 reveals post-translational cleavage. Eur J Biochem *172*, 621-625.

Miller, L.H., Baruch, D.I., Marsh, K., and Doumbo, O.K. (2002). The pathogenic basis of malaria. Nature *415*, 673-679.

Miller, L.H., Good, M.F., and Milon, G. (1994a). Malaria pathogenesis. Science *264*, 1878-1883.

Miller, R.L., Ikram, S., Armelagos, G.J., Walker, R., Harer, W.B., Shiff, C.J., Baggett, D., Carrigan, M., and Maret, S.M. (1994b). Diagnosis of Plasmodium falciparum infections in mummies using the rapid manual ParaSight-F test. Trans R Soc Trop Med Hyg *88*, 31-32.

Mita, T., Tanabe, K., and Kita, K. (2009). Spread and evolution of Plasmodium falciparum drug resistance. Parasitology International *58*, 201-209.

Mitamura, T., and Palacpac, N.M. (2003). Lipid metabolism in Plasmodium falciparum-infected erythrocytes: possible new targets for malaria chemotherapy. Microbes Infect *5*, 545-552.

Mitchell, P. (1975). The protonmotive Q cycle: a general formulation. FEBS Lett *59*, 137-139.

Miyadera, H., Hiraishi, A., Miyoshi, H., Sakamoto, K., Mineki, R., Murayama, K., Nagashima, K.V., Matsuura, K., Kojima, S., and Kita, K. (2003). Complex II from phototrophic purple bacterium Rhodoferax fermentans displays rhodoquinol-fumarate reductase activity. Eur J Biochem *270*, 1863-1874.

Mogi, T., and Kita, K. (2009). Identification of mitochondrial Complex II subunits SDH3 and SDH4 and ATP synthase subunits a and b in Plasmodium spp. Mitochondrion *9*, 443-453.

Mogi, T., Murase, Y., Mori, M., Shiomi, K., Omura, S., Paranagama, M.P., and Kita, K. (2009). Polymyxin B Identified as an Inhibitor of Alternative NADH Dehydrogenase and Malate: Quinone Oxidoreductase from the Gram-positive Bacterium Mycobacterium smegmatis. Journal of Biochemistry *146*, 491-499.

Mokranjac, D., Popov-Celeketic, D., Hell, K., and Neupert, W. (2005). Role of Tim21 in mitochondrial translocation contact sites. J Biol Chem *280*, 23437-23440.

Mokranjac, D., Sichting, M., Neupert, W., and Hell, K. (2003). Tim14, a novel key component of the import motor of the TIM23 protein translocase of mitochondria. EMBO J *22*, 4945-4956.

Molenaar, D., van der Rest, M.E., and Petrovic, S. (1998). Biochemical and genetic characterization of the membrane-associated malate dehydrogenase (acceptor) from Corynebacterium glutamicum. Eur J Biochem *254*, 395-403.

Monaghan, P., and Bell, A. (2005). A Plasmodium falciparum FK506-binding protein (FKBP) with peptidyl-prolyl cis-trans isomerase and chaperone activities. Mol Biochem Parasitol *139*, 185-195.

Monzote, L., and Gille, L. (2010). Mitochondria as a promising antiparasitic target. Curr Clin Pharmacol *5*, 55-60.

Moon, Y., Lee, K.H., Park, J.H., Geum, D., and Kim, K. (2005). Mitochondrial membrane depolarization and the selective death of dopaminergic neurons by rotenone: protective effect of coenzyme Q10. J Neurochem *93*, 1199-1208.

Moorthy, V.S., Imoukhuede, E.B., Keating, S., Pinder, M., Webster, D., Skinner, M.A., Gilbert, S.C., Walraven, G., and Hill, A.V. (2004a). Phase 1 evaluation of 3 highly immunogenic prime-boost regimens, including a 12-month reboosting vaccination, for malaria vaccination in Gambian men. J Infect Dis *189*, 2213-2219.

Moorthy, V.S., Imoukhuede, E.B., Milligan, P., Bojang, K., Keating, S., Kaye, P., Pinder, M., Gilbert, S.C., Walraven, G., Greenwood, B.M.*, et al.* (2004b). A randomised, double-blind, controlled vaccine efficacy trial of DNA/MVA ME-TRAP against malaria infection in Gambian adults. PLoS Med *1*, e33.

Morales, J., Mogi, T., Mineki, S., Takashima, E., Mineki, R., Hirawake, H., Sakamoto, K., Omura, S., and Kita, K. (2009). Novel mitochondrial complex II isolated from Trypanosoma cruzi is composed of 12 peptides including a heterodimeric Ip subunit. J Biol Chem *284*, 7255-7263.

Mossmann, D., Meisinger, C., and Vogtle, F.N. (2011). Processing of mitochondrial presequences. Biochim Biophys Acta.

Mu, J., Ferdig, M.T., Feng, X., Joy, D.A., Duan, J., Furuya, T., Subramanian, G., Aravind, L., Cooper, R.A., Wootton, J.C.*, et al.* (2003). Multiple transporters associated with malaria parasite responses to chloroquine and quinine. Mol Microbiol *49*, 977-989.

Mu, J., Joy, D.A., Duan, J., Huang, Y., Carlton, J., Walker, J., Barnwell, J., Beerli, P., Charleston, M.A., Pybus, O.G.*, et al.* (2005). Host switch leads to emergence of Plasmodium vivax malaria in humans. Mol Biol Evol *22*, 1686-1693.

Muller, I.B., and Hyde, J.E. (2010). Antimalarial drugs: modes of action and mechanisms of parasite resistance. Future Microbiol *5*, 1857-1873.

Muller, S. (2004). Redox and antioxidant systems of the malaria parasite Plasmodium falciparum. Mol Microbiol *53*, 1291-1305.

Murakami, H., Pain, D., and Blobel, G. (1988). 70-kD heat shock-related protein is one of at least two distinct cytosolic factors stimulating protein import into mitochondria. J Cell Biol *107*, 2051-2057.

Murray, J., Zhang, B., Taylor, S.W., Oglesbee, D., Fahy, E., Marusich, M.F., Ghosh, S.S., and Capaldi, R.A. (2003). The subunit composition of the human NADH dehydrogenase obtained by rapid one-step immunopurification. J Biol Chem *278*, 13619-13622.

Musset, L., Bouchaud, O., Matheron, S., Massias, L., and Le Bras, J. (2006). Clinical atovaquone-proguanil resistance of Plasmodium falciparum associated with cytochrome b codon 268 mutations. Microbes Infect *8*, 2599-2604.

Mzhavia, N., Berman, Y.L., Qian, Y., Yan, L., and Devi, L.A. (1999). Cloning, expression, and characterization of human metalloprotease 1: a novel member of the pitrilysin family of metalloendoproteases. DNA Cell Biol *18*, 369-380.

Naamati, A., Regev-Rudzki, N., Galperin, S., Lill, R., and Pines, O. (2009). Dual targeting of Nfs1 and discovery of its novel processing enzyme, Icp55. J Biol Chem *284*, 30200-30208.

Nasirudeen, A.M., and Tan, K.S. (2004). Isolation and characterization of the mitochondrion-like organelle from Blastocystis hominis. J Microbiol Methods *58*, 101-109.

Neupert, W., and Herrmann, J.M. (2007). Translocation of proteins into mitochondria. Annu Rev Biochem *76*, 723-749.

Nicolay, K., Laterveer, F.D., and van Heerde, W.L. (1994). Effects of amphipathic peptides, including presequences, on the functional integrity of rat liver mitochondrial membranes. J Bioenerg Biomembr *26*, 327-334.

Nosten, F., Phillips-Howard, P., and Kuile, F. (2012). Other 4-Methanolquinolines, Amyl Alcohols and Phentathrenes: Mefloquine, Lumefantrine and Halofantrine.

Nosten, F., and White, N.J. (2007). Artemisinin-based combination treatment of falciparum malaria. Am J Trop Med Hyg *77*, 181-192.

Nunnari, J., Fox, T.D., and Walter, P. (1993). A mitochondrial protease with two catalytic subunits of nonoverlapping specificities. Science *262*, 1997-2004.

Nzila, A. (2012). Antifolates: Pyrimethamine, Proguanil, Sulphadoxine and Dapsone.

O'Neill, P.M., Amewu, R.K., Nixon, G.L., Bousejra ElGarah, F., Mungthin, M., Chadwick, J., Shone, A.E., Vivas, L., Lander, H., Barton, V.*, et al.* (2010a). Identification of a 1,2,4,5-tetraoxane antimalarial drug-development candidate (RKA 182) with superior properties to the semisynthetic artemisinins. Angew Chem Int Ed Engl *49*, 5693-5697.

O'Neill, P.M., Barton, V.E., and Ward, S.A. (2010b). The molecular mechanism of action of artemisinin--the debate continues. Molecules *15*, 1705-1721.

O'Neill, P.M., Bishop, L.P., Searle, N.L., Maggs, J.L., Storr, R.C., Ward, S.A., Park, B.K., and Mabbs, F. (2000). Biomimetic Fe(II)-mediated degradation of arteflene (Ro-42-1611). The first EPR spin-trapping evidence for the previously postulated secondary carbon-centered cyclohexyl radical. J Org Chem *65*, 1578-1582.

O'Neill, P.M., and Posner, G.H. (2004). A medicinal chemistry perspective on artemisinin and related endoperoxides. J Med Chem *47*, 2945-2964.

O'Neill, P., Barton, V., Ward, S., and Chadwick, J. (2012). 4-Aminoquinolines: Chloroquine, Amodiaquine and Next-Generation Analogues. In Treatment and Prevention of Malaria, H.M. Staines, and S. Krishna, eds. (Springer Basel), pp. 19-44.

Okamoto, N., Spurck, T.P., Goodman, C.D., and McFadden, G.I. (2009). Apicoplast and mitochondrion in gametocytogenesis of Plasmodium falciparum. Eukaryot Cell *8*, 128-132.

Okombo, J., Kiara, S.M., Rono, J., Mwai, L., Pole, L., Ohuma, E., Borrmann, S., Ochola, L.I., and Nzila, A. (2010). In vitro activities of quinine and other antimalarials and pfnhe polymorphisms in Plasmodium isolates from Kenya. Antimicrob Agents Chemother *54*, 3302-3307.

Olliaro, P. (2001). Mode of action and mechanisms of resistance for antimalarial drugs. Pharmacology & Therapeutics *89*, 207-219.

Olszewski, K.L., Mather, M.W., Morrisey, J.M., Garcia, B.A., Vaidya, A.B., Rabinowitz, J.D., and Llinas, M. (2010). Branched tricarboxylic acid metabolism in Plasmodium falciparum. Nature *466*, 774-778.

Osei-Akoto, A., Orton, L., and Owusu-Ofori, S.P. (2005). Atovaquone-proguanil for treating uncomplicated malaria. Cochrane Database Syst Rev, CD004529.

Ott, M., Prestele, M., Bauerschmitt, H., Funes, S., Bonnefoy, N., and Herrmann, J.M. (2006). Mba1, a membrane-associated ribosome receptor in mitochondria. EMBO J *25*, 1603-1610.

Otto, H., Conz, C., Maier, P., Wolfle, T., Suzuki, C.K., Jeno, P., Rucknagel, P., Stahl, J., and Rospert, S. (2005). The chaperones MPP11 and Hsp70L1 form the mammalian ribosome-associated complex. Proc Natl Acad Sci U S A *102*, 10064-10069.

Pagola, S., Stephens, P.W., Bohle, D.S., Kosar, A.D., and Madsen, S.K. (2000). The structure of malaria pigment beta-haematin. Nature *404*, 307-310.

Pain, A., Renauld, H., Berriman, M., Murphy, L., Yeats, C.A., Weir, W., Kerhornou, A., Aslett, M., Bishop, R., Bouchier, C*., et al.* (2005). Genome of the host-cell transforming parasite Theileria annulata compared with T. parva. Science *309*, 131-133.

Painter, H.J., Morrisey, J.M., Mather, M.W., and Vaidya, A.B. (2007). Specific role of mitochondrial electron transport in blood-stage Plasmodium falciparum. Nature *446*, 88-91.

Painter, H.J., Morrisey, J.M., and Vaidya, A.B. (2010). Mitochondrial Electron Transport Inhibition and Viability of Intraerythrocytic Plasmodium falciparum. Antimicrobial Agents and Chemotherapy *54*, 5281-5287.

Pandey, A.V., Tekwani, B.L., Singh, R.L., and Chauhan, V.S. (1999). Artemisinin, an endoperoxide antimalarial, disrupts the hemoglobin catabolism and heme detoxification systems in malarial parasite. J Biol Chem *274*, 19383-19388.

Pandya, K.P., and King, H.K. (1966). Ubiquinone and menaquinone in bacteria: a comparative study of some bacterial respiratory systems. Arch Biochem Biophys *114*, 154-157.

Pasvol, G. (2005). The treatment of complicated and severe malaria. Br Med Bull *75-76*, 29-47.

Patarroyo, G., Franco, L., Amador, R., Murillo, L.A., Rocha, C.L., Rojas, M., and Patarroyo, M.E. (1992). Study of the safety and immunogenicity of the synthetic malaria SPf66 vaccine in children aged 1-14 years. Vaccine *10*, 175-178.

Patel, V., Booker, M., Kramer, M., Ross, L., Celatka, C.A., Kennedy, L.M., Dvorin, J.D., Duraisingh, M.T., Sliz, P., Wirth, D.F*., et al.* (2008). Identification and characterization of small molecule inhibitors of Plasmodium falciparum dihydroorotate dehydrogenase. J Biol Chem *283*, 35078-35085.

Peel, S.A. (2001). The ABC transporter genes of Plasmodium falciparum and drug resistance. Drug Resistance Updates *4*, 66-74.

Perkins, S.L., and Austin, C.C. (2009). Four new species of Plasmodium from New Guinea lizards: integrating morphology and molecules. J Parasitol *95*, 424-433.

Peters, J.M., Chen, N., Gatton, M., Korsinczky, M., Fowler, E.V., Manzetti, S., Saul, A., and Cheng, Q. (2002). Mutations in cytochrome b resulting in atovaquone resistance are associated with loss of fitness in Plasmodium falciparum. Antimicrob Agents Chemother *46*, 2435-2441.

Petersen, E. (2003). The safety of atovaquone/proguanil in long-term malaria prophylaxis of nonimmune adults. J Travel Med *10 Suppl 1*, S13-15; discussion S21.

Petmitr, S., and Krungkrai, J. (1995). Mitochondrial cytochrome b gene in two developmental stages of human malarial parasite Plasmodium falciparum. Southeast Asian J Trop Med Public Health *26*, 600-605.

Phillips, M.A., Gujjar, R., Malmquist, N.A., White, J., El Mazouni, F., Baldwin, J., and Rathod, P.K. (2008). Triazolopyrimidine-based dihydroorotate dehydrogenase inhibitors with potent and selective activity against the malaria parasite Plasmodium falciparum. J Med Chem *51*, 3649-3653.

Piao, L., Li, Y., Kim, S.J., Byun, H.S., Huang, S.M., Hwang, S.K., Yang, K.J., Park, K.A., Won, M., Hong, J.*, et al.* (2009). Association of LETM1 and MRPL36 contributes to the regulation of mitochondrial ATP production and necrotic cell death. Cancer Res *69*, 3397-3404.

Piechota, J., Kolodziejczak, M., Juszczak, I., Sakamoto, W., and Janska, H. (2010). Identification and characterization of high molecular weight complexes formed by matrix AAA proteases and prohibitins in mitochondria of Arabidopsis thaliana. J Biol Chem *285*, 12512-12521.

Pisciotta, J.M., Coppens, I., Tripathi, A.K., Scholl, P.F., Shuman, J., Bajad, S., Shulaev, V., and Sullivan, D.J., Jr. (2007). The role of neutral lipid nanospheres in Plasmodium falciparum haem crystallization. Biochem J *402*, 197-204.

Ponpuak, M., Klemba, M., Park, M., Gluzman, I.Y., Lamppa, G.K., and Goldberg, D.E. (2007). A role for falcilysin in transit peptide degradation in the Plasmodium falciparum apicoplast. Mol Microbiol *63*, 314-334.

Porter, N.A. (1986). Mechanisms for the autoxidation of polyunsaturated lipids. Accounts of Chemical Research *19*, 262-268.

Posner, G.H., Oh, C.H., Wang, D., Gerena, L., Milhous, W.K., Meshnick, S.R., and Asawamahasadka, W. (1994). Mechanism-based design, synthesis, and in vitro antimalarial testing of new 4-methylated trioxanes structurally related to artemisinin: the importance of a carbon-centered radical for antimalarial activity. J Med Chem *37*, 1256-1258.

Posner, G.H., Wang, D., Cumming, J.N., Oh, C.H., French, A.N., Bodley, A.L., and Shapiro, T.A. (1995). Further evidence supporting the importance of and the restrictions on a carbon-centered radical for high antimalarial activity of 1,2,4-trioxanes like artemisinin. J Med Chem *38*, 2273-2275.

Pradines, B., Rolain, J.M., Ramiandrasoa, F., Fusai, T., Mosnier, J., Rogier, C., Daries, W., Baret, E., Kunesch, G., Le Bras, J.*, et al.* (2002). Iron chelators as antimalarial agents: in vitro activity of dicatecholate against Plasmodium falciparum. J Antimicrob Chemother *50*, 177-187.

Pratje, E., Mannhaupt, G., Michaelis, G., and Beyreuther, K. (1983). A nuclear mutation prevents processing of a mitochondrially encoded membrane protein in Saccharomyces cerevisiae. EMBO J *2*, 1049-1054.

Qbadou, S., Becker, T., Mirus, O., Tews, I., Soll, J., and Schleiff, E. (2006). The molecular chaperone Hsp90 delivers precursor proteins to the chloroplast import receptor Toc64. EMBO J *25*, 1836-1847.

Raabe, C.A., Sanchez, C.P., Randau, G., Robeck, T., Skryabin, B.V., Chinni, S.V., Kube, M., Reinhardt, R., Ng, G.H., Manickam, R.*, et al.* (2010). A global view of the nonprotein-coding transcriptome in Plasmodium falciparum. Nucleic Acids Res *38*, 608-617.

Radloff, P.D., Philipps, J., Nkeyi, M., Hutchinson, D., and Kremsner, P.G. (1996). Atovaquone and proguanil for Plasmodium falciparum malaria. Lancet *347*, 1511-1514.

Raj, D.K., Mu, J., Jiang, H., Kabat, J., Singh, S., Sullivan, M., Fay, M.P., McCutchan, T.F., and Su, X.Z. (2009). Disruption of a Plasmodium falciparum multidrug resistance-associated protein (PfMRP) alters its fitness and transport of antimalarial drugs and glutathione. J Biol Chem *284*, 7687-7696.

Ranson, N.A., White, H.E., and Saibil, H.R. (1998). Chaperonins. Biochem J *333 (Pt 2)*, 233-242.

Refojo, P.N., Teixeira, M., and Pereira, M.M. (2012). The Alternative complex III: Properties and possible mechanisms for electron transfer and energy conservation. Biochim Biophys Acta.

Rehling, P., Model, K., Brandner, K., Kovermann, P., Sickmann, A., Meyer, H.E., Kuhlbrandt, W., Wagner, R., Truscott, K.N., and Pfanner, N. (2003). Protein insertion into the mitochondrial inner membrane by a twin-pore translocase. Science *299*, 1747-1751.

Reyburn, H., Mbatia, R., Drakeley, C., Bruce, J., Carneiro, I., Olomi, R., Cox, J., Nkya, W.M., Lemnge, M., Greenwood, B.M*., et al.* (2005). Association of transmission intensity and age with clinical manifestations and case fatality of severe Plasmodium falciparum malaria. JAMA *293*, 1461-1470.

Rich, P.R. (2003). The molecular machinery of Keilin's respiratory chain. Biochem Soc Trans *31*, 1095-1105.

Richter, C. (1987). Biophysical consequences of lipid peroxidation in membranes. Chem Phys Lipids *44*, 175-189.

Richter, O.M., and Ludwig, B. (2003). Cytochrome c oxidase--structure, function, and physiology of a redox-driven molecular machine. Rev Physiol Biochem Pharmacol *147*, 47-74.

Ridley, R.G. (2002). Medical need, scientific opportunity and the drive for antimalarial drugs. Nature *415*, 686-693.

Robert, A., Benoit-Vical, F., Claparols, C., and Meunier, B. (2005). The antimalarial drug artemisinin alkylates heme in infected mice. Proc Natl Acad Sci U S A *102*, 13676-13680.

Robert, A., Bonduelle, C., Laurent, S.A.L., and Meunier, B. (2006). Heme alkylation by artemisinin and trioxaquines. Journal of Physical Organic Chemistry *19*, 562-569.

Robinson, K.M., and Lemire, B.D. (1996). Covalent attachment of FAD to the yeast succinate dehydrogenase flavoprotein requires import into mitochondria, presequence removal, and folding. J Biol Chem *271*, 4055-4060.

Rogalska, A., Koceva-Chyla, A., and Jozwiak, Z. (2008). Aclarubicin-induced ROS generation and collapse of mitochondrial membrane potential in human cancer cell lines. Chem Biol Interact *176*, 58-70.

Roise, D., Horvath, S.J., Tomich, J.M., Richards, J.H., and Schatz, G. (1986). A chemically synthesized pre-sequence of an imported mitochondrial protein can form an amphiphilic helix and perturb natural and artificial phospholipid bilayers. EMBO J *5*, 1327-1334.

Rosenthal, P.J., and Meshnick, S.R. (1996). Hemoglobin catabolism and iron utilization by malaria parasites. Mol Biochem Parasitol *83*, 131-139.

Ross, R. (1898). The role of the mosquito in the evolution of the malaria parasite. Lancet *ii*, 489.

Rossignol, R., Faustin, B., Rocher, C., Malgat, M., Mazat, J.P., and Letellier, T. (2003). Mitochondrial threshold effects. Biochemical Journal *370*, 751-762.

Rudzinska, M.A. (1969). The fine structure of malaria parasites. Int Rev Cytol *25*, 161-199.

Rye, H.S., Burston, S.G., Fenton, W.A., Beechem, J.M., Xu, Z., Sigler, P.B., and Horwich, A.L. (1997). Distinct actions of cis and trans ATP within the double ring of the chaperonin GroEL. Nature *388*, 792-798.

Sachs, J., and Malaney, P. (2002). The economic and social burden of malaria. Nature *415*, 680-685.

Sadacharan, S.K., Cavanagh, A.C., and Gupta, R.S. (2001). Immunoelectron microscopy provides evidence for the presence of mitochondrial heat shock 10-kDa protein (chaperonin 10) in red blood cells and a variety of secretory granules. Histochem Cell Biol *116*, 507-517.

Sadasivaiah, S., Tozan, Y., and Breman, J.G. (2007). Dichlorodiphenyltrichloroethane (DDT) for Indoor Residual Spraying in Africa: How Can It Be Used for Malaria Control? The American Journal of Tropical Medicine and Hygiene *77*, 249-263.

Sakai, C., Tomitsuka, E., Esumi, H., Harada, S., and Kita, K. (2012). Mitochondrial fumarate reductase as a target of chemotherapy: From parasites to cancer cells. Biochim Biophys Acta *1820*, 643-651.

Saliba, K.J., and Kirk, K. (1999). pH regulation in the intracellular malaria parasite, Plasmodium falciparum. H(+) extrusion via a v-type h(+)-atpase. J Biol Chem *274*, 33213-33219.

Saliba, K.J., Martin, R.E., Broer, A., Henry, R.I., McCarthy, C.S., Downie, M.J., Allen, R.J., Mullin, K.A., McFadden, G.I., Broer, S*., et al.* (2006). Sodium-dependent uptake of inorganic phosphate by the intracellular malaria parasite. Nature *443*, 582-585.

Saraste, M. (1999). Oxidative phosphorylation at the fin de siecle. Science *283*, 1488-1493.

Saruta, F., Kuramochi, T., Nakamura, K., Takamiya, S., Yu, Y., Aoki, T., Sekimizu, K., Kojima, S., and Kita, K. (1995). Stage-specific isoforms of complex II (succinate-ubiquinone oxidoreductase) in mitochondria from the parasitic nematode, Ascaris suum. J Biol Chem *270*, 928-932.

Sato, S., Rangachari, K., and Wilson, R.J. (2003). Targeting GFP to the malarial mitochondrion. Mol Biochem Parasitol *130*, 155-158.

Sato, S., and Wilson, R.J. (2004). The use of DsRED in single- and dual-color fluorescence labeling of mitochondrial and plastid organelles in Plasmodium falciparum. Mol Biochem Parasitol *134*, 175-179.

Sato, S., and Wilson, R.J. (2005). Organelle-specific cochaperonins in apicomplexan parasites. Mol Biochem Parasitol *141*, 133-143.

Schagger, H., and Pfeiffer, K. (2000). Supercomplexes in the respiratory chains of yeast and mammalian mitochondria. EMBO J *19*, 1777-1783.

Scheibel, L.W., Adler, A., and Trager, W. (1979). Tetraethylthiuram disulfide (Antabuse) inhibits the human malaria parasite Plasmodium falciparum. Proceedings of the National Academy of Sciences of the United States of America *76*, 5303-5307.

Scheibel, L.W., and Pflaum, W.K. (1970). Cytochrome oxidase activity in platelet-free preparations of Plasmodium falciparum. J Parasitol *56*, 1054.

Schilling, B., Murray, J., Yoo, C.B., Row, R.H., Cusack, M.P., Capaldi, R.A., and Gibson, B.W. (2006). Proteomic analysis of succinate dehydrogenase and ubiquinol-cytochrome c reductase (Complex II and III) isolated by immunoprecipitation from bovine and mouse heart mitochondria. Biochim Biophys Acta *1762*, 213-222.

Schlitzer, M. (2007). Malaria chemotherapeutics part I: History of antimalarial drug development, currently used therapeutics, and drugs in clinical development. ChemMedChem *2*, 944-986.

Schmid, R., and Gerloff, D.L. (2004). Functional properties of the alternative NADH:ubiquinone oxidoreductase from E. coli through comparative 3-D modelling. FEBS Lett *578*, 163-168.

Schmidt, O., Pfanner, N., and Meisinger, C. (2010). Mitochondrial protein import: from proteomics to functional mechanisms. Nat Rev Mol Cell Biol *11*, 655-667.

Schneider, A., Bursac, D., and Lithgow, T. (2008). The direct route: a simplified pathway for protein import into the mitochondrion of trypanosomes. Trends Cell Biol *18*, 12-18.

Schneider, A., Charriere, F., Pusnik, M., and Horn, E.K. (2007). Isolation of mitochondria from procyclic Trypanosoma brucei. Methods Mol Biol *372*, 67-80.

Schneider, A., Oppliger, W., and Jeno, P. (1994a). Purified inner membrane protease I of yeast mitochondria is a heterodimer. J Biol Chem *269*, 8635-8638.

Schneider, H.C., Berthold, J., Bauer, M.F., Dietmeier, K., Guiard, B., Brunner, M., and Neupert, W. (1994b). Mitochondrial Hsp70/MIM44 complex facilitates protein import. Nature *371*, 768-774.

Schneider, H.C., Westermann, B., Neupert, W., and Brunner, M. (1996). The nucleotide exchange factor MGE exerts a key function in the ATP-dependent cycle of mt-Hsp70-Tim44 interaction driving mitochondrial protein import. EMBO J *15*, 5796-5803.

Scholl, P.F., Tripathi, A.K., and Sullivan, D.J. (2005). Bioavailable iron and heme metabolism in Plasmodium falciparum. Curr Top Microbiol Immunol *295*, 293-324.

Sen, R., Bandyopadhyay, S., Dutta, A., Mandal, G., Ganguly, S., Saha, P., and Chatterjee, M. (2007). Artemisinin triggers induction of cell-cycle arrest and apoptosis in Leishmania donovani promastigotes. J Med Microbiol *56*, 1213-1218.

Sen, T., Sen, N., Tripathi, G., Chatterjee, U., and Chakrabarti, S. (2006). Lipid peroxidation associated cardiolipin loss and membrane depolarization in rat brain mitochondria. Neurochem Int *49*, 20-27.

Senkevich, T.G., White, C.L., Koonin, E.V., and Moss, B. (2000). A viral member of the ERV1/ALR protein family participates in a cytoplasmic pathway of disulfide bond formation. Proc Natl Acad Sci U S A *97*, 12068-12073.

Seymour, K.K., Yeo, A.E., Rieckmann, K.H., and Christopherson, R.I. (1997). dCTP levels are maintained in Plasmodium falciparum subjected to pyrimidine deficiency or excess. Ann Trop Med Parasitol *91*, 603-609.

Sheiner, L., and Soldati-Favre, D. (2008). Protein trafficking inside Toxoplasma gondii. Traffic *9*, 636-646.

Shestopalov, A.I., Bogachev, A.V., Murtazina, R.A., Viryasov, M.B., and Skulachev, V.P. (1997). Aeration-dependent changes in composition of the quinone pool in Escherichia coli. Evidence of post-transcriptional regulation of the quinone biosynthesis. FEBS Lett *404*, 272-274.

Shortt, H., and Garnham, P. (1948). Pre-erythrocytic stages in mammalian malaria parasites. Nature *161*, 126.

Sibmooh, N., Udomsangpetch, R., Kujoa, A., Chantharaksri, U., and Mankhetkorn, S. (2001). Redox reaction of artemisinin with ferrous and ferric ions in aqueous buffer. Chem Pharm Bull (Tokyo) *49*, 1541-1546.

Sidhu, A.B., Uhlemann, A.C., Valderramos, S.G., Valderramos, J.C., Krishna, S., and Fidock, D.A. (2006). Decreasing pfmdr1 copy number in plasmodium falciparum malaria heightens susceptibility to mefloquine, lumefantrine, halofantrine, quinine, and artemisinin. J Infect Dis *194*, 528-535.

Simpson, A.G., and Roger, A.J. (2004). The real 'kingdoms' of eukaryotes. Curr Biol *14*, R693-696.

Sinden, R.E., and Billingsley, P.F. (2001). Plasmodium invasion of mosquito cells: hawk or dove? Trends in Parasitology *17*, 209-211.

Singh, B., Sung, L.K., Matusop, A., Radhakrishnan, A., Shamsul, S.S.G., Cox-Singh, J., Thomas, A., and Conway, D.J. (2004). A large focus of naturally acquired Plasmodium knowlesi infections in human beings. The Lancet *363*, 1017-1024.

Sirrenberg, C., Bauer, M.F., Guiard, B., Neupert, W., and Brunner, M. (1996). Import of carrier proteins into the mitochondrial inner membrane mediated by Tim22. Nature *384*, 582-585.

Skerlj, R.T., Bastos, C.M., Booker, M.L., Kramer, M.L., Barker, R.H., Celatka, C.A., O'Shea, T.J., Munoz, B., Sidhu, A.B., Cortese, J.F.*, et al.* (2011). Optimization of Potent Inhibitors of P. falciparum Dihydroorotate Dehydrogenase for the Treatment of Malaria. ACS Medicinal Chemistry Letters *2*, 708-713.

Slapeta, J., and Keithly, J.S. (2004). Cryptosporidium parvum mitochondrial-type HSP70 targets homologous and heterologous mitochondria. Eukaryot Cell *3*, 483-494.

Smilkstein, M., Sriwilaijaroen, N., Kelly, J.X., Wilairat, P., and Riscoe, M. (2004). Simple and inexpensive fluorescence-based technique for high-throughput antimalarial drug screening. Antimicrob Agents Chemother *48*, 1803-1806.

Smith, D.C., and Sanford, L.B. (1985). Laveran's germ: the reception and use of a medical discovery. Am J Trop Med Hyg *34*, 2-20.

Snyder, C.H., Denke, E., and Trumpower, B.L. (1999). Aromatic amino acids in the Rieske iron–sulfur protein do not form an obligatory conduit for electron transfer from the iron–sulfur cluster to the heme of cytochrome c1 in the cytochrome bc1 complex. Biochimica et Biophysica Acta (BBA) - Bioenergetics *1410*, 237-247.

Sottocasa, G.L., Kuylenstierna, B., Ernster, L., and Bergstrand, A. (1967). An electron-transport system associated with the outer membrane of liver mitochondria. A biochemical and morphological study. J Cell Biol *32*, 415-438.

Srivastava, I.K., Rottenberg, H., and Vaidya, A.B. (1997). Atovaquone, a broad spectrum antiparasitic drug, collapses mitochondrial membrane potential in a malarial parasite. J Biol Chem *272*, 3961-3966.

Srivastava, I.K., and Vaidya, A.B. (1999). A mechanism for the synergistic antimalarial action of atovaquone and proguanil. Antimicrob Agents Chemother *43*, 1334-1339.

Stahl, A., Moberg, P., Ytterberg, J., Panfilov, O., Brockenhuus Von Lowenhielm, H., Nilsson, F., and Glaser, E. (2002). Isolation and identification of a novel mitochondrial metalloprotease (PreP) that degrades targeting presequences in plants. J Biol Chem *277*, 41931-41939.

Steigmiller, S., Turina, P., and Graber, P. (2008). The thermodynamic H+/ATP ratios of the H+-ATPsynthases from chloroplasts and Escherichia coli. Proc Natl Acad Sci U S A *105*, 3745-3750.

Stocks, P.A., Bray, P.G., Barton, V.E., Al-Helal, M., Jones, M., Araujo, N.C., Gibbons, P., Ward, S.A., Hughes, R.H., Biagini, G.A*., et al.* (2007). Evidence for a common non-heme chelatable-iron-dependent activation mechanism for semisynthetic and synthetic endoperoxide antimalarial drugs. Angew Chem Int Ed Engl *46*, 6278-6283.

Stoute, J.A., Gombe, J., Withers, M.R., Siangla, J., McKinney, D., Onyango, M., Cummings, J.F., Milman, J., Tucker, K., Soisson, L*., et al.* (2007). Phase 1 randomized double-blind safety and immunogenicity trial of Plasmodium falciparum malaria merozoite surface protein FMP1 vaccine, adjuvanted with AS02A, in adults in western Kenya. Vaccine *25*, 176-184.

Sullivan, D. (2012). Cinchona Alkaloids: Quinine and Quinidine.

Sun F Fau - Huo, X., Huo X Fau - Zhai, Y., Zhai Y Fau - Wang, A., Wang A Fau - Xu, J., Xu J Fau - Su, D., Su D Fau - Bartlam, M., Bartlam M Fau - Rao, Z., and Rao, Z. Crystal structure of mitochondrial respiratory membrane protein complex II.

Suraveratum, N., Krungkrai, S.R., Leangaramgul, P., Prapunwattana, P., and Krungkrai, J. (2000). Purification and characterization of Plasmodium falciparum succinate dehydrogenase. Mol Biochem Parasitol *105*, 215-222.

Swamy, M. (2006). Blue Native Polyacrylamide Gel Electrophoresis (BN-PAGE) for the Identification and Analysis of Multiprotein Complexes. Science's STKE *2006*, pl4-pl4.

Symersky, J., Pagadala, V., Osowski, D., Krah, A., Meier, T., Faraldo-Gomez, J.D., and Mueller, D.M. (2012). Structure of the c(10) ring of the yeast mitochondrial ATP synthase in the open conformation. Nat Struct Mol Biol *19*, 485-491.

Takashima, E., Takamiya, S., Takeo, S., Mi-ichi, F., Amino, H., and Kita, K. (2001). Isolation of mitochondria from Plasmodium falciparum showing dihydroorotate dependent respiration. Parasitol Int *50*, 273-278.

Takeo, S., Kokaze, A., Ng, C.S., Mizuchi, D., Watanabe, J.I., Tanabe, K., Kojima, S., and Kita, K. (2000). Succinate dehydrogenase in Plasmodium falciparum mitochondria: molecular characterization of the SDHA and SDHB genes for the catalytic subunits, the flavoprotein (Fp) and iron-sulfur (Ip) subunits. Mol Biochem Parasitol *107*, 191-205.

Takken, W., and Knols, B.G. (2009). Malaria vector control: current and future strategies. Trends Parasitol *25*, 101-104.

Tanaka, T.Q., Hirai, M., Watanabe, Y.I., and Kita, K. (2012). Toward understanding the role of mitochondrial complex II in the intraerythrocytic stages of Plasmodium falciparum: Gene targeting of the Fp subunit. Parasitol Int.

Taylor, A.B., Smith, B.S., Kitada, S., Kojima, K., Miyaura, H., Otwinowski, Z., Ito, A., and Deisenhofer, J. (2001). Crystal structures of mitochondrial processing peptidase reveal the mode for specific cleavage of import signal sequences. Structure *9*, 615-625.

Taylor, S.W., Warnock, D.E., Glenn, G.M., Zhang, B., Fahy, E., Gaucher, S.P., Capaldi, R.A., Gibson, B.W., and Ghosh, S.S. (2002). An alternative strategy to determine the mitochondrial proteome using sucrose gradient fractionation and 1D PAGE on highly purified human heart mitochondria. J Proteome Res *1*, 451-458.

ter Kuile, F., White, N.J., Holloway, P., Pasvol, G., and Krishna, S. (1993). Plasmodium falciparum: in vitro studies of the pharmacodynamic properties of drugs used for the treatment of severe malaria. Exp Parasitol *76*, 85-95.

ter Kuile, F.O., Terlouw, D.J., Phillips-Howard, P.A., Hawley, W.A., Friedman, J.F., Kariuki, S.K., Shi, Y.P., Kolczak, M.S., Lal, A.A., Vulule, J.M*., et al.* (2003). Reduction of malaria during pregnancy by permethrin-treated bed nets in an area of intense perennial malaria transmission in western Kenya. Am J Trop Med Hyg *68*, 50-60.

Terrapon, N., Gascuel, O., Marechal, E., and Breehelin, L. (2009). Detection of new protein domains using co-occurrence: application to Plasmodium falciparum. Bioinformatics *25*, 3077-3083.

Theakston, R.D., Howells, R.E., Fletcher, K.A., Peters, W., Fullard, J., and Moore, G.A. (1969). The ultrastructural distribution of cytochrome oxidase activity in Plasmodium Berghei and P. Gallinaceum. Life Sci *8*, 521-529.

Tian, H., Yu, L., Mather, M.W., and Yu, C.A. (1998). Flexibility of the neck region of the rieske iron-sulfur protein is functionally important in the cytochrome bc1 complex. J Biol Chem *273*, 27953-27959.

Tonhosolo, R., Gabriel, H.B., Matsumura, M.Y., Cabral, F.J., Yamamoto, M.M., D'Alexandri, F.L., Sussmann, R.A.C., Belmonte, R., Peres, V.J., and Crick, D.C. (2010). Intraerythrocytic stages of Plasmodium falciparum biosynthesize menaquinone. FEBS Letters *584*, 4761-4768.

Torrentino-Madamet, M., Desplans, J., Travaille, C., James, Y., and Parzy, D. (2010). Microaerophilic respiratory metabolism of Plasmodium falciparum mitochondrion as a drug target. Curr Mol Med *10*, 29-46.

Trager, W. (1994). Cultivation of malaria parasites. Methods Cell Biol *45*, 7-26.

Trager, W., and Jensen, J.B. (1976). Human malaria parasites in continuous culture. Science *193*, 673-675.

Tran, Q.M., Rothery, R.A., Maklashina, E., Cecchini, G., and Weiner, J.H. (2006). The quinone binding site in Escherichia coli succinate dehydrogenase is required for electron transfer to the heme b. J Biol Chem *281*, 32310-32317.

Truscott, K.N., Voos, W., Frazier, A.E., Lind, M., Li, Y., Geissler, A., Dudek, J., Muller, H., Sickmann, A., Meyer, H.E*., et al.* (2003). A J-protein is an essential subunit of the presequence translocase-associated protein import motor of mitochondria. J Cell Biol *163*, 707-713.

Tschan, S., Kremsner, P.G., and Mordmuller, B. (2012). Emerging drugs for malaria. Expert Opin Emerg Drugs *17*, 319-333.

Uhlemann, A.C., and Krishna, S. (2005). Antimalarial multi-drug resistance in Asia: mechanisms and assessment. Curr Top Microbiol Immunol *295*, 39-53.

Uhlemann, A.C., Wittlin, S., Matile, H., Bustamante, L.Y., and Krishna, S. (2007). Mechanism of antimalarial action of the synthetic trioxolane RBX11160 (OZ277). Antimicrob Agents Chemother *51*, 667-672.

Unden, G., and Bongaerts, J. (1997). Alternative respiratory pathways of Escherichia coli: energetics and transcriptional regulation in response to electron acceptors. Biochim Biophys Acta *1320*, 217-234.

Urantowka, A., Knorpp, C., Olczak, T., Kolodziejczak, M., and Janska, H. (2005). Plant mitochondria contain at least two i-AAA-like complexes. Plant Mol Biol *59*, 239-252.

Urban, S., Lee, J.R., and Freeman, M. (2001). Drosophila rhomboid-1 defines a family of putative intramembrane serine proteases. Cell *107*, 173-182.

Uyemura, S.A., Luo, S., Moreno, S.N., and Docampo, R. (2000). Oxidative phosphorylation, Ca(2+) transport, and fatty acid-induced uncoupling in malaria parasites mitochondria. J Biol Chem *275*, 9709-9715.

Uyemura, S.A., Luo, S., Vieira, M., Moreno, S.N., and Docampo, R. (2004). Oxidative phosphorylation and rotenone-insensitive malate- and NADH-quinone oxidoreductases in Plasmodium yoelii yoelii mitochondria in situ. J Biol Chem *279*, 385-393.

Vaidya, A. (2012). Naphthoquinones: Atovaquone, and Other Antimalarials Targeting Mitochondrial Functions.

Vaidya, A.B. (2004). Mitochondrial and plastid functions as antimalarial drug targets. Curr Drug Targets Infect Disord *4*, 11-23.

Vaidya, A.B., Akella, R., and Suplick, K. (1989). Sequences similar to genes for two mitochondrial proteins and portions of ribosomal RNA in tandemly arrayed 6-kilobase-pair DNA of a malarial parasite. Mol Biochem Parasitol *35*, 97-107.

Vaidya, A.B., and Arasu, P. (1987). Tandemly arranged gene clusters of malarial parasites that are highly conserved and transcribed. Mol Biochem Parasitol *22*, 249-257.

Vaidya, A.B., and Mather, M.W. (2009). Mitochondrial evolution and functions in malaria parasites. Annu Rev Microbiol *63*, 249-267.

Vaidya, A.B., Morrisey, J., Plowe, C.V., Kaslow, D.C., and Wellems, T.E. (1993). Unidirectional dominance of cytoplasmic inheritance in two genetic crosses of Plasmodium falciparum. Mol Cell Biol *13*, 7349-7357.

Valnot, I., Kassis, J., Chretien, D., de Lonlay, P., Parfait, B., Munnich, A., Kachaner, J., Rustin, P., and Rotig, A. (1999). A mitochondrial cytochrome b mutation but no mutations of nuclearly encoded subunits in ubiquinol cytochrome c reductase (complex III) deficiency. Hum Genet *104*, 460-466.

van den Berg, H. (2009). Global status of DDT and its alternatives for use in vector control to prevent disease. Environ Health Perspect *117*, 1656-1663.

van der Laan, M., Chacinska, A., Lind, M., Perschil, I., Sickmann, A., Meyer, H.E., Guiard, B., Meisinger, C., Pfanner, N., and Rehling, P. (2005). Pam17 is required for architecture and translocation activity of the mitochondrial protein import motor. Mol Cell Biol *25*, 7449-7458.

van Dooren, G.G., Marti, M., Tonkin, C.J., Stimmler, L.M., Cowman, A.F., and McFadden, G.I. (2005). Development of the endoplasmic reticulum, mitochondrion and apicoplast during the asexual life cycle of Plasmodium falciparum. Mol Microbiol *57*, 405-419.

van Dooren, G.G., Stimmler, L.M., and McFadden, G.I. (2006). Metabolic maps and functions of thePlasmodiummitochondrion. FEMS Microbiology Reviews *30*, 596-630.

van Dooren, G.G., Su, V., D'Ombrain, M.C., and McFadden, G.I. (2002). Processing of an apicoplast leader sequence in Plasmodium falciparum and the identification of a putative leader cleavage enzyme. J Biol Chem *277*, 23612-23619.

Van Geldre, E., Vergauwe, A., and Van den Eeckhout, E. (1997). State of the art of the production of the antimalarial compound artemisinin in plants. Plant Mol Biol *33*, 199-209.

van Schalkwyk, D.A., Chan, X.W., Misiano, P., Gagliardi, S., Farina, C., and Saliba, K.J. (2010). Inhibition of Plasmodium falciparum pH regulation by small molecule indole derivatives results in rapid parasite death. Biochem Pharmacol *79*, 1291-1299.

Vander Jagt, D.L., Hunsaker, L.A., Campos, N.M., and Baack, B.R. (1990). D-lactate production in erythrocytes infected with Plasmodium falciparum. Mol Biochem Parasitol *42*, 277-284.

Vennerstrom, J.L., and Eaton, J.W. (1988). Oxidants, oxidant drugs, and malaria. J Med Chem *31*, 1269-1277.

Verma, R., Varshney, G.C., and Raghava, G.P. (2010). Prediction of mitochondrial proteins of malaria parasite using split amino acid composition and PSSM profile. Amino Acids *39*, 101-110.

Vibat, C.R., Cecchini, G., Nakamura, K., Kita, K., and Gennis, R.B. (1998). Localization of histidine residues responsible for heme axial ligation in cytochrome b556 of complex II (succinate:ubiquinone oxidoreductase) in Escherichia coli. Biochemistry *37*, 4148-4159.

Vogtle, F.N., Wortelkamp, S., Zahedi, R.P., Becker, D., Leidhold, C., Gevaert, K., Kellermann, J., Voos, W., Sickmann, A., Pfanner, N.*, et al.* (2009). Global analysis of the mitochondrial N-proteome identifies a processing peptidase critical for protein stability. Cell *139*, 428-439.

von Ballmoos, C., Cook, G.M., and Dimroth, P. (2008). Unique rotary ATP synthase and its biological diversity. Annu Rev Biophys *37*, 43-64.

Vontas, J., Siden-Kiamos, I., Papagiannakis, G., Karras, M., Waters, A.P., and Louis, C. (2005). Gene expression in Plasmodium berghei ookinetes and early oocysts in a co-culture system with mosquito cells. Mol Biochem Parasitol *139*, 1-13.

Walker, J.E., and Dickson, V.K. (2006). The peripheral stalk of the mitochondrial ATP synthase. Biochim Biophys Acta *1757*, 286-296.

Walker, K., and Lynch, M. (2007). Contributions of Anopheles larval control to malaria suppression in tropical Africa: review of achievements and potential. Medical and Veterinary Entomology *21*, 2-21.

Waller, R.F., Keeling, P.J., Donald, R.G., Striepen, B., Handman, E., Lang-Unnasch, N., Cowman, A.F., Besra, G.S., Roos, D.S., and McFadden, G.I. (1998). Nuclear-encoded proteins target to the plastid in Toxoplasma gondii and Plasmodium falciparum. Proc Natl Acad Sci U S A *95*, 12352-12357.

Walther, M., Thompson, F.M., Dunachie, S., Keating, S., Todryk, S., Berthoud, T., Andrews, L., Andersen, R.F., Moore, A., Gilbert, S.C.*, et al.* (2006). Safety, immunogenicity, and efficacy of prime-boost immunization with recombinant poxvirus FP9 and modified vaccinia virus Ankara encoding the full-length Plasmodium falciparum circumsporozoite protein. Infect Immun *74*, 2706-2716.

Wang, J., Huang, L., Li, J., Fan, Q., Long, Y., Li, Y., and Zhou, B. (2010). Artemisinin directly targets malarial mitochondria through its specific mitochondrial activation. PLoS One *5*, e9582.

Wang, S., Sakai, H., and Wiedmann, M. (1995). NAC covers ribosome-associated nascent chains thereby forming a protective environment for regions of nascent chains just emerging from the peptidyl transferase center. J Cell Biol *130*, 519-528.

Waters, N., and Edstein, M. (2012). 8-Aminoquinolines: Primaquine and Tafenoquine.

Weber, J. (2007). ATP synthase--the structure of the stator stalk. Trends Biochem Sci *32*, 53-56.

Weinstein, E.A., Yano, T., Li, L.S., Avarbock, D., Avarbock, A., Helm, D., McColm, A.A., Duncan, K., Lonsdale, J.T., and Rubin, H. (2005). Inhibitors of type II NADH:menaquinone oxidoreductase represent a class of antitubercular drugs. Proc Natl Acad Sci U S A *102*, 4548-4553.

Wendel, W.B. (1946). The influence of napthoquinones upon the respiratory and carbohydrate metabolism of malarial parasites. Fed Proc *5*, 406.

White, N.J. (2008). Qinghaosu (artemisinin): the price of success. Science *320*, 330-334.

Whitworth, A.J., Lee, J.R., Ho, V.M., Flick, R., Chowdhury, R., and McQuibban, G.A. (2008). Rhomboid-7 and HtrA2/Omi act in a common pathway with the Parkinson's disease factors Pink1 and Parkin. Dis Model Mech *1*, 168-174; discussion 173.

WHO (2010). World Health Organization - World Malaria Report 2010.

Wibrand, F., Ravn, K., Schwartz, M., Rosenberg, T., Horn, N., and Vissing, J. (2001). Multisystem disorder associated with a missense mutation in the mitochondrial cytochrome b gene. Ann Neurol *50*, 540-543.

Wichmann, O., Muehlberger, N., Jelinek, T., Alifrangis, M., Peyerl-Hoffmann, G., Muhlen, M., Grobusch, M.P., Gascon, J., Matteelli, A., Laferl, H.*, et al.* (2004). Screening for mutations related to atovaquone/proguanil resistance in treatment failures and other imported isolates of Plasmodium falciparum in Europe. J Infect Dis *190*, 1541-1546.

Wiedemann, N., Kozjak, V., Chacinska, A., Schonfisch, B., Rospert, S., Ryan, M.T., Pfanner, N., and Meisinger, C. (2003). Machinery for protein sorting and assembly in the mitochondrial outer membrane. Nature *424*, 565-571.

Wiedemann, N., Truscott, K.N., Pfannschmidt, S., Guiard, B., Meisinger, C., and Pfanner, N. (2004). Biogenesis of the protein import channel Tom40 of the mitochondrial outer membrane: intermembrane space components are involved in an early stage of the assembly pathway. J Biol Chem *279*, 18188-18194.

Wiedemann, N., van der Laan, M., Hutu, D.P., Rehling, P., and Pfanner, N. (2007). Sorting switch of mitochondrial presequence translocase involves coupling of motor module to respiratory chain. J Cell Biol *179*, 1115-1122.

Wiedmann, B., Sakai, H., Davis, T.A., and Wiedmann, M. (1994). A protein complex required for signal-sequence-specific sorting and translocation. Nature *370*, 434-440.

Wikstrom, M., and Hummer, G. (2012). Stoichiometry of proton translocation by respiratory complex I and its mechanistic implications. Proc Natl Acad Sci U S A *109*, 4431-4436.

Wilairatana, P., and Krudsood, S. (2009). Cerebral Malaria. In International Neurology (Wiley-Blackwell), pp. 285-289.

Wilkens, S., and Capaldi, R.A. (1998). Electron microscopic evidence of two stalks linking the F1 and F0 parts of the Escherichia coli ATP synthase. Biochim Biophys Acta *1365*, 93-97.

Wilson, C.M., Serrano, A.E., Wasley, A., Bogenschutz, M.P., Shankar, A.H., and Wirth, D.F. (1989). Amplification of a gene related to mammalian mdr genes in drug-resistant Plasmodium falciparum. Science *244*, 1184-1186.

Winstanley, P., and Ward, S. (2006). Malaria chemotherapy. Adv Parasitol *61*, 47-76.

Winter, R.W., Kelly, J.X., Smilkstein, M.J., Dodean, R., Hinrichs, D., and Riscoe, M.K. (2008). Antimalarial quinolones: synthesis, potency, and mechanistic studies. Exp Parasitol *118*, 487-497.

Wirth, D.F. (2002). The parasite genome: Biological revelations. Nature *419*, 495-496.

Wittig, I., Braun, H.-P., and Schägger, H. (2006). Blue native PAGE. Nature Protocols *1*, 418-428.

Wittig, I., Meyer, B., Heide, H., Steger, M., Bleier, L., Wumaier, Z., Karas, M., and Schagger, H. (2010). Assembly and oligomerization of human ATP synthase lacking mitochondrial subunits a and A6L. Biochim Biophys Acta *1797*, 1004-1011.

Wittig, I., and Schagger, H. (2008). Structural organization of mitochondrial ATP synthase. Biochim Biophys Acta *1777*, 592-598.

Wongsrichanalai, C., Pickard, A.L., Wernsdorfer, W.H., and Meshnick, S.R. (2002). Epidemiology of drug-resistant malaria. Lancet Infect Dis *2*, 209-218.

Wu, W.-M., Wu, Y., Wu, Y.-L., Yao, Z.-J., Zhou, C.-M., Li, Y., and Shan, F. (1998). Unified Mechanistic Framework for the Fe(II)-Induced Cleavage of Qinghaosu and Derivatives/Analogues. The First Spin-Trapping Evidence for the Previously Postulated Secondary C-4 Radical. Journal of the American Chemical Society *120*, 3316-3325.

Wu, Y., and Sha, B. (2006). Crystal structure of yeast mitochondrial outer membrane translocon member Tom70p. Nat Struct Mol Biol *13*, 589-593.

Wu, Y., Wang, X., Liu, X., and Wang, Y. (2003). Data-mining approaches reveal hidden families of proteases in the genome of malaria parasite. Genome Res *13*, 601-616.

Wyatt, C.N., and Buckler, K.J. (2004). The effect of mitochondrial inhibitors on membrane currents in isolated neonatal rat carotid body type I cells. J Physiol *556*, 175-191.

Xia, D., Yu, C.A., Kim, H., Xia, J.Z., Kachurin, A.M., Zhang, L., Yu, L., and Deisenhofer, J. (1997). Crystal structure of the cytochrome bc1 complex from bovine heart mitochondria. Science *277*, 60-66.

Xiang, H., McSurdy-Freed, J., Moorthy, G.S., Hugger, E., Bambal, R., Han, C., Ferrer, S., Gargallo, D., and Davis, C.B. (2006). Preclinical drug metabolism and pharmacokinetic evaluation of GW844520, a novel anti-malarial mitochondrial electron transport inhibitor. J Pharm Sci *95*, 2657-2672.

Xiao, K., Liu, X., Yu, C.-A., and Yu, L. (2004). The Extra Fragment of the Iron−Sulfur Protein (Residues 96-107) of Rhodobacter sphaeroides Cytochrome bc1 Complex Is Required for Protein Stability†. Biochemistry *43*, 1488-1495.

Xu, P., Widmer, G., Wang, Y., Ozaki, L.S., Alves, J.M., Serrano, M.G., Puiu, D., Manque, P., Akiyoshi, D., Mackey, A.J.*, et al.* (2004). The genome of Cryptosporidium hominis. Nature *431*, 1107-1112.

Yamamoto, H., Esaki, M., Kanamori, T., Tamura, Y., Nishikawa, S., and Endo, T. (2002). Tim50 is a subunit of the TIM23 complex that links protein translocation across the outer and inner mitochondrial membranes. Cell *111*, 519-528.

Yang, Y.Z., Little, B., and Meshnick, S.R. (1994). Alkylation of proteins by artemisinin. Effects of heme, pH, and drug structure. Biochem Pharmacol *48*, 569-573.

Yankovskaya, V., Horsefield, R., Tornroth, S., Luna-Chavez, C., Miyoshi, H., Leger, C., Byrne, B., Cecchini, G., and Iwata, S. (2003). Architecture of succinate dehydrogenase and reactive oxygen species generation. Science *299*, 700-704.

Yano, M., Terada, K., and Mori, M. (2003). AIP is a mitochondrial import mediator that binds to both import receptor Tom20 and preproteins. J Cell Biol *163*, 45-56.

Yeates, C.L., Batchelor, J.F., Capon, E.C., Cheesman, N.J., Fry, M., Hudson, A.T., Pudney, M., Trimming, H., Woolven, J., Bueno, J.M.*, et al.* (2008). Synthesis and structure-activity relationships of 4-pyridones as potential antimalarials. J Med Chem *51*, 2845-2852.

Yin, H., and Porter, N.A. (2005). New insights regarding the autoxidation of polyunsaturated fatty acids. Antioxid Redox Signal *7*, 170-184.

Ylikallio, E., and Suomalainen, A. (2012). Mechanisms of mitochondrial diseases. Ann Med *44*, 41-59.

Young, J.C., Hoogenraad, N.J., and Hartl, F.U. (2003). Molecular chaperones Hsp90 and Hsp70 deliver preproteins to the mitochondrial import receptor Tom70. Cell *112*, 41-50.

Yung, S., Unnasch, T.R., and Lang-Unnasch, N. (2001). Analysis of apicoplast targeting and transit peptide processing in Toxoplasma gondii by deletional and insertional mutagenesis. Mol Biochem Parasitol *118*, 11-21.

Zara, V., Conte, L., and Trumpower, B.L. (2009). Evidence that the assembly of the yeast cytochrome bc1 complex involves the formation of a large core structure in the inner mitochondrial membrane. FEBS J *276*, 1900-1914.

Zeng, X., Neupert, W., and Tzagoloff, A. (2007). The metalloprotease encoded by ATP23 has a dual function in processing and assembly of subunit 6 of mitochondrial ATPase. Mol Biol Cell *18*, 617-626.

Zhang, J., Krugliak, M., and Ginsburg, H. (1999). The fate of ferriprotorphyrin IX in malaria infected erythrocytes in conjunction with the mode of action of antimalarial drugs. Mol Biochem Parasitol *99*, 129-141.

Zhang, S., and Gerhard, G.S. (2008). Heme activates artemisinin more efficiently than hemin, inorganic iron, or hemoglobin. Bioorg Med Chem *16*, 7853-7861.

Zhang, Y., Marcillat, O., Giulivi, C., Ernster, L., and Davies, K.J. (1990). The oxidative inactivation of mitochondrial electron transport chain components and ATPase. J Biol Chem *265*, 16330-16336.

Zhang, Z., Huang, L., Shulmeister, V.M., Chi, Y.I., Kim, K.K., Hung, L.W., Crofts, A.R., Berry, E.A., and Kim, S.H. (1998). Electron transfer by domain movement in cytochrome bc1. Nature *392*, 677-684.

Zhou, X.W., Kafsack, B.F., Cole, R.N., Beckett, P., Shen, R.F., and Carruthers, V.B. (2005). The opportunistic pathogen Toxoplasma gondii deploys a diverse legion of invasion and survival proteins. J Biol Chem *280*, 34233-34244.